THESE DE DOCTORAT DE
L'UNIVERSITE PIERRE ET MARIE CURIE

Spécialité

Chimie et Physico-Chimie des Polymères
(ED 397, Physique et Chimie des Matériaux)

Présentée par

Mlle Mengxing LI

Pour obtenir le grade de

DOCTEUR DE L'UNIVERSITE PIERRE ET MARIE CURIE

Sujet de la thèse :

Films minces d'hydrogels stimulables

Soutenue le 14/10/2014 devant le jury composé de:

Mme. Catherine AMIEL	Rapporteur
M. Costantino CRETON	
M. Michel GOLDMANN	
Mme. Lay-Theng LEE	Rapporteur
M. Frédéric RESTAGNO	
Mme. Yvette TRAN	

Contents

General introduction 1

Chapter 1: Hydrogel thin films: a general survey 7

Contents 8

1. Polymer hydrogels 9
   - 1.1. Definitions and main characteristics 9
   - 1.2. Various architectures of hydrogels 10
     - 1.2.1 Interpenetrating networks (IPN) hydrogels 11
     - 1.2.2 Double networks (DN) hydrogels 12
     - 1.2.3 Hybrid hydrogels 13
   - 1.3. Stimuli-responsive hydrogels 14
     - 1.3.1 Main characteristics 14
     - 1.3.2 Different stimuli-responsive hydrogels 15
2. Polymer hydrogels at interfaces 17
   - 2.1. Polymer assemblies at interfaces 17
     - 2.1.1. Layer-by-layer assemblies 18
     - 2.1.2. Polymer brushes 19
   - 2.2. Hydrogel thin films: advantage of hydrogels and films 20
     - 2.2.1. Synthesis methods of hydrogel thin films 21
     - 2.2.2. Swelling of hydrogel thin films 22
     - 2.2.3. Flory-Rehner theory extended to one-dimension 22
3. Objectives of the thesis 24
   - 3.1. A simple and versatile strategy 25
   - 3.2. Which responsive properties? 26
   - 3.3. Effect of confinement and constraints on the lateral swelling 27
   - 3.4. Development of new hydrogel films with complex architectures 27

References 29

Chapter 2: Synthesis of hydrogel thin films 39

Contents 40

Introduction 41

1. Strategy of synthesis of surface-attached gel thin films 41
   - 1.1. Thiol-ene click chemistry 41

1.2. Spin-coating of polymers 42
1.3. General strategy 43
2. Synthesis of stimuli-responsive polymers 44
2.1. General strategy 44
2.2. Thermo-responsive polymers 46
2.2.1. Synthesis of poly(AA-co-NIPAM) 46
2.2.2. Ene-functionalization of PNIPAM chains 49
2.3. Photo-responsive polymers 51
2.4. Electro-responsive polymers 53
2.4.1. Synthesis of poly(AA-co-AMPS) 54
2.4.2. Ene-functionalization of PAMPS chains 55
2.5. Deuterated polymers for neutron experiments 55
2.5.1. Synthesis of deuterated PAA (PAA_D) 55
2.5.2. Ene-functionalization of deuterated PAA (PAA_D) 56
3. Synthesis method for hydrogel thin films 57
3.1. Functionalization of substrates 57
3.2. Coating of polymer films 58
3.3. Cross-linking and grafting of polymers 60
4. Formation of single network gel films 60
4.1. Synthesis of single network gel films 60
4.2. Dry thickness 61
4.3. Synthesis of single network gel films for neutron experiments 62
References 64

Chapter 3: Swelling behavior of single network films 65

Contents 66
Introduction 67
1. Swelling ratio 68
1.1. Measure by ellipsometry 68
1.2. Thermo-responsive properties of PNIPAM hydrogel films 71
1.2.1. Effect of the film thickness 71
1.2.2. Effect of the length of polymer chains 73
2. Topography of the free surface 74
2.1. Measurement by AFM 75
2.2. Study of measurement conditions 77
2.2.1. In air 77
2.2.2. In water: approach-retract curves 78

2.2.3. Topography in water 84
2.3. Topography of PNIPAM hydrogel films in air 89
2.4. Topography of PNIPAM hydrogel films in water 92
2.4.1. Thick fims 92
2.4.2. Thin films 94
2.5. Effect of temperature 95
2.6. Conclusion 98
3. Density profile of monomers 98
3.1. Measures in air 99
3.2. Effect of temperature 101
3.3. Effect of the thickness of the film 103
4. Discussion 107
4.1. Each technique has its specification and limitation 107
4.2. Effect of the confinement 108
4.3. Gel film: a model network? 111
References 115

Chapter 4: Development of new hydrogel films with complex architectures 117
Contents 118
Introduction 119
1. Layer-by-layer (LbL) networks gel films 121
1.1. Synthesis 121
1.1.1. General strategy 121
1.1.2. Synthesis of multilayer PNIPAM gel films 123
1.1.3. Synthesis of bilayer PNIPAM gel films for neutron experiments 124
1.2. Structure of multilayer PNIPAM gel films in water 125
1.2.1. Topography 125
1.2.2. Swelling behavior 127
1.2.3. Characterization by neutron reflectivity 128
2. Interpenetrating networks (IPN) gel films 128
2.1. Synthesis 129
2.1.1. General strategy 129
2.1.2. Synthesis of PNIPAM IPN gel films 131
2.1.3. Synthesis of IPN films for neutron reflectivity experiments 132
2.2. Structure of the PNIPAM IPN gel films in water 133
2.2.1. Topography 133

2.2.2. Swelling behavior 134
3. Hybrid gel films 135
3.1. Synthesis 135
3.1.1. General strategy 135
3.1.2. Synthesis of silica-PNIPAM hybrid gel films 137
3.2. Structure of silica-PNIPAM hybrid gel films in water 139
3.2.1. Topography of the free surface 139
3.2.2. Swelling ratio 145
3.2.3. Effect of temperature on the swelling ratio 148
4. LbL or IPN networks? A study by neutron reflectivity 150
4.1. Measures in air 151
4.2. Effect of temperature 156
4.3. Discussion 159
References 163

General conclusion 165

Annexes 173

General introduction

Research interest in stimuli-responsive polymer surfaces and interfaces is due to their wide range of applications for materials, biology or medicine fields. To name a few, wetting, permeability or adhesion properties, can be improved and controlled with suitably switchable systems. Polymer brushes and self-assembled layers are so far examples of materials most studied in this field. Our study goes beyond and focuses on stimuli-responsive hydrogel films. The hydrogel thin films are attractive since they associate both advantages of hydrogels and films.

Why advantage of hydrogels? The architecture of hydrogel in thin films, inspired from the versatile architecture of macroscopic hydrogels, offers much potential in competition with layer-by-layer (LbL) assemblies and grafted polymer layers. On the one hand, the polymer networks are much more stable surface coatings when compared with LbL systems due to their covalent attachment to the surface and their chemical cross-linking. Furthermore, the fabrication of hydrogel thin films is a one-step process and there is no need of cyclic steps as for multilayer systems. The range of thickness reached with hydrogel films or multilayer gel films is of the same order of magnitude. On the other hand, hydrogel films are also more stable when compared with polymer brushes, where polymer chains are grafted to the surface via only one functional group while the polymer network is linked to the surface by multiple anchoring points. Another advantage is that the thickness of the hydrogel layer is not limited by the number of units in a polymer chain as for polymer brushes. In addition, if needed, the hydrogel thin film can be used as a free-standing film thanks to its 3D cross-linked network structure while polymer brushes can't. In summary, hydrogel thin films are very promising as an approach to responsive surfaces and interfaces: they can be easily rendered multifunctional and multiresponsive without compromising their mechanical stability, which is secured by a 3D cross-linked network structure.

Why advantage of films? The decrease of the feature size in thin films is an appropriate way to create structures with fast response without corruption of the mechanical properties of the bulk materials. As known, the swelling/collapse phase transition of hydrogels is a diffusion-limited process, so bulk hydrogels often result in long response time, which is too slow for many applications. Actually, the dependence of the response time, T, required for the volumetric change, is expressed as $T = L^2/D$, where L is the smallest dimension of the hydrogel, and D is the collective diffusion constant of the gel network defined as a ratio of the longitudinal bulk modulus of the network to the coefficient of friction between the network and the solvent. This equation indicates that a small size of hydrogel would give a faster response, for example, the response time is 1 ms for one micron-thick gel films. For this purpose, one straightforward way is to downside the hydrogel structures by using thin films. This approach allows the development of devices with fast responses while maintaining their mechanical robustness.

The properties of these “smart” materials can be interestingly explored for the fabrication of miniaturized devices with fast response time. Since the chemical groups (i.e. polymer chains) define the type of stimulus to which the hydrogels respond, and the physical properties (size and structure) determine the response time, hydrogels can be tuned to desired applications with a wide range of chemical and physical properties. These “smart” hydrogel thin films are then promising materials for a broad range of applications, from sensors to actuators. They can offer endless opportunities for the development of coatings for drug delivery systems, tunable optical systems and many other advanced applications. Among the numerous possibilities of applications, hydrogel thin films served as microfluidic valves and flow switches are very attractive. A stimuli-responsive hydrogel thin film embedded inside a microfluidic channel can work as a valve (functional gate) which opens or closes the channel for a water flow. “Smart” hydrogel valves eliminate the need of bulky external control and thus allow the creation of handy and autonomous “lab-on-a-chip” systems for analytics.

The hydrogel films we are interested in are chemical polymer networks that are covalently grafted to the surface, with the size ranging from nanometers to hundred of microns. One of our objectives is to develop surface-attached hydrogel films with a wide range of thicknesses and with the desired responsiveness nature.

Which strategy for the synthesis of hydrogel films? The strategy adopted should be very simple and very versatile. It should allow easily the adjustment of chemical properties (e.g. responsiveness) and physical properties (e.g. size and structure) of the films. The strategy chosen to synthesize chemically cross-linked hydrogels consists in cross-linking preformed and functionalized polymers through thiol-ene click chemistry. It is preferred to the synthesis starting from monomers which are then polymerized and cross-linked at the same time. Our approach allows a better control of the synthesis because there is no caution of controlled atmosphere and no addition of any initiator.

Which stimuli-responsive properties? Among different external stimuli, we choose the temperature, the light and the electric field. Though the temperature is not a local stimulus, it is a handy parameter to control and it can be easily varied on a wide range. The thermo-sensitive hydrogel films are obtained using PNIPAM for its LCST (around 32°C) properties. As the temperature is convenient to control as external stimulus, we will always use hydrogel films containing PNIPAM networks to study the phase transition of model networks films. The electric field and the light stimuli have the advantages of rapid and local activation which is very helpful for applications such as the function of hydrogel-based microvalves in microfluidic devices. The microfluidic geometry renders the possibility to show for the first time the sensitivity of polymer *films* to electric field.

The range of thickness targeted in this present study goes from nanometer to microns, which allows the characterization by usual reflectivity techniques such as ellipsometry or neutron reflectivity.

We investigate the structure of these stimuli-responsive hydrogel films to make clear the effects of confinement and lateral constraints on their responsive behaviors. Actually, the swelling of hydrogels in the confinement state such as films is likely rather anisotropic than isotropic as for macroscopic hydrogels. The constraints on lateral swelling due to the covalent attachment of the hydrogel film on the solid substrate may induce a mechanical stress which causes the deformation of the free surface of the hydrogel film. Taking thermo-responsive hydrogel films as an example, we try to tackle these fundamental aspects: what is the effect of the confinement on the swelling of the gel films? How does the surface-attachment affect the free surface of the gel films?

Correspondingly, systematic studies will be carried out with three different and complementary techniques: ellipsometry, neutron reflectivity and atomic force microscopy. Ellipsometry is employed to determine the swelling ratio of the hydrogel films in the direction normal to the substrate. Neutron reflectivity experiments are performed for defining the interface width on the free surface side of the hydrogel films. The density profile of the gel films obtained from neutron reflectivity is coupled with a topographic (in-plane) description of the free surface, resulting from AFM experiments.

The promising feature of the hydrogel films is the development of new and complex hydrogel films with various architectures of the polymer networks, inspired from the versatile architecture of macroscopic hydrogels. The objective is to achieve multifunctional hydrogel films with targeted architecture of the network. We aim to elaborate architectures such as multilayer hydrogel films through layer-by-layer assembly, interpenetrating networks (IPN) hydrogel films and hybrid hydrogel films containing solid particles such as silica nanoparticles. Multilayer hydrogel films are very promising as simple way to achieve multifunctional films with long-terme stability. For example, they can be rendered the responsive properties to various stimuli. They hopefully are as versatile as layer-by-layer assemblies. Along with that, the interpenetrating networks (IPN) hydrogel films are the alternative architecture to bilayers hydrogel films. Interpenetrating networks have two cross-linked structures which are not joined together. The properties of each network can be interestingly maintained within the interpenetrating networks. The IPN architecture can be exploited to develop double networks (DN) hydrogel films, which are expected to be

mechanically strengthened by analogy with macroscopic DN hydrogels. Meanwhile, silica-polymer hybrid hydrogel films are also supposed to have their mechanical behaviors reinforced similarly to macroscopic hybrid hydrogels.

This manuscript is divided into four chapters.

The first chapter is devoted to an overview of hydrogels and polymer assemblies at interfaces. The main characteristics of hydrogels are presented, along with their various architectures and responsive properties to different stimuli. Polymer assemblies at interfaces, in particular layer-by-layer assemblies and polymer brushes, are described. The overview allows then the introduction of the objectives of the thesis.

The second chapter is dedicated to the strategy of synthesis of hydrogel films with responsive properties to different stimuli. In this chapter, we describe the synthesis and characterization of stimuli-responsive polymers and finally the formation of single-network hydrogel films.

In Chapter 3, effect of confinement and lateral constraints on the swelling behavior of single-network hydrogel films is studied, in terms of the swelling ratio of the hydrogel films in the direction normal to the substrate by ellipsometry, the interface width on the free surface side of the hydrogel films by neutron reflectivity, and a topographic (in-plane) description of the free surface by AFM.

In Chapter 4, development of various architectures such as multilayer hydrogel films, interpenetrating networks hydrogel films and hybrid hydrogel films containing silica nanoparticles are presented, together with the studies on their structures and swelling properties.

Finally, the main contributions of this work will be recalled and summarized in a concluding part, along with the prospects.

Chapter 1

Hydrogel thin films: a general survey

Contents

Contents 8

1. Polymer hydrogels 9

    1.1. Definitions and main characteristics 9

    1.2. Various architectures of hydrogels 10

        1.2.1 Interpenetrating networks (IPN) hydrogels 11

        1.2.2 Double networks (DN) hydrogels 12

        1.2.3 Hybrid hydrogels 13

    1.3. Stimuli-responsive hydrogels 14

        1.3.1 Main characteristics 14

        1.3.2 Different stimuli-responsive hydrogels 15

2. Polymer hydrogels at interfaces 17

    2.1. Polymer assemblies at interfaces 17

        2.1.1. Layer-by-layer assemblies 18

        2.1.2. Polymer brushes 19

    2.2. Hydrogel thin films: advantage of hydrogels and films 20

        2.2.1. Synthesis methods of hydrogel thin films 21

        2.2.2. Swelling of hydrogel thin films 22

        2.2.3. Flory-Rehner theory extended to one-dimension 22

3. Objectives of the thesis 24

    3.1. A simple and versatile strategy 25

    3.2. Which responsive properties? 26

    3.3. Effect of confinement and constraints on the lateral swelling 27

    3.4. Development of new hydrogel films with complex architectures 27

References 29

1. Polymer hydrogels

Synthetic polymer hydrogels have been developed for the past several decades. Due to their significant water content, polymer hydrogels possess a degree of flexibility very similar to natural tissue, which renders them special attention in biology engineering. In addition, their diverse important properties, such as responsive behavior to external stimuli, ability to store chemical or biological species, and low interfacial tension at gel-water interface, make them become promising candidate materials in numerous application fields.

1.1. Definitions and main characteristics

Hydrogel is a three-dimensional cross-linked network of hydrophilic polymer chains, which can absorb up to 90% (by weight) water when submerged in water. One of the most remarkable properties of hydrogels is the very low polymer content. Due to the special structure, hydrogels are soft materials behaving as soft solids, with the properties ranging from soft and weak to hard and tough. In water, the hydrogel system can be treated as a dispersion of water molecules within a solid in which the solid is the continuous phase and the liquid is the discontinuous phase.

Owing to specific interactions between the polymer chains and water and many possible structures of the networks, kinds of complex polymer hydrogels are available. These two key parameters can be initially designed to obtain particular materials with required properties. Based on the type of cross-linking, hydrogels are classified in two groups: chemically cross-linked hydrogels and physically cross-linked hydrogels. For chemically cross-linked hydrogels, the polymer chains are cross-linked through covalent bonds, which are irreversible if no chemical degradation occurs. These hydrogels behave as elastic solids, with the conservation of the permanent shape under self-weight (no flowing phenomenon) and no physical modification. On the contrary, in the case of physically cross-linked hydrogels, the interactions between the polymer chains at the cross-linking points are reversible, including Van der Waals interactions [1]: hydrogen bonding [2], ionic [3, 4] or hydrophobic interactions [5, 6], etc.

In this study, we will focus on hydrogels based on covalently cross-linked polymer chains, as schematically represented in **Figure 1**.

Many inherent properties of polymer hydrogels predetermine their irreplaceable position for numerous applications, among which the most important is their high water content that makes them biocompatible and allows the diffusion process of water soluble compound through the polymer networks [7]. This leads to the fact that hydrogels are able to absorb, store and release large amounts of water as well as aqueous solutions containing active

substances. Based on this property, various uses of hydrogels have been explored in biomedicine engineering, including contact lenses [8, 9], super-absorbants [10], and so on.

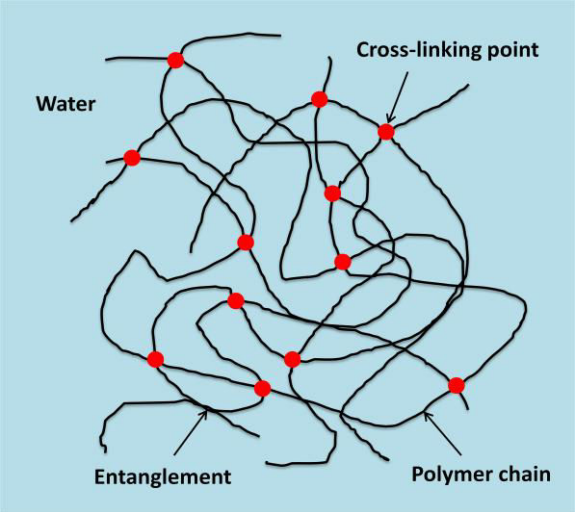


***Figure 1**: Schematic representation of a (chemically or physically) cross-linked polymer network.*

Hydrogels are also employed in scaffolds for tissue engineering to control the distribution of cells or molecular species [11-13]. In addition, introduced into agriculture, hydrogels can hold moisture in arid areas [14]. The number of scientific publications and applications concerning hydrogels has been increasing drastically during the last thirty years. However one main limitation remains: the poor mechanical properties of hydrogels.

Overall, hydrogels are highly swollen 3D cross-linked networks with a wide range of properties. Their mechanical and swelling properties are influenced by the life-time of the cross-linking points (infinite for chemical cross-linked gels, while temporary for physical cross-linked gels) and also by structural parameters of the networks (such as the mesh size, the presence and type of inhomogeneities).

1.2. Various architectures of hydrogels

As mentioned above, under some conditions hydrogels are not ideal materials because of their poor mechanical behaviors. Several strategies have been developed in order to reinforce their mechanical properties. Particularly, the design of hydrogels with various architectures has been a hot topic in recent years, as these complex systems allow to tailor their structures to obtain well-controlled properties over a large range [15]. According to Walter Richtering and Brian R. Saunders, well-studied hydrogels in recent years can be summarized in **Figure 2** depending on their various structures [15].

In this part, we will focus on some of them that are mostly studied.

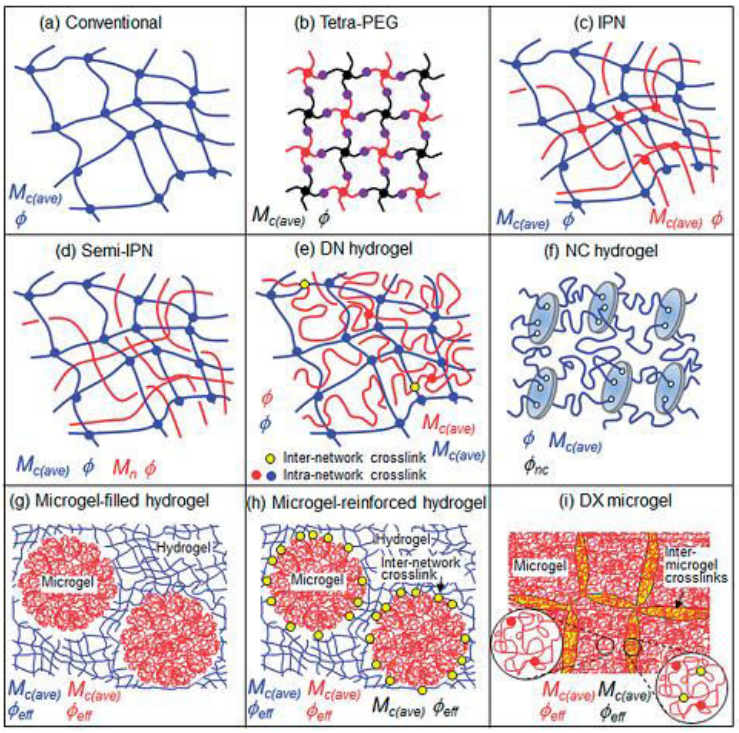


***Figure 2**: Depiction of the structures of well-studied hydrogels [15].*

1.2.1. Interpenetrating networks (IPN) hydrogels

An interpenetrating networks (IPN) hydrogel is a system composed of two or more cross-linked polymer networks which are interlaced at the molecular scale but not covalently bonded to each other. The contained networks are supposed to be concatenated through entanglements. However, simply mixing two or more polymer networks cannot yield an IPN hydrogel. Here, we take IPN hydrogels comprising two polymer networks as an example to show their synthesis and characterizations.

IPN hydrogels can be prepared while each of the two polymer networks is independently cross-linked at the same time using orthogonal chemistry [16]. Another way to produce IPN hydrogels is to prepare the second polymer network in the presence of the first one, which may result in the formation of interpolymer complexes due to physical interaction like hydrogen bonding [17]. In fact, as special IPN hydrogels, there are also semi-IPN hydrogels, in which one of the two components is in the form of polymer chains that are not cross-linked [16, 18].

Generally, IPN hydrogels have improved properties compared with the corresponding single-network hydrogels, due to the integration of properties of the two polymer networks, various interactions between the two polymer networks, and so on. For example, Wen-FuLee et al. developed PNIPAAm/chitosan semi-IPN and IPN hydrogels which had both temperature-sensitivity (resulting from PNIPAAm) and pH-sensitivity (resulting from chitosan)

[16]. It is the same case for PMAA/PNIPAAm IPN hydrogels prepared by Jing Zhang et al., in which the properties of each polymer network were maintained [19]. Moreover, semi-IPN hydrogels based on cross-linked PAAm network containing PNIPAAm chains inside presented improved mechanical properties with a higher elastic modulus compared to PAAm hydrogels [18].

1.2.2. Double networks (DN) hydrogels

A few years ago, Gong et al. developed a new concept of strong hydrogels by introducing the double-network (DN) structure to combine various hydrophilic polymers. Their DN hydrogels exhibit excellent mechanical performances while containing 60-90% water [20]. The mechanically enhanced DN hydrogels consist of two polymer networks with totally asymmetric structures. The first network is made of tightly cross-linked rigid polymer chains, while the second one is a loosely, or even not, cross-linked flexible polymer network. In addition, it is required that the molar concentration of the second network is 20–30times that of the first network [21]. As schematically represented in **Figure 3**, the neutral poly(acrylamide) (PAAm) network (the 2nd network) is incorporated within the polyelectrolyte network of poly(2-acrylamido-2-methylpropanesulfonic acid) (PAMPS) (the 1st network) [22]. The main idea is to find an optimal combination of the first rigid and brittle polyelectrolyte network and the second soft and ductile neutral network.

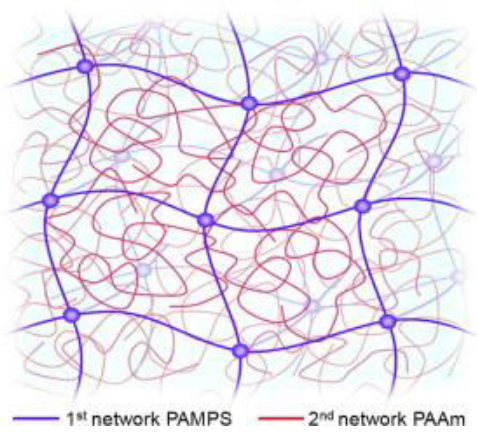


***Figure 3**: Schematic representation of the structure of double network hydrogels [22].*

The mechanical properties of double networks hydrogels are strongly improved compared with that of the composing single network hydrogels, in terms of stiffness (elastic modulus), strength and toughness. This mechanically reinforcement is due to the special structure of double networks with the optimized combination parameters of the two networks [21, 23-25]. Uniaxial tensile tests are applied on Gong's PAMPS/PAAm DN hydrogels, showing a necking phenomenon: narrowed zones ("necks") appear along the samples and then grow up with elongation. After the necks' propagation, the gels become extremely soft [21, 24].

Correspondingly, cyclic experiments of loading-unloading on double network hydrogels indicate a significant hysteresis during the first cycle, which is never observed in a second cycle [26]. These experimental findings can be explained as follows: the first PAMPS network breaks into small clusters, because of its intrinsic fragility, and then the formed clusters play a role of physical cross-linking points of the long flexible PAAm chains, behaving as sliding cross-linkers, due to the low cross-linking density of the PAAm network and the high molecular weight of PAAm [21].

The highly enhanced mechanical performances have brought DN hydrogels great attention aiming for various useful applications, especially in biomedical area. Therefore, many different hydrogel systems with a double-network structure have been developed inspired by Gong's concept, such as the biocompatible hydrogels based on double networks with the combination of natural polymers (bacterial cellulose, jellyfish or alginate gels) and synthetic ones (gelatin or PAAm) [27-29]. Thanks to their high water content and relatively high mechanical strength, some DN hydrogels serve as advantageous candidates for cartilage and cornea replacement [30-34].

1.2.3. Hybrid hydrogels

Hydrogels which contain two or more components are normally referred to as hybrid hydrogels. During the last decade, various hybrid hydrogels with improved properties have been developed by different research groups. Minko et al. exploited a kind of hybrid gel with gold nanoparticles contained in a responsive polymer gel, which enables the transduction of external stimuli into a strong optical effect [35]. Thermo-responsive PNIPAM was encapsulated in silica to form a hybrid gel membrane, whose permeability can be controlled by the swelling/shrinking behavior of PNIPAM, presented by López et al. [36]. Haraguchi et al. developed hybrid hydrogels with extraordinary mechanical properties, due to the introduction of exfoliated clay platelets into the polymer networks [37].

What we are interested in is hybrid hydrogels with silica nanoparticles. As known, classical organic hydrogels present poor mechanical properties because of inhomogeneities in their structures and low dissipation of energy, which limit their applications. As an inorganic component, silica nanoparticles are incorporated in the polymer networks to reinforce the mechanical properties of hydrogels. This idea is inspired by Haraguchi group, but compared with clay platelets, silica nanoparticles can be spherical, preventing any anisotropic effect. Moreover, silica nanoparticles have some other advantages, presented as follows: their aqueous colloidal suspensions are stable; they are commercially available with various sizes; their surface can be easily functionalized, leading to a wide range of grafting or interactions with polymers.

Different from the reinforced networks prepared by polymerizing the monomer in aqueous solution of inorganic particles [37], Van Durme et al. developed hybrid networks by stirring the mixture of PNIPAM and silica nanoparticles in water, which exhibit a much faster thermal response thanks to the interactions between PNIPAM chains and silica particles [38]. On the basis of this, Petit et al. succeeded in creating hybrid hydrogels based on the assembly of silica nanoparticles and a graft copolymer designed with adsorbing grafts in aqueous media [39]. Adsorption isotherms and calorimetric studies showed that N-alkylacrylamide derivatives irreversibly interact with silica nanoparticles. So when PNIPAM was grafted onto a non-adsorbing and water-soluble poly(acrylamide-co-sodium acrylate) backbone, a binding process of the adsorbing side-chains was observed [39]. In addition, due to the thermo-responsive behavior of PNIPAM in water, the hybrid networks indicate responsive properties with a sol/gel transition upon heating. It is pointed out that both the amount of PNIPAM grafts between silica particles (acting as cross-linkers) and the concentration of silica particles have great influence on the viscoelastic properties of these physical networks [39].

Two different systems have been developed by Hourdet et al. on the basis of the elaboration of hybrid hydrogels. The first system is based on the hybrid hydrogels prepared by free radical polymerization of DMA in water in the presence of silica nanoparticles, without any chemical cross-linker. These hybrid gels present highly enhanced mechanical properties in terms of initial modulus, strain at failure and energy dissipation, thanks to the strong interactions between PDMA chains and silica particles. In fact, the silica particles perform as physical cross-linkers, and the cross-linking density can be tuned by varying the polymer concentration or the ratio between silica particles and polymer chains, which may induce changes in the mechanical behaviors correspondingly. However, a self-crosslinking phenomenon induced by transfer reactions has been observed in this system, which results in chemical cross-linking [40]. The second system is similar to the first one except that it contains a high concentration of chemical cross-linker (N,N'-methylenebisacrylamide, MBA), and it has been studied at swollen state [41]. Hybrid hydrogels developed with acrylamide (which does not adsorb on silica particles) have no specific reinforcement in their mechanical properties [42]. Based on the former work, Séverine et al. studied the time-dependent dissipative mechanisms and recovery process of hybrid hydrogel containing PDMA covalent network and silica nanoparticles [43]. Moreover, dynamic light scattering (DLS) was employed to investigate the dynamics of the network and the nanoparticles in PAAm/silica hybrid hydrogel and P(AAm-co-DMA)/silica hybrid hydrogel respectively [44, 45].

1.3. Stimuli-responsive hydrogels

1.3.1. Main characteristics

Thanks to their chemical diversity (coming from the composition) and the possibility to tune

their structures thus their properties, hydrogels have been employed to develop kinds of new materials. Polymer hydrogels with stimuli-responsive properties are interesting materials for a variety of different applications, due to their large volume change by absorption or expulsion of water upon receiving an external signal. The volumetric change is observed as a transition in the swelling degree of the gel in the solution, which may cause variation of many properties of the gel: permeability, elastic modulus, interfacial tension, adhesion, etc [46]. These smart hydrogels can respond to various stimuli such as pH, salt concentration, temperature, light, electric or magnetic field. A slight change in the environmental conditions may in turn generate great modifications of their macroscopic properties. The reversibility of the volume transition is an additional advantage for the applications of these hydrogels as responsive materials.

As a matter of fact, the sharp volume phase transition of hydrogels is the key point during the responsive process. There are three major mechanisms that are responsible for the stimuli-induced volume change: changes in osmotic pressure or charge density (e.g., pH-responsive hydrogels); changes in solvent affinity of the polymer chains (e.g., thermo-responsive hydrogels); changes in the cross-linking density of polymer chains [47]. The reversible volume phase transition is often referred as swelling-shrinking transition in literatures.

The responsiveness of hydrogels upon external stimuli in the form of changing their physical properties has been explored for numerous applications in various fields. For example, they can be employed as chemical valves to regulate flow or permeability [48], or for encapsulation and the triggered release of active substances in drug delivery systems [49-52], or as chemical sensors [53, 54] and actuators.

1.3.2. Different stimuli-responsive hydrogels

Volume phase transitions in stimuli-responsive hydrogels are induced via various physical and chemical stimuli. In fact, the responsiveness of hydrogels to changes in their surrounding environment is due to the natural properties of the polymer chains used to make the gels. Thus, by varying the cross-linked polymer chains which hold the initial responsive properties, we are able to develop hydrogels that can respond to different stimuli.

Stimuli-responsive polymers are smart polymers which can respond to external stimuli in the form of changing their own properties. Usually, slight changes in the environment are sufficient to induce significant changes in the structures and/or properties of these polymers. Actually, their responsive properties lie in their inherent nature. The response of each individual unit in the polymer chains to the stimuli is weak. However, these weak responses, when compounded hundreds or thousands of times, can create a considerable change in the

polymer's macroscopic properties. The essence underlying the stimuli-responsive behaviors of these smart polymers is their conformational and chemical changes on receiving an external signal. At the macromolecular level, polymer chains can be modified in various ways, including changes in conformation or solubility, alteration of the hydrophilic/hydrophobic balance, degradation and so on. And these modifications, in turn, will cause detectable behavioral changes of the polymer [55].

The presence of various stimuli-responsive polymers makes it possible to explore different stimuli-responsive hydrogels. In this study, we will focus on the following three kinds of hydrogels: thermo-responsive hydrogels, light-responsive hydrogels and electro-responsive hydrogels.

As one of the most widely studied smart materials, thermo-responsive hydrogels have attracted an increasing interest and been more and more studied in the past several years, because of the easy controllability of temperature and more importantly their promising applications in various fields [56]. Normally, thermo-responsive hydrogels are prepared from polymers which exhibit a critical solution temperature in water, around which the interactions between polymer chains and water vary between hydrophilic state and hydrophobic state dramatically within a small temperature range. Resulting from the expansion or contraction of polymer chains in water, thermo-responsive hydrogels indicate volume phase transition around the lower critical solution temperature (LCST) or upper critical solution temperature (UCST) depending on the polymers. For hydrogels made of polymers with LCST (e.g. poly(*N*-isopropylacrylamide), PNIPAM), when the temperature lowers below LCST, the gels swell due to the diffusion of water into the polymer networks, because water molecules form hydrogen-bonds with the polar groups on the polymer chains. However, the efficiency of the hydrogen-bonding decreases with the rise in temperature, and when the temperature is above LCST, the hydrophobic property of the polymer chains starts dominating, causing the hydrogels shrink. As a matter of fact, the LCST of thermo-responsive polymers (thus hydrogels) can be strongly altered by incorporating certain comonomers into the polymer chains [46, 57]. Moreover, Franck Ilmain et al. developed an interpenetrating networks (IPN) hydrogel composed of poly(acrylamide) (PAAm) and poly(acrylic acid) (PAAc) which showed a UCST in aqueous solution, due to the cooperative "zipping" interactions resulting from hydrogel bonding between molecules [2]. On the basis of this, Liang-Yin Chu et al. designed PAAm/PAAc-based IPN hydrogel membranes working as functional gates with reversible thermo-responsive permeation properties [48].

Light has become one of the most favorable stimuli thanks to the quick, easy and remote variation of its spatial, wavelength, and intensity parameters [58]. Taking advantage of this, researchers have developed different kinds of light-responsive hydrogels which are highly

advantageous for multiple applications. Actually, the light sensitivity of these smart hydrogels comes from the light-absorbing chromophores incorporated in the polymer chains, such as spirobenzopyran [59], azobenzene [60, 61], chlorophyllin [62]. Generally, upon the irradiation of light with certain wavelengths, these chromophores reveal changes in their properties, such as color, molecular polarity, molecular size and shape, or transform between ionic state and nonionic state. The variation of the merged chromophores in different forms induces macroscopic changes in the structures and thus the properties of the hydrogels, including adhesion, color, permeability, hydrophilicity, ionizability, etc. Base on this, light-responsive hydrogels have been employed to manage size-selective mass transport (electron, gas, inorganic and organic ions) [63], to trigger gel-to-sol and sol-to-gel phase transition [60], to realize swelling-shrinking transition [59], and to control cell adhesion [64]. In addition, spirobenzopyran and azobenzene groups render hydrogels reversible light-responsive property owing to the reversibility of their isomerization, which is of great use for their applications.

Electric field is used as an external stimulus due to the precise control of related parameters, like the magnitude of the current, the duration of an electrical pulse, and the interval between pulses [65]. Accordingly, electro-responsive hydrogels have been the hot point studied by numerous researchers since long time ago [66-69]. The responsive behavior of hydrogels to an external electric field depends on the cross-linked polymer chains. Typical polymers employed to make electro-responsive hydrogels are polyelectrolytes, including polycations and polyanions, whose repeating units bear an electrolyte group. Once polyelectrolytes are dissolved in water, these groups will dissociate, resulting in charged polymers and counterions. So in the solution of polyelectrolyte hydrogels, the applied electric field can create osmotic pressure gradients of free mobile ions which may induce the shrinking or swelling of the hydrogels [67, 69]**.** And normally the responsive property of electro-responsive hydrogels to electric field is reversible.

2. Polymer hydrogels at interfaces

2.1. Polymer assemblies at interfaces

Surfaces that provide specific properties (such as wettability, permeability, adhesive, adsorptive, and responsive properties) have drawn considerable attention in various research fields, including biomedicine, chemical engineering and so on. Correspondingly, different polymer assemblies at interfaces with dynamically modulated properties have been developed. We describe here the two most usual of them: layer-by-layer assemblies and polymer brushes.

2.1.1. Layer-by-layer assemblies

Layer-by-Layer (LbL) assembly is a fabrication technique of thin films. The films are prepared by depositing alternating layers of oppositely charged materials with wash steps in between. This technique was firstly implemented by R. K. Iler, who succeeded in obtaining multilayers of colloidal nanoparticles in 1960s [70]. Afterwards, it was revitalized by Gero Decher in 1990s, who extended its applicability from particles to a wide range of polyelectrolytes (PEs) [71-74]. Nowadays, layer-by-layer assembly has become a universal approach for the facile fabrication of multicomponent films on solid supports. It is important to note that during the preparation of LbL assemblies, apart from electrostatic attraction, some other interactions are involved in this process, including hydrophobic attraction [75]. Moreover, for water-soluble non-ionic polymers and some polyelectrolytes, hydrogen bonding can also be exploited to produce multilayer films based on LbL assembly [76-78]. In fact, besides polyelectrolytes, a wide variety of materials can be deposited by LbL, such as nanoparticles, colloids, and biological molecules, to form functionalized conformal nanostructured interfaces.

The LbL assembly technology has found widespread applications because of its simplicity and versatility for surface modification. In particular, polyelectrolyte multilayer films have attracted wide attention due to their pH-responsive properties. For example, PAH/PSS multilayer films showed pH-sensitive properties when assembled at a certain pH [79]. The mechanism of the pH-responsive swelling behavior exhibited by polyelectrolyte LbL films containing PAH was exhaustively studied by Rubner et al. [80]. It was found that the pH during assembly process played an important role in determining the swelling properties of the multilayer films, including swelling ratio, surface roughness and refractive index [80]. However, besides pH, some other stimuli have been exploited to trigger response of LbL films. For instance, based on hydrogen-bonding interactions, neutral thermo-responsive PVME was introduced to produce multilayer thin films with PMAA using layer-by-layer assembly method, which showed temperature-responsive properties when deposited onto porous support membranes [78].

In addition to its simplicity and versatility, the main advantages of LbL assembly lie in that it is possible to control the structure and chemical composition of the film, and that it is adaptable on substrates of any shape and in confined environments [46]. Furthermore, it allows the fine control over the dry thickness of the multilayer film, which arises according to the linear growth with the number of layers. So if a single layer can be as thin as 1 nm, this method offers an easy control over the thickness with 1 nm resolution. Also the process of LbL assembly is not complicated and can be carried out easily. However, in some conditions, LbL films may become unstable due to large swelling force, dissociation of ionic bonds, etc.,

leading to decomposition of films, film detachment from the substrate, or phase separation [81, 82]. In order to ensure their stability, the films can be prepared by forming internally crosslinked polymer networks which are chemically grafted to the substrate. For instance, PAH and PAA chains were firstly functionalized with photoreactive groups (benzophenone) separately, which enabled the crosslinking of multilayer polymer chains with UV light after LbL assembly [83]. Moreover, PAH/PAA LbL multilayer films could also be crosslinked via a heat-induced amidation reaction [84].

2.1.2. Polymer brushes

Polymer brush refers to a monolayer of polymer chains which are grafted by one end onto a surface or an interface. The grafting density is so high that the polymer chains are crowded and forced to stretch away from the surface or interface to avoid overlapping, exhibiting a stretched conformation [85]. Actually, the behavior of polymer brushes is dominated by the combination of strong entropic repulsion between polymer chains, entropic stretching costs and frozen constraints due to the irreversible grafting [86]**.** Generally, there are two ways to prepare polymer brushes: physisorption and covalent attachment, while the covalent attachment can be achieved by either "grafting to" or "grafting from" approaches. The "grafting from" method is preferable because it allows high grafting density, and the control over the length of polymer chains and thus the brush thickness, thanks to *in situ* surface-initiated polymerization, usually surface radical polymerization such as RAFT or ATRP [87-89]. However, it was shown that the "grafting to" method allows the formation of brushes with various types of polymers and on a wide range of grafting densities. "Grafting to" technique has also the advantage of the simplicity since it does not require sophisticated chemistry [90].

Polymer brushes have been employed to stabilize colloids, reduce friction between surfaces, and to provide lubrication in artificial joints in various fields. Recent years, "smart" polymer brushes, which can respond to external stimuli reversibly, have drawn great attention, because they make it possible to fabricate adaptive and responsive surfaces and interfaces. Several examples of actuation and transduction based on polymer brushes have already been explored [91]. In particular, Jinghong Li et al. developed switchable PNIPAM, PAA and P(NIPAM-co-AA) brush interfaces which were able to reversibly respond to temperature, ionic strength and pH, independently or simultaneously [92]. Polymer brushes can be generated on planar and curved surfaces, which is a very useful advantage. Moreover, a wide range of possible chemical functionalities can be introduced into polymer brushes by controlling their chemical composition [91].

Some significant publications of Yim et al. dealt with thermo-responsive properties of PNIPAM brushes [93-96]. These brushes were synthesized on gold and silicon by a "grafting from" method using ATRP. The temperature-dependence of chains conformation was

studied by neutron reflectivity. Other studies of the temperature transition of PNIPAM brushes were carried out by Surface Plasmon Resonance [97], Quartz Crystal Microbalance [98] or a combination of AFM and QCM or also by contact angle of air-bubble underneath PNIPAM grafted membranes in water. The temperature transition was also characterized by surface force measurements for PNIPAM brushes synthesized by surface-initiated ATRP [99, 100] and brushes obtained by Langmuir-Blodgett deposition [101]. Although various studies have been reported on the synthesis of PNIPAM brushes and their conformational changes with temperature, only a few experimental works were devoted to the adsorption properties of brushes in the presence of added macromolecules or colloïds. The ability of grafted PNIPAM chains to trap, store and deliver microparticles was described by Chen et al. [102] Liu et al. [103] quantified the reversibility of the adsorption: they found that only 30 % of polystyrene particles adsorbed on PNIPAM brushes were released. The adsorption of bovine serum albumin (BSA) was investigated by Xue et al. by ellipsometry [104]. Burkert et al. [105] studied the adsorption of BSA on poly(2-vinyl pyridine) and PNIPAM mixed brushes using the combination of ellipsometry and ATR-IR spectroscopy.

2.2. Hydrogel thin films: advantage of hydrogels and films

Recent advances in nanotechnology have led to increased interest in hydrogel thin films, as they can be rendered multifunctional and multiresponsive. The hydrogel thin films are very promising since they associate both advantages of hydrogel and films.

On the one hand, hydrogel thin films are attractive as an approach to responsive surfaces and interfaces, where the hydrogel architecture offers much potential in competition with layer-by-layer (LbL) assemblies and grafted polymer layers.

On the other hand, the decrease of the feature size in thin films is an appropriate way to create structures with fast response. Actually, the swelling/collapse phase transition of hydrogels is a diffusion-limited process and so bulk hydrogels often result in long response time (minutes to hours), which is too slow for many applications. For this purpose, one straightforward way is to downside the hydrogel structures by using thin films. This approach allows the development of devices with fast responses while maintaining their mechanical robustness.

To our best knowledge, hydrogel thin films are scarcely investigated despite their huge potential. In the following, we report the few works dedicated to the synthesis and the swelling of hydrogel thin films. We also describe the scaling laws for the swelling by detailing the Flory-Rehner theory extended to one dimension.

2.2.1. Synthesis methods of hydrogel thin films

Thin films of chemically cross-linked hydrogels are usually prepared by the following two methods:

i. cross-linking copolymerization by mixing monomers and multifunctional comonomers;
ii. cross-linking functionalized (co)polymers with reactive groups or with high-energy irradiation.

In the first approach, copolymerization and cross-linking take place simultaneously. Solvent-based free radical polymerization techniques are widely employed. The reaction mixture containing monomers, the cross-linker and the initiator is confined between two planar substrates (one is functionalized to attach the hydrogel film and the other is non-sticky to detach the film) separated by spacers, and then is polymerized and cross-linked in situ [106]. Among all the free radical polymerization techniques, UV-initiated polymerization has drawn great attention because it realizes micro-patterning of hydrogel films by using a projection mask [106-109]. However, this technique may have its limits for thick hydrogel films due to the volume absorption of the UV beam. Plasma polymerization is another attractive deposition technique used to fabricate highly cross-linked hydrogel thin films (typical thickness ranging from tens to hundreds of nanometers), thanks to its advantageous features, like one-step, solvent-free and vapor-phase. Here crosslinkers are not needed because cross-linking results from the ion or electron bombardment of the material during deposition [110-113]. And the dry thickness of the hydrogel film can be conveniently controlled by varying the polymerization time and plasma power.

In the second approach, crosslinking of polymer chains in dry state is carried out after coating a thin film of functionalized (co)polymers to obtain hydrogel. So far, various techniques for coating have been developed, like spin-coating, dip-coating, spray-coating, etc. As for crosslinking, different techniques are available according to the chemical composition of the polymer. For example, after spin-coating, thin layers of mixed PVA/PAA chains are dried and then thermally crosslinked at 130°C via esterification reaction to produce pH-responsive hydrogel thin films [114, 115].

While for copolymers that contain photo-reactive pendent groups or monomers, their crosslinking can be achieved either by the addition of photoinitiators [116] or by UV irradiation [47, 117-121]. The crosslinking technique based on UV irradiation is broadly used, because it is compatible with photolithography and allows the preparation of hydrogel films with a wide range of dry thickness (from nanometres to tens of microns) [122, 123]. As a matter of fact, high-energy irradiation (e.g., electron beam, γ-rays, UV-light) on polymer chains induces random chain scission resulting in free-radicals, which are then recombinated,

leading to the formation of a crosslinked polymer network [46]. The crosslinking density is supposedly decided by the ratio of crosslinkers and/or the irradiation dose.

2.2.2. Swelling of hydrogel thin films

The swelling of isotropic bulk hydrogels is uniform in all directions. In contrast, the swelling of surface-attached hydrogel thin films is highly anisotropic. In fact, their in-plane (lateral) swelling is restricted by the chemical attachment of the polymer networks to the surface, and their volumetric expansion is available only in the direction normal to the substrate plane [124]. Thus, the swelling behavior of the hydrogel thin films is strongly influenced by the surface confinement.

It has been observed that the surface-attached polymer networks swell much less than the non-attached bulk networks of the same cross-link density. For example, bulk PNIPAM gels showed a total volume change of 100-fold compared to the 15-fold change for the 4 microns-thick surface-attached PNIPAM gel films [106]. However, the swelling of the surface-attached polymer networks is larger than that suggested by simple geometric considerations for swelling in one dimension. In particular, the results found with surface-attached poly(dimethylacrylamide) gel films are in good qualitative agreement with the Flory-Rehner theory [125] extended to one-dimension swelling [124].

Moreover, the transition temperature of the surface-attached PNIPAM gel films was found to be affected: it started to decrease above some critical film thickness. The constraints of the fixed substrate also limited the collapse of the hydrogel thin films at temperatures above the transition temperature [106, 126-129]. So far, only thermo-sensitive hydrogel films using PNIPAM were investigated, there is no study on the responsiveness such as UV-light or electric field.

The surface confinement has also an effect on the surface topography of the hydrogel thin films apart from their swelling properties. Actually, the strong osmotic force in the lateral dimension can induce a mechanical stress which may cause the delamination of the hydrogel films from the substrate [130, 131] and the wrinkling of the free surface of the gel films. In particular, the wrinkling was observed in 100 mm-thick gel films [132] and 150 nm-thick gel membranes [133, 134].

2.2.3. Flory-Rehner theory extended to one-dimension

The extension of Flory-Rehner theory for the swelling of hydrogels to one dimension is described in the following. It is extracted from Toomey et al. [124].

1. Simple geometric considerations

For surface-attached gel films, the volumetric swelling ratio S_F is the ratio of the volume fraction of polymer in air Φ_a to the volume fraction of polymer in water Φ_w. If attached networks swell only perpendicularly to the surface with no swelling parallel to the surface, then the linear swelling ratio and the volumetric swelling ratio is the same, in other words:

$$S_F = \frac{\Phi_a}{\Phi_w} = \frac{h_w}{h_a} \qquad [\mathbf{eq.\ 1}]$$

For bulk polymer gels, the swelling ratio S_V can be defined as the ratio of the mass of the polymer gel in the equilibrium swollen state to the mass of the polymer gel in dry state. Assuming the density of the polymer network is close to 1, S_V is also the ratio of volume fractions like in equation 1.

If the swelling of bulk hydrogels is presumed to be isotropic, the swelling ratio is equal in the three dimensions. Therefore, from simple geometric considerations, it may be expected that the swelling ratios are linked by:

$$S_F = S_v^{1/3}$$

2. Extension of Flory-Rehner theory to one dimension

However, the swelling of surface-attached polymer networks is experimentally larger than what is suggested through simple geometric considerations for swelling in one dimension. It is consistently observed that the linear swelling ratio of the surface-attached networks exceeds the linear swelling ratio of the bulk networks.

This observation is consistent by considering a simple phenomenological model based on a Flory-Rehner expression for the free energy. Upon immersion in a good solvent, the equilibrium structure of a polymer network is subject only to two opposing forces: the thermodynamic force of mixing, which favors swelling, and the elastic retractile force of the network, which opposes swelling. The free energy of the system can be written as

$$\Delta G = \Delta G_{mix} + \Delta G_{elastic}$$

The mixing free energy is

$$\frac{\Delta G_{mix}}{kT} = n_1 \ln(1 - \Phi) + \chi n_1 \Phi$$

where k is the Boltzmann constant, T is the absolute temperature, n_1 is the number of solvent molecules, Φ is the polymer fraction in the swollen gel, and χ is the Flory polymer-solvent interaction parameter. The expression for the elastic free energy is

$$\frac{\Delta G_{elastic}}{kT} = v\left(\frac{d}{2}\right)[\alpha^2 - 1 - ln\alpha]$$

where v is the number of cross-links in the network and d is the number of dimensions in which the network can swell. Noting that the polymer volume fraction Φ in the swollen network is related to its linear deformation α through

$$\Phi = \frac{\Phi_0}{\alpha^d}$$

Minimization of the free energy ΔG of the swollen network yields the following relationship between the equilibrium linear deformation of the gel α and the degrees of freedom in which the network can swell:

$$\alpha \approx [\frac{1}{(1/2 - \chi)\Phi_0 N_c}]^{-1/(d+2)}$$

As swelling is confined to fewer dimensions, α shows a stronger dependence on the cross-linking density $1/N_c$, where N_c is the number of segments between cross-linking points. Since the volumetric swelling degree $S = \alpha^d$, the scaling laws of both S and α can be determined for three-dimensional and one-dimensional swelling in a good solvent:

$$\alpha_V \approx [\frac{1}{\Phi_0 N_c}]^{-1/5} \quad S_V \approx [\frac{1}{\Phi_0 N_c}]^{-3/5} \qquad [\mathbf{eq.2}]$$

and

$$\alpha_F \approx [\frac{1}{\Phi_0 N_c}]^{-1/3} \quad S_F \approx [\frac{1}{\Phi_0 N_c}]^{-1/3} \qquad [\mathbf{eq.3}]$$

Equations 2 and 3 predict that the volumetric degree of swelling in the surface-attached network should be approximately the square root of the degree of swelling in the unconstrained network:

$$S_F = {S_V}^{5/9}$$

3. Objectives of the thesis

The hydrogel films we are interested in are chemical polymer networks that are covalently grafted to the surface. One of our objectives is to obtain surface-attached hydrogel films with a wide range of thicknesses and with the desired responsiveness nature. Which simple and versatile strategy for the synthesis hydrogel films? Which responsive properties for the hydrogel films? What is the effect of confinement and constraints on the lateral swelling of hydrogel films? How to develop new hydrogel films with complex architectures inspired from macroscopic hydrogels?

3.1. A simple and versatile strategy

We have developed a very simple and versatile strategy which allows easily the adjustment of chemical properties (e.g. responsiveness) and physical properties (e.g. size and structure) of the films. The strategy chosen to synthesize chemically cross-linked hydrogels consists in cross-linking preformed and functionalized polymers in preference to polymerizing and cross-linking monomers. This method is preferred as it allows a better control of the synthesis. Actually, the radical polymerization should be performed with caution and in particular with controlled atmosphere to avoid from oxygen. A lack of caution would have disastrous consequences on the formation of the hydrogel thin films much more than for macroscopic hydrogels. Also, we adopted the strategy of cross-linking reactive polymer chains through click chemistry which takes place efficiently without caution of controlled atmosphere and without addition of any initiator.

The click chemistry selected is based on thiol-ene chemistry. The surface-attached hydrogel films are obtained by coating ene-functionalized polymers in the presence of dithiol molecules as cross-linkers on thiol-modified substrate. The thiol-ene reaction allows both the chemical cross-linking of the polymer chains and their covalent attachment to the surface. The thiol-ene reaction is performed under air atmosphere and can be activated without initiator by temperature or UV-irradiation (at 250 nm). In addition to the convenience of the activation, the use of thiol function is also judicious for surface modification: glass and silicon substrates can be usually functionalized with thiol and gold surfaces can be even more easily thiol-modified with dithiol molecules. In addition, dithiol molecules used for the cross-linking (and gold surface modification) can be widely purchased.

The range of thickness targeted in this present study goes from nanometer to microns, which allows the characterization by usual reflectivity techniques such as ellipsometry or neutron reflectivity. The coating method suitable for this range of thickness is the spin-coating which has the additional advantage to use a little polymer to obtain a film of polymer in the melt state.

The response of the hydrogel films to external stimuli results from the polymer chains used for cross-linking. So, different polymers are chosen according to their specific responsiveness properties. Most synthesis process of ene-functionalized polymers is carried out in water, which is another advantage of the thiol-ene strategy. The ene-functionalized polymers are obtained after two steps: the copolymerization of acrylic acid and monomers with responsive properties and the ene-functionalization of the copolymers with simple peptide reaction using allylamine. The copolymerization can be performed by free radical technique because there is no need to obtain polymer chains with low polydispersity. The free radical polymerization is much less binding than controlled radical techniques for example since

extreme purification is not required. In fact, the purification of polymers is performed with the dialysis of synthesized polymers against water.

3.2. Which responsive properties?

We synthesize hydrogel films which can response to three different stimuli: temperature, light and electric field.

The thermo-sensitive hydrogel films are obtained using PNIPAM for its LCST properties. Both steps of the synthesis, copolymeration of these acrylamide-like monomers and acrylic acid and ene-functionalization, can be performed in water.

The light-responsive properties of the hydrogel films are achieved with the addition of azobenzene UV-activated groups on the PNIPAM chains. The UV-irradiation induces the change of trans-conformation to cis-conformation which renders the polymer more hydrophilic, resulting in the shift of the LCST to higher temperature, even with a small ratio of azobenzene in the hydrogel.

The response to electric field is achieved using polyelectrolyte hydrogels. With the electric field applied on the hydrogel film, the change of the osmotic pressure due to the moving of the counterions from inside to outside of the hydrogel should induce the swelling to collapse phase transition of the hydrogel film. Weak polyelectrolyte such as PAA hydrogels used at high pH for a complete ionization and strong polyelectrolyte such as PAMPS are suitable. Ene-functionalized PAMPS chains can be synthesis in water like ene-functionalized PNIPAM. For PAA chains, they are even more easily to obtain since the ene-functionalization can be performed directly with (commercial) PAA homopolymers.

Why the choice of these stimuli? The electric field and the light stimuli are easy to control. They have also the advantages of rapid and local activation which is very helpful for applications such as the function of hydrogel-based microvalves in microfluidic devices. The microfluidic geometry renders the possibility to show for the first time the sensitivity of polymer *films* to electric field. Actually, the electric field that should be applied to achieve the phase transition of polymer films is very high. For example, a field of 30 kV/m is required for the swelling-collapse transition of a micrometric polyelectrolyte hydrogel film. However, though a high value of electric field, the voltage applied is accessible since it less than 1 V for micrometric channels.

Moreover, the hydrogel films can response to electric field at any work temperature, ambient temperature for example. While for photo-responsive hydrogel films, the transition can be observed for temperature close to the LCST, exactly between the shifted and no-shifted LCST.

Though the temperature is not a local stimulus, it is very convenient because it can be easily varied on a wide range. In addition, as the LCST of PNIPAM is around 32°C, the phase transition can be comfortably investigated. As the temperature is easy to control as external stimulus, we always use hydrogel films containing PNIPAM networks to study the phase transition of model networks films.

3.3. Effect of confinement and constraints on the lateral swelling

We investigate the structure of these stimuli-responsive hydrogel films to make clear the effects of confinement and lateral constraints on their responsive behaviors. Actually, the swelling of hydrogels in the confinement state such as films is likely rather anisotropic than isotropic as for macroscopic hydrogels. The constraint on lateral swelling due to the covalent attachment of the hydrogel film on the solid substrate may induce a mechanical stress which causes the deformation of the free surface of the hydrogel film. Taking thermo-responsive hydrogel films as an example, we try to tackle these fundamental aspects: what is the effect of the confinement on the swelling of the gel films? How does the surface-attachment affect the free surface of the gel films?

Correspondingly, systematic studies have been carried out with three different and complementary techniques: ellipsometry, neutron reflectivity and atomic force microscopy. Ellipsometry has been employed to determine the swelling ratio of the hydrogel films in the direction normal to the substrate. Neutron reflectivity experiments have been performed for defining the interface width on the free surface side of the hydrogel films. The density profile of the gel films obtained from neutron reflectivity is coupled with a topographic (in-plane) description of the free surface, resulting from AFM experiments.

As explained above, a few studies have been performed on the phase transition of thermo-responsive PNIPAM films. But there was no interest in the effect of the confinement and lateral constraints through the study of hydrogel films with a wide range of thickness. In addition, there was a lack of combination of in-plane studies of the free surface of the hydrogels and studies in the direction normal to the surface. Using the three complementary characterizations, we attempt to answer the following questions. How is the scale affected by the surface attachment and the film geometry? How is the deformation of the free surface of the hydrogel?

3.4. Development of new hydrogel films with complex architectures

Last but not least, in order to achieve multifunctional hydrogel films and to improve their mechanical properties, we have exploited new and complex hydrogel films by targeting the architecture of the polymer networks. Thanks to the versatility of our hydrogel systems, we

aim to elaborate various architectures such as multilayer hydrogel films through layer-by-layer assembly, interpenetrating networks (IPN) hydrogel films and hybrid hydrogel films containing silica nanoparticles.

Multilayer hydrogel films are very promising as a simple way to achieve multifunctional films with long-term stability. For example, they can be rendered the responsive properties to various stimuli. They hopefully are as versatile as layer-by-layer assemblies. The alternative architecture to bilayers hydrogel films is the interpenetrating networks for which both have cross-linked structures but are not joined together. The properties of each network can be interestingly maintained within the interpenetrating networks. The IPN architecture can be exploited to develop double networks (DN) hydrogel films, which are expected to be mechanically strengthened by analogy with macroscopic DN hydrogels. Meanwhile, silica-polymer hybrid hydrogel films are also supposed to have their mechanical behaviors reinforced similarly to macroscopic hybrid hydrogels.

The structure and swelling properties of these complex systems are investigated by the three techniques as for single-network (SN) hydrogel films, and then comparisons are made among them.

References

1. Rubinstein, M. and A.V. Dobrynin, *Associations leading to formation of reversible networks and gels.* Current Opinion in Colloid & Interface Science, 1999. **4**(1): p. 83-87.
2. Ilmain, F., T. Tanaka, and E. Kokufuta, *Volume transition in a gel driven by hydrogen bonding.* Nature, 1991. **349**(6308): p. 400-401.
3. Skouri, R., et al., *Swelling and Elastic Properties of Polyelectrolyte Gels.* Macromolecules, 1995. **28**(1): p. 197-210.
4. Karakasyan, C., et al., *Cold Gelation of Alginates Induced by Monovalent Cations.* Biomacromolecules, 2010. **11**(11): p. 2966-2975.
5. Tuncaboylu, D.C., et al., *Tough and Self-Healing Hydrogels Formed via Hydrophobic Interactions.* Macromolecules, 2011. **44**(12): p. 4997-5005.
6. Miquelard-Garnier, G., C. Creton, and D. Hourdet, *Synthesis and Viscoelastic Properties of Hydrophobically Modified Hydrogels.* Macromolecular Symposia, 2007. **256**(1): p. 189-194.
7. Buenger, D., F. Topuz, and J. Groll, *Hydrogels in sensing applications.* Progress in Polymer Science, 2012. **37**(12): p. 1678-1719.
8. Peppas, N.A., *Hydrogels in medicine and pharmacy*. 1986, Boca Raton, FL: CRC Press.
9. Mirejovsky, D., A.S. Patel, and G. Young, *Water properties of hydrogel contact lens materials: a possible predictive model for corneal desiccation staining.* Biomaterials, 1993. **14**(14): p. 1080-1088.
10. Buchholz, F.L. and A.T. Graham, *Modern superabsorbent polymer technology.* Wiley-VCH, 1998.
11. Lee, K.Y. and D.J. Mooney, *Hydrogels for Tissue Engineering.* Chemical Reviews, 2001. **101**(7): p. 1869-1880.
12. Balakrishnan, B. and R. Banerjee, *Biopolymer-Based Hydrogels for Cartilage Tissue Engineering.* Chemical Reviews, 2011. **111**(8): p. 4453-4474.
13. Lee, K.Y. and D.J. Mooney, *Alginate: Properties and biomedical applications.* Progress in Polymer Science, 2012. **37**(1): p. 106-126.
14. Rudzinski, W., et al., *Hydrogels as controlled release devices in agriculture.* Designed monomers and polymers, 2002. **5**(1): p. 39-65.
15. Richtering, W. and B.R. Saunders, *Gel architectures and their complexity.* Soft Matter, 2014. **10**(21): p. 3695-3702.
16. Lee, W.-F. and Y.-J. Chen, *Studies on preparation and swelling properties of the N-isopropylacrylamide/chitosan semi-IPN and IPN hydrogels.* Journal of Applied Polymer Science, 2001. **82**(10): p. 2487-2496.

17. Aoki, T., et al., *Temperature-Responsive Interpenetrating Polymer Networks Constructed with Poly(acrylic acid) and Poly(N,N-dimethylacrylamide).* Macromolecules, 1994. **27**(4): p. 947-952.
18. Muniz, E.C. and G. Geuskens, *Compressive Elastic Modulus of Polyacrylamide Hydrogels and Semi-IPNs with Poly(N-isopropylacrylamide).* Macromolecules, 2001. **34**(13): p. 4480-4484.
19. Zhang, J. and N.A. Peppas, *Synthesis and Characterization of pH- and Temperature-Sensitive Poly(methacrylic acid)/Poly(N-isopropylacrylamide) Interpenetrating Polymeric Networks.* Macromolecules, 1999. **33**(1): p. 102-107.
20. Gong, J.P., et al., *Double-Network Hydrogels with Extremely High Mechanical Strength.* Advanced Materials, 2003. **15**(14): p. 1155-1158.
21. Gong, J.P., *Why are double network hydrogels so tough?* Soft Matter, 2010. **6**(12): p. 2583-2590.
22. Haque, M.A., T. Kurokawa, and J.P. Gong, *Super tough double network hydrogels and their application as biomaterials.* Polymer, 2012. **53**(9): p. 1805-1822.
23. Na, Y.-H., et al., *Structural Characteristics of Double Network Gels with Extremely High Mechanical Strength.* Macromolecules, 2004. **37**(14): p. 5370-5374.
24. Na, Y.-H., et al., *Necking Phenomenon of Double-Network Gels.* Macromolecules, 2006. **39**(14): p. 4641-4645.
25. Tanaka, Y., et al., *Determination of Fracture Energy of High Strength Double Network Hydrogels.* The Journal of Physical Chemistry B, 2005. **109**(23): p. 11559-11562.
26. Webber, R.E., et al., *Large Strain Hysteresis and Mullins Effect of Tough Double-Network Hydrogels.* Macromolecules, 2007. **40**(8): p. 2919-2927.
27. Nakayama, A., et al., *High mechanical strength double-network hydrogel with bacterial cellulose.* Advanced Functional Materials, 2004. **14**(11): p. 1124-1128.
28. Wang, X., H. Wang, and H.R. Brown, *Jellyfish gel and its hybrid hydrogels with high mechanical strength.* Soft Matter, 2011. **7**(1): p. 211-219.
29. Sun, J.-Y., et al., *Highly stretchable and tough hydrogels.* Nature, 2012. **489**(7414): p. 133-136.
30. Yasuda, K., et al., *Biomechanical properties of high-toughness double network hydrogels.* Biomaterials, 2005. **26**(21): p. 4468-4475.
31. Azuma, C., et al., *Biodegradation of high-toughness double network hydrogels as potential materials for artificial cartilage.* Journal of Biomedical Materials Research Part A, 2007. **81**(2): p. 373-380.
32. Yasuda, K., et al., *A Novel Double-Network Hydrogel Induces Spontaneous Articular Cartilage Regeneration in vivo in a Large Osteochondral Defect.* Macromolecular bioscience, 2009. **9**(4): p. 307-316.

33. Kitamura, N., et al., *Induction of Spontaneous Hyaline Cartilage Regeneration Using a Double-Network Gel Efficacy of a Novel Therapeutic Strategy for an Articular Cartilage Defect.* The American journal of sports medicine, 2011. **39**(6): p. 1160-1169.
34. Myung, D., et al., *Glucose-permeable interpenetrating polymer network hydrogels for corneal implant applications: A pilot study.* Current eye research, 2008. **33**(1): p. 29-43.
35. Tokarev, I., I. Tokareva, and S. Minko, *Gold-Nanoparticle-Enhanced Plasmonic Effects in a Responsive Polymer Gel.* Advanced Materials, 2008. **20**(14): p. 2730-2734.
36. Rama Rao, G.V. and G.P. López, *Encapsulation of Poly(N-Isopropyl Acrylamide) in Silica: A Stimuli-Responsive Porous Hybrid Material That Incorporates Molecular Nano-Valves.* Advanced Materials, 2000. **12**(22): p. 1692-1695.
37. Haraguchi, K., T. Takehisa, and S. Fan, *Effects of Clay Content on the Properties of Nanocomposite Hydrogels Composed of Poly(N-isopropylacrylamide) and Clay.* Macromolecules, 2002. **35**(27): p. 10162-10171.
38. Durme, K.V., et al., *Introduction of silica into thermo-responsive poly(N-isopropyl acrylamide) hydrogels: A novel approach to improve response rates.* Polymer, 2005. **46**(23): p. 9851-9862.
39. Petit, L., et al., *Responsive Hybrid Self-Assemblies in Aqueous Media†.* Langmuir, 2006. **23**(1): p. 147-158.
40. Carlsson, L., et al., *Nano-hybrid self-crosslinked PDMA/silica hydrogels.* Soft Matter, 2010. **6**(15): p. 3619-3631.
41. Lin, W.-C., et al., *Large Strain and Fracture Properties of Poly(dimethylacrylamide)/Silica Hybrid Hydrogels.* Macromolecules, 2010. **43**(5): p. 2554-2563.
42. Lin, W.-C., et al., *Effect of polymer-particle interaction on the fracture toughness of silica filled hydrogels.* Soft Matter, 2011. **7**(14): p. 6578-6582.
43. Rose, S., et al., *Time Dependence of Dissipative and Recovery Processes in Nanohybrid Hydrogels.* Macromolecules, 2013. **46**(10): p. 4095-4104.
44. Rose, S., et al., *Dynamics of Hybrid Polyacrylamide Hydrogels Containing Silica Nanoparticles Studied by Dynamic Light Scattering.* Macromolecules, 2013. **46**(11): p. 4567-4574.
45. Rose, S., et al., *Dynamics of Hybrid Poly(acrylamide-co-N,N-dimethylacrylamide) Hydrogels Containing Silica Nanoparticles Studied by Dynamic Light Scattering.* Macromolecules, 2013. **46**(13): p. 5329-5336.
46. Tokarev, I. and S. Minko, *Stimuli-responsive hydrogel thin films.* Soft Matter, 2009. **5**(3): p. 511-524.
47. Kuckling, D., *Responsive hydrogel layers—from synthesis to applications.* Colloid and Polymer Science, 2009. **287**(8): p. 881-891.

48. Chu, L.-Y., et al., *Negatively Thermoresponsive Membranes with Functional Gates Driven by Zipper-Type Hydrogen-Bonding Interactions.* Angewandte Chemie International Edition, 2005. **44**(14): p. 2124-2127.
49. Hoare, T.R. and D.S. Kohane, *Hydrogels in drug delivery: progress and challenges.* Polymer, 2008. **49**(8): p. 1993-2007.
50. Oh, J.K., et al., *The development of microgels/nanogels for drug delivery applications.* Progress in Polymer Science, 2008. **33**(4): p. 448-477.
51. Qiu, Y. and K. Park, *Environment-sensitive hydrogels for drug delivery.* Advanced drug delivery reviews, 2001. **53**(3): p. 321-339.
52. Ankareddi, I. and C.S. Brazel, *Synthesis and characterization of grafted thermosensitive hydrogels for heating activated controlled release.* International journal of pharmaceutics, 2007. **336**(2): p. 241-247.
53. Jiang, C., et al., *Freely suspended nanocomposite membranes as highly sensitive sensors.* Nat Mater, 2004. **3**(10): p. 721-728.
54. Dong, L., et al., *Adaptive liquid microlenses activated by stimuli-responsive hydrogels.* Nature, 2006. **442**(7102): p. 551-554.
55. Schmaljohann, D., *Thermo- and pH-responsive polymers in drug delivery.* Advanced Drug Delivery Reviews, 2006. **58**(15): p. 1655-1670.
56. Zhang, L., T. Xu, and Z. Lin, *Controlled release of ionic drug through the positively charged temperature-responsive membranes.* Journal of Membrane Science, 2006. **281**(1–2): p. 491-499.
57. Pareek, P., H.-J. Adler, and D. Kuckling, *Tuning the Swelling Behavior of Chemisorbed Thin PNIPAAm Hydrogel Layers by N,N-Dimethyl Acrylamide Content*, in *Characterization of Polymer Surfaces and Thin Films*, K. Grundke, M. Stamm, and H.-J. Adler, Editors. 2006, Springer Berlin Heidelberg. p. 145-151.
58. White, E.M., et al., *Advances in smart materials: Stimuli-responsive hydrogel thin films.* Journal of Polymer Science Part B: Polymer Physics, 2013. **51**(14): p. 1084-1099.
59. Szilágyi, A., et al., *Rewritable Microrelief Formation on Photoresponsive Hydrogel Layers.* Chemistry of Materials, 2007. **19**(11): p. 2730-2732.
60. Zhao, Y.-L. and J.F. Stoddart, *Azobenzene-Based Light-Responsive Hydrogel System†.* Langmuir, 2009. **25**(15): p. 8442-8446.
61. Friedrich, T., et al., *Photoisomerizable and Thermoresponsive N-isopropylacrylamide–Surfmer Copolymer Hydrogels Prepared upon Electrostatic Self-Assembly of an Azobenzene Bolaamphiphile.* Macromolecular Rapid Communications, 2013. **34**(5): p. 393-398.
62. Suzuki, A. and T. Tanaka, *Phase transition in polymer gels induced by visible light.* Nature, 1990. **346**(6282): p. 345-347.

63. Kumar, S.K. and J.-D. Hong, *Photoresponsive Ion Gating Function of an Azobenzene Polyelectrolyte Multilayer Spin-Self-Assembled on a Nanoporous Support.* Langmuir, 2008. **24**(8): p. 4190-4193.
64. Edahiro, J.-i., et al., *In Situ Control of Cell Adhesion Using Photoresponsive Culture Surface.* Biomacromolecules, 2005. **6**(2): p. 970-974.
65. Cabane, E., et al., *Stimuli-Responsive Polymers and Their Applications in Nanomedicine.* Biointerphases, 2012. **7**(1-4): p. 1-27.
66. TANAKA, T., et al., *Collapse of Gels in an Electric Field.* Science, 1982. **218**(4571): p. 467-469.
67. Osada, Y., H. Okuzaki, and H. Hori, *A polymer gel with electrically driven motility.* Nature, 1992. **355**(6357): p. 242-244.
68. Gong, J.P., T. Nitta, and Y. Osada, *Electrokinetic Modeling of the Contractile Phenomena of Polyelectrolyte Gels. One-Dimensional Capillary Model.* The Journal of Physical Chemistry, 1994. **98**(38): p. 9583-9587.
69. Morales, D., et al., *Electro-actuated hydrogel walkers with dual responsive legs.* Soft Matter, 2014. **10**(9): p. 1337-1348.
70. Iler, R.K., *Multilayers of colloidal particles.* Journal of Colloid and Interface Science, 1966. **21**(6): p. 569-594.
71. Decher, G. and J.-D. Hong, *Buildup of ultrathin multilayer films by a self-assembly process, 1 consecutive adsorption of anionic and cationic bipolar amphiphiles on charged surfaces.* Makromolekulare Chemie. Macromolecular Symposia, 1991. **46**(1): p. 321-327.
72. Decher, G. and J.D. Hong, *Buildup of Ultrathin Multilayer Films by a Self-Assembly Process: II. Consecutive Adsorption of Anionic and Cationic Bipolar Amphiphiles and Polyelectrolytes on Charged Surfaces.* Berichte der Bunsengesellschaft für physikalische Chemie, 1991. **95**(11): p. 1430-1434.
73. Decher, G., J.D. Hong, and J. Schmitt, *Buildup of ultrathin multilayer films by a self-assembly process: III. Consecutively alternating adsorption of anionic and cationic polyelectrolytes on charged surfaces.* Thin Solid Films, 1992. **210–211, Part 2**(0): p. 831-835.
74. Decher, G., *Fuzzy Nanoassemblies: Toward Layered Polymeric Multicomposites.* Science, 1997. **277**(5330): p. 1232-1237.
75. Kotov, N.A., *Layer-by-layer self-assembly: The contribution of hydrophobic interactions.* Nanostructured Materials, 1999. **12**(5–8): p. 789-796.
76. Quinn, J.F. and F. Caruso, *Facile Tailoring of Film Morphology and Release Properties Using Layer-by-Layer Assembly of Thermoresponsive Materials.* Langmuir, 2003. **20**(1): p. 20-22.

77. Quinn, J.F., et al., *Next generation, sequentially assembled ultrathin films: beyond electrostatics.* Chemical Society Reviews, 2007. **36**(5): p. 707-718.
78. Kharlampieva, E., et al., *Hydrogen-Bonded Multilayers of Thermoresponsive Polymers.* Macromolecules, 2005. **38**(25): p. 10523-10531.
79. Hiller, J.A. and M.F. Rubner, *Reversible Molecular Memory and pH-Switchable Swelling Transitions in Polyelectrolyte Multilayers.* Macromolecules, 2003. **36**(11): p. 4078-4083.
80. Itano, K., J. Choi, and M.F. Rubner, *Mechanism of the pH-Induced Discontinuous Swelling/Deswelling Transitions of Poly(allylamine hydrochloride)-Containing Polyelectrolyte Multilayer Films.* Macromolecules, 2005. **38**(8): p. 3450-3460.
81. Sukhishvili, S.A. and S. Granick, *Layered, Erasable, Ultrathin Polymer Films.* Journal of the American Chemical Society, 2000. **122**(39): p. 9550-9551.
82. Dubas, S.T. and J.B. Schlenoff, *Polyelectrolyte Multilayers Containing a Weak Polyacid: Construction and Deconstruction.* Macromolecules, 2001. **34**(11): p. 3736-3740.
83. Park, M.-K., S. Deng, and R.C. Advincula, *pH-Sensitive Bipolar Ion-Permselective Ultrathin Films.* Journal of the American Chemical Society, 2004. **126**(42): p. 13723-13731.
84. Dai, J., et al., *Controlling the Permeability of Multilayered Polyelectrolyte Films through Derivatization, Cross-Linking, and Hydrolysis.* Langmuir, 2001. **17**(3): p. 931-937.
85. Zhao, B. and W.J. Brittain, *Polymer brushes: surface-immobilized macromolecules.* Progress in Polymer Science, 2000. **25**(5): p. 677-710.
86. Stuart, M.A.C., et al., *Emerging applications of stimuli-responsive polymer materials.* Nat Mater, 2010. **9**(2): p. 101-113.
87. Sanjuan, S., et al., *Synthesis and swelling behavior of pH-responsive polybase brushes.* Langmuir, 2007. **23**(10): p. 5769-5778.
88. Sanjuan, S. and Y. Tran, *Stimuli-responsive interfaces using random polyampholyte brushes.* Macromolecules, 2008. **41**(22): p. 8721-8728.
89. Sanjuan, S. and Y. Tran, *Synthesis of random polyampholyte brushes by atom transfer radical polymerization.* Journal of Polymer Science Part A: Polymer Chemistry, 2008. **46**(13): p. 4305-4319.
90. Sudre, G., et al., *Reversible adhesion between a hydrogel and a polymer brush.* Soft Matter, 2012. **8**(31): p. 8184-8193.
91. Comrie, J.E. and W.T.S. Huck, *Exploring Actuation and Mechanotransduction Properties of Polymer Brushes.* Macromolecular Rapid Communications, 2008. **29**(7): p. 539-546.

92. Zhou, J., et al., *Temperature, ionic strength and pH induced electrochemical switching of smart polymer interfaces.* Chemical Communications, 2006(46): p. 4820-4822.
93. Yim, H., et al., *Effects of grafting density and molecular weight on the temperature-dependent conformational change of poly (N-isopropylacrylamide) grafted chains in water.* Macromolecules, 2006. **39**(9): p. 3420-3426.
94. Yim, H., et al., *Temperature-dependent conformational change of PNIPAM grafted chains at high surface density in water.* Macromolecules, 2004. **37**(5): p. 1994-1997.
95. Yim, H., et al., *Study of the conformational change of poly(N-isopropylacrylamide)-grafted chains in water with neutron reflection: Molecular weight dependence at high grafting density.* Journal of Polymer Science Part B: Polymer Physics, 2004. **42**(17): p. 3302-3310.
96. Yim, H., et al., *Conformation of end-tethered PNIPAM chains in water and in acetone by neutron reflectivity.* Macromolecules, 2003. **36**(14): p. 5244-5251.
97. Balamurugan, S., et al., *Thermal response of poly (N-isopropylacrylamide) brushes probed by surface plasmon resonance.* Langmuir, 2003. **19**(7): p. 2545-2549.
98. Annaka, M., et al., *Real-time observation of coil-to-globule transition in thermosensitive poly (N-isopropylacrylamide) brushes by quartz crystal microbalance.* Polymer, 2007. **48**(19): p. 5713-5720.
99. Malham, I.B. and L. Bureau, *Density effects on collapse, compression, and adhesion of thermoresponsive polymer brushes.* Langmuir, 2009. **26**(7): p. 4762-4768.
100. Plunkett, K.N., et al., *PNIPAM chain collapse depends on the molecular weight and grafting density.* Langmuir, 2006. **22**(9): p. 4259-4266.
101. Zhu, X., et al., *End-grafted low-molecular-weight PNIPAM does not collapse above the LCST.* Langmuir, 2007. **23**(1): p. 162-169.
102. Chen, T., et al., *Fabrication of Micropatterned Stimulus-Responsive Polymer-Brush 'Anemone'.* Advanced Materials, 2009. **21**(18): p. 1825-1829.
103. Liu, R., et al., *Thermally-responsive surfaces comprising grafted poly(N-isopropylacrylamide) chains: Surface characterisation and reversible capture of dispersed polymer particles.* Journal of Colloid and Interface Science, 2009. **340**(2): p. 166-175.
104. Xue, C., et al., *Protein adsorption on poly (N-isopropylacrylamide) brushes: dependence on grafting density and chain collapse.* Langmuir, 2011. **27**(14): p. 8810-8818.
105. Burkert, S., et al., *Protein Resistance of PNIPAAm Brushes: Application to Switchable Protein Adsorption.* Langmuir, 2009. **26**(3): p. 1786-1795.
106. Harmon, M.E., et al., *A Surface Plasmon Resonance Study of Volume Phase Transitions in N-Isopropylacrylamide Gel Films.* Macromolecules, 2002. **35**(15): p. 5999-6004.

107. Bhatta, D., et al., *Holographic sensors for the detection of bacterial spores.* Biosensors and Bioelectronics, 2007. **23**(4): p. 520-527.
108. Bashir, R., et al., *Micromechanical cantilever as an ultrasensitive pH microsensor.* Applied Physics Letters, 2002. **81**(16): p. 3091-3093.
109. Liang, L., et al., *Temperature-sensitive membranes prepared by UV photopolymerization of N-isopropylacrylamide on a surface of porous hydrophilic polypropylene membranes.* Journal of Membrane Science, 1999. **162**(1–2): p. 235-246.
110. Pan, Y.V., et al., *Plasma Polymerized N-Isopropylacrylamide: Synthesis and Characterization of a Smart Thermally Responsive Coating.* Biomacromolecules, 2000. **2**(1): p. 32-36.
111. Tamirisa, P.A. and D.W. Hess, *Water and Moisture Uptake by Plasma Polymerized Thermoresponsive Hydrogel Films.* Macromolecules, 2006. **39**(20): p. 7092-7097.
112. Bullett, N.A., et al., *Chemical and thermo-responsive characterisation of surfaces formed by plasma polymerisation of N-isopropyl acrylamide.* Surface and Interface Analysis, 2006. **38**(7): p. 1109-1116.
113. Förch, R., et al., *Recent and Expected Roles of Plasma-Polymerized Films for Biomedical Applications.* Chemical Vapor Deposition, 2007. **13**(6-7): p. 280-294.
114. Richter, A., et al., *Characterization of a microgravimetric sensor based on pH sensitive hydrogels.* Sensors and Actuators B: Chemical, 2004. **99**(2–3): p. 579-585.
115. Sorber, J., et al., *Hydrogel-Based Piezoresistive pH Sensors: Investigations Using FT-IR Attenuated Total Reflection Spectroscopic Imaging.* Analytical Chemistry, 2008. **80**(8): p. 2957-2962.
116. Aussenegg, F.R., et al., *The metal island coated swelling polymer over mirror system (MICSPOMS): a new principle for measuring ionic strength.* Sensors and Actuators B: Chemical, 1995. **29**(1–3): p. 204-209.
117. Guenther, M., et al., *Chemical sensors based on multiresponsive block copolymer hydrogels.* Sensors and Actuators B: Chemical, 2007. **126**(1): p. 97-106.
118. Gupta, S., et al., *Synthesis and characterization of stimuli-sensitive micro- and nanohydrogels based on photocrosslinkable poly(dimethylaminoethyl methacrylate).* Journal of Polymer Science Part A: Polymer Chemistry, 2007. **45**(4): p. 669-679.
119. von Recum, H.A., et al., *Novel thermally reversible hydrogel as detachable cell culture substrate.* Journal of Biomedical Materials Research, 1998. **40**(4): p. 631-639.
120. Matsukuma, D., K. Yamamoto, and T. Aoyagi, *Stimuli-Responsive Properties of N-Isopropylacrylamide-Based Ultrathin Hydrogel Films Prepared by Photo-Cross-Linking.* Langmuir, 2006. **22**(13): p. 5911-5915.
121. Heijl, J.M.D. and F.E. Du Prez, *Fast, multi-responsive microgels based on photo-crosslinkable poly(2-(dimethylamino)ethyl methacrylate).* Polymer, 2004. **45**(20): p. 6771-6778.

122. Hoffmann, J., et al., *Photopatterning of thermally sensitive hydrogels useful for microactuators.* Sensors and Actuators A: Physical, 1999. **77**(2): p. 139-144.
123. Liu, H. and Y. Ito, *Gradient micropattern immobilization of a thermo-responsive polymer to investigate its effect on cell behavior.* Journal of Biomedical Materials Research Part A, 2003. **67A**(4): p. 1424-1429.
124. Toomey, R., D. Freidank, and J. Rühe, *Swelling Behavior of Thin, Surface-Attached Polymer Networks.* Macromolecules, 2004. **37**(3): p. 882-887.
125. Flory, P.J. and J. Rehner, *Statistical Mechanics of Cross-Linked Polymer Networks II. Swelling.* The Journal of Chemical Physics, 1943. **11**(11): p. 521-526.
126. Kuckling, D., M.E. Harmon, and C.W. Frank, *Photo-Cross-Linkable PNIPAAm Copolymers. 1. Synthesis and Characterization of Constrained Temperature-Responsive Hydrogel Layers.* Macromolecules, 2002. **35**(16): p. 6377-6383.
127. Harmon, M.E., D. Kuckling, and C.W. Frank, *Photo-Cross-Linkable PNIPAAm Copolymers. 2. Effects of Constraint on Temperature and pH-Responsive Hydrogel Layers.* Macromolecules, 2002. **36**(1): p. 162-172.
128. Harmon, M.E., D. Kuckling, and C.W. Frank, *Photo-Cross-Linkable PNIPAAm Copolymers. 5. Mechanical Properties of Hydrogel Layers.* Langmuir, 2003. **19**(26): p. 10660-10665.
129. Harmon, M.E., et al., *Photo-Cross-Linkable PNIPAAm Copolymers. 4. Effects of Copolymerization and Cross-Linking on the Volume-Phase Transition in Constrained Hydrogel Layers.* Langmuir, 2003. **19**(26): p. 10947-10956.
130. Sharp, J.S. and R.A.L. Jones, *Micro-buckling as a Route Towards Surface Patterning.* Advanced Materials, 2002. **14**(11): p. 799-802.
131. Sharp, J.S. and R.A.L. Jones, *Swelling-induced morphology in ultrathin supported films of poly(d,l-lactide).* Physical Review E, 2002. **66**(1): p. 011801.
132. Tanaka, T., et al., *Mechanical instability of gels at the phase transition.* Nature, 1987. **325**(6107): p. 796-798.
133. Orlov, M., et al., *pH-Responsive Thin Film Membranes from Poly(2-vinylpyridine): Water Vapor-Induced Formation of a Microporous Structure.* Macromolecules, 2007. **40**(6): p. 2086-2091.
134. Tokarev, I., et al., *An Electrochemical Gate Based on a Stimuli-Responsive Membrane Associated with an Electrode Surface.* The Journal of Physical Chemistry B, 2007. **111**(42): p. 12141-12145.

Chapter 2

Synthesis of hydrogel thin films

Contents

Contents 40

Introduction 41

1. Strategy of synthesis of surface-attached gel thin films 41
    1.1. Thiol-ene click chemistry 41
    1.2. Spin-coating of polymers 42
    1.3. General strategy 43
2. Synthesis of stimuli-responsive polymers 44
    2.1. General strategy 44
    2.2. Thermo-responsive polymers 46
        2.2.1. Synthesis of poly(AA-co-NIPAM) 46
        2.2.2. Ene-functionalization of PNIPAM chains 49
    2.3. Photo-responsive polymers 51
    2.4. Electro-responsive polymers 53
        2.4.1. Synthesis of poly(AA-co-AMPS) 54
        2.4.2. Ene-functionalization of PAMPS chains 55
    2.5. Deuterated polymers for neutron experiments 55
        2.5.1. Synthesis of deuterated PAA (PAA_D) 55
        2.5.2. Ene-functionalization of deuterated PAA (PAA_D) 56
3. Synthesis method for hydrogel thin films 57
    3.1. Functionalization of substrates 57
    3.2. Coating of polymer films 58
    3.3. Cross-linking and grafting of polymers 60
4. Formation of single network gel films 60
    4.1. Synthesis of single network gel films 60
    4.2. Dry thickness 61
    4.3. Synthesis of single network gel films for neutron experiments 62

References 64

Introduction

This first experimental chapter focuses on the synthesis of surface-attached hydrogel thin films. We choose the method of "cross-linking chains" which consists in starting from preformed and functionalized polymer chains instead of "cross-linking monomers" which consists in starting from monomers and polymerizing and cross-linking them. The strategy is based on thiol-ene click chemistry. Ene-functionalized polymer chains are coated in melt state onto the thiol-modified surface with dithiol as cross-linkers. The thiol-ene reaction allows both the surface grafting and the cross-linking of chains. This method is appreciated for its simplicity and versatility. It allows the synthesis of gel film of well-controlled thickness and of targeted properties, the stimuli-responsive properties of gel film depending on the polymer used for cross-linking. In the following, we report the synthesis and characterization of different kinds of responsive hydrogel films (with temperature, light and electric field).

1. Strategy of synthesis of surface-attached gel thin films

1.1. Thiol-ene click chemistry

Click chemistry is a term applied to chemical synthesis tailored to generate substances quickly and reliably by joining small units together. It is not a single specific reaction, but describes a way of generating products that follows examples in nature, which also generates substances by joining small modular units. Characteristics of a desirable click chemistry include high chemical yields with by-products (if any) that are easily removable by non-chromatographic processes, insensitivity to oxygen or water, solventless (or aqueous) reaction conditions, amenability to a wide variety of readily available starting compounds, and so on [1, 2].

Thiol-ene reaction involves the addition of a S-H bond across a double bond by either a free radical or ionic mechanism. It is essentially the sulfur version of the hydrosilylation reaction. Thiol-ene reaction is considered to be a "click" reaction as it carries all the desirable features of a click reaction, being highly efficient, simple to execute with no side products and proceeding rapidly to high yield [2].

We follow a straightforward strategy based on thiol-ene reaction [3] (see **Figure 1**) to

synthesize the surface-attached hydrogel films. The thiol-ene click chemistry offers many advantages. It is conveniently realized in air and there is no caution of controlled atmosphere. It can be activated by either temperature or UV-irradiation (usually at 250 nm) without any initiator. The principle consists in using thiol-modified silicon wafers, ene-functionalized polymers, and bifunctional thiol molecules as crosslinkers, to obtain covalently cross-linked hydrogel networks which are covalently grafted onto the surface of silicon wafers. The polymers are copolymers containing ene-reactive groups and monomer units with stimuli-responsive properties. This new approach allows easily the variation of the chemical functions of the polymers, thus the responsive properties of the hydrogel films.

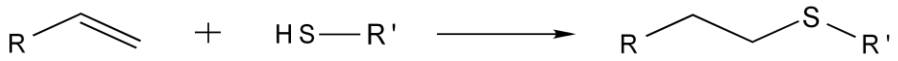


***Figure 1**: Principle of the thiol-ene reaction.*

1.2. Spin-coating of polymers

We choose the spin-coating as the method to coat polymer melt on a substrate with desired thickness. Spin-coating is the dominant technique employed to produce uniform thin films with a wide range of thickness. The controllability of the spin-coating process is excellent when it comes to creating a well-defined film with a homogeneous lateral and vertical polymer distribution. Compared with spin-coating, to get a polymer film of the same thickness dip-coating needs much more polymers, and it is more difficult to make a homogeneous film with dip-coating. Flow-coating and spray-coating have the same problem, i.e. it is harder to control the homogeneity of polymer films. The choice is motivated mainly by the high controllability and reproducibility of the film thicknesses [4]. And also the thickness of the gel films obtained from spin-coating ranges from nanometer to micrometers, including the thicknesses that are suitable for measurements with ellipsometry (hundreds of nms) and neutron reflectivity (tens of nanometers).

After spin-coating of the polymer solution on the flat substrate, the viscous force and surface tension causes a thin residual film to be retained on the substrate. It has been established that the initial volume of the fluid dispensed onto the rotating disk and the rate of fluid delivery (i.e., dispense speed during a brief period of slow rotation preceding spinning to spread out the fluid) have a negligible effect on the final film thickness [5]. In fact the thickness of the residual film depends on the final spinning speed and the viscosity of the solution [6]. The viscosity of a polymer solution is decided by the molar mass of the polymer and the concentration [7]**.** That is to say, by controlling the spinning speed, the molar mass of the polymer and the concentration of the polymer solution, we can easily get the hydrogel film of desired thickness.

1.3. General strategy

Based on thiol-ene click chemistry, the synthesis of hydrogel films does not require very sophisticated chemistry. It needs quite easy processes: free radical polymerization, polymers functionalization by ene group and surface modification by silane. The copolymerization of monomers (with responsive properties) and acrylic acid (necessary for the further functionalization) is performed by free radical technique. The radical polymerization is the best choice for acrylic acid and acrylamide derivatives. In addition, there is here no need to synthesized polymer chains with low polydispersity by controlled radical polymerization methods, for example, which are more binding. The polymers functionalization by ene group is obtained by a simple peptide reaction using allylamine. Both the free radical polymerization and the peptide reaction can be achieved in water, which is very convenient for the purification and the recovery of polymers since the copolymers can be purified by dialysis against water. The silanization of surface (silicon wafers or glass substrates) is now very usual even if a few cautions are required.

Our general strategy (see **Figure 2**) is as follows:

- synthesize and ene-functionalize the copolymer with stimuli-responsive property;
- the ene-functionalized copolymer is solubilized in proper solvent and then the bifunctional thiol molecules are introduced into the solution as cross-linkers which are proportional to the ene groups in the polymer;
- the solution is deposited on the thiol-modified silicon wafer and then spin-coated;
- cross-linking and grafting-to-surface processes are achieved simultaneously by the thiol-ene reaction under certain conditions.

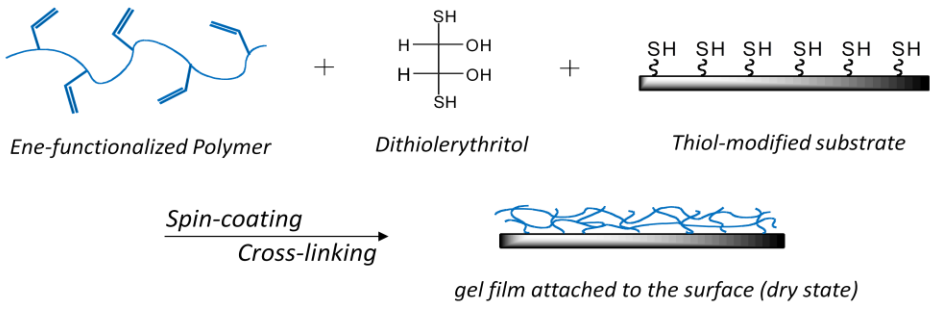


***Figure 2**: Synthesis of hydrogel thin films based on thiol-ene reaction.*

Specially, the thickness of the hydrogel thin films can be easily controlled by adjusting polymers with different molar mass, the concentration of the solutions and the final spinning speed. The surface attachment and the cross-linking by the thiol-ene reaction occur in air

atmosphere at high temperature (typically 120°C) or under UV-irradiation (at 250 nm). The heat was necessary for the formation of the hydrogel film (under 80°C, there was no film). It probably both contributes to activate thiol-ene reaction and allows the mobility of polymer chains. As the hydrogel films we studied are macroscopically uniform (the size is usually more than cm^2), all the samples were synthesized by heating at 120°C. Here, we were not interested in patterning hydrogels using local activation by UV-irradiation, which is involved in another thesis.

2. Synthesis of stimuli-responsive polymers

In the present study, we develop hydrogel thin films which can respond to external stimuli such as temperature, light and electric field. The responsive properties of hydrogel films to external stimuli come from the polymer chains used for cross-linking. So the polymers are suitably chosen for their responsive properties. The synthesis of stimuli-responsive polymers consists in free radical copolymerization and ene-functionalization of the polymers (and also functionalization with photo-reactive groups for the light-responsive polymer).

2.1. General strategy

The polymers are firstly synthesized by free radical polymerization at ambient temperature (see **Figure 3**). Since all the monomers exploited have carbon-carbon double bond (ene), and there is no need to specially control the polymer distribution index (PDI) of the polymer chains which are going to be cross-linked to form three-dimensional networks, free radical polymerization is the best choice, as it is already widely employed on polymer synthesis and it is much easier to realize compared to other polymerization methods (like ATRP, RAFT and so on).

The initiator we apply to initiate the polymerization is the redox couple ammonium persulfate ($(NH4)_2S_2O_8$)/sodium metabisulfite ($Na_2S_2O_5$) or ammonium persulfate ($(NH4)_2S_2O_8$)/ N,N,N',N'-Tetramethylethylenediamine (TEMED). By varying the concentration of the reducing agent ($Na_2S_2O_5$), which is inversely proportional to the molecular weight (Mw), we can obtain polymer chains with different Mw, as shown in **Figure 4** [8].

The reactions take place in water as all the chemicals we used here are hydrophilic and it is facile to recover the copolymers after the polymerization simply by dialysis in water and freeze-drying.

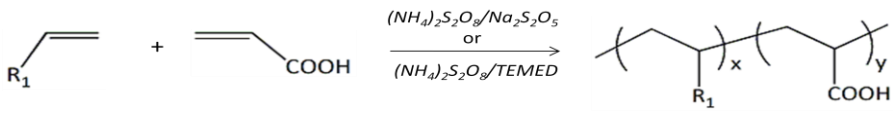


***Figure 3**: Synthesis of copolymers by free radical polymerization.*

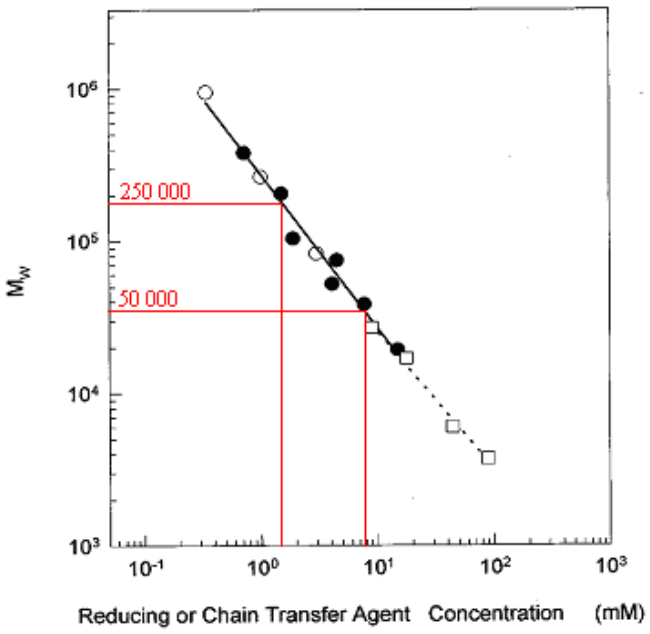


***Figure 4**: The weight-average molar mass, Mw, as a function of the concentration of the reducing agent in the redox couple used, as extracted from Bokias et al. [8].*

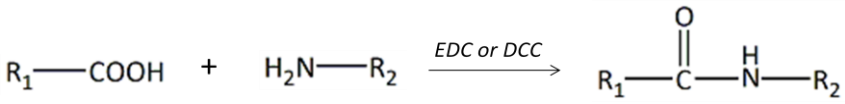


***Figure 5**: Functionalization of ene or azobenzene groups by peptide reaction.*

After polymerization, the polymer chains are randomly functionalized with ene groups by peptide reaction. Ene groups are required for the cross-linking and grafting to the surface (see **Figure 5**). Because we have carboxyls (-COOH) in our polymer chains and allylamine has both amino (-NH_2) and double bond which we need, peptide reaction is exploited to graft allylamine onto the polymer chains. This peptide reaction (between polymer chains and allylamine) can be easily carried out in water, in the presence of 1-(3-Dimethyl-aminopropyl)-3-ethylcarbodiimide hydrochloride (EDC) as the dehydration. The excess of EDC and the byproduct EDU which is also hydrophilic are able to be removed by dialysis in water.

For the light-responsive polymer, before ene-functionalization an additional step is required to graft the azobenzene groups to the polymer (using aminoazobenzene), which is also realized by peptide reaction for its light-responsive property. But as aminoazobenzene is not soluble in water, this peptide reaction takes place in N-Methyl-2-pyrrolidone (NMP) in the presence of N,N'-Dicyclohexylcarbodiimide (DCC) as the dehydration agent.

We need to point out that polymerization happens before ene-functionalization, because if ene-functionalization is performed before polymerization, the grafted ene groups may take

part in the free radical polymerization. So then there will be no more double bonds left on the polymer chains for the cross-linking.

The chemical reactants used in this chapter are listed in **Table 1**. Their main characteristics are also presented here.

All the chemicals are used as received without any further purification. All the salts used are analytical grade reagents. For all the experiments, water is purified with a Millipore system by reverse osmosis (Millipore filter Milli Ro3+) followed by deionization (MilliQ+).

2.2. Thermo-responsive polymers

To obtain thermo-responsive hydrogel films we choose poly(N-isopropylacrylamide) (PNIPAM) whose Lower Critical Solution Temperature (LCST) is around 32°C which is convenient for study with temperature. When the temperature is changed from below LCST to above LCST, aqueous solution of PNIPAM shows a phase separation between the polymer and water. So correspondingly, the hydrogel films made of PNIPAM present the swelling/collapse phase transition when temperature changes due to their large volume change by absorption or expulsion of water. In the following, we report the synthesis of copolymer poly(AA-co-NIPAM) in which acrylic acid (AA) is used for grafting ene groups, and the functionalization of ene groups onto the polymer chains by peptide reaction.

2.2.1. Synthesis of poly(AA-co-NIPAM)

*The synthesis of poly(AA-co-NIPAM) is carried out in water by free radical polymerization initiated by the redox couple ammonium persulfate/sodium metabisulfite under nitrogen at room temperature (see **Figure 6**). After the dissolution of 53.5 mg NH_4Cl, 10.74 g NIPAM (0.095 mol) and 0.36 g AA (0.005 mol) in 100 ml water, the pH of the solution is adjusted to 3-4 with NaOH solution at the concentration of 1 M. Then the mixture is deoxygenated with a bubbling of nitrogen for 1 h before the introduction of initiators (the amount depends on the molecular weight we aim, as shown in **Figure 4**), which are already dissolved separately in 2 ml water and deoxygenated beforehand. The reaction is allowed to proceed for 24 hours. The final solution is dialyzed in Milli-Q water changed twice a day during 4 days, and the polymer is recovered by freeze-drying.*

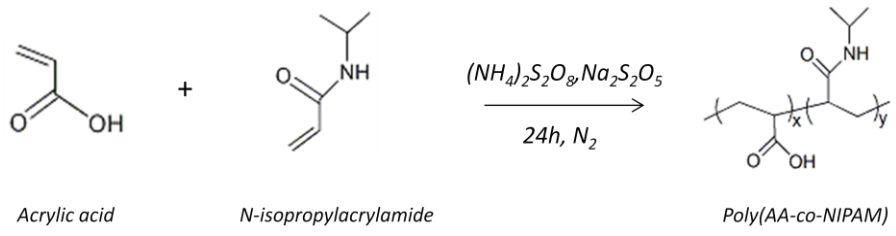


***Figure 6**: Synthesis of copolymer P(AA-co-NIPAM).*

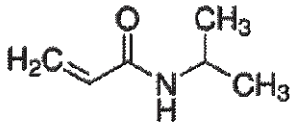
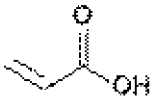
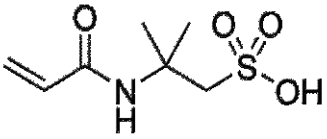
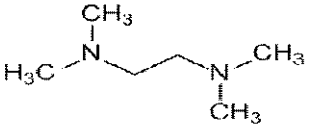
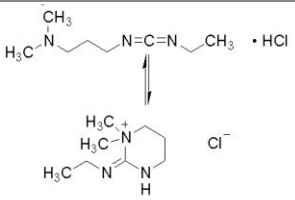
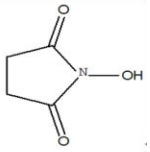
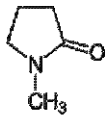
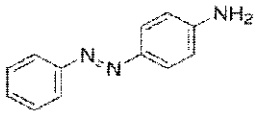
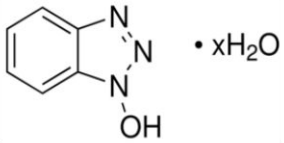
Notation	Chemical name	Semi-developed formula	Molar mass (g/mol)	Purity	Origin
NIPAM	N-isopropylacrylamide		113.2	97%	Aldrich
AA	acrylic acid		72.1	99.0%	Fluka
AMPS	2-acrylamido-2-methylpropane sulfonic acid		207.3	99%	Aldrich
APS	ammonium persulfate	$(NH4)_2S_2O_8$	228.2	98%	Acros
-	sodium metabisulfite	$Na_2S_2O_5$	190.1	-	Acros
TEMED	N,N,N',N'-tetramethylethylenediamine		116.2	99%	Millipore
-	allylamine		57.1	98%	Acros
EDC	1-(3-dimethyl-aminopropyl)-3-ethylcarbodiimide hydrochloride		191.7	98.0%	Aldrich
NHS	N-hydroxysuccinimide		115.1	98%	Aldrich
NMP	N-methyl-2-pyrrolidone		99.1	99.7%	Carlo Erba
-	4-aminoazobenzene		19.2	-	Aldrich
HOBT·1H_2O	1-hydroxy-benzotriazole hydrate		153.1	-	Aldrich
DCC	N,N'-dicyclohexylcarbodiimide		206.3	99%	Acros

***Table 1**: Chemical reactants.*

The reaction process can be followed in time by size exclusion chromatography (SEC). In **Figure 7**, the blue curve is the SEC result from passing the solution taken at the time t = 0, i.e. before the addition of the initiators. While the red curve is the SEC result from passing the solution taken at the time t = 24h, i.e. 24 hours after the addition of the initiators. Since the molecular weight of the copolymer is much bigger than that of the monomers, the peak of the copolymer should come out earlier than that of the monomers. By comparing the two curves, we can figure out all the peaks, as shown in the figure (the minus peak refers to the solvent). It tells that after 24 hours, there are no more monomers, which means that the polymerization is totally finished.

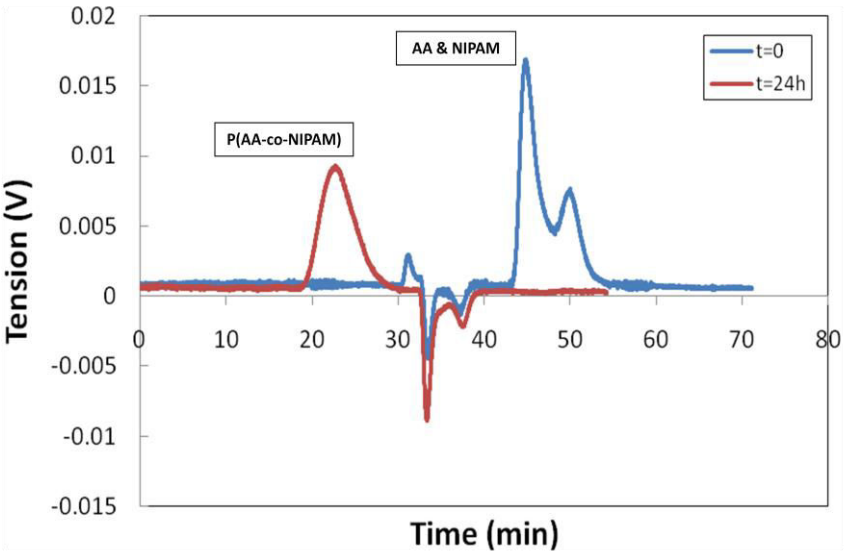


***Figure 7**: Monitoring of the synthesis process of P(AA-co-NIPAM) by SEC.*

After synthesis, the copolymer P(AA-co-NIPAM) is characterized by (calibrated) SEC and ^{1}H NMR spectroscopy. SEC provides the weight-average molar mass (Mw) and polymer dispersity index (PDI) of the copolymer, while ^{1}H NMR gives the ratio of AA in the copolymer.

The ^{1}H NMR spectrum shown in **Figure 8** is an example of spectra obtained with P(AA-co-NIPAM) copolymers in D_2O.

In **Figure 8**, the peak at 1.0-1.2 ppm corresponds to the protons on the methyl group (marked as “a”), the peak at 3.8-4.0 ppm corresponds to the proton connected to the secondary carbon of the isopropyl group (marked as “b”), and the peaks at 1.3-2.2 ppm correspond to the protons connected to the carbon on the main chain (marked as “c” and “d”).

The ratio of AA in the polymer can be determined by comparing the integral of the peak. The calculation process is shown as follows:

$$\begin{cases} 3x + 9y = 9.40 \\ y = 1.00 \end{cases}$$

$$\Longrightarrow \quad \frac{x}{x+y} = 11.7\%$$

We found here a ratio of AA in the copolymer equal to 11.7%.

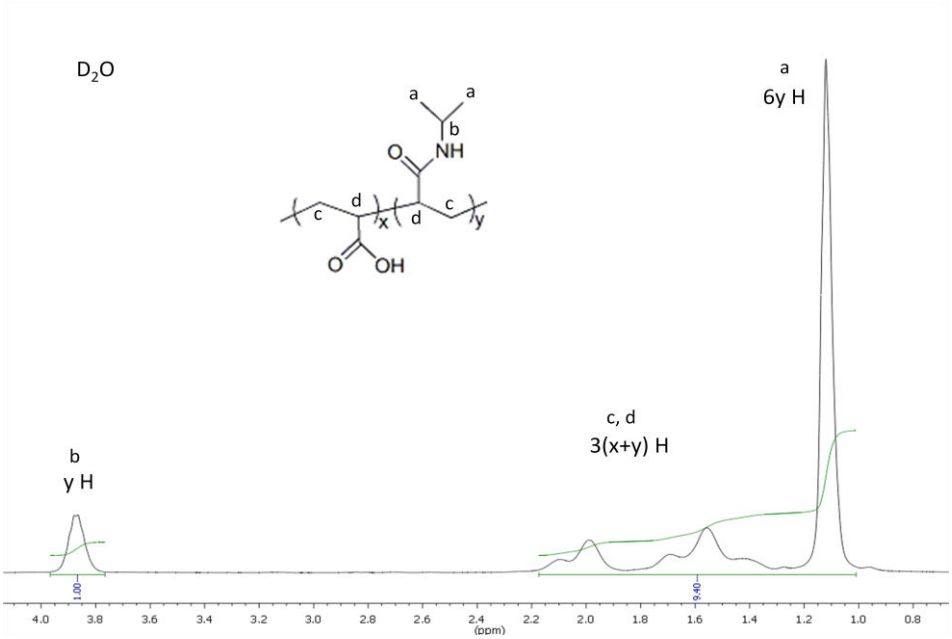


***Figure 8**: ^{1}H NMR spectra of copolymer P(AA-co-NIPAM) in D_2O.*

2.2.2. Ene-functionalization of PNIPAM chains

*The copolymer P(AA-co-NIPAM) is ene-functionalized by allylamine in water at room temperature in the presence of EDC as the dehydration agent and NHS as the addition agent to increase yields and decrease side reactions (see **Figure 9**). After 4.54 g P(AA-co-NIPAM) (0.042 mol, if the ratio of AA in the copolymer is 10%) is dissolved in 150 ml water, allylamine is added into the solution under stirring. Then the pH of the solution is adjusted to 5 (as EDC is effective at pH 4-6) with concentrated hydrochloric acid (1 M), before the introduction of EDC and NHS. The molar ratio (AA)/(Allylamine)/(EDC)/(NHS) is set equal to 1/2/4/2. The reaction is allowed to proceed for 24 hours. The final solution is dialyzed firstly in NaCl solution (to remove the unreacted EDC) with the concentration of 0.1 mol/L for 4 days, and then in Milli-Q water for 4 days, solvent changed twice a day. Finally the polymer is recovered by freeze-drying.*

Like the polymerization, the ene-functionalization process can be followed in time by size exclusion chromatography (SEC). In **Figure 10**, the red curve is the SEC result from passing the solution taken at the time t=0, i.e. before the addition of EDC and NHS. While the green curve is the SEC result from passing the solution taken at the time t=20 min, i.e. 20 minutes after the addition of EDC and NHS. Other curves have similar meanings with the time to take

the solution different. Since the molecular weight of the copolymer is the biggest among all the solutes in the solution, the peak which comes out first should refer to the copolymer. Since the minus peaks refer to the solvent, from the red curve we can easily determine the peak for allylamine, as shown in the figure. By comparing all the curves, we can figure out that after the reaction starting for 1 hour, there's almost no more decrease in the amount of allylamine, which is added in excess in the very beginning. It is reasonable as EDC is efficient only in the first hours.

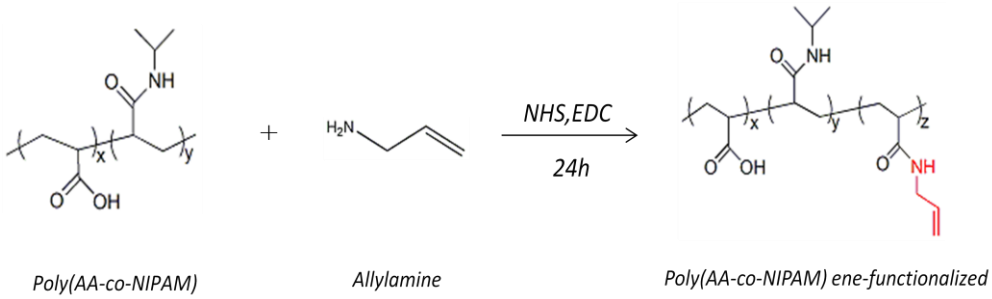


***Figure 9**: Ene-functionalization of copolymer P(AA-co-NIPAM).*

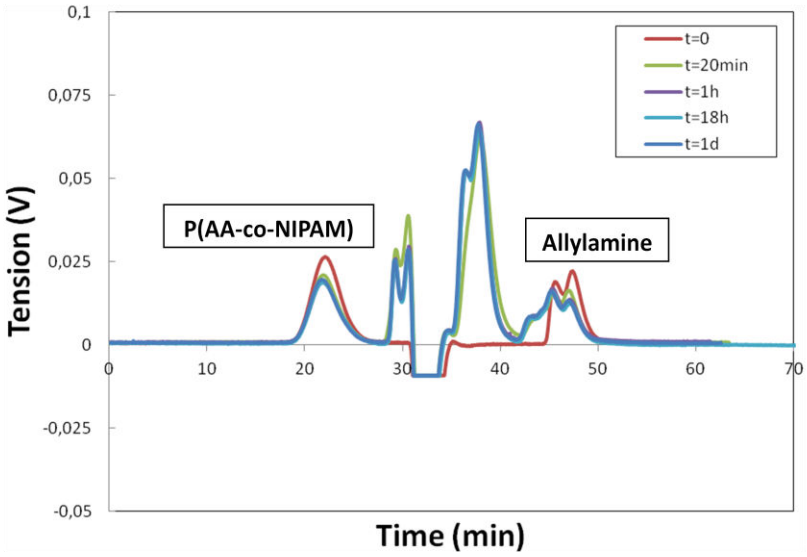


***Figure 10**: Monitoring the ene-functionalization process of P(AA-co-NIPAM) by SEC.*

The ene-functionalized copolymer P(AA-co-NIPAM) is also characterized by ^{1}H NMR spectroscopy in D_2O to determine the ratio of ene groups in the copolymer (see **Figure 11**).

In **Figure 11**, the peak at 1.0-1.2 ppm corresponds to the protons on the methyl group (marked as "a"), the peak at 3.8-4.0 ppm corresponds to the proton connected to the secondary carbon of the isopropyl group and the one connected to the primary carbon on the allyl group (marked as "b" and "e" respectively), the peaks at 1.3-2.2 ppm correspond to the protons connected to the carbon on the main chain (marked as "c" and "d"), and the

peaks at 5.8 ppm and 5.2 ppm correspond to the protons on the ene group (marked as “f” and “g” respectively).

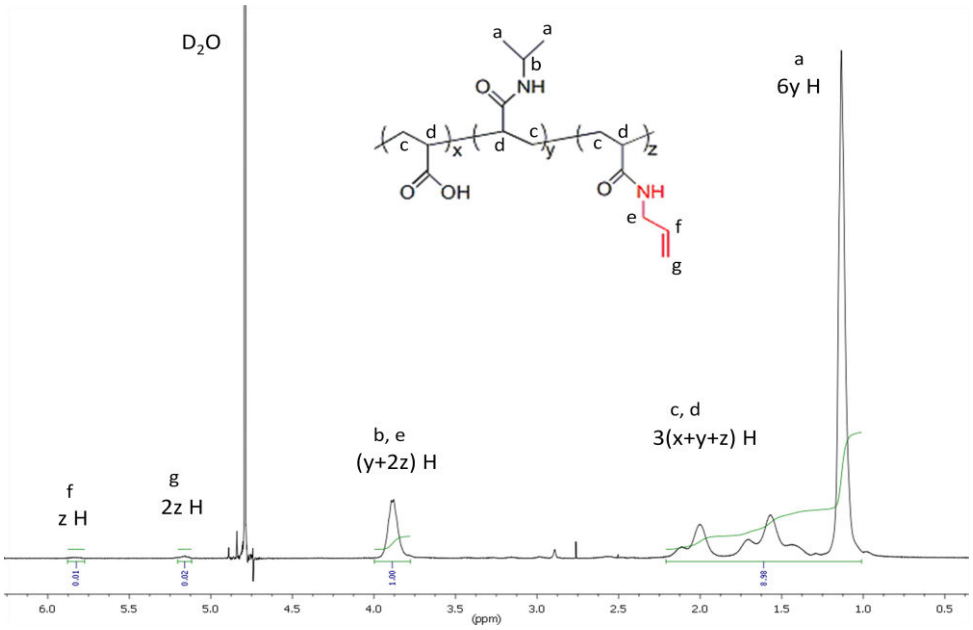


***Figure 11**: [1]H NMR spectra of ene-functionalized copolymer P(AA-co-NIPAM) in D_2O.*

The ratio of ene-functionalization can be determined with the following calculation process:

$$\begin{cases} 3x + 9y + 3z = 8.98 \\ y + 2z = 1 \\ 2z = 0.02 \end{cases}$$

$$\Longrightarrow \quad \frac{z}{x+y+z} = 1\%$$

The result shows that the ratio of ene groups in the copolymer is 1%.

2.3. Photo-responsive polymers

The thermo-responsive phase transition of the PNIPAM hydrogels can also be tuned by light. The principle lies in that a shift of LCST of PNIPAM is observed when photo-active groups (such as azobenzene) are grafted onto the polymer chains [9]. Since azobenzene has two isomers (trans- and cis-conformation), the azobenzene-modified PNIPAM has two shifted LCST ($LCST_{trans}$ and $LCST_{cis}$). When irradiated by blue light or ultraviolet light, the isomerization of azobenzene groups occurs, and therefore the LCST of the azobenzene-modified polymer changes which may induce the phase separation between the polymer and water. So if we fix the environmental temperature (T_0) at a value which is between the two LCST (see **Figure 12**), the PNIPAM hydrogels can respond to light by the

swelling/collapse phase transition in water.

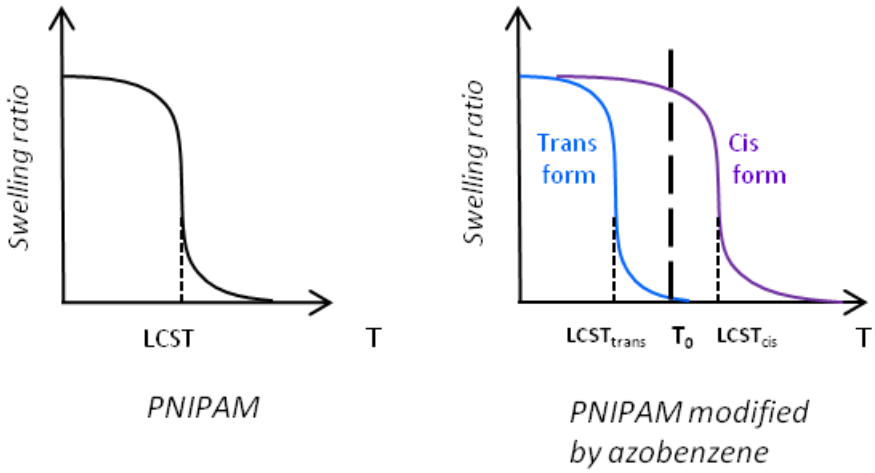


***Figure 12**: Schematic representation of the principle for the photo-responsiveness of azobenzene-modified PNIPAM.*

To graft the azobenzene groups onto the PNIPAM chains by peptide reaction, we firstly make the synthesis of copolymer P(AA-co-NIPAM) in which acrylic acid (AA) is used for grafting both azobenzene groups and ene groups, like what has been done for thermo-responsive polymers. As the yield of the reaction between AA and azobenzene groups is low, we increase the ratio of AA in the copolymer to 20%, and that's also why azobenzene-functionalization is carried out before ene-functionalization. Since azobenzene is not soluble in water, the azobenzene-functionalization takes place in NMP in the presence of DCC as the dehydration agent and HOBT used to suppress the racemization of single-enantiomer chiral molecules and to improve the efficiency of peptide synthesis. (see **Figure 13**).

In a flask of 250 ml, 2.5 g copolymer P(AA-co-NIPAM) (0.024 mol) is dissolved in 50 ml NMP, and then the mixture is heated at 70°C for one night to help dissolution of the copolymer. 2.37 g 4-Aminoazobenzene (0.012 mol) is solubilized in 3 ml NMP, heated for 5 minutes using the heating gun, and then introduced to the reaction solution under stirring. After the solution is homogeneous, 0.44 g HOBT·1H_2O (0.0029 mol) is solubilized in 1 ml NMP, and then added into the reaction solution under stirring. At last, 0.74 g DCC (0.0036 mol) is solubilized in 1 ml NMP, and then added into the reaction solution under stirring. The molar ratio (AA)/(4-Aminoazobenzene)/(DCC)/(HOBT·1H_2O) is set equal to 1/2.5/0.6/0.75 as we aim to modify half of AA in the polymer chains with azobenzene groups (the other half of AA is kept for ene-functionalization afterwards). The reaction is allowed to proceed for 24 h at 70°C with the solution stirred.

The final solution is cooled down till room temperature and then diluted with Milli-Q water by 10 times (volume of solution to 500 ml). The diluted solution is dialyzed in Milli-Q water for 4 days, water changed twice a day. Since there is precipitate (containing excess of azobenzene, DCC and HOBT) coming out in the solution, the solution is filtered to remove the precipitate. Then the filtered solution is dialyzed again in Milli-Q water for another 4 days, water changed twice a day. Finally the polymer

is recovered by freeze-drying.

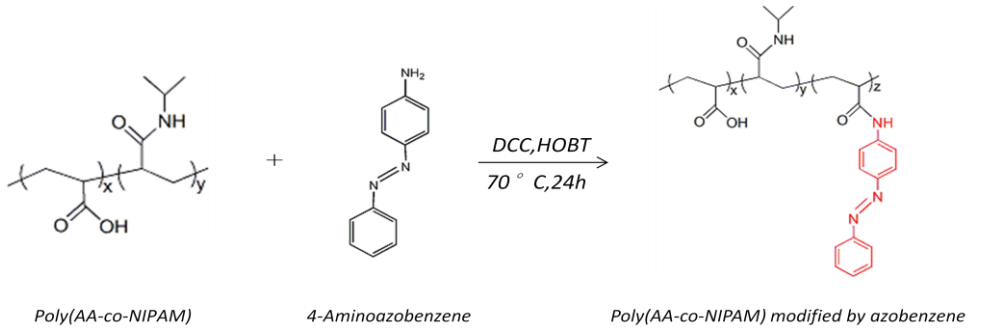


***Figure 13**: Modification of copolymer P(AA-co-NIPAM) by grafting azobenzene groups.*

The azobenzene-functionalized copolymer P(AA-co-NIPAM) is characterized by ^{1}H NMR spectroscopy to determine the ratio of azobenzene groups in the copolymer (see **Annex 1**).

After azobenzene-functionalization, ene-functionalization of the copolymer to graft ene groups onto the polymer chains is carried out like what has been done for thermo-responsive polymers.

The ene-functionalized copolymer P(AA-co-NIPAM) modified by azobenzene is also characterized by ^{1}H NMR spectroscopy to determine the ratio of ene groups in the copolymer (see **Annex 1**).

However, this experiment has been done once so that we cannot draw any conclusion about the effect of azobenzene groups on the ene-functionalization.

2.4. Electro-responsive polymers

The electro-responsive property can be achieved with polylectrolyte hydrogels. The response to electric field is due to the change of the osmotic pressure inside the gels. The application of an electric field, which is against the osmotic pressure responsible for the swelling of the gels, induces the displacement of the counterions confined inside the gels, resulting in the decrease of the osmotic pressure and thus the collapse of the gels (see **Figure 14**).

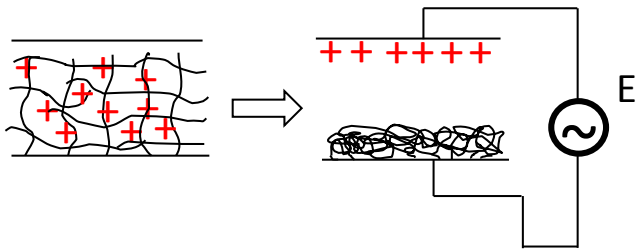
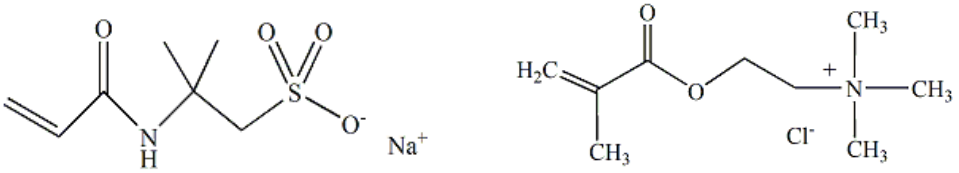


***Figure 14**: Schematic representation of the principle for the electro-responsiveness of polylectrolyte hydrogels.*

Poly(2-Acrylamido-2-methylpropane sulfonic acid) (polyAMPS) is a water-soluble and strong anionic polyelectrolyte. The hydrogels made of polyAMPS in their ionized form are polyelectrolyte gels which can respond to the electric field. Similar to polyAMPS, Poly(2-methacryloyloxy ethyl trimethylammonium chloride) (polyMAETAC) is a strong cationic polyelectrolyte, the hydrogels made of whom in the ionized form are also able to respond to the electric field with the same principle as polyAMPS hydrogels. The chemical formula of AMPS and MAETAC in the ionized form is shown in **Figure 15**. Here we take the polyAMPS as an example to report the copolymerization and ene-functionalization of poly(AA-co-AMPS). Like thermo-responsive PNIPAM, we make the synthesis of poly(AA-co-AMPS) copolymer in which acrylic acid (AA) is used for grafting ene groups.

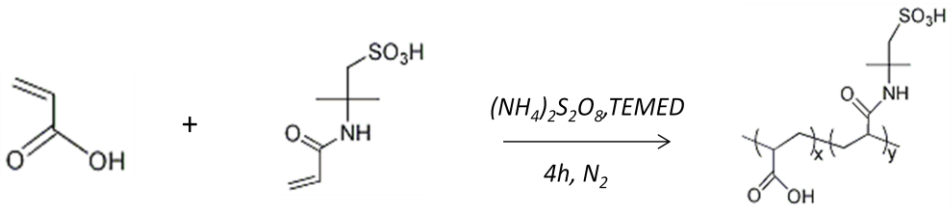


AMPS MAETAC

***Figure 15**: Chemical formula of AMPS and MAETAC in the ionized form.*

2.4.1. Synthesis of poly(AA-co-AMPS)

*The synthesis of poly(AA-co-AMPS) is carried out by aqueous free radical polymerization initiated by the redox couple ammonium persulfate/N,N,N',N'-Tetramethylethylenediamine (TEMED) under nitrogen at room temperature (see **Figure 16**). After the dissolution of 10.39 g AMPS (0.05 mol) and 405.9 mg AA (0.0056 mol) in 100 ml water, 248.5 mg ammonium persulfate (0.0011 mol) is introduced into the solution. Then the pH of the solution is adjusted to 9 with NaOH solution at the concentration of 2 M. The solution is deoxygenated with a bubbling of nitrogen for 1 hour before the introduction of 250 mg TEMED (0.0022 mol). The reaction is allowed to proceed for 4 hours. The final solution is dialyzed in Milli-Q water changed twice a day during 4 days, and the polymer is recovered by freeze-drying.*



Acrylic acid *AMPS* *Poly(AA-co-AMPS)*

***Figure 16**: Synthesis of copolymer P(AA-co-AMPS).*

The reaction process can be followed in time by size exclusion chromatography (SEC), and the synthesized copolymer P(AA-co-AMPS) is characterized by (calibrated) SEC and ^{1}H NMR

spectroscopy (see **Annex 1**).

2.4.2. Ene-functionalization of PAMPS chains

The copolymer P(AA-co-AMPS) is ene-functionalized by allylamine in water in the presence of EDC and NHS (see **Figure 17**). Except that the reaction takes place at 60°C, the others are exactly the same as what has been done for P(AA-co-NIPAM).

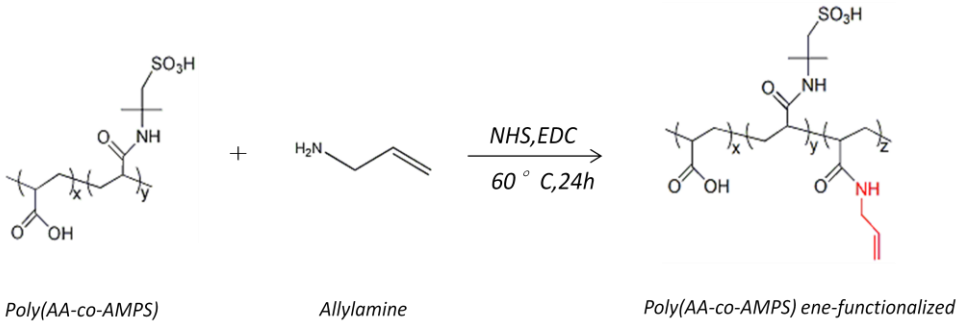


***Figure 17**: Ene-functionalization of copolymer P(AA-co-AMPS).*

The reaction process can be followed in time by size exclusion chromatography (SEC) and the ene-functionalized copolymer P(AA-co-AMPS) is characterized by ^{1}H NMR spectroscopy to determine the ratio of ene groups in the copolymer (see **Annex 1**).

2.5. Deuterated polymers for neutron experiments

Deuterated PAA chains are required for measurements with neutron reflector in liquid.

2.5.1. Synthesis of deuterated PAA (PAA_D)

The synthesis of homopolymer PAA_D is very similar to that of poly(AA-co-NIPAM), as shown in **Figure 18**, except that here the monomer is only deuterated AA.

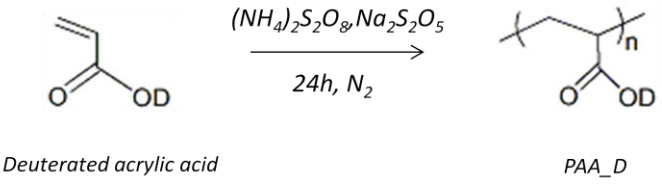


***Figure 18**: Synthesis of homopolymer PAA_D.*

The synthesis of PAA_D is carried out by aqueous free radical polymerization initiated by the redox couple ammonium persulfate/sodium metabisulfite under nitrogen at room temperature. After the dissolution of 13.9 mg NH_4Cl and 2 g deuterated AA in 25 ml water, the pH of the solution is adjusted to 3-4 with NaOH solution at the concentration of 1 M. Then the mixture is deoxygenated with a bubbling of nitrogen for 1 h before the introduction of initiators (the amount depends on the

*molecular weight we aim, as shown in **Figure 4**), which are already dissolved separately in 1 ml water and deoxygenated beforehand. The reaction is allowed to proceed for 24 h under nitrogen. The final solution is dialyzed in Milli-Q water changed twice a day during 4 days, and the polymer is recovered by freeze-drying.*

After synthesis, the homopolymer PAA_D is characterized by SEC which gives us the weight-average molar mass (Mw) and polymer dispersity index (PDI) of the copolymer.

2.5.2. Ene-functionalization of deuterated PAA (PAA_D)

The ene-functionalization of PAA _D is almost the same as that of poly(AA-co-AMPS), as shown in **Figure 19**, except that there's a difference on the amount of allylamine added as PAA _D is a homopolymer with only deuterated AA molecular units.

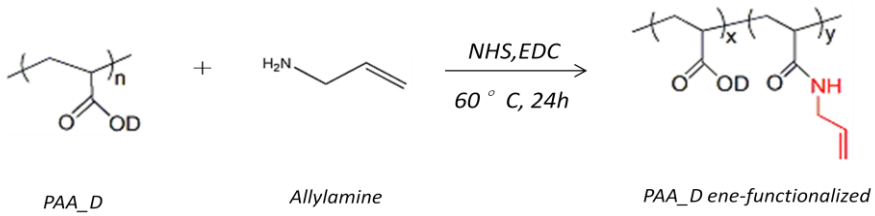


***Figure 19**: Ene-functionalization of homopolymer PAA_D.*

After polymerization, the homopolymer PAA_D is ene-functionalized by allylamine in water at room temperature in the presence of EDC as the dehydration agent and NHS as the addition agent to increase yields and decrease side reactions. After 0.3 g PAA_D is dissolved in 20 ml water, allylamine is added into the solution under stirring. Then the pH of the solution is adjusted to 5 with NaOH solution (1 M), before the introduction of EDC and NHS. The molar ratio (AA)/(Allylamine)/(EDC)/(NHS) is set equal to 10/1/2/1. The reaction is allowed to proceed for 24 h at 60°C. The final solution is dialyzed firstly in NaCl solution (to remove the unreacted EDC) with the concentration of 0.1 mol/L for 4 days, and then in Milli-Q water for 4 days, solvent changed twice a day. The polymer is recovered by freeze-drying.

The ene-functionalized homopolymer PAA_D is characterized by ^{1}H NMR spectroscopy to determine the ratio of ene groups in the polymer (see **Annex 1**).

All of the synthesis that has been carried out is listed in **Table 2 and Table 3**.

From **Table 2** and **Table 3** we can see that all the polymers have small PDI (around 2) in consideration of free radical polymerization. And overall polymers with higher molecular weight (Mw) have smaller PDI. The ratios of AA in the copolymers are mostly well controlled as the ratio obtained is the same as the ratio expected. But the ratios of ene groups in most of the polymers are less than 3%, even an excess of allylamine is added, which means the

yield of this reaction is low. While the grafting of azobenzene groups by peptide reaction in organic solvent is better, with a higher ratio (5%) of azobenzene groups obtained.

Polymer	Mw (Kg/mol)	PDI	Ratio of AA		Ratio of ene
			expected	obtained	
P(AA-co-NIPAM)	681	1.9	10%	11%	3%
	669	1.6	10%	10%	2%
	629	1.8	10%	10%	1%
	510	2.0	20%	20%	-
	474	1.8	5%	5%	3%
	405	1.8	10%	12%	2%
	254	1.8	5%	6%	3%
	195	1.6	10%	9%	1%
	67	2.5	20%	20%	-
	66	2.2	10%	12%	1%

***Table 2**: Characteristics of synthesized poly(AA-co-NIPAM). PDI is the polymer dispersity index, defined as the Mw/Mn ratio, where Mw is the weight average molecular weight and Mn is the number average molecular weight.*

Polymer	Mw (Kg/mol)	PDI	Ratio of AA		Ratio of ene	Ratio of azo
			expected	obtained		
P(AA-co-NIPAM)_azo	510	2.0	20%	20%	0.4%	5%
P(AA-co-AMPS)	454	3.1	10%	10%	2%	-
PAA_D	92	1.9	-	-	5%	-
P(AA_H-co-NIPAM_D)	38	1.9	5%	2%	1%	-

***Table 3**: Characteristics of synthesized copolymers.*

3. Synthesis method for hydrogel thin films

3.1. Functionalization of substrates

Silicon wafers are used as the substrates. Besides its availability and relative low cost, the silicon wafer – made out of a monocrystal – is rough at the atomic scale and carries at its surface a 15 Å-thick layer of native silica. On top of it, silanol functions are chemically reactive with different types of small molecules including some silanes with which they form covalent bonds. As they are atomically rough and totally reflective for UV, visible light and neutrons at air and at water interface, the silicon wafers are perfectly suitable for techniques used to characterize the interfacial structure such as ellipsometry and neutron reflectivity. In

addition, they are almost transparent for neutrons (whereas water absorb), so neutron reflectivity can also be applied to characterize the silicon-liquid interface, as ellipsometry.

The geometry of the silicon wafers used for our study strongly depends on the characterization techniques used. For ellipsometry, rectangle silicon wafers with the size of 1 cm x 2 cm and a 1-mm thickness, polished on a single side can be suitable. While for neutron reflectivity, classical silicon wafers with a 2-inch diameter and a 3 to 5-mm thickness, polished on a single side, are selected. Thick silicon wafers are required for silicon-water measurements since the neutron beam passes through silicon medium so that the edge should be thick enough for usually grazing incidence.

Prior to any chemical modification of the silicon wafers, it is necessary to activate the silanol functions of the native layer of silica. The wafers are cleaned in a freshly prepared "piranha" solution (70 vol% of sulfuric acid (>95%), 30 vol% of hydrogen peroxide (35%) heated at 150°C. They are immersed in this very exothermic and oxidative solution until ebullition stops (20 to 30 min). Piranha is supposed to remove all traces of pollutants on the surface of silicon wafers. The wafers are then extensively rinsed in Milli-Q water and sonicated in Milli-Q water during 1 min and finally dried with nitrogen flow. Afterwards the thickness of the silica layer is measured by ellipsometry: different measurements performed on the same sample must give a thickness ideally close to 0.2 nm with a standard deviation lower than 10% of the mean thickness.

Silanization with mercaptopropyltrimethoxysilane is carried out on the piranha-cleaned silicon wafers to realize the thiol-modification of the surface for thiol-ene reaction which is responsible to form surface-attached hydrogel films, as shown in **Figure 20**. After irradiated by UV for 15 minutes to activate the silanol functions, the silicon wafers are quickly transferred into a sealed reactor in which N_2 flow is then introduced to remove the air inside. Once the reactor is all filled with N_2, the solution of dry toluene with 3 vol% of mercaptopropyltrimethoxysilane which is already deoxidized before is introduced into the reactor under nitrogen. The wafers are kept immersed in the solution under nitrogen for 3 hours. Once the reaction finishes, the wafers are rinsed in toluene immediately and sonicated in toluene during 1 min and finally dried with nitrogen flow. Afterwards the thickness of the thiol layer is measured by ellipsometry, which is supposed to be around 1 nm with a standard deviation lower than 10% of the mean thickness.

3.2. Coating of polymer films

For the spin-coating process of the polymer solution on the thiol-modified silicon wafer, the polymer is first solubilized in a certain solvent (blend) at a certain concentration. Then the polymer solution is infused slowly onto the wafer fixed on the disc (which is either static or

rotating at a low angular velocity), and when the solution is well dispersed over the wafer without any bubbles, the disc is rapidly accelerated to a certain angular velocity, lasting for a certain time. During this process, the film thins by the combination of the outward fluid flow of the polymer solution and the evaporation of the solvent [10]. Several parameters are crucial in order to get a homogeneous film with a certain thickness, such as the solvent (blend), the concentration, the final angular velocity and the spinning time.

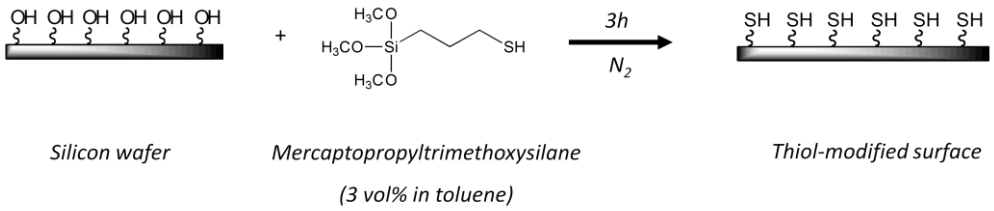


***Figure 20**: Thiol-modification of the silicon wafer.*

The choice of the solvent is very important. Former studies indicate that the thickness of the film is qualitatively related to the volatility of the solvent [11, 12]. Solvents with higher volatility result in thicker films for a given viscosity of the polymer solution. But too high volatility of solvents can also cause non-uniformities in the films due to the significant chilling effect. In order to decrease the defects in the films, we can use a bi-solvent blend, which contains a high- and a low-volatility solvent [13]. Furthermore, greater solvent/polymer compatibility results in more uniform films, i.e. less topographical variation on the surface of polymer films [12, 14]. Besides that, the solvent/substrate interaction, which is affected by the surface tension of the solvent on the substrate, is also a key factor in obtaining a homogeneous film. For example, if the wettability of the solvent on the substrate is not good, there will be no film left on the substrate after spin-coating.

Except the volatility of the solvent, the film thickness is also strongly affected by the solution viscosity and the final angular velocity [11]. For a given polymer solution, higher angular velocity gives thinner films. While for a given angular velocity, polymer solutions with higher viscosity give thicker films.

In fact, the spin-coating process is not only influenced by the angular velocity and the physical properties of the solution, but can, in addition, be very sensitive to parameters such as temperature, airflow velocity, relative humidity and thermal surroundings for the evaporating solvent (heat transfer). Thus in order to perform systematic studies or reproduce polymer films, it is necessary to obtain a fixed set of operational conditions for a given spin-coating apparatus [4].

Considering all of the parameters, bi-solvent blend is chosen with proper boiling point and

surface tension for each solvent. For example, we choose the mixture of butanol and methanol (V/V = 1/1) as the solvent blend for P(AA-co-NIPAM) and azobenzene-modified P(AA-co-NIPAM) for spin-coating. The final spinning speed is fixed at 3000 rpm during 30 s. So by changing the polymer molecular weight and the polymer concentration, we can easily obtain films with different thickness.

3.3. Cross-linking and grafting of polymers

After spin-coating, the thiol-ene reaction is carried out to accomplish the cross-linking and grafting of the polymers, using dithioerythritol (DTE) as the cross-linker. DTE has the structure of two thiols (-SH) in one molecular, which makes it work as a bridge to connect the polymer chains by covalent bonds through thiol-ene reaction.

The films are subsequently annealed at 120°C for 12 hours in vacuum after spin-coating to relax the film and to remove the residual solvent. If the annealing time is not enough, the thiol-ene reaction cannot finish completely, which may result in the detachment of the film from the substrate or the decrease of the thickness of the film or the inhomogeneity in the thickness of the film.

We have also made some preliminary tests for the time and temperature needed to get a homogeneous gel film which is well-attached to the substrate. After spin-coating of the 1% solution of PNIPAM chains (Mw=400Kg/mol), 2 hours' annealing at 120°C can make a homogeneous gel film. But if it is annealed at 80°C, even 3 hours' annealing is not enough. Correspondingly, after spin-coating of the 0.3% solution of PNIPAM chains (Mw=400Kg/mol), 1 hours' annealing at 120°C is enough. It is consistent that the annealing time is related to the amount of the polymer chains left on the substrate after spin-coating. Unfortunately, only a few experiments on the effect of time and temperature were performed but not systematic studies.

4. Formation of single network gel films

4.1. Synthesis of single network gel films

Based on the ene-functionalized polymers and the thiol-modified silicon wafers, the synthesis of single network gel film contains two main steps: spin-coating of the polymer solution on the silicon wafer, and then cross-linking of polymer chains and simultaneously grafting of the polymer onto the silicon wafer. We will take the thermo-responsive P(AA-co-NIPAM) as an example to show how to make the single network gel films.

Firstly the polymer is dissolved in the mixture of butanol and methanol (V/V = 1/1) at a certain concentration, the solution stirred for one night to help dissolution. Then the cross-linker, of an access

with respect to a certain ratio (typically 30 times) of the ene groups in the polymer chains, is added into the solution. The solution is spin-coated on the silicon wafer at 3000 rpm for 30 s. After spin-coating, the wafer is put under vacuum at 120°C. The cross-linking process is allowed to proceed for one night. The silicon wafer is taken out of the oven and cools down naturally. It is rinsed in methanol (or water) using ultrasonic bath for 1 minute to remove the unreacted polymers and then dried with N_2 flow. The thickness of the obtained film is measured by ellipsometry.

In **Table 4**, we list out some of the PNIPAM single network gel films and their characteristics.

Name of samples	Mw of polymer (Kg/mol)	Concentration of polymer (wt%)	Thickness in air (nm)
SN65	400	1.0%	65
SN80	400	1.0%	80
SN83	681	1.0%	83
SN93	66	1.5%	93
SN149	681	1.5%	149
SN248	681	2.5%	248
SN421	681	3.5%	421

***Table 4**: Formulation of PNIPAM single network gel films. The number in the name is the value of the thickness of the SN gel film in air.*

From **Table 4**, we can see that single network gel films made from copolymers of different molar mass or at different polymer concentrations are available, resulting in various thicknesses. These samples are stored at room temperature for later use.

In **Table 5**, we list out the solvent blends which are suitable for spin-coating to get uniform gel films. The solvent blends used to solubilize different polymers are preferably organic solvents with low surface tension and high volatility.

Polymer	PNIPAM	PAMPS	PMAETAC	PAA
Solvent for spin-coating	Butanol + Methanol (V/V=1/1)	Methanol + Formic acid (V/V=7/3)	Butanol + Methanol (V/V=4/6)	Methanol + Formic acid (V/V=7/3)

***Table 5**: Solvent for spin-coating for all the polymers synthesized.*

4.2. Dry thickness

Figure 21 displays the variation of the film thickness as function of the concentration of the polymer solution used for spin-coating. The ene-functionalized P(AA-co-NIPAM) is prepared in the mixture of butanol and methanol (V/V = 1/1) with concentrations varying from 1% to 10%. For all solutions, the excess of cross-linkers is kept 30 times. We show that for a given

molecular weight, higher polymer concentration gives thicker films; while for a given concentration, polymer with higher molecular weight results in thicker films. So, the thickness of the film is controlled by the molecular weight of the polymer and the concentration of the polymer solution. We demonstrate that hydrogel films can be obtained with a very wide range of thickness from nanometer to more than 1 micron. This large range of thickness is achieved with a comfortable variation of molecular weight (from 60 to 700 kg/mol) and of concentration of spin-coating solutions (from 0.1 to 10%).

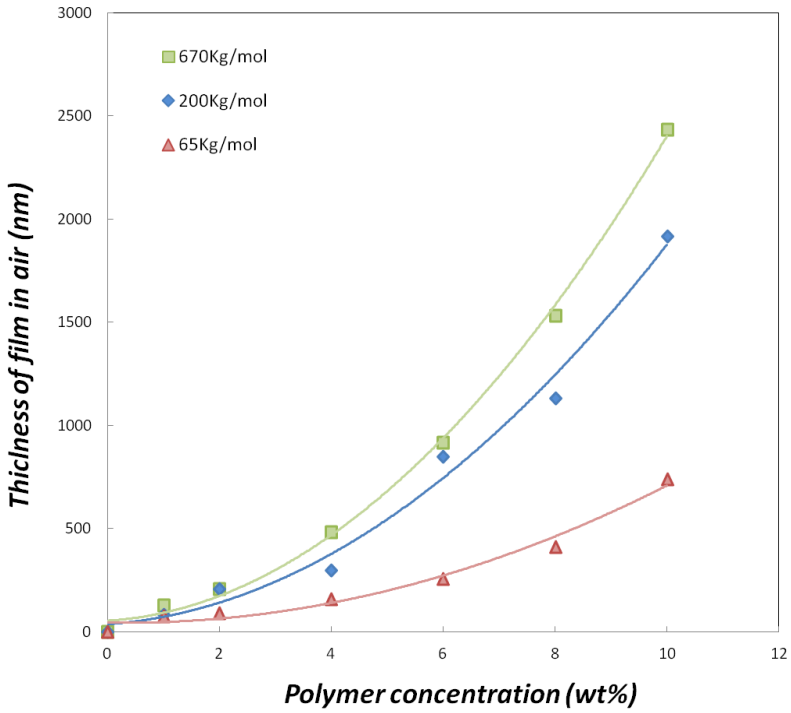


***Figure 21**: Dry thickness of films as function of polymer concentration for different polymers.*

4.3. Synthesis of single network gel films for neutron experiments

Very thin single network PNIPAM gel films are required to determine their swelling behaviors in liquid by neutron reflectivity. In **Table 6**, we list out all the single network PNIPAM gel hydrogel films prepared for neutron experiments.

Name of samples	Mw of polymer (Kg/mol)	Concentration of polymer (wt%)	Thickness in air (nm)
SN6	681	0.1%	6.4
SN7	681	0.1%	6.9
SN9	66	0.5%	8.8
SN12	681	0.2%	12.4
SN36	681	0.5%	36.2
SN63	681	0.8%	63.4

***Table 6**: Formulation of PNIPAM single network gel films for neutron experiments. The number in the name is the value of the thickness of the SN gel film in air.*

From **Table 6**, we can see that very thin single network gel films made from PNIPAM chains with various thicknesses in air are available. These samples are stored at room temperature for later use.

References

1. Kolb, H.C., M.G. Finn, and K.B. Sharpless, *Click Chemistry: Diverse Chemical Function from a Few Good Reactions.* Angewandte Chemie International Edition, 2001. **40**(11): p. 2004-2021.
2. Hoyle, C.E. and C.N. Bowman, *Thiol–Ene Click Chemistry.* Angewandte Chemie International Edition, 2010. **49**(9): p. 1540-1573.
3. Hoyle, C.E., T.Y. Lee, and T. Roper, *Thiol–enes: Chemistry of the past with promise for the future.* Journal of Polymer Science Part A: Polymer Chemistry, 2004. **42**(21): p. 5301-5338.
4. Norrman, K., A. Ghanbari-Siahkali, and N.B. Larsen, *6 Studies of spin-coated polymer films.* Annual Reports Section "C" (Physical Chemistry), 2005. **101**(0): p. 174-201.
5. Flack, W.W., et al., *A mathematical model for spin coating of polymer resists.* Journal of Applied Physics, 1984. **56**(4): p. 1199-1206.
6. Sahu, N., B. Parija, and S. Panigrahi, *Fundamental understanding and modeling of spin coating process: A review.* Indian Journal of Physics, 2009. **83**(4): p. 493-502.
7. Brandrup J, I.E., *Polymer handbook.* John Wiley & Sons, 1989.
8. Bokias, G., A. Durand, and D. Hourdet, *Molar mass control of poly(N-isopropylacrylamide) and poly(acrylic acid) in aqueous polymerizations initiated by redox initiators based on persulfates.* Macromolecular Chemistry and Physics, 1998. **199**(7): p. 1387-1392.
9. Irie, M., *Stimuli-responsive poly(N-isopropylacrylamide). Photo- and chemical-induced phase transitions*, in *Responsive Gels: Volume Transitions II*, K. Dušek, Editor. 1993, Springer Berlin Heidelberg. p. 49-65.
10. Lawrence, C.J. and W. Zhou, *Spin coating of non-Newtonian fluids.* Journal of Non-Newtonian Fluid Mechanics, 1991. **39**(2): p. 137-187.
11. Chen, B.T., *Investigation of the solvent-evaporation effect on spin coating of thin films.* Polymer Engineering & Science, 1983. **23**(7): p. 399-403.
12. Spangler, L.L., J.M. Torkelson, and J.S. Royal, *Influence of solvent and molecular weight on thickness and surface topography of spin-coated polymer films.* Polymer Engineering & Science, 1990. **30**(11): p. 644-653.
13. Schubert, D. and T. Dunkel, *Spin coating from a molecular point of view: its concentration regimes, influence of molar mass and distribution.* Materials Research Innovations, 2003. **7**(5): p. 314-321.
14. Lai, J.H., *An investigation of spin coating of electron resists.* Polymer Engineering & Science, 1979. **19**(15): p. 1117-1121.

Chapter 3

Swelling behavior of single network films

Contents

Contents 66

Introduction 67

1. Swelling ratio 68
    1.1. Measure by ellipsometry 68
    1.2. Thermo-responsive properties of PNIPAM hydrogel films 71
        1.2.1. Effect of the film thickness 71
        1.2.2. Effect of the length of polymer chains 73
2. Topography of the free surface 74
    2.1. Measurement by AFM 75
    2.2. Study of measurement conditions 77
        2.2.1. In air 77
        2.2.2. In water: approach-retract curves 78
        2.2.3. Topography in water 84
    2.3. Topography of PNIPAM hydrogel films in air 89
    2.4. Topography of PNIPAM hydrogel films in water 92
        2.4.1. Thick fims 92
        2.4.2. Thin films 94
    2.5. Effect of temperature 95
    2.6. Conclusion 98
3. Density profile of monomers 98
    3.1. Measures in air 99
    3.2. Effect of temperature 101
    3.3. Effect of the thickness of the film 103
4. Discussion 107
    4.1. Each technique has its specification and limitation 107
    4.2. Effect of the confinement 108
    4.3. Gel film: a model network? 111

References 115

Introduction

The structural investigation of the surface-attached hydrogel thin films with responsive properties tackles a fundamental aspect of confined and constrained systems. We study the effects of confinement and lateral constraints on the swelling/collapse phase transition of the gel films in two aspects: the one-dimensional swelling behavior in the direction perpendicular to the substrate and the in-plane observation of the free surface of the gel films. Correspondingly we apply three different experimental techniques to characterize the swelling behavior of the gel films.

Ellipsometry is chosen to determine the swelling ratio of the films in water in the direction normal to the substrate as a function of various physico-chemical parameters. We try to make clear: what is the effect of the confinement on the swelling ratio of the gel films? Are the experimental data consistent with the scaling laws of Flory-Rehner theory for the swelling of hydrogels extended to one-dimension swelling?

The one-dimension (normal to the substrate) swelling behavior is further studied by neutron reflectivity to obtain the density profile of the gel films both in air and in liquid. We attempt to answer the following questions: how is the interface width of the free surface of the gel films both in air and in water? How smooth or abrupt is the profile of the gel film in the direction perpendicular to the surface?

The lateral (or in-plane) exploration of the free surface of the gel films is achieved using Atomic Force Microscopy (AFM). If the characterization of the hydrogel films in air seems to be unproblematic, what about the study in water? How is the topography of the free surface of the gel? How is the “roughness” of the free surface?

Since PNIPAM hydrogel is interesting for its thermo-responsive properties and temperature is easier to control as an external stimulus, here we choose PNIPAM hydrogel thin films as the studied object to investigate their swelling behavior and responsive properties.

1. Swelling ratio

The swelling ratio is defined as the ratio between the mean thickness of the gel film in water and its thickness in air. It is determined at various temperatures to find out the transition temperature. The effect of the film thickness on the transition temperature is also investigated. Another physico-chemical parameter considered is the molecular weight of polymer chains used for the synthesis of the gel films by spin-coating.

The swelling ratio of the surface-attached hydrogel films in water was obtained using a spectroscopic ellipsometer. The measurements were performed with a liquid cell which can be regulated in temperature to determine the swollen thickness of the gel films in water. The swelling ratio of the films was then deduced. All the liquid experiments were achieved by recording the data after 30 minutes of immersion of the gel films in water at a fixed temperature, the equilibrium being undoubtedly reached. Actually, the time required for the volumetric change of the gel network is expressed as $T = h^2/D$ where h is the smallest dimension of the hydrogel or the thickness of the gel film and D the collective diffusion constant of the gel. Taking h ~ 1 μm and D ~10^{-9} m^2 s^{-1} (water diffusion), we have T ~ 1 ms.

1.1. Measure by ellipsometry

The swollen thickness of the hydrogel thin films was measured using an Accurion spectroscopic ellipsometer (see **Annex 2**).

The thickness of all the gel films is in the optical range, giving rise to sufficient features in the recorded data to infer the swollen thickness and the refractive index. A multilayer model of a flat film is applied for the fitting of the experimentally measured ellipsometric angles Ψ and Δ, including the native silica layer, the thiol layer and the gel layer from the substrate to the film-liquid interface. The refractive index of the native silica layer and thiol layer is the same, equaling to 1.46, while that of PNIPAM chains is 1.52. To simplify the fitting, a simple model of the refractive index profile of the gel films in water is generated (see **Figure 1**). The one-step function is employed to approximate the real density profile of the gel films in water, which is very soft due to the large volume fraction of water in the films. During the fitting based on the model, the swollen thickness and the refractive index of the gel film are adjusted to minimize the difference between the fitting and the experimental data.

From the swollen thickness in water (h_w) and the thickness in air (h_a), we can then deduce the swelling ratio r of the gel film, which is defined as $r = h_w/h_a$, giving the stretching degree of the polymer chains in water. The swelling ratio of PNIPAM hydrogel films as a function of temperature is also investigated.

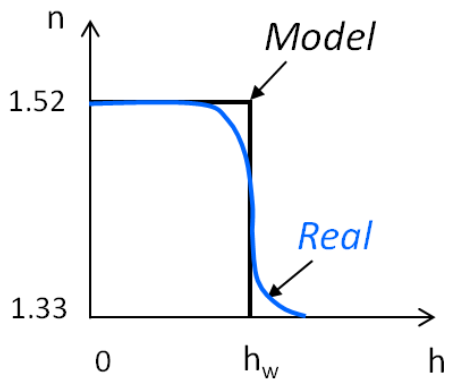


***Figure 1**: Model of the refractive index profile of the gel films in water. n is the refractive index of the film, h the thickness of the film, h_w the swollen thickness of the film in water. The refractive index of PNIPAM chains is 1.52 and that of water is 1.33.*

Since the gel films are attached to the substrate by covalent bonds, the amount of the polymer chains in the films should always keep the same when immersed in water. Based on this, we are able to use a numerical test to ensure that the fitting of the experimental data from ellipsometry is reliable.

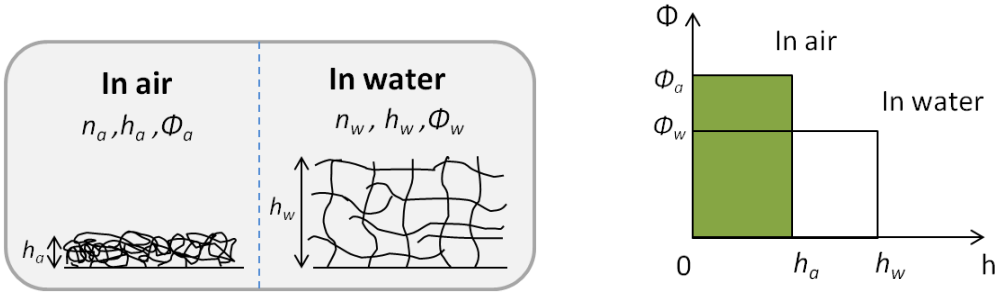


***Figure 2**: Sketch of the gel film in air and in water. n_a is the refractive index of the gel film in air, h_a the thickness of the gel film in air, ϕ_a the volume fraction of the polymer chains in air; n_w the refractive index of the gel film in water, h_w the swollen thickness of the film in water, ϕ_w the volume fraction of the polymer chains in water.*

In **Figure 2**, the sketch of the gel film in air and in water is shown, with all the related parameters listed out. If the variation of the refractive index is considered as linear with the fraction of polymer, we have (the refractive index of PNIPAM chains and water is 1.52 and 1.33 respectively):

$$n(\phi) = 1.52 \times \phi + 1.33 \times (1 - \phi) \qquad \textbf{[eq. 1]}$$

In air, it is found that the volume fraction of the polymer chains in the film ϕ_a is about 0.90. Using equation [1], we can calculate the refractive index of the gel film in air n_a which is equal to 1.50. When the film is immersed in water, since the film swells by absorbing water,

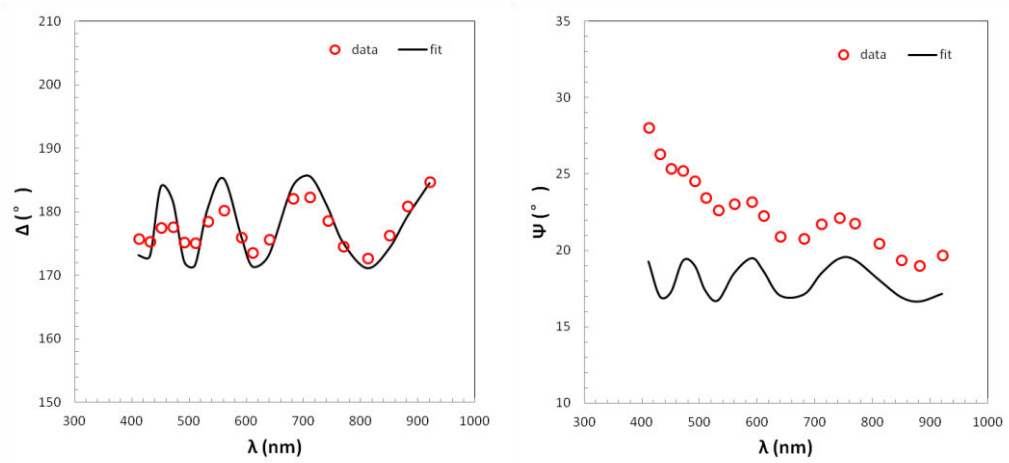
both the refractive index of the film and the volume fraction of the polymer chains in the film change. Since the gel films are attached to the substrate by covalent bonds, the amount of the polymer chains in the films should always keep the same when immersed in water. So we have:

$$n_w = \frac{1.50 - 1.33}{0.9}\phi_w + 1.33 \qquad \textbf{[eq. 2]}$$

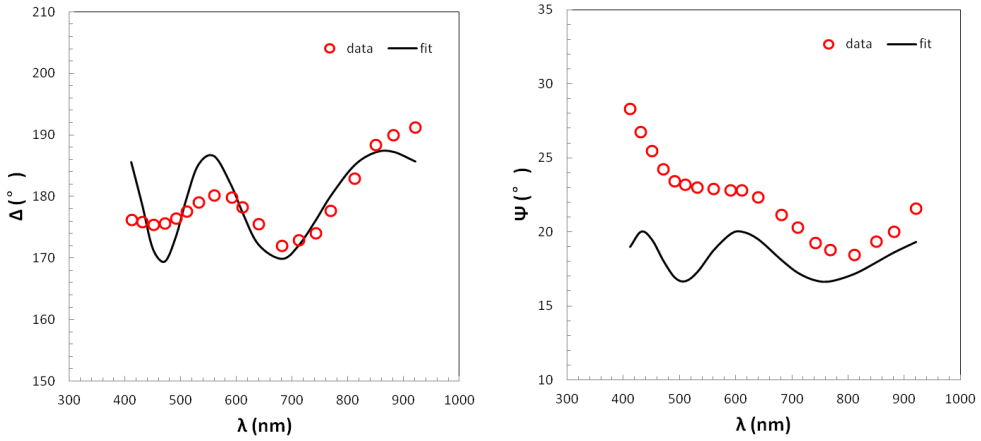
$$h_w \times \phi_w = h_a \times \phi_a \qquad \textbf{[eq. 3]}$$

Using these equations, we are able to use a numerical test to ensure that the fitting of the experimental data from ellipsometry is reliable. Once we adjust the swollen thickness h_w and the refractive index of the film in water n_w, we can deduce the thickness of the film in air h_a (ϕ_a is fixed at 0.9). We compare then the calculated h_a with the measured h_a. If the two are close, it means that the fitting is reliable; otherwise we need to redo the fitting.

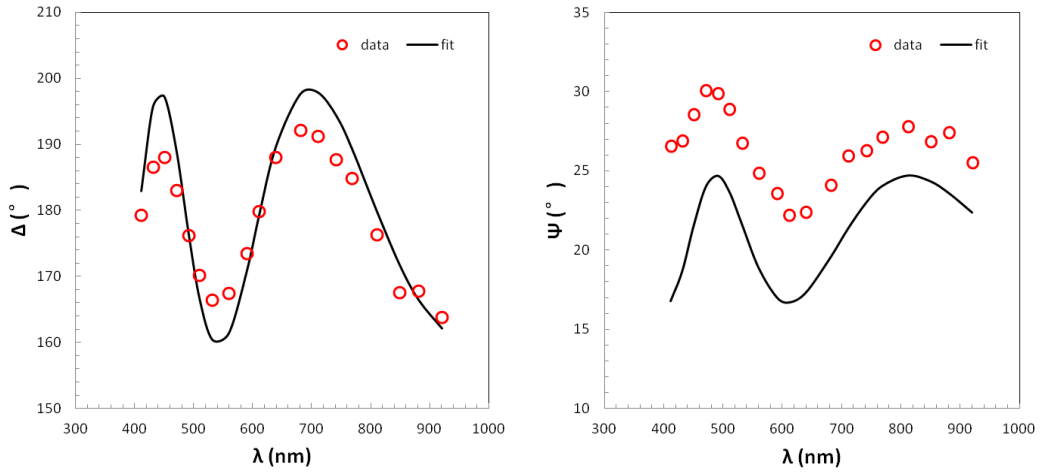
Figure 3 displays an example of fitting of the ellipsometric angles Δ and Ψ. The sample is a PNIPAM gel film (with h_a = 421 nm) measured in water at three different temperatures.



(a) *25°C (h_w = 1695 nm, n_w = 1.37)*



(b) *35°C (h_w = 970 nm, n_w = 1.40)*



(c) *40°C (h_w = 655 nm, n_w = 1.44)*

Figure 3*: An example of fitting of the ellipsometric angles Δ and Ψ. The sample is a PNIPAM gel film (with h_a = 421 nm) measured in water at (a) 25°C, (b) 35°C and (c) 40°C.*

For the three fittings shown in **Figure 3**, the difference between the calculated h_a and the measured h_a is within 5%, which means that the fittings are reliable. It could be observed that comparing to Ψ, the fitting of Δ is closer to the experimental data. In fact, even if the average value of Ψ of the fitting is lower than that of the experimental data, the fitting of the oscillations of both ellipsometric angles, Δ and Ψ, is quite satisfactory. As the thickness of the layer is directly relied to the oscillations, the thickness extracted from the fitting can be considered as reliable. Moreover, the difference between the fitting and the experimental data for 40°C (collapsed state) is smaller than that for 25°C (swollen state) and 35°C (volume transition process), because at 40°C in collapsed state, the refractive index profile (**Figure 1**) is closer to the one-step model. The proximity of the box model in collapsed state rather than swollen state will be also demonstrated with the other techniques, AFM and neutron reflectivity.

1.2. Thermo-responsive properties of PNIPAM hydrogel films

1.2.1. Effect of the film thickness

The swelling ratio of PNIPAM hydrogel thin films of various thicknesses is measured by ellipsometry to make clear the effect of the film thickness on their thermo-responsive properties. Single network PNIPAM gel films SN149 (h_a = 149 nm), SN248 (h_a = 248 nm) and SN421 (h_a = 421 nm) (see Chapter 2) are used for study, with results shown in **Figure 4**.

Note that the normalized representation in swelling ratio instead of swollen thickness allows the comparison of samples with various thicknesses (in air).

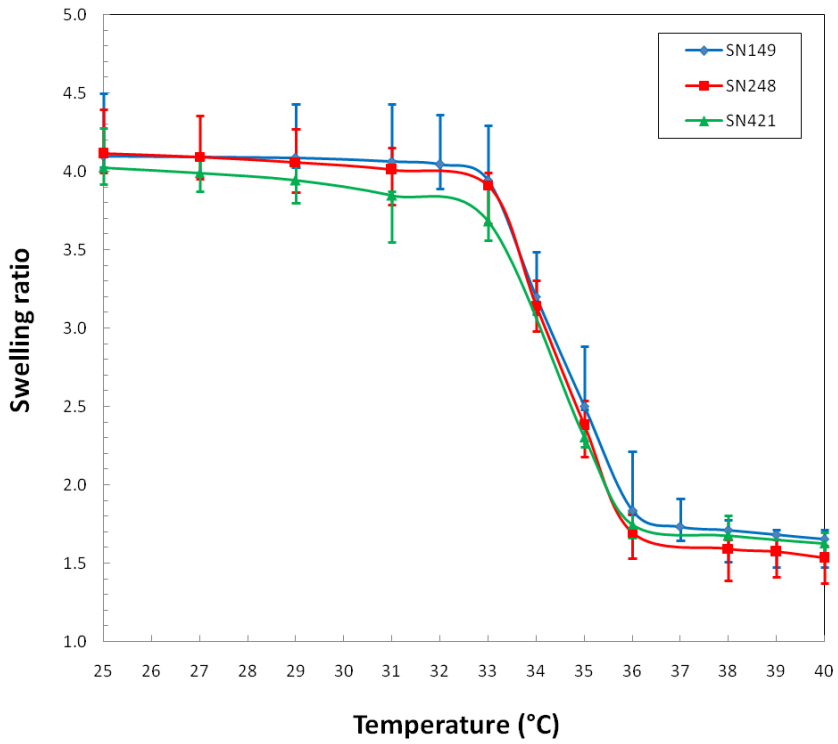


***Figure 4**: Swelling ratio of PNIPAM hydrogel films of different thickness. The swelling ratio is investigated as a function of temperature.*

In **Figure 4**, the swelling ratio of PNIPAM hydrogel films is plotted as a function of temperature for films of different thickness. The error bars just give an indication of the reliability of the fitting. The error bars include the fitting results which are estimated to be reasonably close to the experimental data (considering oscillations for example). The three samples exhibit very similar swelling ratio and responsive behavior to temperature, showing that the swelling behavior of the gel films is independent of the film thickness in the range from 150 nm to 420 nm. The swelling ratio decreases from about 4 at 25°C to about 1.5 at 40°C, showing a LCST around 34°C. The swelling ratio of the gel films is high at temperatures below the LCST, where the gel films are hydrophilic and highly swollen with a large volume fraction of water (77.5%). The swelling ratio is low at temperatures above the LCST, where the gel films are hydrophobic and collapsed, containing less water (40%). The swelling ratio around 1.5 at 40°C indicates that the films are unable to fully collapse as in air (only 10% of water).

With the increase of temperature, the phase transition of the PNIPAM gel films starts at 33°C and ends at 36°C. Outside the range of temperature 33-36°C, the swelling ratio is quite constant (4 below the LCST and 1.5 above the LCST). This range is much smaller than that found by Vidyasagar et al. [1]. They studied the collapse with temperature of a 25 nm-thick (in air) PNIPAM gel film using neutron reflectivity. They showed that the gel film collapses abruptly at 32°C containing 35% water. The thickness of the film in water decreases almost

linearly with temperature from 15°C to 30°C: about 110 nm to 70 nm. It was explained by a decrease of the osmotic pressure which favors the dilution against the entropic penalty of chains stretching opposing the dilution. However their PNIPAM film is much thinner and in our case, the results were obtained on three samples with different thickness. Moreover, PNIPAM brushes [2-5] are shown to collapse around 32°C on a temperature range of 5°C at the maximum, the less dense brushes collapsing more abruptly.

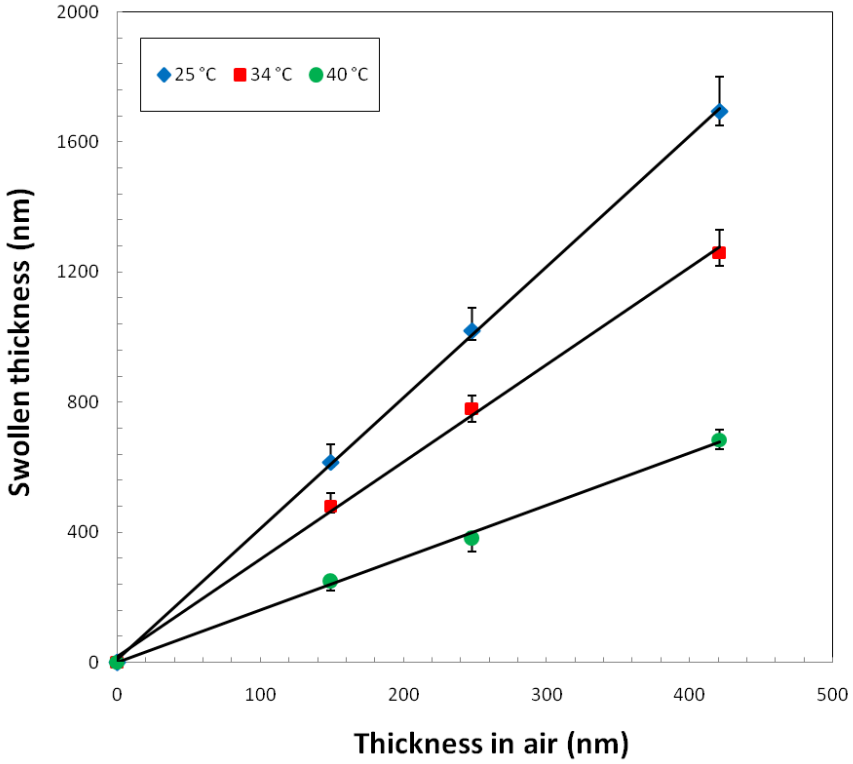


***Figure 5**: Swollen thickness of PNIPAM hydrogel films as a function of the film thickness in air, at three different temperatures: 25°C, 34°C and 40°C.*

In **Figure 5**, the swollen thickness of each PNIPAM hydrogel film is plotted as a function of the film thickness in air at three different temperatures. At each temperature, the swollen thickness of the gel films increases linearly with the growth of the film thickness. Actually, the slopes of the lines give out the swelling ratio of the gel films. Therefore, gel films of different thicknesses indicate the same swelling ratio at a given temperature, which shows a decrease when the temperature rises.

1.2.2. Effect of the length of polymer chains

The swelling ratio of PNIPAM hydrogel thin films of similar thickness made from polymers of different molecular weights is also measured by ellipsometry to make clear the effect of the length of polymer chains on their thermo-responsive properties. Single network PNIPAM gel films SN93 (Mw = 66 Kg/mol), SN80 (Mw = 405 Kg/mol) and SN83 (Mw = 681 Kg/mol) (see

Chapter 2) are used for study, with results shown in **Figure 6**.

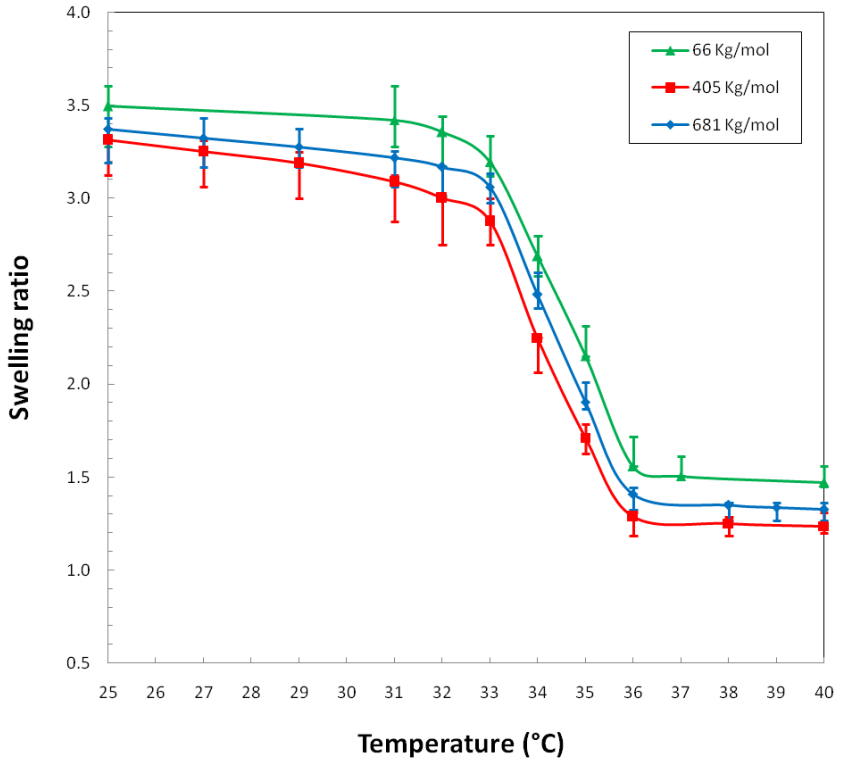


***Figure 6**: Swelling ratio of PNIPAM hydrogel films of similar thickness but made from polymers of different molecular weights as a function of temperature.*

In **Figure 6**, the swelling ratio of each PNIPAM hydrogel film is plotted as a function of temperature for films of similar thickness but made from polymers of different molecular weights. The three samples exhibit very similar swelling ratio and responsive behavior to temperature, showing that the swelling behavior of the gel films is independent of the length of polymer chains used for the synthesis. Here, the swelling ratio decreases from about 3.5 at 25°C to about 1.4 at 40°C, showing a LCST around 34°C. A swelling ratio of 3.5 for temperatures below the LCST is obtained here for PNIPAM gel films with thickness in air is 80 to 93 nm whereas the value of 4 was found for films with thickness in air higher than 100 nm. Note that the range of the transition temperature, from 32°C to 36°C, is the same as that observed previously for thicker films.

2. Topography of the free surface

The topography of the free surface (in dry state and in water) of the hydrogel is investigated in this section. The swelling of a film (covalently attached to the substrate) immersed in water could induce lateral constraints on the free surface. This could cause the deformation of the free surface of the hydrogels. Observations of the free surface (in-plane topography) by Atomic Force Microscopy have been performed in air and in water in order to address this

question.

The AFM experiments in water are not straightforward for hydrogels and require the determination the good imaging conditions: indeed, hydrogels are very soft and easily indented by almost all cantilever. The first part will be devoted to the determination of the experimental conditions for hydrogels imaging. In the second part, the different morphologies of the film and their change with temperature will be analyzed.

PNIPAM hydrogel films are expected to show a swollen/collapsed phase transition across the LCST. It will be then interesting to observe the variation of the topography of thermo-responsive films around the phase transition temperature. These studies are complementary with those performed by neutron reflectivity. AFM imaging experiments will be carried out on hydrogel films with a higher range of thicknesses (hundreds of nanometers) than those studied by neutron reflectivity (50 nm at the maximum) because the effect of the solid substrate is strong for ultra-thin films less than 100 nm.

2.1. Measurement by AFM

Three AFM techniques can be used for the imaging of the PNIPAM hydrogel film in air or in liquid state: the tapping mode, the contact mode and the so-called QNM or Quantitative Nano-Mechanics measurement. All techniques will be used in this study while the last one (QNM) is preferred when imaging the soft gel in water. The QNM mode is supposed to enable an on-line quantitative measurement of a set of properties such as elastic modulus, adhesion of the tip on the surface, deformation of the sample and dissipation of energy. These properties are extracted from high frequency on-line approach-retract curves through a defined model ("DMT" or Sneddon). Due to the particular conditions of our study (very low values of Young's modulus of the PNIPAM hydrogel in water, typically a few tens of kPa), the QNM mode is employed only to probe the surface topography. The other properties (modulus etc…) are not taken into account in this study.

A QNM experiment can be viewed as a succession of approach-retract of a cantilever on the surface at high frequency (typically 1 kHz or 2 kHz). Each approach of the cantilever on the surface is limited by a force setpoint. Once the force setpoint is reached, the cantilever begins to retract away from the surface. In a simplistic view, the force setpoint is equivalent to a deflection setpoint of the cantilever. Before presenting the results, two definitions need to be specified: the approach-retract curve and the indentation. A schematic representation of the approach-retract curve is displayed in **Figure 7**.

Δh is the variation of height imposed to the cantilever and Δd is the deviation of the cantilever (expressed in Volt). The curve $\Delta d = f(\Delta h)$ measured at one point of the sample is

called approach curve (respectively retract curve) in the case of decreasing Δh (respectively increasing Δh). An approach-retract curve obtained on a rigid sample (as a silicon wafer) allows the determination of the relationship between the deviation Δd in Volt and the deviation in nanometer through a calibration factor. In the following, Δd will be expressed in nm. The value of the slope of the approach curve is equal to 1 on a rigid sample and lower than 1 on a soft surface indented by the tip-cantilever system. If the cantilever is viewed as a simple spring, the force imposed to the cantilever is the product of k and Δd, where k is the stiffness of the cantilever. The value k, usually provided by the manufacturer, can be properly measured through the acquisition of frequency spectrum of the cantilever thermally excited. The indentation δ is equal to Δh-Δd and represents the deformation of the sample or the depth of penetration of the tip in the material. During the approach experiment, the value Δh_0 is defined as the contact point between the tip and the surface. Just before the contact between the tip and the surface, the tip is attracted by the surface by Van der Waals forces, displaying a jump to contact at Δh_0.

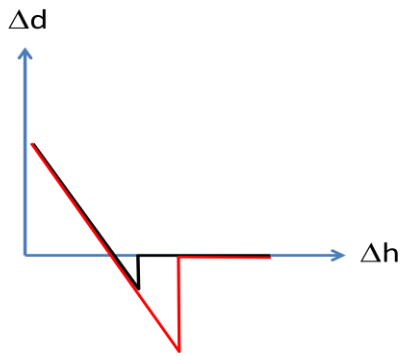


***Figure 7**: Schematic representation of the approach-retract curve. Black line: approach; red line: retract. Δh is the variation of height imposed to the cantilever and Δd is the deviation of the cantilever.*

In situ imaging of the grafted PNIPAM hydrogel thin films on silicon wafers is performed using an ICON microscope equipped with a Nanoscope V controller (Bruker). The QNM mode is used with the lowest possible force set point in order to minimize the damage to the gel film, especially in the liquid state. Triangular cantilevers of different stiffness with a silicon nitride tip (NanoProbe, Olympus) are used. All of the measurements in liquid are conducted in Milli-Q water. For the measurements in water, the gel films grafted to the silicon wafers is positioned on a specially designed temperature-controllable cell with a few of water droplets on them, and the temperature is regulated within ± 0.1°C. At each temperature, the system is left during 15 minutes for equilibration to ensure the stability of the gel surface. All the AFM images displayed below are height images. Along with each AFM height image, we also show the height histogram of the image at the top, and the cross-sectional plot of the image along the diagonal direction (called X) at the bottom, in which Z refers to the direction

of the height. In addition, the value of full width at half maximum (FWHM) of the height histogram curve is also indicated in the histogram image.

2.2. Study of measurement conditions

2.2.1. In air

The easiest way to study the topography of the PNIPAM hydrogel film in air is the well-known tapping mode. This technique allows a very high lateral resolution and is suitable to get simple topographic information. In **Figure 8**, a typical image obtained is displayed. The half width of the height histogram is 0.5 nm. The cantilever used is a budget Sensor Tap 300 with a resonance frequency equal to 300 kHz and a stiffness of 40 N/m. The amplitude reduction is equal to 0.95. The phase image is not displayed. Indeed, the sample is very homogeneous and no particular phase contrast is expected. Concerning the study of the topography of the film in dry state, QNM mode can also be used, giving very similar results as showed on the **Figure 9**.

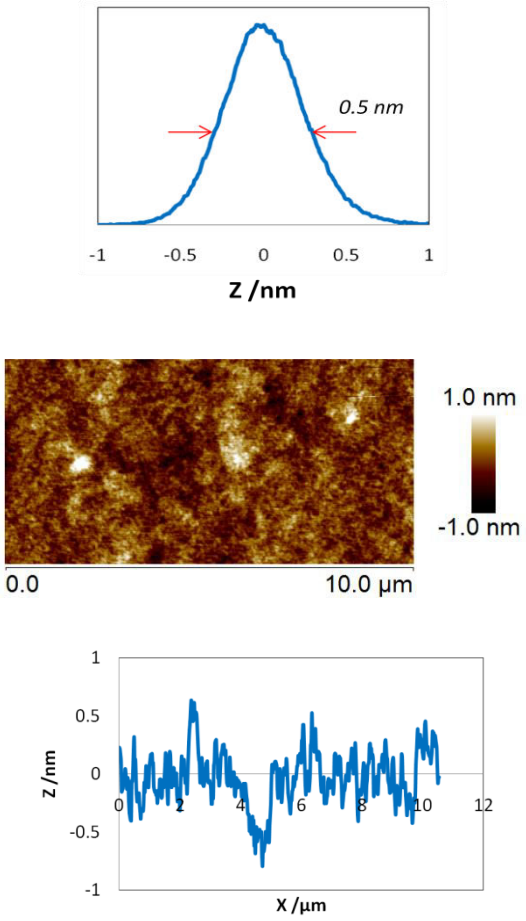


***Figure 8**: AFM images of SN233 (single network film with thickness equal to 233 nm) in air probed in tapping mode with a standard tapping cantilever (k = 40 N/m) and a resonance frequency equal to 300 kHz.*

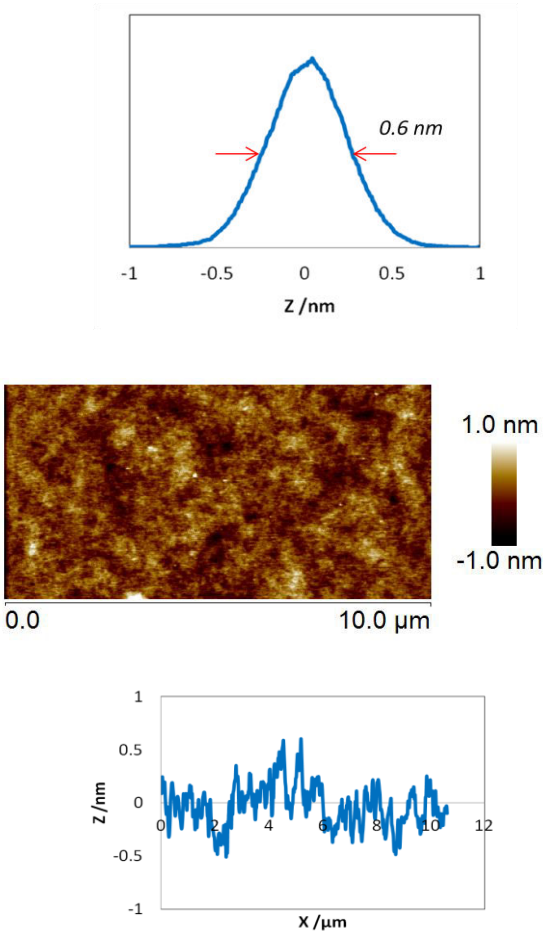


***Figure 9**: AFM topography image of SN182 in air obtained with QNM (force set point equal to 100 pN, the stiffness of the cantilever is equal to 0.06 N/m.*

2.2.2. In water: approach-retract curves

AFM is extensively used to image *in situ* soft matter in liquid state. In particular AFM has been employed to probe the topography of PNIPAM hydrogel films and its variation with temperature [6]. However, measuring the topography of hydrogels in water is rather more complicated than in air for several reasons. In our case, tapping experiments in water are avoided. Even if the tapping mode in water is usually expected, we believe that this experiment is not so easy to interpret; the main difficulty comes from the shape of the resonance curve of the cantilever excited in water. Two other techniques are then available: the contact mode and the QNM mode. Both could be suitable to measure the topography. But imaging a material as soft as a hydrogel film raises a fundamental problem: the stiffness of most standard AFM cantilevers is too high for the gel in liquid state. Using a cantilever with a stiffness k equal to 0.1 N/m, Kuckling et al. [7] showed that the cantilever indents the sample on a distance of 300 nm: the indentation δ can be almost equal to the height variation Δh. It means that in such conditions, the sample is crashed under the action of the cantilever during the measurement. What is then the meaning of the topography

measurement in these conditions? And how to observe a surface which is deeply modified by the AFM tip during imaging? The same problem is encountered by Ishida et al. [8] and Wiedemair et al. [9]. Montagne et al. [10] prefer to study the free surface with very soft cantilever (k = 0.06 N/m) with the amplitude modulation mode. Some authors, interested in mechanical properties of hydrogels used colloidal tips. It is then possible to extract properties such as the Young's modulus from approach-retract curves when experiments are made with colloidal modified tips (curvature radius of few micrometers) [7]. With this kind of tip, the Herzian model is used to obtain reliable values for the Young's modulus. But the imaging problem is not solved. Indeed, the use of a colloidal tip with large tip radius induces a loss of image resolution. In our study, we aim to evaluate the topography with different AFM techniques.

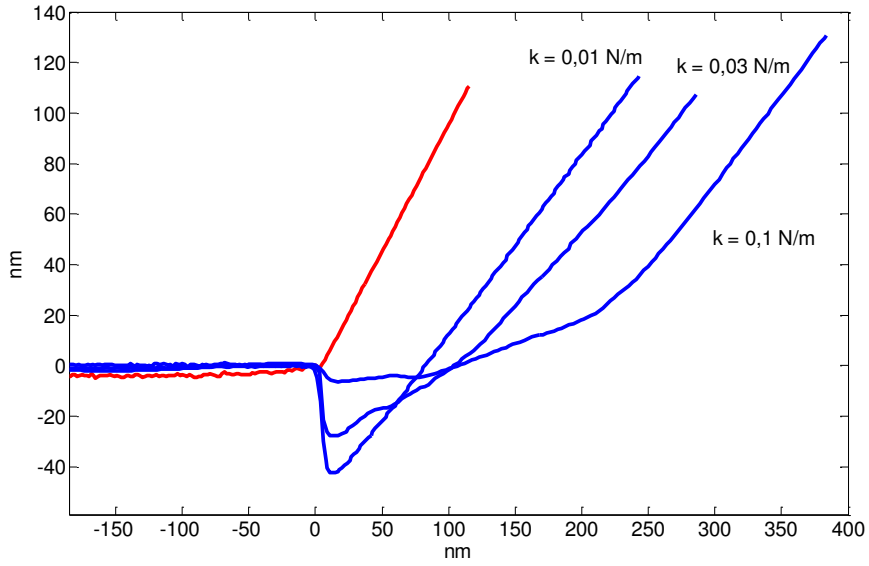
Effect of the stiffness of cantilevers

We checked the ability of the QNM mode to image the PNIPAM hydrogel films in water. In order to find out the proper conditions, different approach-retract curves are acquired on the sample SN237 in water at 25°C (**Figure 10**) with cantilevers of different stiffness. The red curve corresponds to the approach curve on a silicon wafer in water to calibrate the cantilever (the slope is equal to one by definition). Actually, for each cantilever, the exact calibration factor in nm/V is determined on a silicon wafer before approach-retract measurements on the hydrogel films in water. The value of the stiffness displayed in **Figure 10** is the one given by the probe manufacturer and was not independently measured.

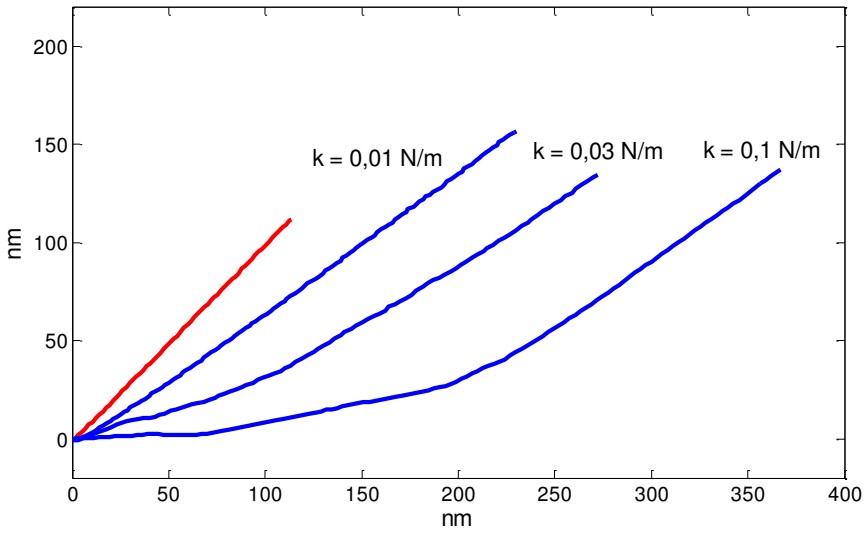
In **Figure 10a**, all curves have been positioned so that the contact point Δh_0 between the tip and the surface matches. On the **Figure 10b,** all the curves are superposed so that their points after the contact jump coincide (at this point, all the derivative $\Delta h'(\Delta d)$ are the same). We first note that the jump to the contact is higher than expected in water. This jump clearly depends on the stiffness of the cantilever: 40 nm for k = 0.01 N/m, 30 nm for k = 0.03 N/m and 5 nm for k = 0.1 N/m. We attribute this jump to an adhesion between the hydrogel-polluted tip and the surface of the hydrogel film. Just after the jump, we observe in all cases an indentation with constant force (contact stiffness equal to zero) on a range of 5 nm and then an increase of the contact stiffness. For high values of indentation, the slopes of the curves are equal to 0.7 nm/nm. For a value of k typically above 0.01 N/m, we observe two regimes of indentation, the second one corresponding to the same slope 0.7 nm/nm. This behavior is expected for PNIPAM hydrogel in water [11].

The same kind of experiment is carried out on the same sample with another set of cantilevers (**Figure 11**). The same results are obtained, except that a weaker adhesion is observed. The drawback is that the Δh_0 value corresponding to the contact between the tip and the surface is not precisely known. Indeed, no contact jump is observed for k=0.06 N/m.

The slope of the curve corresponding to a stiffness k = 0.06 N/m is about 0.6 nm/nm for a Δh height variation above 100 nm. These results are consistent with the previous ones, and the slopes are expected to be the same for Δh equal to more than 250 nm.



(a)



(b)

Figure 10*: (a) Approach curves acquired in water at 25°C at 1 Hz with cantilevers of different stiffness. The blue curves correspond to the approach on the PNIPAM hydrogel film SN237 (the swollen thickness h_w is 950 nm). The red curve corresponds to the approach on a silicon wafer. (b) The same curves are displayed with a different vertical positioning of the curves.*

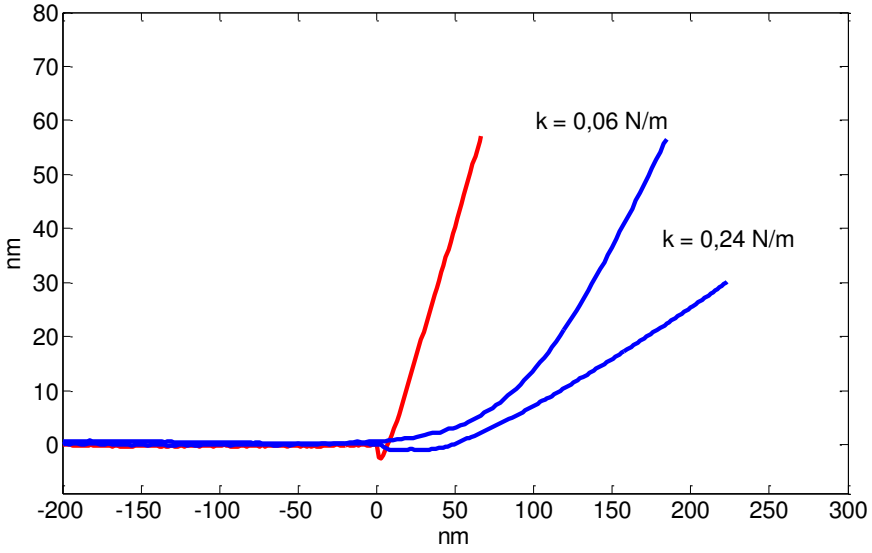


***Figure 11**: Approach curves acquired in water at 25°C at 1 Hz with cantilevers of different stiffness. The blue curves correspond to the approach on the PNIPAM hydrogel film SN237 (for which the thickness in air h_a is 237 nm and the swollen thickness in water is h_w is 950 nm). The red curve corresponds to the approach on a silicon wafer.*

Effect of the film thickness

A thinner PNIPAM hydrogel film SN42 is studied in the same way (**Figure 12**). The red curve corresponds to the rigid reference with a slope equal to 1 for all the stiffness. The dark-green curve (cantilever stiffness k = 0.5 N/m) shows two regimes: for high Δh values, the contact stiffness is infinitely rigid. It can be easily explained by the effect of the silicon wafer which is a rigid surface at a depth equal to 170 nm. For lower values of Δh, the indentation of the tip in the film is observed. It has to be noticed that even for very low cantilever stiffness k = 0.01 N/m, the film is indented. Moreover, the curve k = 0.03 N/m (light green) is very close to the curve k = 0.5 N/m (dark green). The same slope for all stiffness at high values of Δh is expected.

The results obtained on the thin film can be compared to those obtained previously on a thick film. The **Figure 12** shows that even a cantilever with a low k (0.01 N/m) indents the thin film. However two points have to be considered:

(i) The stiffness k is ill-defined in the range of low stiffness values (typically 0.02 N/m). The difference between the stiffness measured in air with a thermal tune and the value given by manufacturer can reach 100%.

(ii) There is precisely a critical value of stiffness around 0.01 N/m. Indeed, a cantilever with stiffness higher than this order of magnitude can definitely indent the hydrogel. For example, the approach curves obtained with a cantilever of stiffness k equal to

0.06 N/m are very similar whatever the film. *A contrario*, approach curves obtained with a labeled stiffness of 0.01 N/m present a high variability.

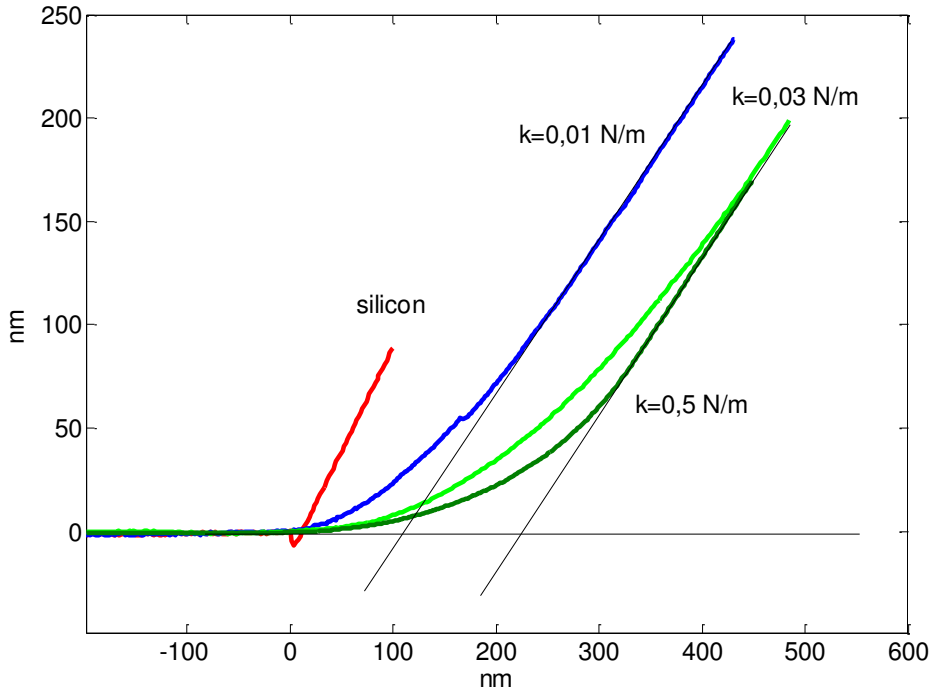


***Figure 12**: Approach curves on the PNIPAM hydrogel film SN42 (the thickness in air h_a is 42 nm and the swollen thickness in water h_w is 170 nm) acquired in water at 25°C at 1 Hz with cantilevers of different stiffness. Red curve: approach on a silicon wafer; blue curve: approach on the PNIPAM gel film with k = 0.01 N/m, light green: k = 0.03 N/m and dark green: k = 0.5 N/m.*

Effect of the frequency

In order to validate the QNM measurements, we performed the approach-retract curves at different frequencies varying between 0.1 Hz and 40 Hz and using a cantilever of stiffness k = 0.06 N/m (which is constant for different frequencies). The approach-retract curves are not readable above 40 Hz. On **Figure 13**, the red curve is typical of an approach curve: all approach curves obtained at different frequencies overlap. Retract curves for all frequencies (blue curves) are also very similar. The approach-retract curve at 80 Hz is not displayed but gives the same result. We conclude that the visco-elastic effects do not depend on the solicitation frequency in the range 0.1 Hz – 80 Hz. Secondly, approach and retract curves match for all frequencies indicating that visco-elastic effects are weak.

The same kind of experiment can be done on the same sample, using another value of stiffness. The result is displayed on the **Figure 14**. Using a cantilever of stiffness 0.03 N/m (MLCT Bruker), approach-retract curves display visco-elastic effects and adhesion effects.

The difference between the **Figure 13** and **Figure 14** can be explained as following: in the case of **Figure 14**, the stiffness reaches a critical value for which visco-elastic effects begin to appear. It means that the approach curve and retract curve no longer match. The jump to contact of the tip during approach is attributed to a polymer pollution of the tip. Moreover, even if visco-elastic effects could depend on the frequency, the **Figure 14** indicates that they are not. However, the adhesion effects strongly depend on the frequency.

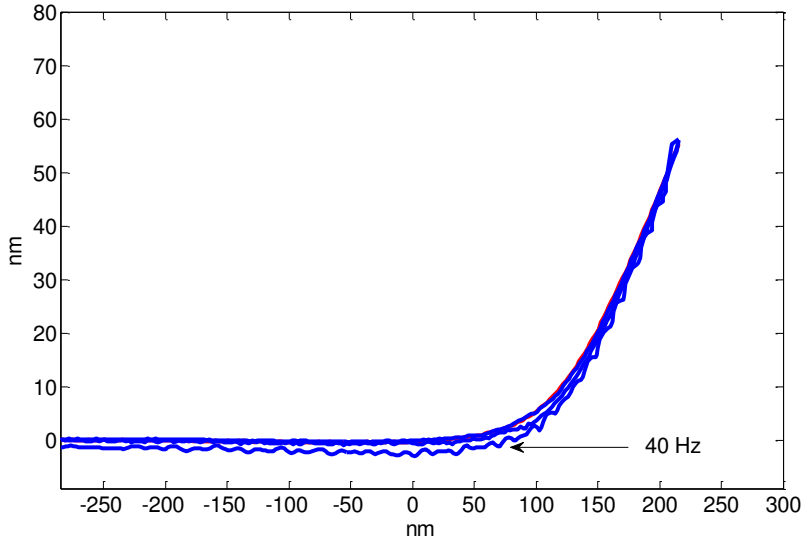


***Figure 13**: Approach-retract curves on the PNIPAM hydrogel film SN237 acquired in water at 25°C with different frequencies (0.1 Hz up to 40 Hz), using a cantilever of stiffness k = 0.06 N/m. The red curve corresponds to approach curve and the blue curves correspond to retract curves.*

This frequency study of approach-retract experiments are very useful to validate QNM experiment: indeed, the base of a QNM experiment is a succession of approach-retract experiments at high frequency (1kHz), so that we must know the response of the hydrogel under a solicitation at this frequency. It will be assessed in this study that the behavior at 1 kHz is not drastically different from the behavior at lower frequency. This argument is supported by the results from **Figure 13** and **Figure 14** showing that between 0.1 Hz and about 100 Hz (3 decades), the visco-elastic effects do not depend on the frequency. Another conclusion is that the study of the topography by AFM results from a compromise between several effects. If the stiffness of the cantilever is higher than 0.03 N/m, the hydrogel surface is highly indented. If the stiffness is too weak, the dominating adhesion effects and the visco-elastic effects can prevent from obtaining a reliable image. Images should be ideally acquired with a cantilever of stiffness lower than 0.03 N/m. However, the pollution of the tip after a first contact with the sample is difficult to avoid inducing difficulties to perform a QNM

experiment. Knowing all these problems, we now aim to properly evaluate the roughness of the free surface in water.

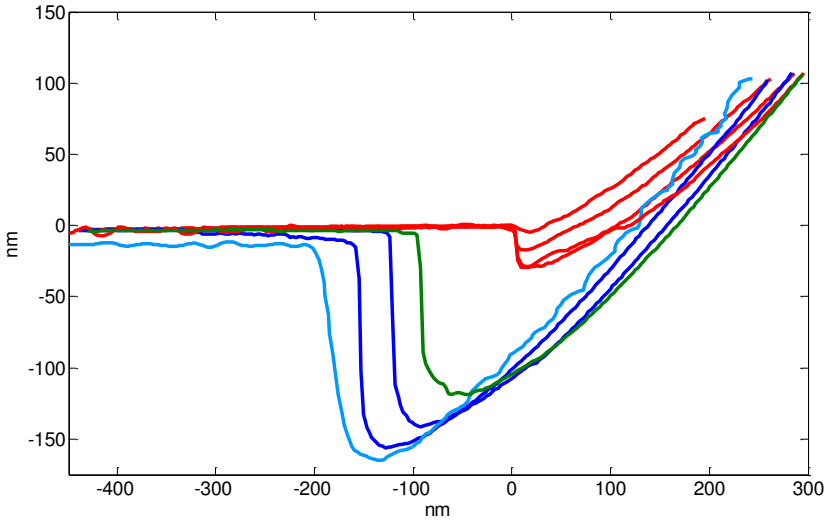


***Figure 14**: Approach-retract curves on the PNIPAM hydrogel film SN237 acquired in water at 25°C with different frequencies (0.1 Hz up to 80 Hz), using a cantilever of stiffness k = 0.03 N/m (MLCT Bruker). The red curves correspond to the approach curves, the green curve to the 0.1 Hz retract curve with 0.1Hz and the light blue to the retract curve with 80 Hz.*

2.2.3. Topography in water

Effect of the cantilever stiffness on images obtained in contact mode

The effect of cantilever stiffness on height images is investigated. The **Figure 15** gathers two images acquired in contact mode with the same feedback set point value (which corresponds to a vertical deviation of 10 nm). The **Figure 15** perfectly illustrates how the stiffness of the cantilever affects the height distribution, the measured roughness and the resolution. Using a cantilever of high stiffness leads to an under-estimation of the roughness of a factor 2. Actually, we find a half width of the height histogram equal to 6.0 nm for the stiffness k = 0.01 N/m and equal to 2.5 nm for k = 0.1 N/m. As expected from the results of the section 1.2.2 (approach-retract curves), the distribution of the height depends on the stiffness: with a value of k = 0.1 N/m, the indentation value can easily reach a value of 200 nm. Using the contact mode with very soft cantilever would be suitable to probe the surface of PNIPAM hydrogel films in water.

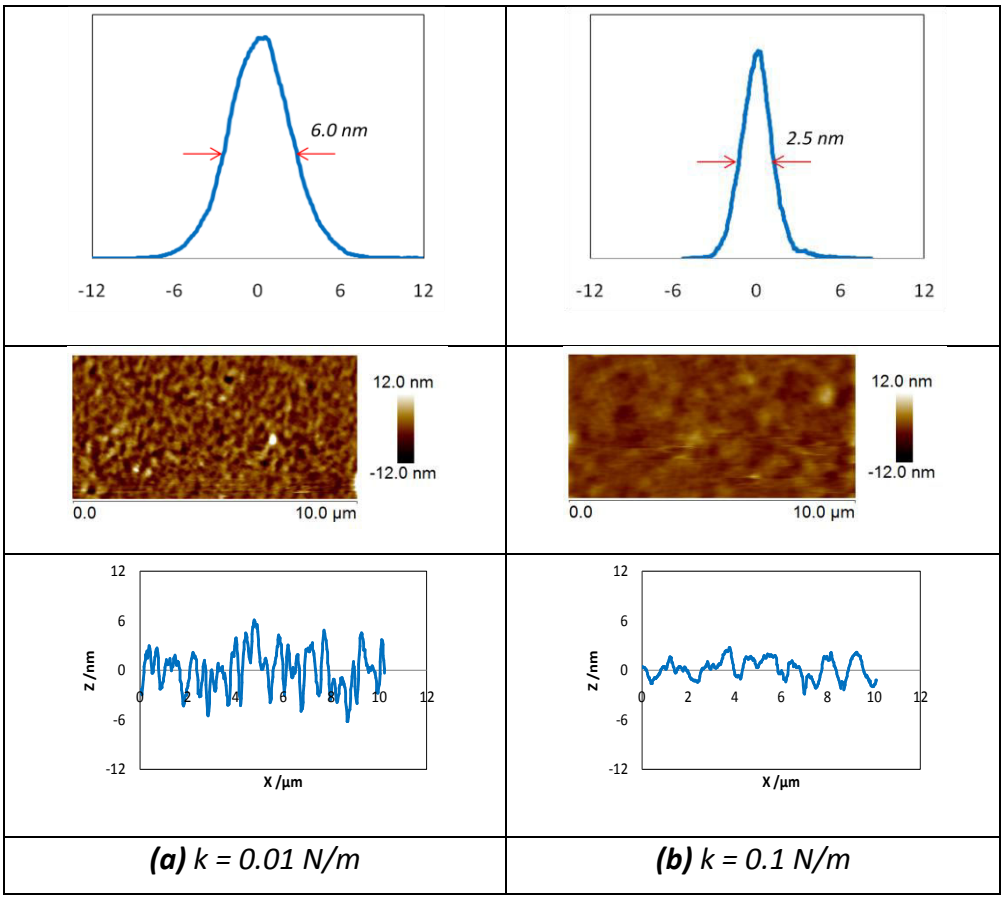
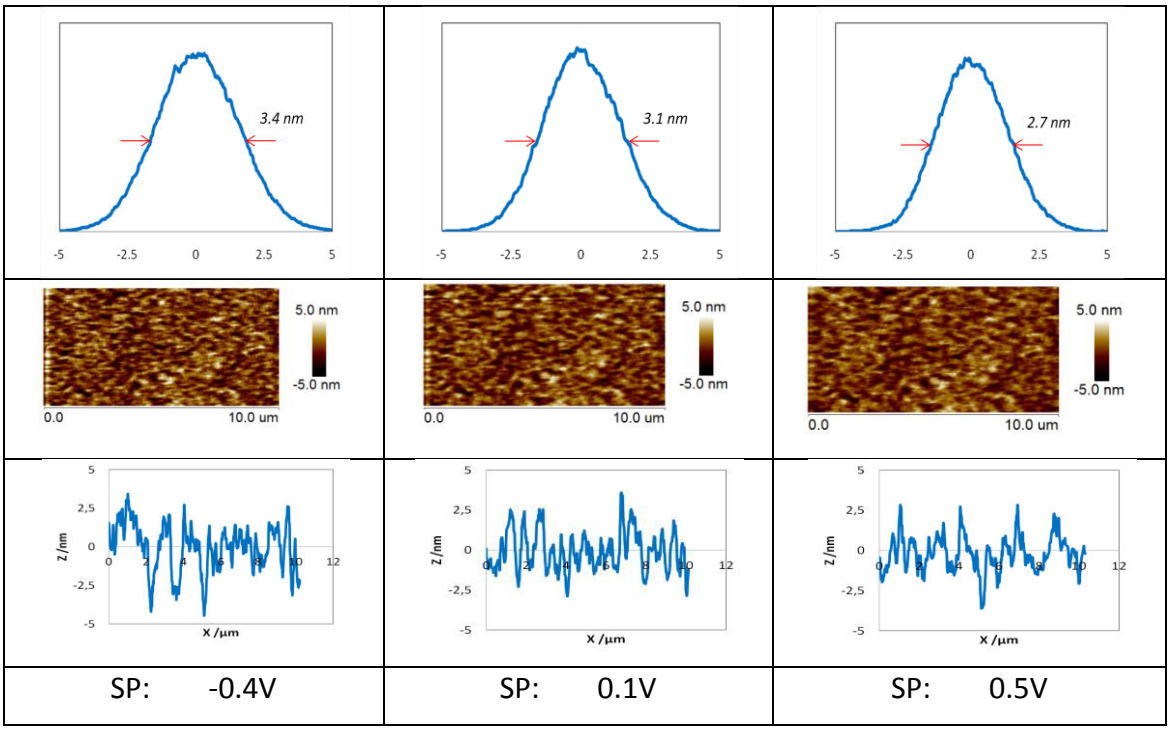


***Figure 15**: AFM contact images of SN237 acquired in water at 25°C (the swollen thickness h_w is 950 nm) with a cantilever of stiffness k = 0.01 N/m (a) and k = 0.1 N/m (b). The feedback set point equal to 0.3 V is the same for both experiments.*

Effect of the set point in contact mode

The effect of the stiffness on the evaluation of the roughness has been evidenced in the previous section. We now have to check the dependence of the roughness as a function of the applied force, for a given stiffness. For this purpose, height images in contact mode with different values of set point using a cantilever of stiffness k = 0.05 N/m are displayed in **Figure 16**. The set point value has a weak effect on the height distribution.



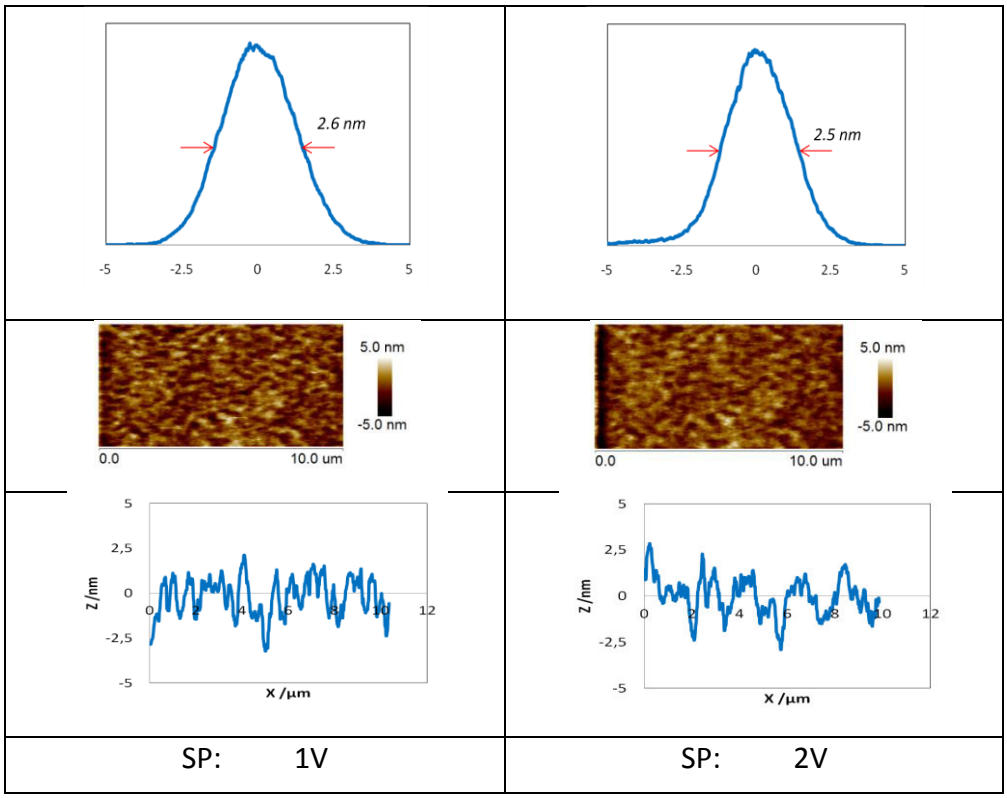


***Figure 16**: AFM contact images of SN182 in water at 25°C (the swollen thickness h_w is 750 nm) probed with different set point values using a cantilever of stiffness k = 0.05 N/m. SP: setpoint.*

Effect of the cantilever stiffness in QNM mode

The same area of the same sample was probed in QNM mode with a cantilever stiffness of

0.5 N/m, which is much higher than that in contact mode. The height image is displayed **Figure 17**. Surprisingly, the height distribution is of the same order of magnitude as that obtained in contact mode with low k, the half width of the height histogram being equal to 6.5 nm. As a result, the QNM mode seems to be appropriate to probe the surface of PNIPAM hydrogel films in water. In comparison with the contact mode, it is expected to find an under-estimated roughness for high stiffness in QNM mode, which is not the case.

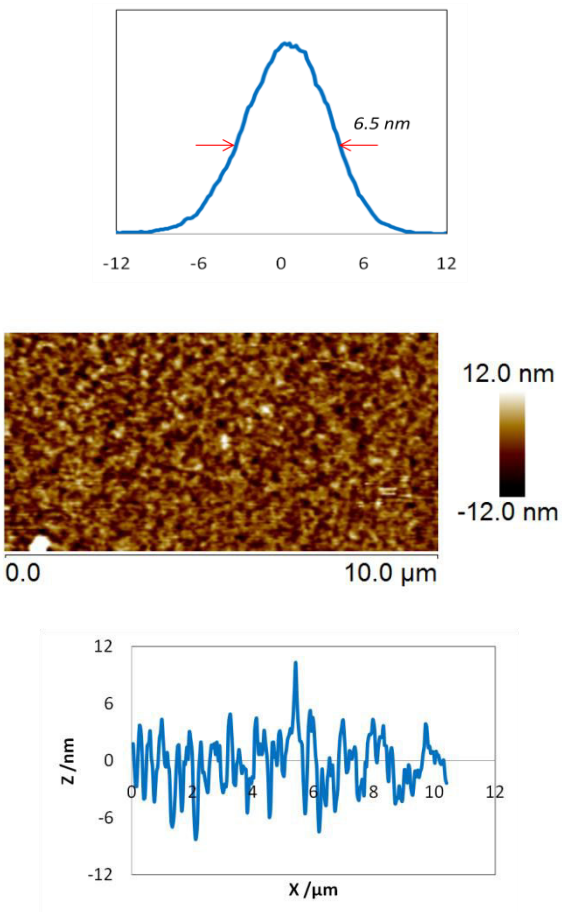
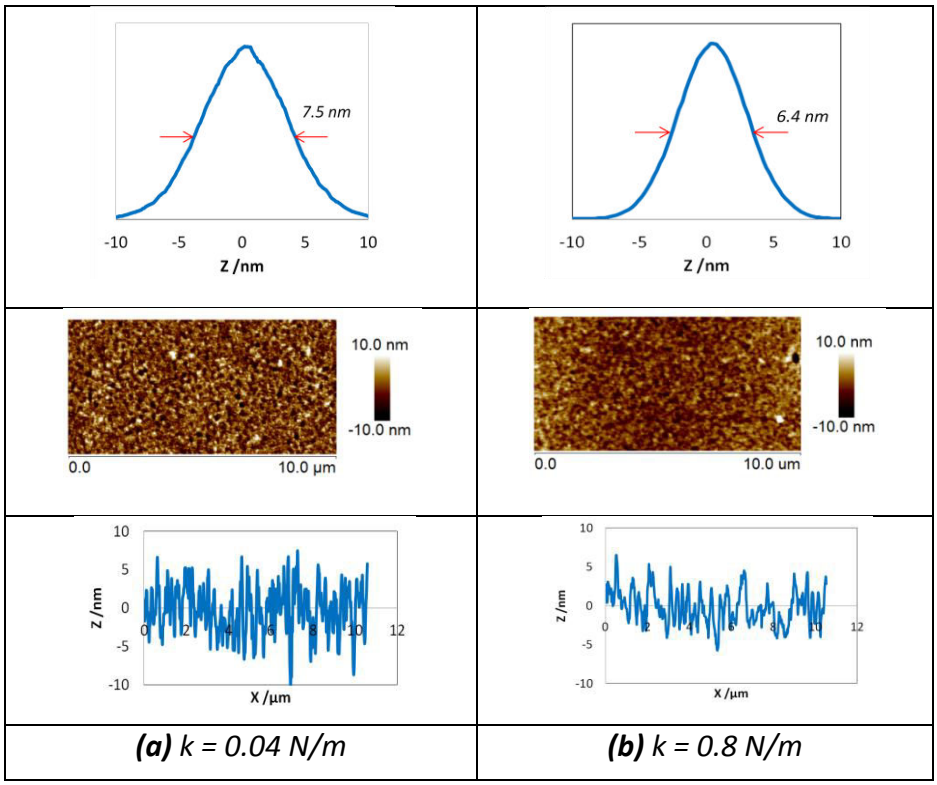


***Figure 17**: AFM QNM images of SN237 acquired in water at 25°C (the swollen thickness h_w is 950 nm) with a cantilever of stiffness k = 0.5 N/m and the feedback set point equal to 0.3 V (about 4 nN in force).*

The imaging conditions have to be fully optimized: the roughness found in QNM found can also depend on the stiffness of the cantilever in the same way as for contact mode.

Experiments were then carried out in QNM mode with a cantilever of lower stiffness (k = 0.04 N/m). In **Figure 18**, the height images (with the height histogram) obtained with cantilevers of stiffness k = 0.04 N/m and k = 0.8 N/m are compared. In the same conditions, the half width of the height histogram is 7.5 nm for k = 0.04 N/m while 6.4 nm for k = 0.8 N/m. We can conclude that the order of magnitude of the roughness obtained with QNM is not so dependent on the imaging conditions.



(a) *k = 0.04 N/m* | ***(b)*** *k = 0.8 N/m*

Figure 18*: AFM QNM images of SN182 probed in water at 25°C (the swollen thickness h_w is 750 nm). The images are obtained at the same area on the surface. (a) The image is obtained with a stiffness of 0.04 N/m. (b) The image is obtained with a stiffness of 0.8 N/m.*

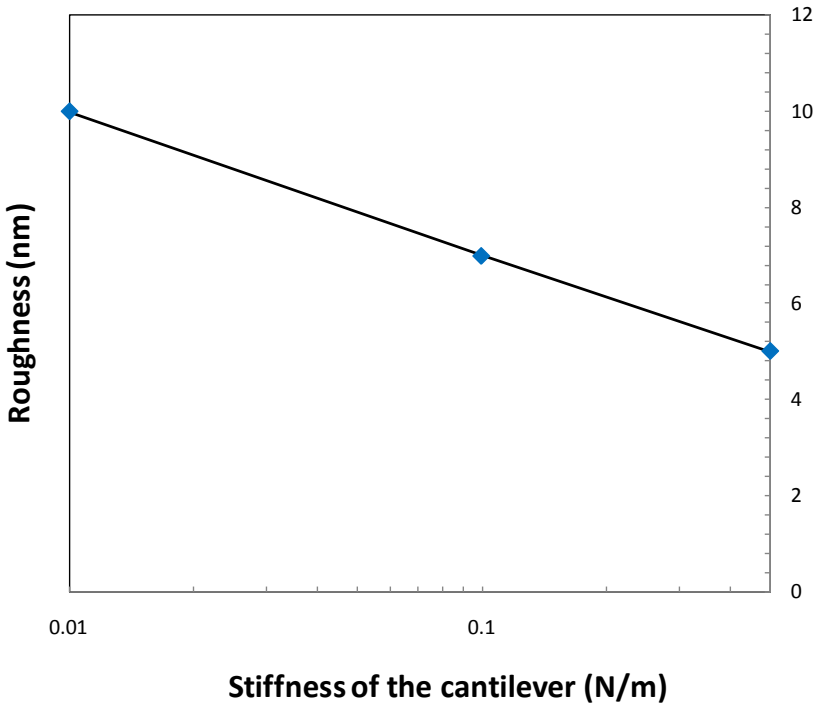


Figure 19*: QNM Rroughness measured on the hydrogel surface versus the stiffness of the cantilever used to acquire the QNM images. The sample is SN249 immersed in water at 25°C.*

More precisely, the **Figure 19** shows that if the value of the stiffness used to image the surface decreases of one order of magnitude, the QNM roughness increases of about 3 nm. Even it would be possible to use a cantilever softer than 0.01 N/m, the roughness would be close to the value obtained by our experiments.

Experiments with different set point value using a cantilever with stiffness equal to 0.05 N/m were also carried out to determine its effect on the topography (**Figure 20)**. The patterns observed are the same and the width of the height histogram around 4 nm is comparable for all conditions. The height images obtained do not depend on the set point value so that it is a proof that the experiments are properly carried out with suitable conditions.

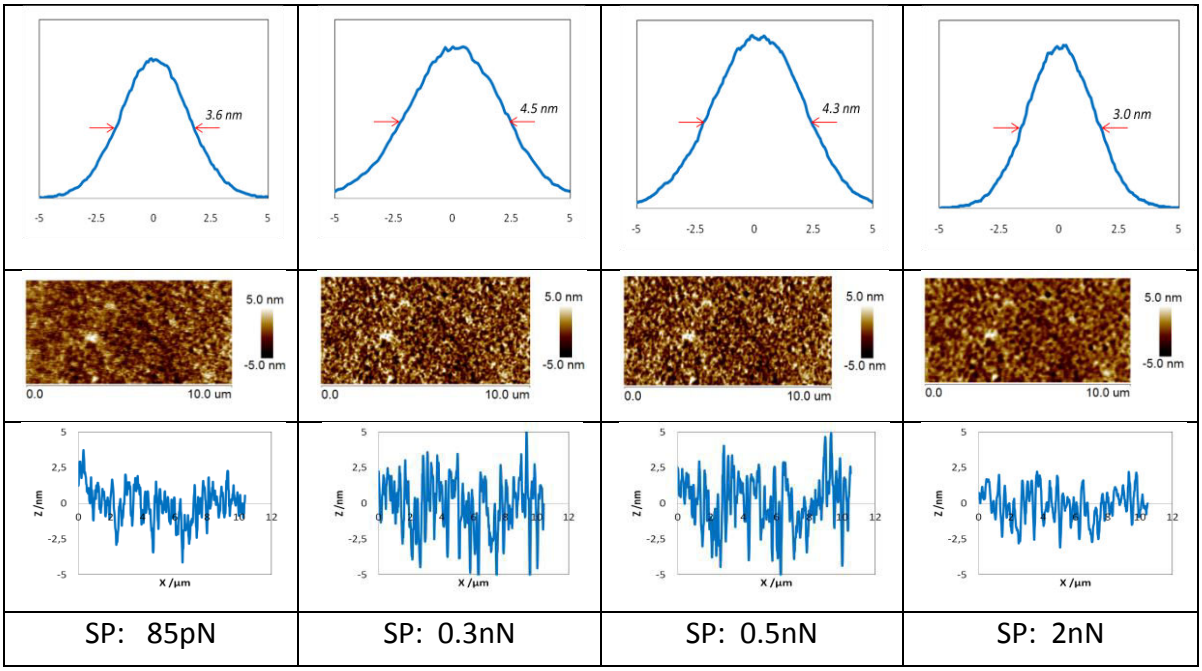


***Figure 20**: AFM QNM images of SN182 in water at 25°C (the swollen thickness h_w is 750 nm) probed with different set point values using a cantilever of stiffness k = 0.05 N/m. All the images are obtained at the same area on the surface. SP: setpoint.*

2.3. Topography of PNIPAM hydrogel films in air

PNIPAM single network films with different thickness are probed by AFM in air. The typical observed morphology is shown on **Figure 21**: seven different samples have been studied in air; for each observation, several areas were investigated. No particular pattern shows up except randomly distributed shallow holes. The half width of the height histogram found is around 0.6 nm. It can be noticed that the images obtained with a scan size of 20 micron present the same roughness value of 0.6 nm. The same morphology and the same value of half width are obtained in QNM mode using cantilevers with different stiffness, from 0.05 N/m to 40 N/m. This morphology was also observed by Montagne et al. [10].

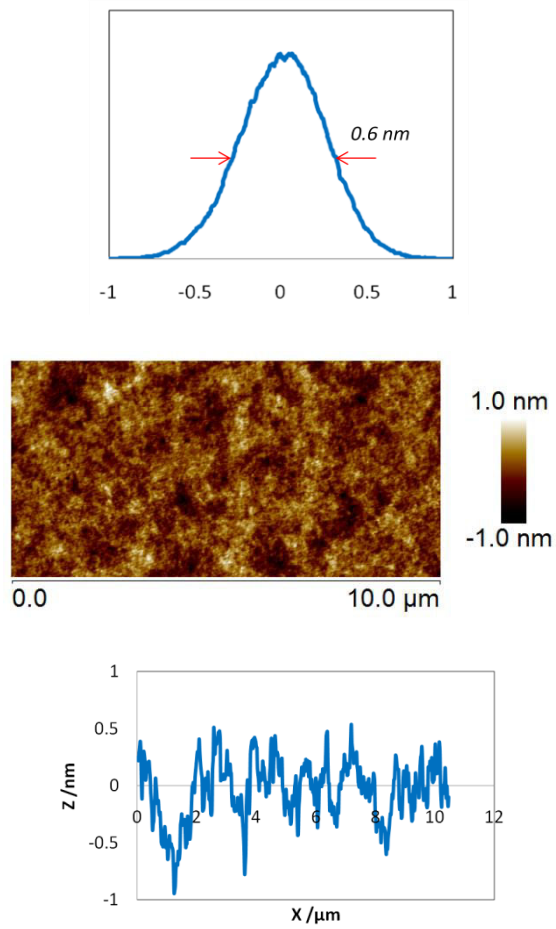


***Figure 21**: height AFM tapping image of SN239 (with thickness in air h_a equal to 239 nm) in air obtained with a cantilever of stiffness k = 40 N/m.*

Most of the samples have no particular patterns. Nevertheless on some samples the holes are clearly observable (**Figure 22 (a)**). In this case, the width of the height histogram is higher than the value of 0.6 nm obtained with the previous morphology. However, in all cases, the width of the height histogram remains under 5 nm. The morphology with holes has already been observed on similar systems by Beines et al. [12].

The **Figure 23** shows the height image and the height histogram for thinner films (with thickness in air h_a equal to 36 nm and swollen thickness in water h_w equal to 150 nm). The morphologies observed – no particular patterns - are similar to those obtained with thick films. The width of the histogram is 0.8 nm.

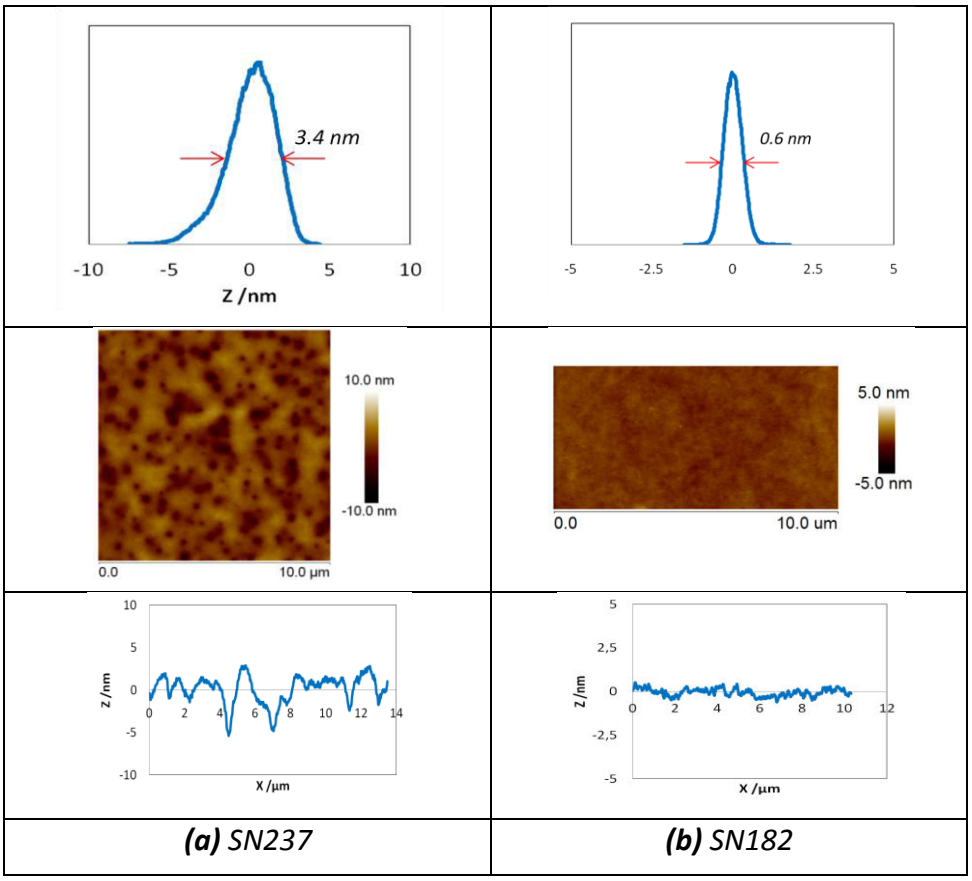


***Figure 22**: AFM QNM images of SN237 (a), and SN182 (b) probed in air with the same peak force set point (100 pN) using a cantilever of stiffness k = 0.06 N/m.*

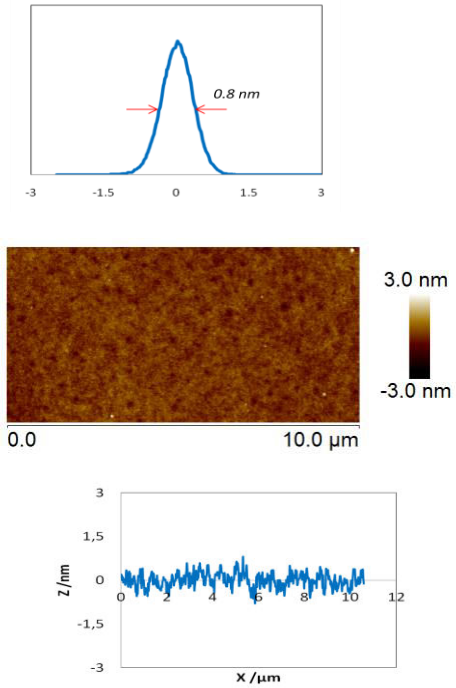
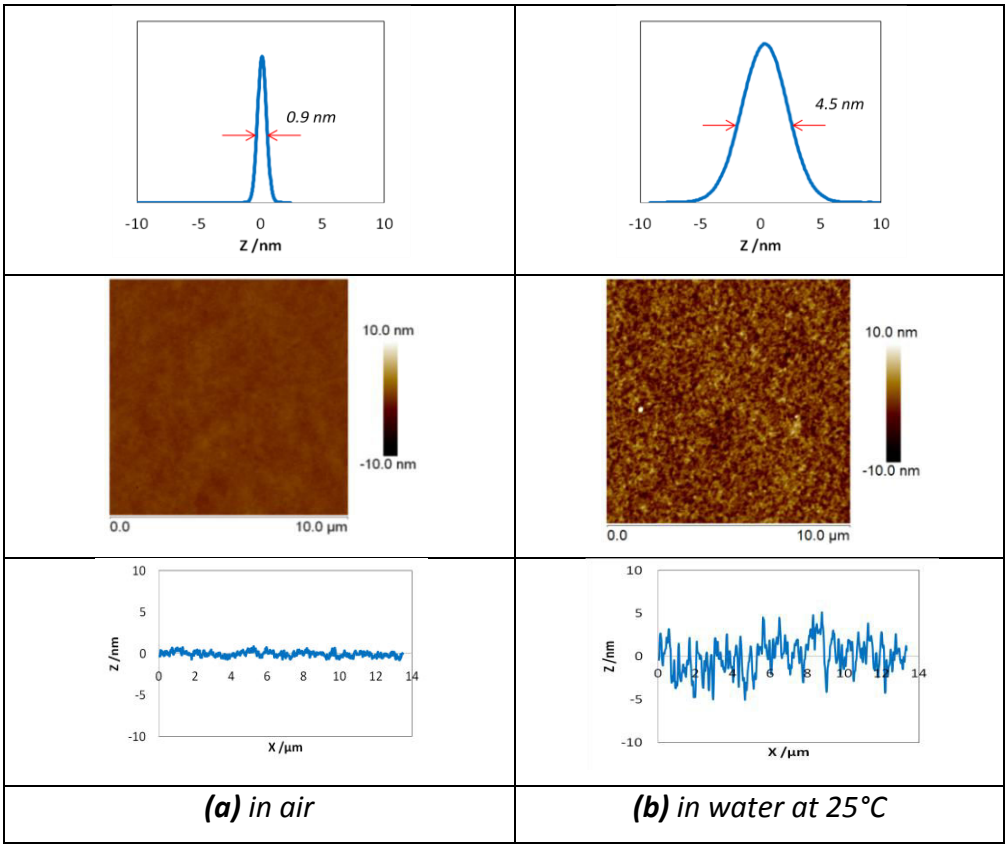


***Figure 23**: Height AFM QNM image of SN36 acquired in air with a cantilever of stiffness k = 0.18 N/m.*

2.4. Topography of PNIPAM hydrogel films in water

2.4.1. Thick fims

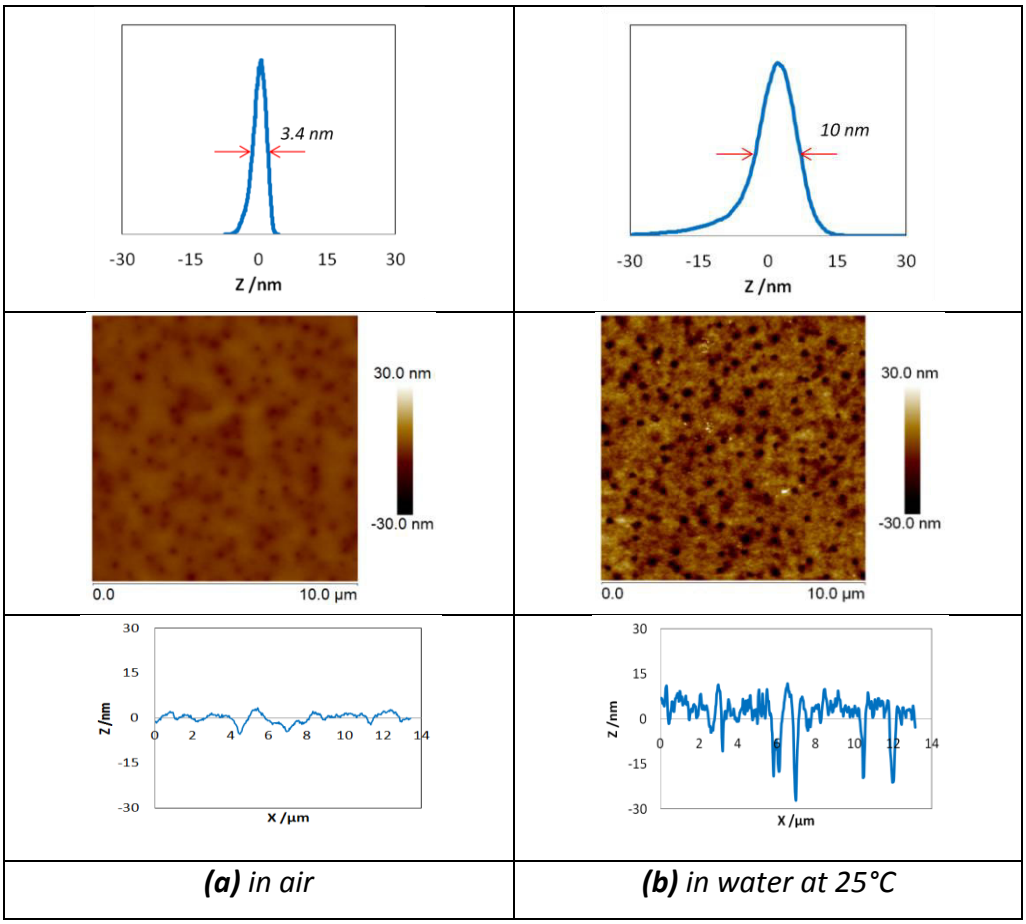
In order to study the effect of the swelling on the surface, we acquire images of the free surface in water at 25°C (below the LCST of the PNIPAM). The height images and the height histograms of PNIPAM hydrogel films in air and in water are displayed on the **Figure 24**. The images in air and in water obtained by QNM are compared. It is showed that if no pattern is observed in air, then there is no pattern in water. The same observation was also made by Montagne et al. [10] using tapping mode in water and by Ishida et al [8]. But the roughness (here defined by the width of the height histogram) in water is 4.5 nm which is 5 times the roughness measured in air for the same scan size of 10 microns. The increase of the roughness is consistent with the swelling of PNIPAM hydrogel films in water (the ratio of swelling is around 3 as shown in part 1). The swelling of the hydrogel emphasizes the irregularities at the free surface. Nevertheless, the roughness is weak (with FWHM around 4.5 nm) in comparison with the thickness of the swollen film (close to 1 micron). One of the aim of this chapter is to answer the question: do we observe any change in morphology due to lateral stress? It seems that the swelling is rather homogeneous and axial.



***(a)** in air* | ***(b)** in water at 25°C*

***Figure 24**: AFM QNM images of SN249 in air (a) and in water at 25°C (b) probed with a cantilever of stiffness k = 0.7 N/m.*

PNIPAM hydrogel films with morphology of hole-like patterns are also studied in water. As shown in **Figure 25,** the distribution and the size of the holes remain almost the same in water as in air. As expected, the holes become deeper when films are immersed in water, which yields to a histogram width of 10 nm. The swelling of the hydrogel leads to an increase of the roughness or an enhancement of the irregularities of the free surface, which is observable with the increase of the width of height histogram. On the contrary, the (lateral) size of the holes does not greatly change with the swelling of the hydrogel film. Indeed, if the holes grow 3 or 4 times in agreement with the (vertical) swelling ratio, it should have been detectable. It demonstrates that the swelling of the hydrogel is rather vertical than horizontal, which is consistent with the constraints of the covalent attachment of the hydrogel to the surface.



***(a)** in air* | ***(b)** in water at 25°C*

***Figure 25**: AFM QNM images of SN237 in air (a) and in water at 25°C (b) probed with a cantilever of stiffness k = 0.06 N/m.*

Experiments on the same sample with two different set point values using a soft cantilever (stiffness of 0.05 N/m) were also carried out to determine its effect on the topography (**Figure 26)**. The same hole-like patterns are observed with a similar width of the height histogram around 8 nm.

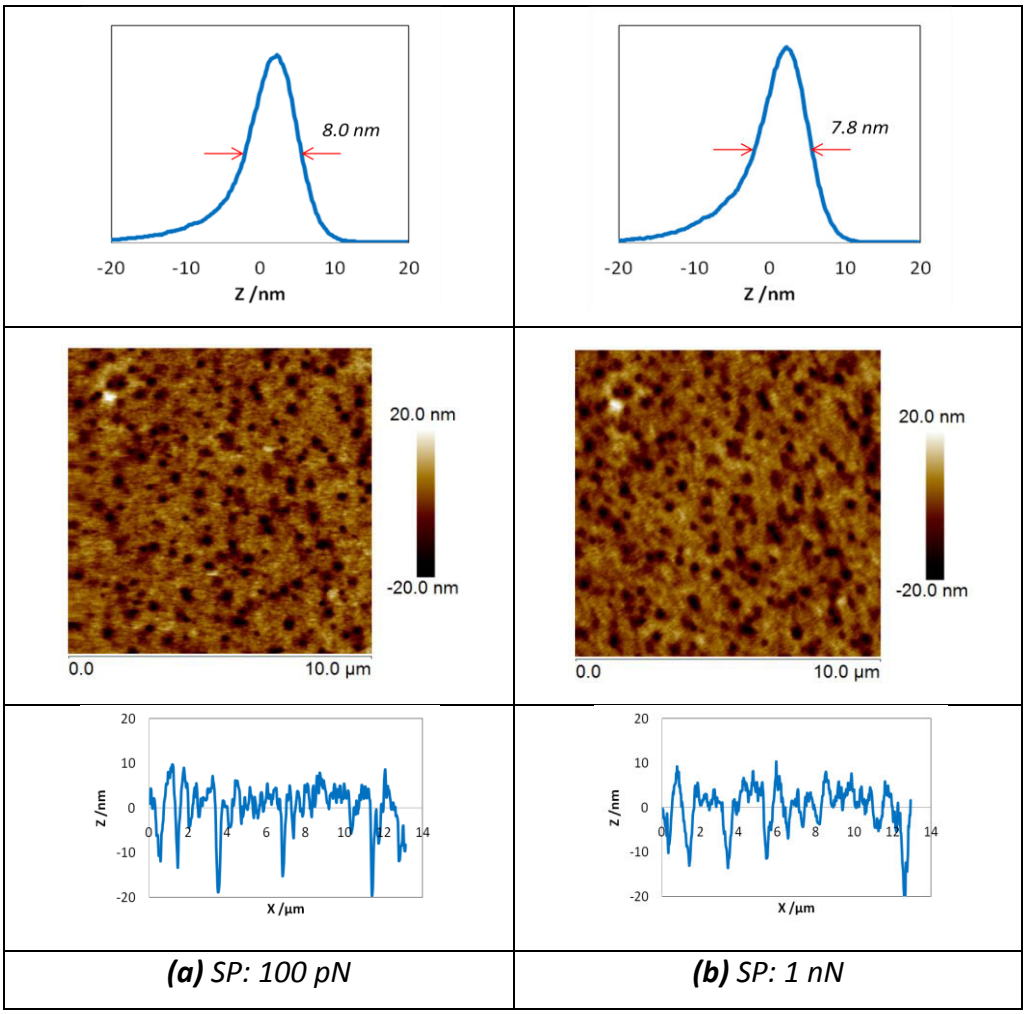


***Figure 26**: AFM QNM images of SN237 in water at 25°C (the swollen thickness h_w is 950 nm) probed with two different set point values using a cantilever of stiffness k = 0.06 N/m. Both of the images are obtained at the same area on the surface. SP: setpoint.*

2.4.2. Thin films

Thin PNIPAM hydrogel films are studied in water in both contact mode and QNM mode. The example shown in **Figure 27** and **Figure 28** is a film with a swollen thickness of 150 nm. However, the topography obtained is the same for all experiments and the reduced images shown are just necessary for the determination of the height histogram and the cross-sectional plot. The morphology observed with no particular patterns is the same as that observed with thick films. The values obtained both in contact mode and in QNM mode are about 2.5 nm for an image of scan size equal to 10 micrometer. These values are similar to those obtained on thicker films for which the swollen thickness of the hydrogel film is close to 1 micron.

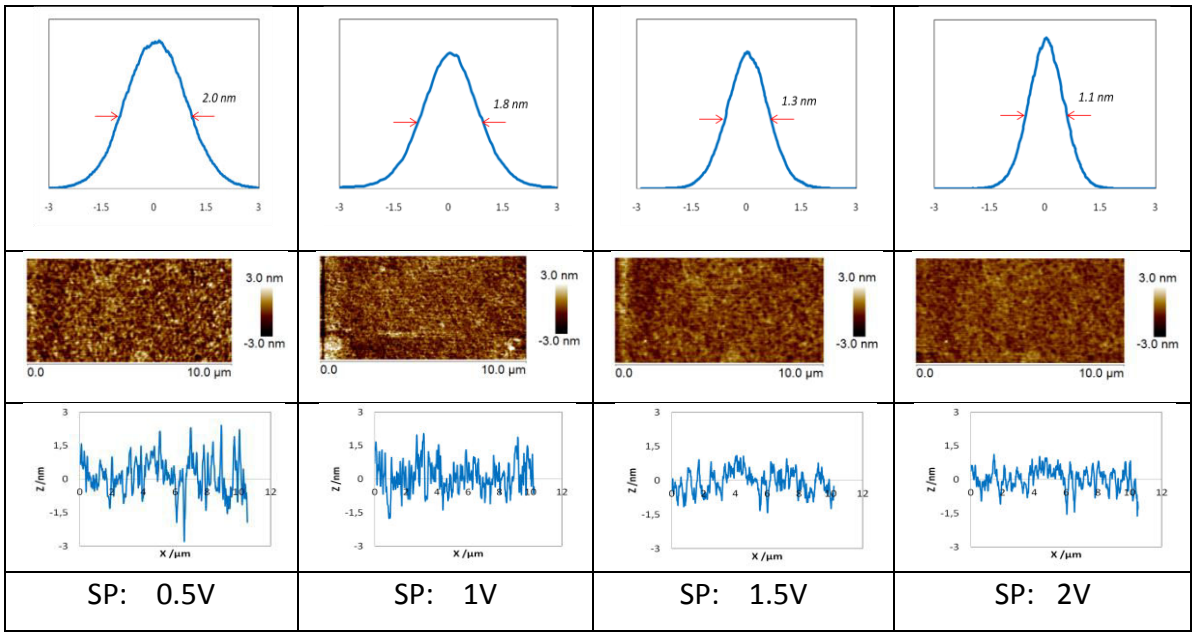


***Figure 27**: AFM contact images of SN36 in water at 25°C (the swollen thickness h_w is 150 nm) probed with different set point values using a cantilever of stiffness k = 0.18 N/m. All the images are obtained at the same area on the surface. SP: setpoint.*

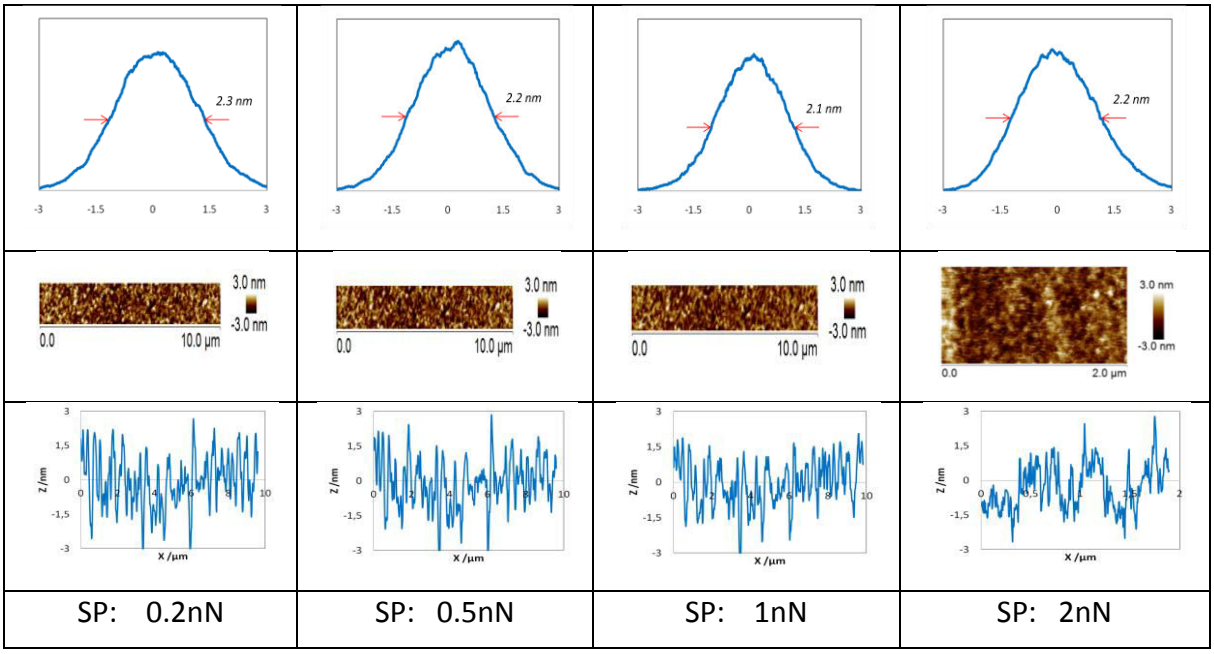


***Figure 28**: AFM QNM images of SN36 in water at 25°C (the swollen thickness h_w is 150 nm) probed with different set point values using a cantilever of stiffness k = 0.18 N/m. All the images are obtained at the same area on the surface. SP: setpoint.*

2.5. Effect of temperature

The effect of temperature on the morphology of the free surface of the PNIPAM hydrogel films in water was investigated. The temperature is varied from 25°C (below the LCST) to

42°C (above the LCST) to determine the influence of the phase transition on the morphology. As shown in **Figure 29**, the width of the height histogram decreases from 4.5 nm to 1.6 nm with the rise of temperature from 25°C to 42°C. The width at 42°C is consistently much closer to the value observed in air. Above the LCST, the PNIPAM hydrogel collapses so that the irregularities of the free surface are reduced. These results are comparable to those found by other groups on PNIPAM films [6, 7, 13, 14].

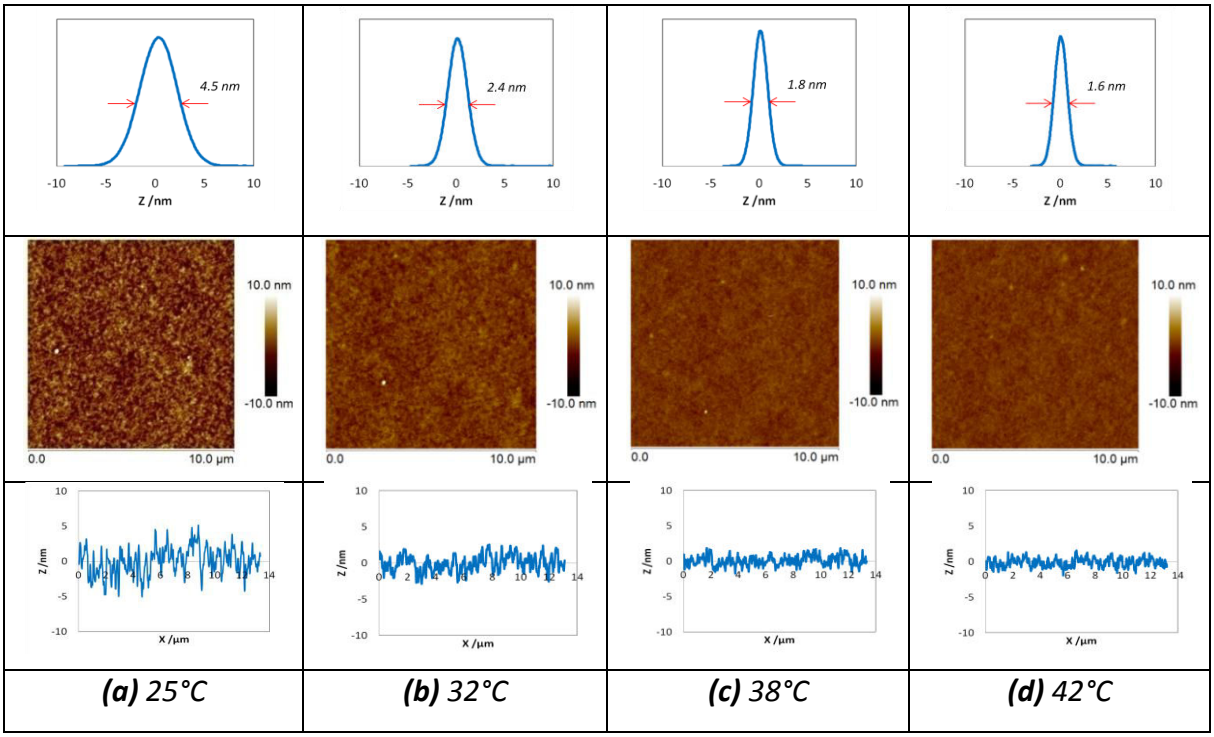


***Figure 29**: AFM QNM images of SN249 in water at different temperatures (a) 25°C, (b) 32°C, (c) 38°C and (d) 42°C probed with a cantilever of stiffness k = 0.7 N/m at the same area on the surface.*

Figure 30 shows the variation of the width of the height histogram with the study temperature. The width decreases with the rise of temperature. The maximum is reached at 25°C below the LCST with the swollen hydrogel film. Nevertheless, the average value found is very weak since it is lower than 5 nm for films with thickness close to 1 micron. As temperature increases, the PNIPAM hydrogel swells to a progressively smaller degree so that the width of height histogram decreases.

PNIPAM hydrogel films with morphology of hole-like patterns are also studied in water at different temperatures. As shown in **Figure 31,** the distribution and the size of the holes remain almost the same. The width of the height histogram decreases from 10 nm to 5.3 nm for increasing temperature to come close to the value obtained in air. The comments on the variation of the (vertical) roughness and the sameness of the (horizontal) size of the holes provided for the comparison between the experiments in air and in water at 25°C are also

applicable when comparing the swollen hydrogel at 25°c and the collapsed state at 42°C. The swelling of the hydrogel is rather vertical than horizontal.

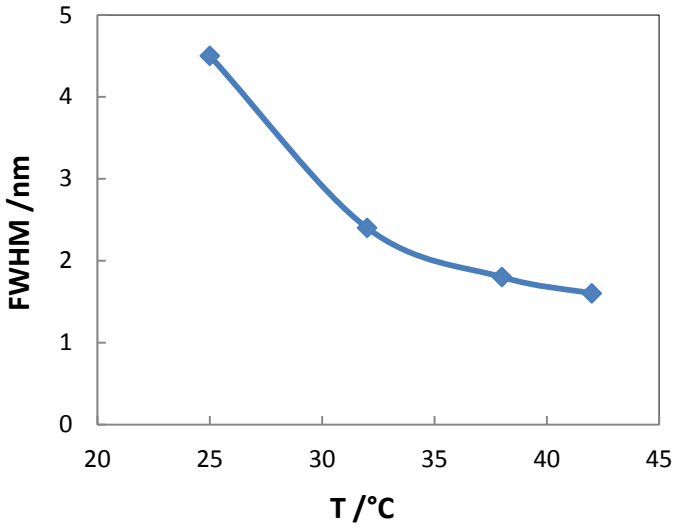


***Figure 30**: Full width at half maximum (FWHM) of height histogram as the function of temperature for SN249 in water.*

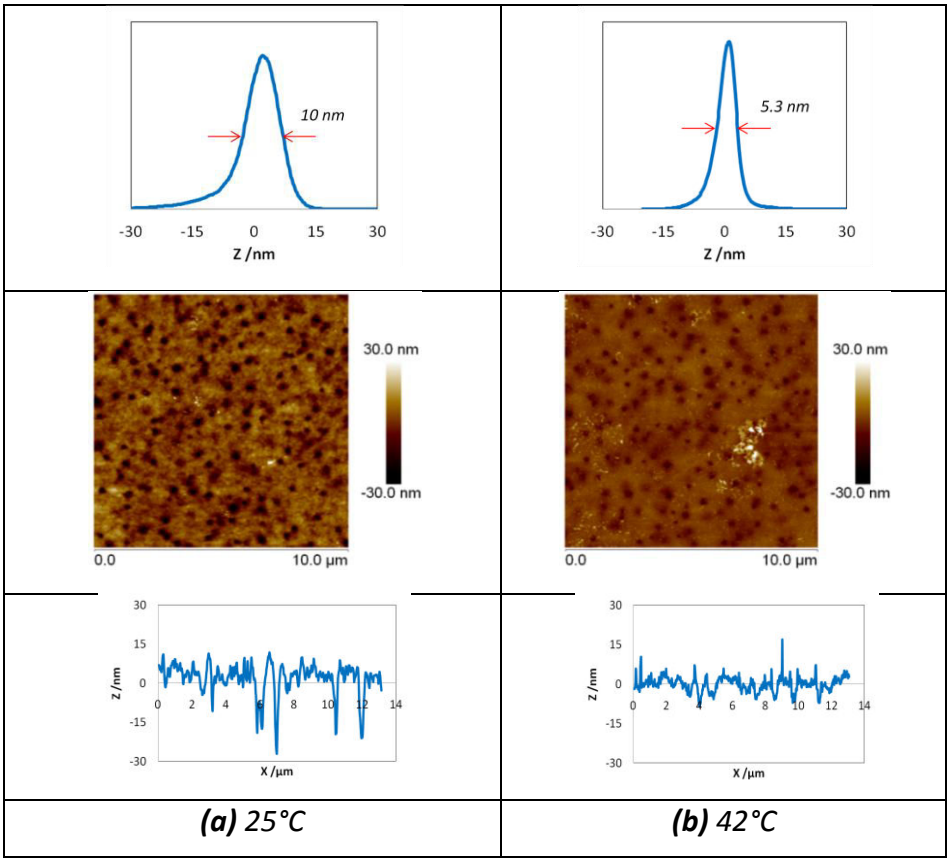


***Figure 31**: AFM QNM images of SN237 in water at different temperatures (a) 25°C, (c) 42°C probed with the same peak force set point (300 pN) using a cantilever of stiffness k = 0.06 N/m at the same area on the surface.*

2.6. Conclusion

Appropriate conditions were found to probe properly the free surface of the hydrogel films in air and in water. High resolution tapping mode is perfectly suitable for the study of gel films in air. For the studies in water, we evidenced that the value of the stiffness used for imaging the surface of hydrogel is a key parameter for the measure of the roughness. This has been clearly confirmed by contact mode images. We proposed a method to properly measure the roughness of hydrogel in water with the AFM QNM mode. The use of cantilevers of low stiffness (ideally less than 0.03 N/m) is required for the study in water as the hydrogel film is very soft with Young's modulus lower than 100 kPa.

The morphology of all hydrogel films shows no particular patterns and no structure. Some samples display shallow holes. The depth contrast between holes and the surface is accentuated when the hydrogel films are swollen in water. The hydrogel films are flat, the roughness being small in comparison with the thickness of the film. In air, the values of the width of the height histogram are a few nanometers for 300 nm-thick films for images of 10 microns-size. For swollen hydrogel films in water, the width of the height histogram is at the maximum 10 nm for images of 10 microns-size (holes-like morphologies) while the thickness of the films can reach 1 micron. We also observe an effect of temperature on the roughness of the surface, with a decrease of the width of the height histogram at high temperatures above the LCST for collapsed hydrogels.

The last point is that the topography of the free surface seems to demonstrate that the swelling of the hydrogel is rather vertical (in the z direction perpendicular to the surface) than horizontal (in the x-y plane). The comparison between the experiments in air and in water indicates that the swelling leads to an increase of the (vertical) roughness while it has no obvious effect on the (horizontal) size of the irregularities. It is consistent with the covalent attachment of the hydrogel to the surface.

3. Density profile of monomers

Neutron reflectivity was also used to characterize the gel films in air and in water. This technique allowed the determination of the composition of the film, its thickness and the width of the free interface of the gel layer. The density profiles of monomers in the direction perpendicular to the surface could be then deduced.

As explained in detail in the annex, the analysis of the neutron reflectivity consisted of fitting the best the data experimental data with a model of layers characterized by a scattering length density Nb_i, a fixed thickness h_i for the layer i and a width σ_i which connects two adjacent layers. As the reflectivity decreases sharply with the wave vector (as k^{-4}), the log-log

representation was usually preferred. This representation allows a better evaluation of the relevance of the fit. Note that for all the samples studied in this part, a single-layer model provides very satisfactory fits.

The gel films were measured in air (at silicon-air interface) and in water (at silicon-D_2O interface). The measures in water were performed at various temperatures to make clear the LCST behavior. The gel films of different thickness (from 5 nm to 60 nm in air) were investigated. What is the effect of the film thickness on the swelling ratio and on the free interface width of the gel?

3.1. Measures in air

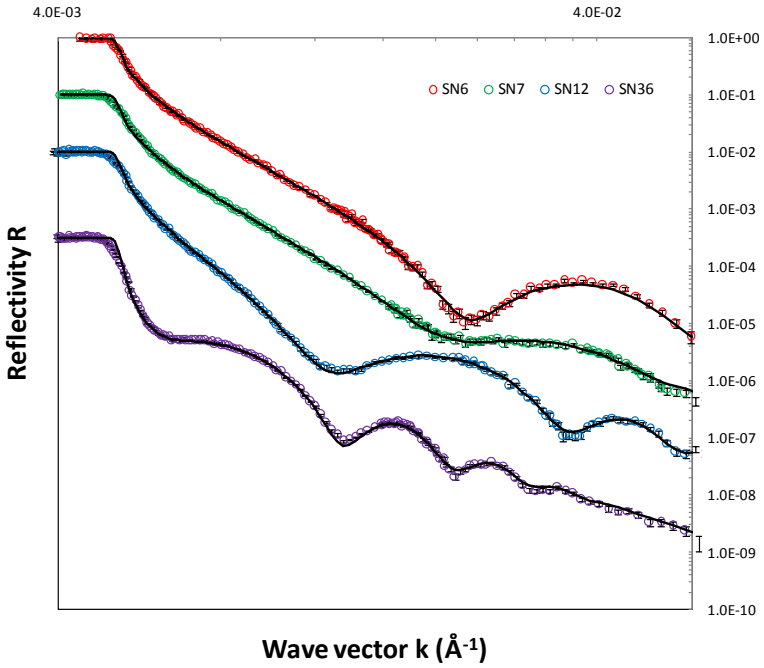


***Figure 32**: Neutron reflectivity curves of single-network films in air and their best fittings. The characteristics of the fittings are indicated in **Table 1**. Circle: data; line: fitting.*

The neutron reflectivity curves of different single-network films are displayed in **Figure 32**. The best fits of the experimental data are also represented. The samples studied have different values of thickness from 6 nm to 36 nm. The characteristics of the gel film corresponding to the neutron reflectivity curve that best fits the experimental data are shown in **Table 1**. The thickness h_a measured in air by neutron reflectivity is compared with the value obtained by ellipsometry. Are also reported the free interface width σ and the scattering length density Nb.

The values of thickness measured in neutron reflectivity and ellipsometry are very similar for all samples with a little difference of a few angstroms. The width of the free interface of the

gel in air varies from 0.5 nm to 3 nm. It increases with the film thickness. For all samples, it is about 10% of the film thickness.

Samples	h_a (nm) by ellipsometry	h_a (nm) by neutrons	σ (nm)	Nb (10^{-6} Å^{-2})
SN6	6.4	6.7	0.5	0.90
SN7	6.9	7.5	1.7	0.88
SN12	12.4	12.5	1.1	0.90
SN36	36.2	36.4	3.0	0.94

***Table 1**: Characteristics of the PNIPAM gel film measured in air. Neutron reflectivity allows the determination of the thickness h_a (which is compared with the value found by ellipsometry), the free interface width σ using erf error function and the scattering length density Nb of the PNIPAM layer.*

The scattering length density found is about 0.9 10^{-6} Å^{-2} (from 0.88 10^{-6} to 0.94 10^{-6} Å^{-2}). From this value, the water content of the PNIPAM gel film in air can be calculated. The water content in the gel film was determined as function of the humidity ratio by ellipsometry. The results were discussed previously (see part 1 of the Chapter 3). It was shown that the water content is in order of 10% in air (with humidity ratio between 20% and 70%). To get water content of 10%, the scattering length density found for the PNIPAM gel film in air and in dry state (pure PNIPAM without any water) should be equal to 0.90 10^{-6} Å^{-2} and 1.05 10^{-6} Å^{-2} respectively (as the scattering length density of water is -0.56 10^{-6} Å^{-2}).

The results obtained in neutron reflectivity are consistent with those found by ellipsometry even if it is difficult to calculate exactly the scattering length density of pure PNIPAM gel film for many reasons: (i) for the synthesis of PNIPAM gel films, we used linear chains containing 95% of NIPAM and 5% of AA, 2% of AA being ene-functionalized to react with dithiol cross-linkers (see chapter 2), (ii) the density of a PNIPAM gel film is not easily determined with precision, Vidyasagar et al. used 1.2 g/cm^2 as the surface density whereas the volume density of PNIPAM chains given by Polymer Handbook is 1.1 g/cm^3. Vidyasagar at al. estimated the scattering length density to be 0.96 10^{-6} Å^{-2} and their PNIPAM gel films were synthesized with a benzophenone UV-irradiated cross-linker. In our case, we obtained by calculation for PNIPAM a scattering length density equal to 0.89 10^{-6} Å^{-2} (using ρ = 1.2 g/cm^3 as the density), for polyacrylic acid 1.5 10^{-6} Å^{-2} (ρ = 1.3 g/cm^3) and for poly(sodium acrylate) 2.24 10^{-6} Å^{-2} (ρ = 1.6 g/cm^3). It means that it is not possible to calculate with high precision the scattering length density but 1 10^{-6} Å^{-2} could be a reasonably estimated value.

Neutron experiments under dry (nitrogen) atmosphere which could not be performed due to lack of time should allow the determination of the scattering length density of PNIPAM gel film in dry state and then the determination of water content with higher precision.

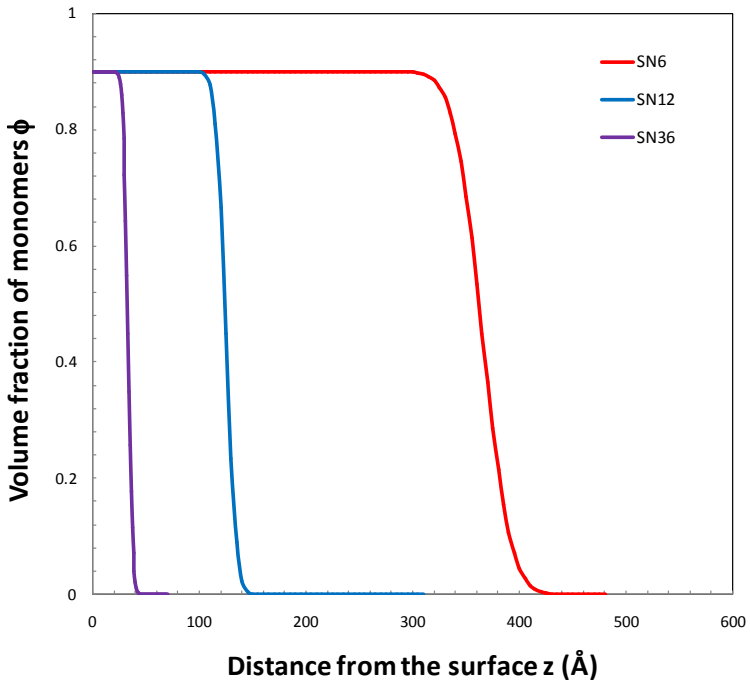


***Figure 33**: Profiles of volume fraction of monomers of single-network films in air.*

The profiles of the volume fraction of monomers in the direction perpendicular to the surface are plotted in **Figure 33**. The maximum of the volume fraction is fixed at 0.9, the mean thickness of the layer corresponding to h_a and the free interface width σ, the continuous shape of the profile being defined by erf mathematical function (see **Annex 4**).

3.2. Effect of temperature

The neutron reflectivity curves of PNIPAM single-network films in water are displayed in **Figure 34**. The best fittings of the experimental data are also represented. The PNIPAM gel film, which is 36.4 nm-thick in air, is measured in water at three different temperatures: 25°C, 32.5°C and 40°C. Note that the range of wave vector here goes from 4 10^{-3} $Å^{-1}$ to 5 10^{-2} $Å^{-1}$ whereas it usually goes at least 0.1 $Å^{-1}$. Actually, the silicon wafer used here is excessively thin (only 1 mm-thick instead of 5 mm-thick wafers which are more suitable) providing high background at wave vectors above 0.05 $Å^{-1}$.

The reflectivity curve at 40°C has highest number of Kiessig fringes which are most pronounced compared to 32.5°C and 25°C. It is the signature of a thicker layer with a steeper density profile at 40°C as shown by the profiles of the volume fraction of monomers in the direction perpendicular to the surface in **Figure 35**. Below the LCST at 25°C, the PNIPAM gel is swollen with a thickness equal to 110.7 nm and a free interface width equal to 18.8 nm whereas above the LCST at 40°C, the PNIPAM gel is contracted with a thickness equal to 81.2 nm and a free interface width equal to 3.5 nm. The profile of the gel film at 32.5°C is reasonably between that at 25°C and 40°C.

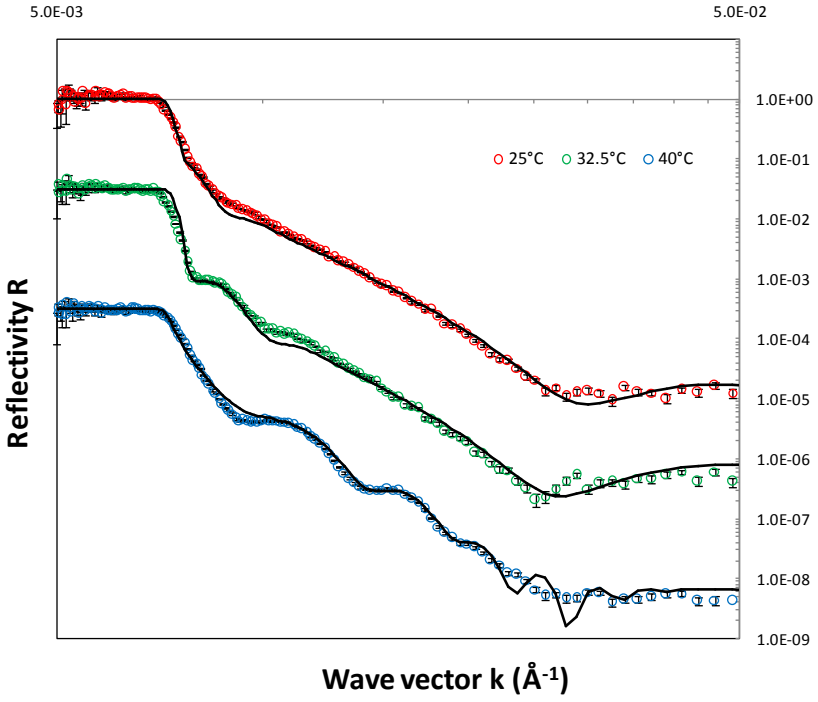


***Figure 34**: Neutron reflectivity curves of the single-network film SN36 in water at three temperatures 25°C, 32.5°C and 40°C. Also are shown the best fittings of the experimental data. The corresponding volume fraction profiles are displayed in **Figure 35**. Circle: data; line: fitting.*

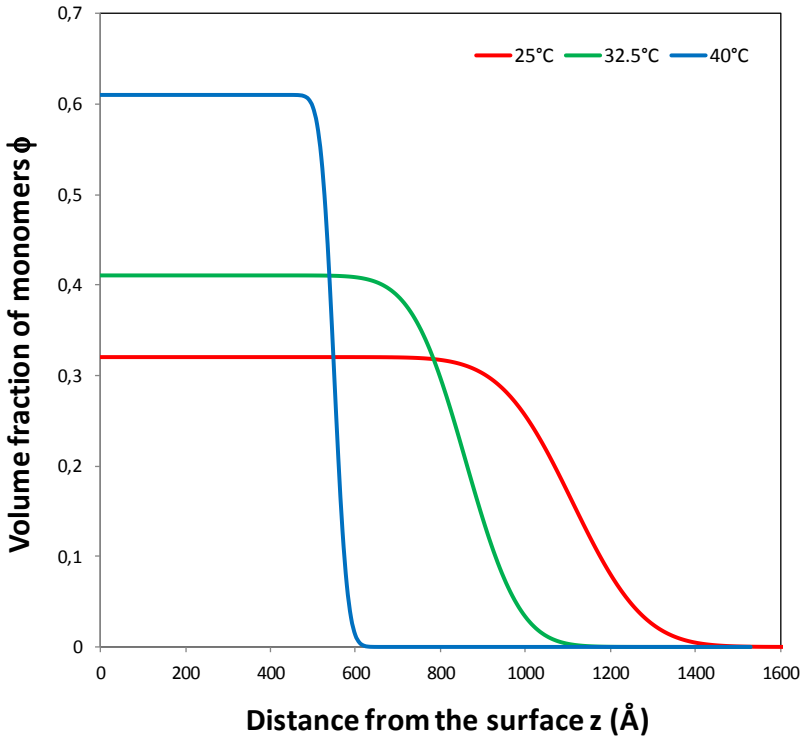


***Figure 35**: Profiles of volume fraction of monomers of the single-network film SN36 in water at three temperatures 25°C, 32.5°C and 40°C.*

3.3. Effect of the thickness of the film

The neutron reflectivity curves and their best fittings in water are displayed in **Figures 36**. The samples are measured in water at three different temperatures: 25°C, 32.5°C and 40°C. The thickness of the PNIPAM gel films in air is 6.7 nm (**Figure 36**, left) and 12.4 nm (**Figure 36**, right). Note that the range of wave vector of SN12 (12.4 nm) goes from 4 10^{-3} $Å^{-1}$ to 5 10^{-2} $Å^{-1}$ for the same reason as SN36 (36.4 nm).

As explained in the previous part with SN36, the reflectivity curve at 40°C has highest number of Kiessig fringes which are most pronounced compared to 32.5°C and 25°C providing thinner layer with steeper density profile. The profiles of the volume fraction of monomers are shown in **Figures 37**.

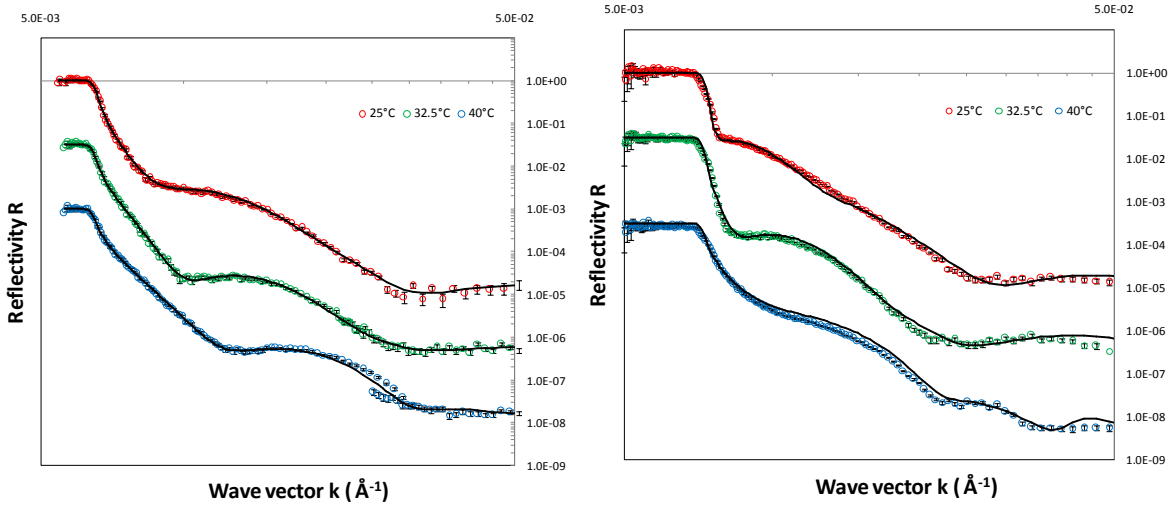


***Figure 36**: Neutron reflectivity curves of the single-network films SN6 (left) and SN12 (right) in water at three temperatures 25°C, 32.5°C and 40°C. Also are shown the best fittings of the experimental data. The corresponding volume fraction profiles are displayed in **Figure 37**. Circle: data; line: fitting.*

All the characteristics of the PNIPAM gel films corresponding to the best fit of the reflectivity data are shown in **Table 2**. The thickness in air measured by neutron reflectivity h_a is reminded. Three parameters are extracted from the fits: h_w the thickness in water, σ the free interface width and the scattering length density Nb. The volume fraction of the layer ϕ is calculated from Nb assuming that the scattering length density of pure PNIPAM is 10^{-6} $Å^{-2}$ and then -1.07 10^{-6} $Å^{-2}$ at silicon-water interface with the scattering length density of silicon equal to 2.07 10^{-6} $Å^{-2}$. As the polymer amount is constant, the product ϕ x h_w should be equal to ϕ_a x h_a (with ϕ_a = 0.9). This comparison is a good tool to assess the accuracy of the fit.

The interface width σ obtained in water is higher at 25°C (and 32.5°C) than at 40°C. If σ it increases with the thickness of the gel film, the ratio σ/h_w decreases with the thickness h_w.

The interface width was found to be about 10% of the thickness of the film in air. The ratio σ/h_w is the same in water at 25°C and 32.5°C, it is about 36% for SN6, 28% for SN12 and 16% for SN36. It is much lower for collapsed film at 40°C, 25% for SN6 and 6% for SN12 and SN36. As observed with the density profiles shown in **Figure 37**, the thicker the gel film, the lower is the ratio σ/h_w. The density profile is the sharpest for the thickest film in the collapsed state at 40°C.

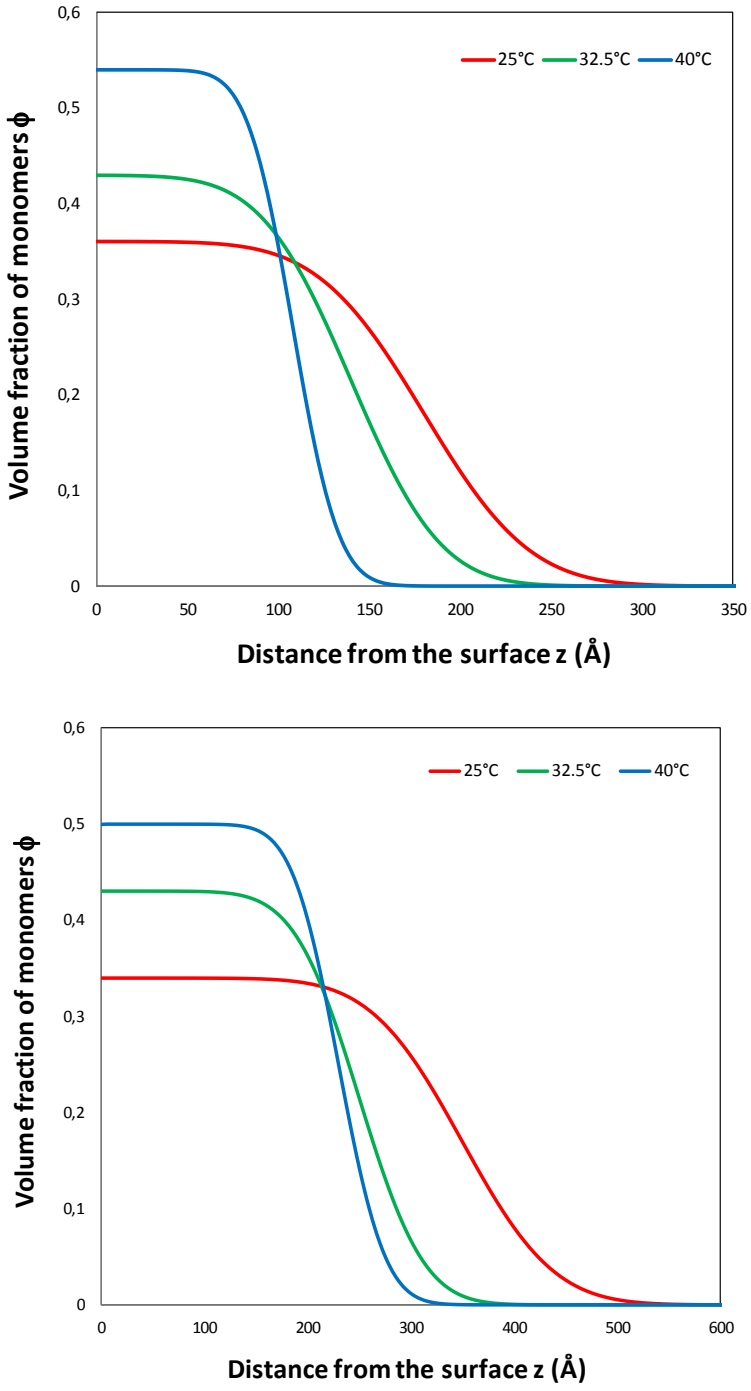


***Figure 37**: Profiles of volume fraction of monomers of the single-network films SN6 (top) and SN12 (bottom) in water at three temperatures 25°C, 32.5°C and 40°C.*

Samples	h_a (nm)	h_w (nm)	σ (nm)	Nb (10^{-6} Å^{-2})	ϕ	h_w/h_a
SN6-air	6.7		0.5	0.90		
SN6-25C	6.7	18.0	6.5	2.36	0.36	2.7
SN6-34C	6.7	14.1	5.5	2.02	0.43	2.1
SN6-40C	6.7	11.0	2.8	1.44	0.54	1.6
SN12-air	12.5		1.1	0.90		
SN12-25C	12.5	35.4	9.9	2.50	0.34	2.8
SN12-34C	12.5	25.0	7.0	2.00	0.43	2.0
SN12-40C	12.5	22.6	1.1	1.65	0.50	1.8
SN36-air	36.4		3.0	0.94		
SN36-25C	36.4	110.7	18.8	2.60	0.32	3.0
SN36-34C	36.4	85.6	14.2	2.10	0.41	2.4
SN36-35C	36.4	81.2	12.8	2.00	0.43	2.2
SN36-40C	36.4	55.5	3.5	1.00	0.61	1.5

***Table 2**: Characteristics of the PNIPAM gel film measured in water. Are reported the thickness h_w (the thickness in air h_a is reminded), the free interface width σ using erf error function and the scattering length density Nb. The volume fraction of the layer ϕ is calculated from Nb assuming that the scattering length density of pure PNIPAM is 10^{-6} Å^{-2} and that of silicon equal to 2.09 10^{-6} Å^{-2}. The swelling ratio h_w/h_a is also calculated.*

In **Figure 38**, the thickness in water h_w is plotted as function of the thickness in air h_a. It seems that a same swelling ratio h_w/h_a (corresponding to the slope of the straight line) is found for each temperature. At 25°C below the LCST, the swelling ratio is about 2.8. Near the transition, it is around 2.2 and at 40°C above the LCST, it is 1.6. At 25°C, the swelling varies from 2.7 to 3.0 (**Table 2**) with increasing thickness, but it is difficult to interpret any variation due to the uncertainty of measurements. It seems that there is no effect of the thickness of the film on the swelling ratio in this range of thickness investigated by neutron reflectivity (up to 100 nm).

The neutron reflectivity curves of SN63 in water at 25°C and 32.5°C are displayed in **Figure 39**. The best fittings of the experimental data are also represented. SN63 is PNIPAM single-network film which thickness in air is 63.4 nm. If this sample is thin enough to be measured in air by neutron reflectivity, it is too thick (compared to the resolution in wave vector) when it is swollen in water. Its thickness at 25°C and at 32.5°C is expected to be about 200 nm and 140 nm respectively.

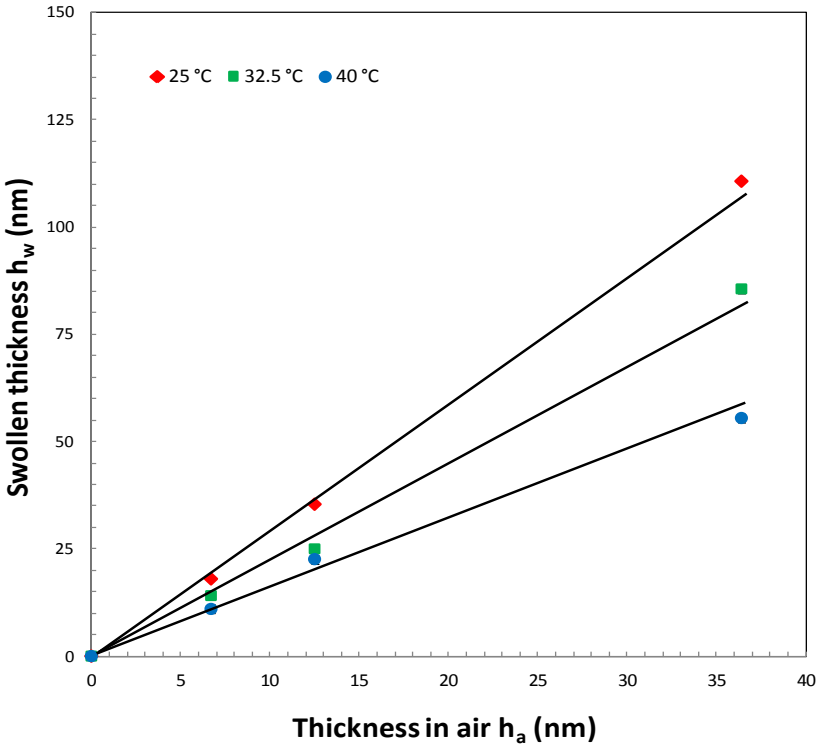


***Figure 38**: Swollen thickness of PNIPAM single-network films as a function of the thickness in air, at three different temperatures: 25°C, 32.5°C and 40°C.*

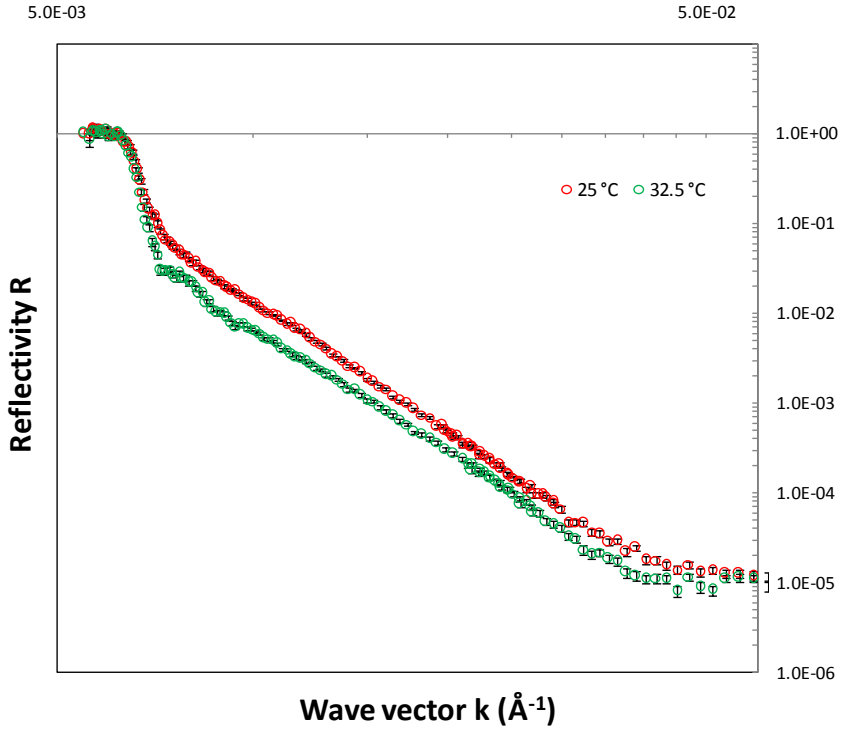


***Figure 39**: Neutron reflectivity curves of the single-network film SN63 in water at 25°C and 32.5°C.*

4. Discussion

4.1. Each technique has its specification and limitation

Three experimental techniques were applied to characterize the swelling/collapse phase transition of the gel films: ellipsometry, atomic force microscopy and neutron reflectivity. In the following, we remind the specific characteristics of the gel films extracted from each technique and we also discuss the limitations of each technique.

Ellipsometry was used to determine the swelling ratio of the films in water in the direction normal to the substrate. The range of thickness measured by ellipsometry is supposed to vary from angstrom to a few microns. This range is accessible for ideal layers with a box model. The range of thickness of gel films measured in air remains quite large: from nanometer to two microns at a maximum. If the interface width of the gel films is weak (it is shown to be 10% of the thickness for films lower than 100 nm), a box model can be applied. For films which thickness is larger than 1 micron, the fitting of the data is less easy but still feasible. For the measures in water, the gel films are far from a box model. The distance from a box model is higher for thicker films since the interface width becomes larger (it is around 35% of the thickness for 100 nm-thick films as an indication). It means that it is very tricky to measure by ellipsometry gel thin films because the addition of thin layer and large interface. However, the measure of gel films which thickness in water is between 300 nm and 1500 nm is achievable since the number of oscillations in the wavelength range studied is enough to allow (reasonably) relevant fitting of the data.

Atomic force microscopy provided information on the topography of the free surface of the gel films. The tapping mode was carried out in air. But Quantitative Nano Mechanics QNM mode was required for the measures in water since the Young modulus of the hydrogel films in water is very low (few tens of kPa) and close to the aqueous environment. Consequently, the measures by AFM are more appropriate for gel films which thickness in air is higher than 100 nm. The morphology of the free surface of the PNIPAM hydrogel films could be then investigated and compared in air and in water at various temperatures.

Neutron reflectivity allowed the determination of the composition of the film, its thickness and the width of the free surface of the gel layer. The range of the thickness easily reachable by neutron reflectivity is roughly from 1 nm (the limit is given by the range of wave vector) to 150 nm (the limit is given by the resolution of wave vector). Also, we chose to use neutron reflectivity to characterize PNIPAM gel films which thickness in air (respectively in water) varies from 6 nm to 36 nm (respectively up to 110 nm). As ellipsometry, specular neutron reflectivity provided information on the slice of the film or in the direction perpendicular to

the substrate, considering the composition of the x-y plane homogeneous. Actually, the specular neutron reflection does not allow the distinction between the roughness and the interdiffusion of a layer if the size of the in-plane irregularities is smaller than the coherent length of neutrons. For thermal neutrons (with a typical wavelength of a few angstroms), the coherent length is on the order of a few microns. In-plane morphologies of the PNIPAM gel films were determined by AFM. If it was shown that the topography could vary a little in water with temperature, the size of the in-plane patterns is lower than 100 nm. It means that the smoothness of the free surface of the hydrogel can be attributable to a diffuse interface as well as a rough interface.

4.2. Effect of the confinement

In **Figure 5** and **Figure 38**, the swelling ratio of PNIPAM gel films is plotted as function of the thickness of the film (in air). Two ranges of thickness were concerned: below 50 nm for the data obtained neutron reflectivity and from 100 nm to 500 nm for the data from ellipsometry. What about thicker films?

As it is tricky to determine the swelling gel films whose thickness (in air) is higher than 500 nm (the thickness in water can be more than 2 microns), we used microfluidic tools to characterize a micron-thick film. This study was performed as part of Benjamin Chollet's thesis on the microfluidic applications of stimuli-responsive hydrogel films as microvalves. This work is currently achieved with the collaboration of Gulliver laboratory in ESPCI. The principle is simple: the swelling-collapse transition of PNIPAM gel films is exploited to control hydrodynamic flows in microfluidic channels [15]. The flow Q in a channel (on which one wall is covalently covered by a PNIPAM gel film) is proportional to the pressure variation ΔP as:

$$Q = R\,\Delta P$$

with R the hydrodynamic resistance. R is relied to the characteristics of the channel by:

$$R = \frac{12\mu L}{h^3 w}$$

where L is the length of the channel, w the width of the channel, μ the viscosity of water. In this equation, h corresponds to the height of channel for the flow with $h = h_c - h_w$ where h_c is the height of the channel and h_w is the height of the swollen hydrogel which obstructs the fluid circulation. The flow through the channel was measured as function of temperature for a given pressure (3 bars for example). The thickness of the gel film h_w could be then deduced. The results obtained with a 1200 nm-thick PNIPAM gel film are shown in **Figure 40**. The swelling ratio of SN1200 characterized by microfluidics is compared with that of thinner films characterized by ellipsometry. The big error bars in microfluidic measurements are due to

the uncertainty of the flow measurements (precision of 10 nL/min). The values of swelling ratio below and above the LCST (4.0 and 1.5) are comparable to those found by ellipsometry. Note that the transition with temperature is quite large, almost 10°C. However, due to the great error bars, it is tricky to settle that the large transition with temperature is attributable to the high thickness of the gel film.

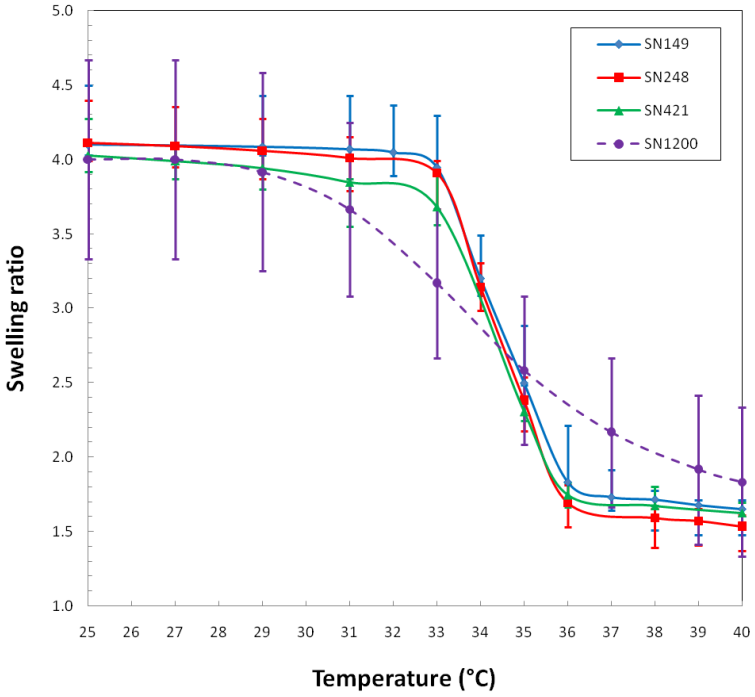


***Figure 40**: Swelling ratio of PNIPAM hydrogel films (of different thickness) as a function of temperature.*

In **Figure 41**, the swollen ratio of PNIPAM hydrogel films is plotted as a function of the film thickness in air for three temperatures 25°C, 34°C and 40°C. It should be highlighted that the combination of ellipsometry, neutron reflectivity and microfluidics allows the plot on a very large range of thickness from nanometer to micron.

At 25°C for swollen gels, the swelling ratio is about 3 for thickness (in air) less than 50 nm. It increases to 3.5 at 90 nm to reach 4.0 for thickness up to 1.2 microns. If the distribution of the cross-links is supposedly homogeneous in the whole film, it means that the surface attachment has a strong effect on the swelling of the films, particular for very thin films below 100 nm. From 100 nm to 1.2 microns, the swelling ratio is the same. It is audacious to point out the transition thickness (which is located between domains of neutron reflectivity and ellipsometry) as it is tricky to interpret any little increase of the swelling ratio for thickness below 50 nm (domain of neutron reflectivity).

At 40°C for collapsed gels, the swelling ratio is 1.5 for the whole range of thickness studied. If the surface attachment of the gel films has a clear effect on the swelling of the films, it has

less influence on the collapse of the films.

These results are quite divergent from those found in the few works dedicated to surface-attached hydrogel films. Indeed, only four papers were interested in the swollen-collapse phase transition of gel films with temperature: two from Kucking's group [7, 16] and the two others from Toomey and co-authors [1, 17]. They all used UV-irradiation to cross-link the chromophore-functionalized chains which were previously spin-coated on the substrate. Like our strategy using the thiol-ene reaction, we can consider that the cross-links are distributed homogeneously in the direction perpendicular to the surface.

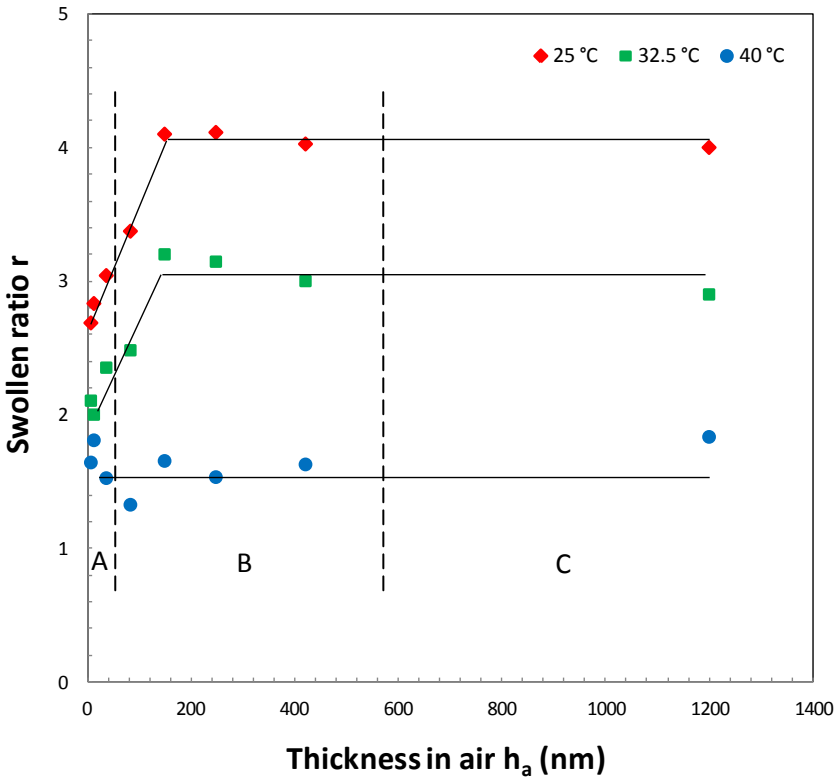


***Figure 41**: Swollen ratio of PNIPAM hydrogel films as a function of the film thickness in air, at three different temperatures: 25°C, 32.5°C and 40°C. A: neutron reflectivity; B: ellipsometry; C: microfluidics.*

Kuckling's group studied PNIPAM gel films which thickness varies from a few hundred nanometers to 2 microns. Using Surface Plasmon Resonance (SPR) they measured the refractive index of the films as function of temperature. They found that the refractive index is the same at high temperatures in the collapsed state for thickness above 280 nm and it decreases with decreasing thickness. For thin films below 280 nm, they explain that the film is unable to fully collapse, which is contrary to Toomey's results and our results. Indeed, this divergence could be explained by a weak sensitivity of the SPR measurements for thin films. In addition, the swollen gel layer is far from a one-step model with a very soft profile (as we

showed by neutron reflectivity), providing supplementary difficulties to measure correctly the gel film immersed in water.

Toomey and co-authors characterized a 25 nm-thick PNIPAM film by neutron reflectivity [1]. The film was obtained from a 3 mol% functionalized copolymer. The swelling ratio at high temperature is around 1.2, which is a little lower than the value of 1.5 we obtained. The swelling ratio at low temperatures can reach 4.4, which is much higher than the ratio of 3 we found. The large amplitude of the swelling ratio (from 1.2 to 4.4) obtained by Toomey could be explained by a weak ratio of cross-linking which is probably much lower than 3 mol%.

In the other article [17], they were interested in the effect of the cross-linking ratio on the swelling of (100 nm-thick) PNIPAM gel films at ambient temperature using variable-angle nulling ellipsometry. The decrease of the modification ratio of the copolymer (1% to 0.05%) leads to an increase of the swelling ratio (400 nm to 1400 nm). However, the swelling ratio of 13 (thickness at 1400 nm) obtained should be considered with caution since the volume fraction of polymers in that case is lower than 10%, which is tricky to measure. They found additionally that the interface width (using error function-type interface) could reach 200 nm, which is very high, and they estimate the precision to be $\pm$ 50 nm.

Nevertheless, the analysis of the scaling laws in this article is helpful so it is summarized in the annex. The scaling laws predicted for the swelling of hydrogels by Flory-Rehner [18] are extended to one-dimension swelling. The volumetric swelling ratio for surface-attached gel films S_F and for bulk networks S_V corresponds to the ratio ϕ_a/ϕ_w between the volume fraction of polymer in air ϕ_a and that in water ϕ_w. With simple geometric considerations, the power law should be $S_F = S_V^{1/3}$. However, the swelling of surface-attached polymer networks is experimentally larger than what is suggested through simple geometric considerations for swelling in-one dimension. It is consistently observed that the linear swelling ratio of the surface-attached networks exceeds the linear swelling ratio of the bulk networks. Also, an extension of Flory-Rehner theory to one dimension which gives $S_F = S_V^{5/9}$ is more appropriate.

The supposed cross-linking ratio (or more exactly the corresponding ratio of functionalization of copolymers with chromophores) is 1 mol% for a swelling ratio of surface-attached films about 3 to 4, which is consistent with our gel films. The corresponding swelling ratio of bulk hydrogels (which is in good agreement with the scaling laws $S_F = S_V^{5/9}$) is about 10 to 20. It indicates that all the hydrogel films investigated are far from a bulk hydrogel, the effect of the surface attachment remaining strong.

4.3. Gel film: a model network?

How far is the gel film a from model network? An attempt to answer is to consider at least

two aspects: the chemical distribution of the cross-linking segments and the interface width of the gel film.

It is reasonable to suppose that the strategy of synthesis provides a homogeneous distribution of the cross-linkers in the whole hydrogel layer. Actually, the ene-functionalized chains and the dithiol cross-linkers are mixed before being coated on the surface and the thiol-ene reaction is initiated by temperature (or even UV-irradiation). This strategy of synthesis is different from the strategy which consists in polymerizing and cross-linking the monomers to obtain the surface-attached gel film. Actually, it has been shown that the surface of hydrogels contains fewer polymers than the volume for gels synthesized in the presence of the substrate. The polymerization is affected by the presence of the substrate with the change of the diffusion of monomers and cross-linkers at the vicinity of the surface [19]. On the other hand, it is not easy to characterize the cross-linking ratio on thin films since it is lower than 5% (even using X-ray Photoelectron Spectroscopy) and it is not presently possible to determine any gradient of the cross-linking.

Even though the distribution of cross-links is supposedly homogeneous, it does not eliminate the presence of pendant chains at the outside edge of the film. These peripheral chains provide a more diffuse interface. The free surface of the gel becomes more diffuse for lower cross-linking ratios since the semi-free polymer chains are less confined to the interface. It can be reasonably supposed that the interface width is a strong function of the molecular weight of chains used for the synthesis.

Another point is the mechanical constraints on the gel film induced by the surface attachment. Harmon et al. [20] illustrated it as shown in **Figure 42**. The hydrogel layer is cross-linked in a reference state (B) and surface-attached gel remains in this reference. The elastic energy of the network acts as compression when the layer is swollen (C) relative to the reference state and as elongation when the layer is more collapsed than the reference state (A). The compression or elongation increases and is greatest at the free surface of the gel. The exact shape of the gel with lateral swelling depends on both the film thickness and the aspect ratio of the gel layer. In our case, the hydrogel film is synthesized in melt condition (in air for UV-irradiation and under vacuum for temperature activation). In water, in swollen state at 25°C or in collapsed state at 40°C, the hydrogel layer is more swollen than the synthesis state so that the elastic energy acts as compression. How is the effect of the compression due to the surface attachment on the free surface of the hydrogel?

We observed by ellipsometry and neutron reflectivity that the gel layer is far from a box model with a step profile. As one-step model is used in ellipsometry, the proximity of the fitting of the ellipsometric angles Ψ and Δ and the experimental data is indicative of the width of the free interface. It should be helpful to improve the model used for the fit by

adding smoothness at the outer edge of the profile. For example, the smoothness added to a step profile should be described by an error function as used in the analysis of the data for neutron reflectivity.

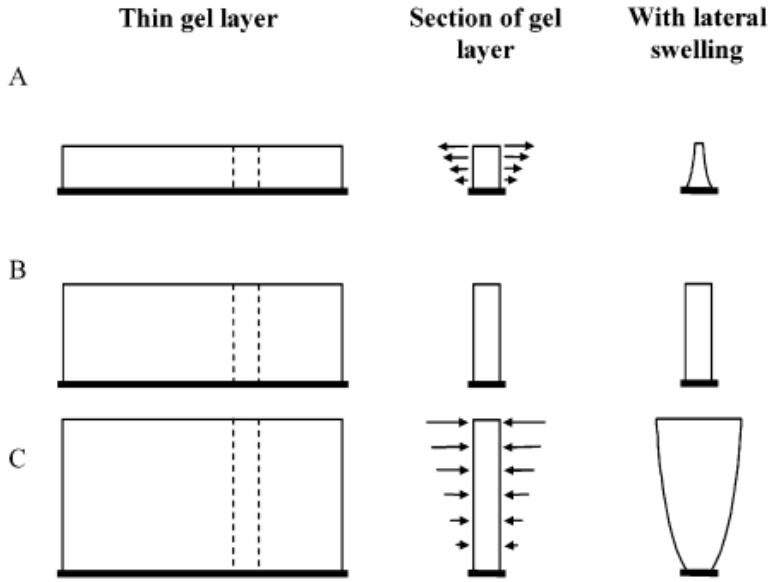


***Figure 42**: Compression of gels [20].*

Neutron reflectivity allows the determination of the free interface width by using a box model with an error function-type interface. However, the technique is sensitive for films whose swollen thickness in water is less than 150 nm. As the size of the in-plane irregularities is much smaller than the coherent length of neutrons, specular neutron reflection cannot distinguish a diffuse film from a rough film. It is then helpful to compare the roughness of the surface of the hydrogel film determined by AFM and the free interface width deduced from neutron reflectivity.

The characteristics extracted from AFM and neutron experiments are displayed in **Table 3**. Using AFM, films with different thickness (36 nm and 249 nm in air) were studied. The full width at half maximum FWHM was determined in air and in water at various temperatures. The sample SN36 studied by neutron reflectivity is compared here, the interface width σ being calculated with error function. The roughness and width of the interface can be quantitatively estimated with a simple normalization to the thickness of the layer. The ratio FWHM/h obtained is quite weak for the roughness. It is the same in any environment in air or water; it is about 0.5% for SN249 and 1.7% for SN36. In contrast, the ratio σ/h is much higher, notably in water at 25°C in the swollen state with a ratio equal to 17% whereas in air and in collapsed state, it is equal to 8%. The discrepancy between the ratios FWHM/h and σ/h is the proof that the smoothness of the free surface of the hydrogel is not only due to the roughness (in-plane irregularities) but also to the diffusion of the interface. The surface is

most diffuse in the swollen state. The diffuse surface might be explained by the presence of pendant chains at the outside edge of the film as suggested above. The peripheral chains are more likely to penetrate into the aqueous environment (rather than into the network, which is entropically unfavorable) giving rise to a more diffuse interface.

Samples	h (nm)	σ (nm)	FWHM (nm)	σ/h or FWHM/h
SN36_air	36.4	3.0		8%
SN36_25C	110.7	18.8		17%
SN36_40C	55.5	3.5		7%
SN36_air	36		0.8	1.6%
SN36_25C	110		1.1 to 2.0	1.8%
SN249_air	249		0.9	0.4%
SN249_25C	960		4.5	0.5%
SN249_40C	360		1.6	0.5%

***Table 3**: Characteristics extracted from AFM and neutron experiments.*

References

1. Vidyasagar, A., J. Majewski, and R. Toomey, *Temperature induced volume-phase transitions in surface-tethered poly (N-isopropylacrylamide) networks.* Macromolecules, 2008. **41**(3): p. 919-924.
2. Yim, H., et al., *Conformation of end-tethered PNIPAM chains in water and in acetone by neutron reflectivity.* Macromolecules, 2003. **36**(14): p. 5244-5251.
3. Yim, H., et al., *Temperature-dependent conformational change of PNIPAM grafted chains at high surface density in water.* Macromolecules, 2004. **37**(5): p. 1994-1997.
4. Yim, H., et al., *Effects of grafting density and molecular weight on the temperature-dependent conformational change of poly (N-isopropylacrylamide) grafted chains in water.* Macromolecules, 2006. **39**(9): p. 3420-3426.
5. Malham, I.B. and L. Bureau, *Density effects on collapse, compression, and adhesion of thermoresponsive polymer brushes.* Langmuir, 2009. **26**(7): p. 4762-4768.
6. Junk, M.J., R.d. Berger, and U. Jonas, *Atomic force spectroscopy of thermoresponsive photo-cross-linked hydrogel films.* Langmuir, 2010. **26**(10): p. 7262-7269.
7. Harmon, M.E., D. Kuckling, and C.W. Frank, *Photo-Cross-Linkable PNIPAAm Copolymers. 5. Mechanical Properties of Hydrogel Layers.* Langmuir, 2003. **19**(26): p. 10660-10665.
8. Ishida, N. and S. Biggs, *Direct Observation of the Phase Transition for a Poly(N-isopropylacryamide) Layer Grafted onto a Solid Surface by AFM and QCM-D.* Langmuir, 2007. **23**(22): p. 11083-11088.
9. Wiedemair, J., et al., *In-Situ AFM Studies of the Phase-Transition Behavior of Single Thermoresponsive Hydrogel Particles†.* Langmuir, 2006. **23**(1): p. 130-137.
10. Montagne, F., et al., *Poly(N-isopropylacrylamide) Thin Films Densely Grafted onto Gold Surface: Preparation, Characterization, and Dynamic AFM Study of Temperature-Induced Chain Conformational Changes.* Langmuir, 2008. **25**(2): p. 983-991.
11. Sui, X., et al., *Probing the Collapse Dynamics of Poly (N-isopropylacrylamide) Brushes by AFM: Effects of Co-nonsolvency and Grafting Densities.* Small, 2011. **7**(10): p. 1440-1447.
12. Beines, P.W., et al., *Responsive thin hydrogel layers from photo-cross-linkable poly (N-isopropylacrylamide) terpolymers.* Langmuir, 2007. **23**(4): p. 2231-2238.
13. Melzak, K.A., et al., *Simultaneous Measurement of Mechanical and Surface Properties in Thermoresponsive, Anchored Hydrogel Films.* Langmuir, 2012. **28**(35): p. 12871-12878.

14. Cole, M.A., et al., *Colloid probe AFM study of thermal collapse and protein interactions of poly (N-isopropylacrylamide) coatings.* Soft Matter, 2010. **6**(12): p. 2657-2667.
15. Vergne, C., *Thèse de Doctorat.* Paris VI, 2013.
16. Harmon, M.E., D. Kuckling, and C.W. Frank, *Photo-Cross-Linkable PNIPAAm Copolymers. 2. Effects of Constraint on Temperature and pH-Responsive Hydrogel Layers.* Macromolecules, 2002. **36**(1): p. 162-172.
17. Toomey, R., D. Freidank, and J. Rühe, *Swelling Behavior of Thin, Surface-Attached Polymer Networks.* Macromolecules, 2004. **37**(3): p. 882-887.
18. Flory, P.J. and J. Rehner, *Statistical Mechanics of Cross-Linked Polymer Networks II. Swelling.* The Journal of Chemical Physics, 1943. **11**(11): p. 521-526.
19. Sudre, G., et al., *Structure of Surfaces and Interfaces of Poly (N, N-dimethylacrylamide) Hydrogels.* Langmuir, 2012. **28**(33): p. 12282-12287.
20. Harmon, M.E., et al., *Photo-Cross-Linkable PNIPAAm Copolymers. 4. Effects of Copolymerization and Cross-Linking on the Volume-Phase Transition in Constrained Hydrogel Layers.* Langmuir, 2003. **19**(26): p. 10947-10956.

Chapter 4

Development of new hydrogel films with complex architectures

Contents

Contents 118
Introduction 119
1. Layer-by-layer (LbL) networks gel films 121
    1.1. Synthesis 121
        1.1.1. General strategy 121
        1.1.2. Synthesis of multilayer PNIPAM gel films 123
        1.1.3. Synthesis of bilayer PNIPAM gel films for neutron experiments 124
    1.2. Structure of multilayer PNIPAM gel films in water 125
        1.2.1. Topography 125
        1.2.2. Swelling behavior 127
        1.2.3. Characterization by neutron reflectivity 128
2. Interpenetrating networks (IPN) gel films 128
    2.1. Synthesis 129
        2.1.1. General strategy 129
        2.1.2. Synthesis of PNIPAM IPN gel films 131
        2.1.3. Synthesis of IPN films for neutron reflectivity experiments 132
    2.2. Structure of the PNIPAM IPN gel films in water 133
        2.2.1. Topography 133
        2.2.2. Swelling behavior 134
3. Hybrid gel films 135
    3.1. Synthesis 135
        3.1.1. General strategy 135
        3.1.2. Synthesis of silica-PNIPAM hybrid gel films 137
    3.2. Structure of silica-PNIPAM hybrid gel films in water 139
        3.2.1. Topography of the free surface 139
        3.2.2. Swelling ratio 145
        3.2.3. Effect of temperature on the swelling ratio 148
4. LbL or IPN networks? A study by neutron reflectivity 150
    4.1. Measures in air 151
    4.2. Effect of temperature 156
    4.3. Discussion 159
References 163

Introduction

This chapter focuses on the development of multiple networks gel films with targeted architectures and their characterization by ellipsometry, AFM and neutron reflectivity, based on the former study of single-network gel films. In this chapter, the objective is to develop complex networks gel films based on the same strategy for single-network films using thiol-ene chemistry. We are guided by the wide variety of architectures of macroscopic gels [1] and of thin films [2] to tailor innovative architectures for hydrogel thin films to achieve well-controlled and improved properties. In this chapter, we describe three architectures issued from the combination of macroscopic gels and thin films: multilayers networks, interpenetrating networks and hybrid networks.

Among the methods developed to make thin films, the layer-by-layer (LbL) assemblies have attracted numerous attentions due to their simplicity and versatility [3, 4]. The popularity of the LbL technique is also based on its advantage of enabling nanoscale control of the thickness, the structure and the composition of the films [5]. Here, we aim to develop surface-attached hydrogel thin films which are inspired from LbL assemblies. Besides easily controlled thickness, LbL-inspired hydrogel films can combine two or more desirable properties (like responsiveness to different stimuli) in the multilayer gel films coming from different composites.

Interpenetrating networks (IPN) are gels of two polymers for which both have cross-linked structures but are not joined together. The properties of each network are maintained within the IPN. A very interesting class of IPN is double network (DN) gels developed by Gong's group [6, 7]. While the DN hydrogels contain 90% of water, they show remarkable mechanical performances like natural cartilage with high elastic modulus, high failure compression and elongation strengths and high fracture energies. The transfer from IPN macroscopic hydrogels to nanoscale IPN gel films raises significant challenges. First, the very high swelling capability of polyelectrolytes in water (due to the osmotic pressure of counterions) cannot be used in gel films in the melt state. Second, mixing of two networks in the absence of a common solvent is not easy to achieve. However some relatively simple strategies will be applied to solve the problems. To realize the swelling of the first network, and then the interpenetration of the second network, we implement one procedure before the cross-linking of the second network to prestretch the polymer chains of the first network.

These studies give the opportunity to tackle some fundamental problems of polymer physics which are here applied in confined systems (or thin films) such as the interdiffusion of chains in the preformed network with the reptation theory and the mixture of polymers with Flory theory.

Besides the fabrication of hydrogel films from the former-synthesized polymers using different synthesis methods (SN, IPN and LbL), we also introduce silica nanoparticles into the gel networks to develop hybrid hydrogel thin films. Especially for the hybrid gel films, how the introduction of silica nanoparticles modifies the general properties of the gel network is investigated.

The same surface techniques used to characterize single-network film like ellipsometry, AFM and neutron reflectivity are employed to study the properties of these three kinds of multiple networks gel films, in terms of swelling behavior, topography and internal structure.

1. Layer-by-layer (LbL) networks gel films

Different from the widely studied polyelectrolyte multilayers, here we employ covalent chemistry for multilayer fabrication by thiol-ene reaction. We expect that due to the formation of strong covalent bonds, stable multilayer hydrogel thin films which are covalently grafted to the substrate can be obtained through LbL-inspired assemblies.

The polymer chains with ene groups synthesized in Chapter 2 are applied to realize cross-linking of the multilayer networks and attachment to the thiol-modified substrate in the presence of cross-linkers, while indicating their responsive properties. Different polymers with responsiveness to different stimuli can be combined in one multilayer network by LbL deposition as different composition of each layer, if proper conditions are chosen (e.g. the amount of cross-linkers, the solvent for spin-coating for each layer, the cross-linking time and so on). We believe that in the interface of two layers, a thin interpenetrating network exists, including both covalent connections through cross-linkers and/or physical entanglements to enable the connection between the two layers.

To make clear the structure of multilayer gel films and to understand the effect of LbL assembly on the properties of the gel films, we investigate the structure of multilayer gel films using ellipsometry, AFM and neutron reflectivity. The LbL networks gels are usually compared with the single-network gel films. Since the environmental parameter temperature is easier to control compared with light and electric field, for the study of properties of the multilayer gel films, we choose thermo-responsive PNIPAM chains in the multilayer networks as the studied object.

1.1. Synthesis

1.1.1. General strategy

For the synthesis of the first layer of the LbL gel film, we follow exactly the same process as presented in Chapter 2. Based on thiol-ene click chemistry, the synthesis does not require very sophisticated chemistry (see **Figure 1**). The principle consists in using thiol-modified silicon wafers, ene-functionalized polymers, and bifunctional thiol molecules as cross-linkers, to obtain covalently cross-linked hydrogel networks which are covalently grafted onto the surface of silicon wafers. The polymers are copolymers containing monomer units with stimuli-responsive properties and ene-reactive groups.

To prepare the second layer of the LbL gel film, we use the same synthesis method as for the first one (see **Figure 2**). The only difference is that the solution of the ene-functionalized polymer is spin-coated on the first layer instead of the thiol-modified silicon wafer. It is

important to choose a solvent for spin-coating the top layer that is close to a good solvent for the first layer as well. Selection of a poor solvent cannot yield a good wetting of the second layer on the first one. During the formation of the bilayer network, a thin interpenetrating network, which results in covalent connections through cross-linkers and/or physical entanglements between the two layers, should be formed to enable the connection between the two layers.

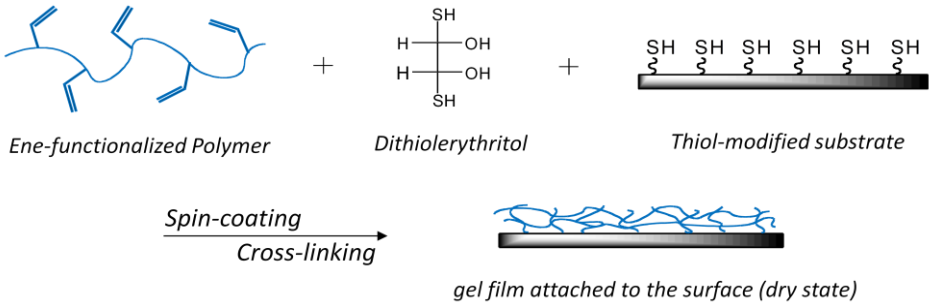


***Figure 1**: Synthesis of hydrogel thin films based on thiol-ene reaction.*

Multilayer gel films are available by successive deposition of a new layer on top of the former layer (using a proper solvent), as what is done for the preparation of the second layer on the first layer. The film thickness of each layer can be easily controlled by adjusting polymers with different molar mass, the concentration of the solution and the final spinning speed in coating. Thus the thickness of the multilayer network gel film is controllable, ranging from nanometers to micrometers.

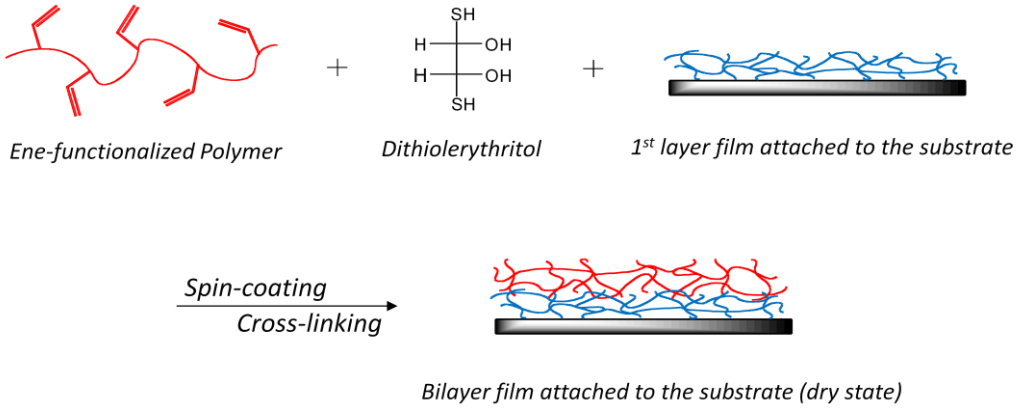


***Figure 2**: Synthesis of a bilayer network gel film based on thiol-ene reaction.*

Our general strategy to prepare multilayer networks hydrogel films by LbL assembly is summarized as follows:

1) the solution of an ene-functionalized polymer is deposited on the thiol-modified silicon wafer in the presence of cross-linkers and then spin-coated; the cross-linking and grafting-to-surface processes are achieved

simultaneously by the thiol-ene reaction;

2) the solution of another (or the same) ene-functionalized polymer is deposited on the former layer film in the presence of cross-linkers and then spin-coated; the cross-linking of the 2nd layer and connecting-to-former layer processes are achieved simultaneously by the thiol-ene reaction
3) repeat step 1) and step 2) if necessary.

As mentioned before, through the LbL deposition method, multifunctional gel films can be obtained, by combining various polymers with different properties in multilayer networks as different composition for each layer.

1.1.2. Synthesis of multilayer PNIPAM gel films

Here we take the thermo-responsive multilayer hydrogel films made from poly(AA-co-NIPAM) as an example to show the details of LbL assembly.

Synthesis of the 1st layer and the other layers

Poly(AA-co-NIPAM) is dissolved in the mixture of butanol and methanol (V/V = 1/1) at a certain concentration, the solution stirred for one night to help dissolution. Then the cross-linker dithioerythritol (DTE), of an access with respect to a certain ratio (typically 30 times) of the ene groups in the polymer chains, is added into the solution. When the cross-linker is totally solubilized, the solution is spin-coated on the silicon wafer at 3000 rpm for 30 s. After spin-coating, the wafer is immediately put into the oven at 120°C. The cross-linking process is allowed to proceed in vacuum at 120°C for one night. Afterwards the silicon wafer is taken out of the oven and cools down naturally. It is rinsed in methanol using ultrasonic bath for 1 minute to remove the unreacted polymers and then dried with N_2 flow. The thickness of the obtained film is measured by ellipsometry. In addition, the thickness of the film after cross-linking before rinsed is also measured to control the final thickness.

This provided a PNIPAM cross-linked network, which is used as a solid substrate for coating the second layer.

To prepare the 2nd layer, 3rd layer, …, the fabrication is almost the same as that of the 1st layer, the solution of the polymer and the cross-linker being spin-coated on top of the former layer gel film.

The samples can be stored at room temperature for later use.

In **Table 1**, we list out some of the multilayer PNIPAM gel films and their compositions.

Name of samples	Mw of polymer (Kg/mol)	Concentration of polymer (wt%)	Thickness of 1st layer in air (nm)	Number of layer: Thickness in air (nm)
LbL_128	400	1.0%	65	2 layers: 128
LbL_219	400	0.3%	15	17 layers: 219
LbL_456	400	2.5%	230	2 layers: 456
LbL_541	400	1.0%	65	9 layers: 541
LbL_668	400	2.5%	230	3 layers: 668

Table 1*: Formulation of multilayer PNIPAM gel films.*

The samples in **Table 1** are all made from the same copolymer P(AA-co-NIPAM) with Mw = 400 Kg/mol. For one sample, each layer is prepared with polymer solution of the same concentration. We can see that multilayer gel films are available by LbL assembly, no matter that the deposition starts from very thin film (15 nm) or relatively much thicker film (230 nm). Till now, we realize maximum 17 layers assembly. The principle is as simple as for alternated polylectrolyte multilayers in layer-by-layer assemblies. One can deposit as many layers as he wants.

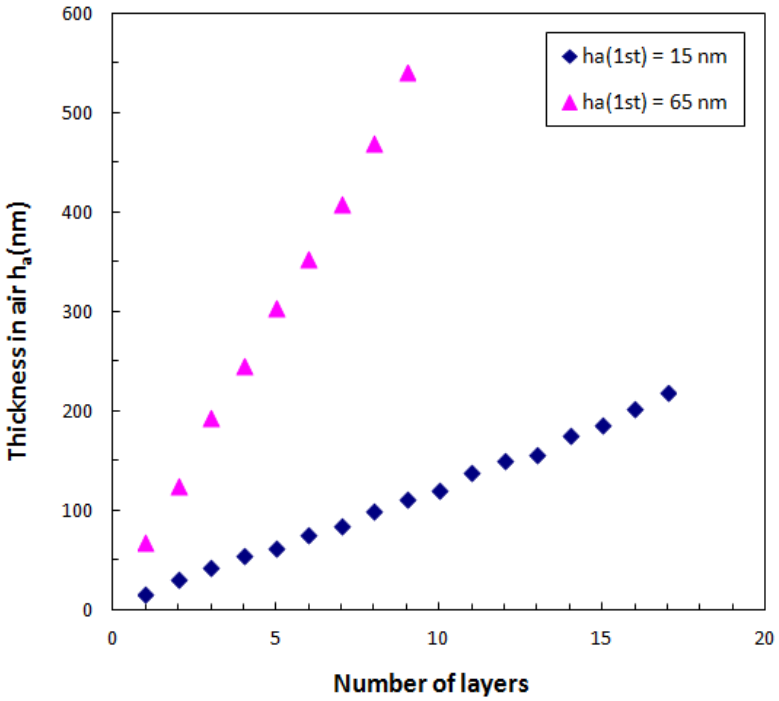


***Figure 3**: Linear increase of film thickness in air with the number of layers for multilayer gel films. $h_a(1^{st})$ is the thickness of the 1^{st} layer in air.*

The linear increase of film thickness in air with the number of deposited layers is demonstrated in **Figure 3**, up to 17 layers (h_a = 219 nm) for $h_a(1^{st})$ = 15 nm and 9 layers (h_a = 541 nm) for $h_a(1^{st})$ = 65 nm. The figure shows that the thickness of a multilayer gel film in air is linear to the number of layers.

1.1.3. Synthesis of bilayer PNIPAM gel films for neutron experiments

Multilayer gel films which have isotopic contrast are required to determine their internal structures in air (dry state) and also in liquid (swollen state) by neutron reflectivity. Thus multilayer hydrogel films of deuterated poly(acrylic acid) (PAA-d) gels and protonated poly(N-isopropylacrylamide) (PNIPAM-h) gels are synthesized, poly(acrylic acid) being used here for its unresponsiveness to temperature. For the study in liquid, PAA-d gel can be contrast-matched with D_2O/H_2O mixture, leaving only PNIPAM gel visible.

Only bilayer gel films containing PAA-d gel as the first layer and PNIPAM-h gel as the second layer are prepared for simplicity of interpretation. The bilayer gel films are chosen to study the effect of one-side confinement (from PAA-d network) on the swelling and collapse phase transition of PNIPAM-h network.

The fabrication process of the bilayers is similar to that of pure PNIPAM multilayer gel films, with the only difference that we use deuterated poly(acrylic acid) (PAA-d) to prepare the first layer. The solvent for spin-coating PAA-d chains as the first layer is a blend of methanol and formic acid with the ratio V/V = 7/3.

In **Table 2**, we list out all the bilayer hydrogel films for neutron experiments. Very thin bilayer films made from PAA-d chains and PNIPAM-h chains with various thicknesses in air are available. However, the uncertainty of thickness shows up when preparing gel films with low polymer concentration.

Name of samples	Number of layers	Polymer	Mw of polymer (Kg/mol)	Concentration of polymer (wt%)	Thickness in air (nm)	Solvent for spin-coating
BL4	1st	PAA Deuterated	92	0.18%	12.5	Methanol+Formic acid V/V=7/3
	2nd	P(AA-co-NIPAM)	66	0.50%	4.2	Butanol+Methanol V/V=1/1
BL7	1st	PAA Deuterated	92	0.18%	12.4	Methanol+Formic acid V/V=7/3
	2nd	P(AA-co-NIPAM)	66	1.50%	6.5	Butanol+Methanol V/V=1/1
BL9	1st	PAA Deuterated	92	0.18%	9.2	Methanol+Formic acid V/V=7/3
	2nd	P(AA-co-NIPAM)	681	0.20%	9.5	Butanol+Methanol V/V=1/1
BL10	1st	PAA Deuterated	92	0.20%	7.9	Methanol+Formic acid V/V=7/3
	2nd	P(AA-co-NIPAM)	66	0.20%	10.0	Butanol+Methanol V/V=1/1
BL26	1st	PAA Deuterated	92	0.40%	17.7	Methanol+Formic acid V/V=7/3
	2nd	P(AA-co-NIPAM)	66	0.50%	25.9	Butanol+Methanol V/V=1/1

***Table 2**: Formulation of bilayer (BL) hydrogel films for neutron experiments. The number in the name is the value of the thickness (in air) of PNIPAM network in the bilayer films.*

1.2. Structure of multilayer PNIPAM gel films in water

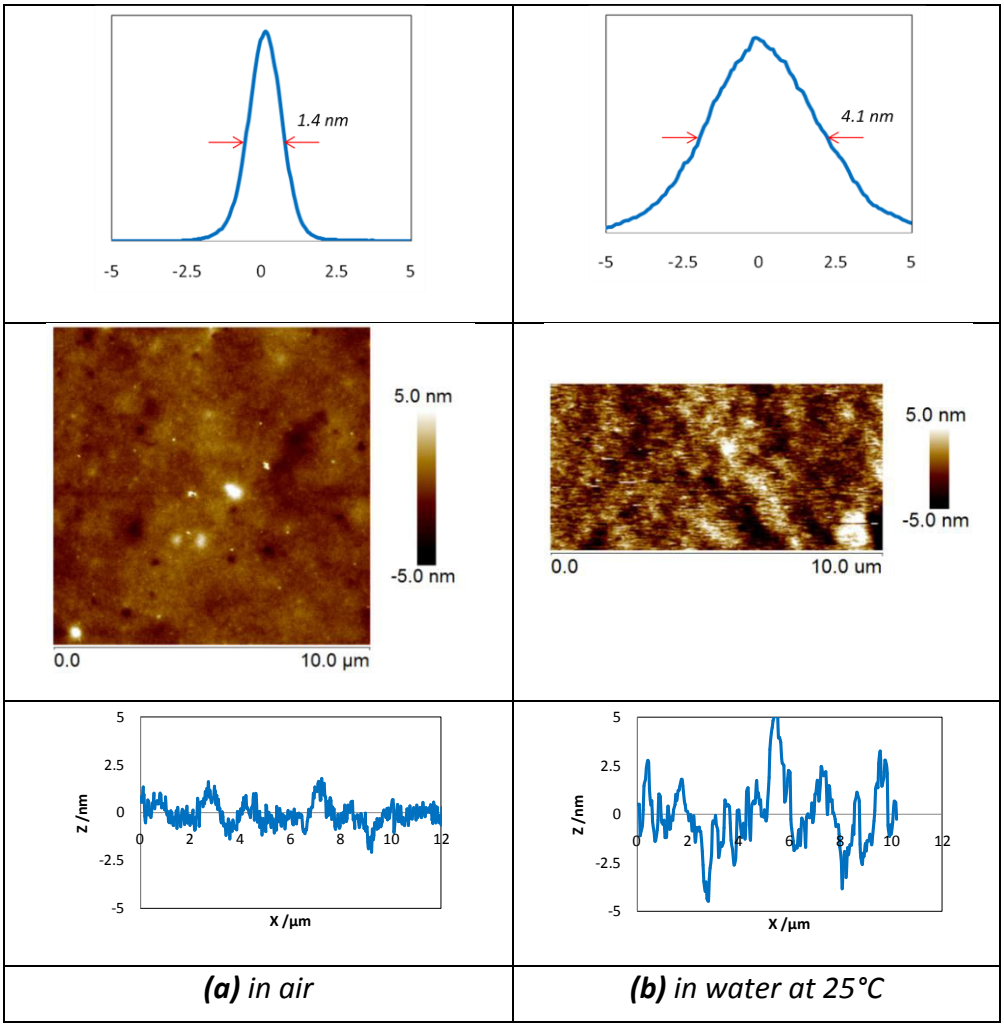
In order to explore properties of multilayer gel films developed through LbL assembly, AFM, ellipsometry and neutron reflectivity are employed to study their free surface topography, swelling behavior and density profile. Since PNIPAM hydrogel is interesting for its thermo-responsive properties and temperature is easier to control as an external stimulus, here we choose networks made of PNIPAM chains in the multilayer gel films as the studied object.

1.2.1. Topography

AFM can provide information on the topography and roughness of the free surface of the gel

films. All the AFM images displayed below are height images as for the characterization of single-network films. Along with each AFM height image, we also show the height histogram of the image at the top, and the cross-sectional plot of the image along the diagonal direction (called X) at the bottom, in which Z refers to the direction of the height.

Here we choose sample LbL_219 in **Table 1** to perform AFM investigation. Sample LbL_219 has the total thickness of 219 nm in air with 17 layers deposition.



***(a)** in air* | ***(b)** in water at 25°C*

***Figure 4**: AFM image of LbL_219 in air (a) and in water at 25°C (b), with thickness in air h_a = 219 nm.*

Peak Force QNM mode is used to characterize the free surface topography of multilayer gel films. AFM images of LbL_219 in air and in water at 25°C are presented in **Figure 4**. The small roughness (a few nanometers) in comparison with the thickness of the film (219 nm in air) implies the formation of uniform and continuous patterns on the multilayers hydrogel film. As obtained with single-network films, the LbL hydrogel film is rather flat with uniform patterns. The seemly continuous patterns observed in air and in water by AFM indicate that there is no effect of the constraints of the surface-attachment on the lateral swelling.

1.2.2. Swelling behavior

Swelling behavior of multilayers PNIPAM gel films in water at 25°C (swollen state) and 40°C (collapsed state) is determined by ellipsometry. Two samples LbL_219 (thickness of the first layer is 15 nm) and LbL_541 (thickness of the first layer is 65 nm) in **Table 1** are used for the study. In addition, to make a comparison with single network gel films, the samples SN12, SN248, SN65 and SN421 (see Chapter 2) are also investigated together. Results are shown in **Table 3**.

As for each sample, all the layers are made from the same polymer, when we treat the experimental data of multilayers films obtained from ellipsometry, we suppose the multilayers network as a single network. Also, it is taken into account that the refractive index of water is temperature independent.

Name of samples	Thickness in air h_a (nm)	Swollen thickness h_w (nm)		Swelling ratio $r = h_w/h_a$	
		in water at 40°C	in water at 25°C	in water at 40°C	in water at 25°C
SN12[(1)]	12	18	36	1.5	3.0
LbL_219	219	335	650	1.5	3.0
SN248	248	380	1020	1.5	4.1
SN65[(2)]	65	100	221	1.5	3.4
LbL_541	541	770	1630	1.4	3.0
SN421	421	685	1695	1.6	4.0

(1) Since the film is too thin for the measurements in water by ellipsometry, the results are from neutron reflectivity experiments.

(2) The film is too thick for the measurements in water by neutron reflectivity. It is at the limit of detection (thin layers) for the measurements in water by ellipsometry, mainly due to the width of the interface.

***Table 3**: Swelling behavior of multilayer PNIPAM gel films is compared with single-network gel films. The samples are characterized by ellipsometry.*

The swollen thickness and swelling ratio of each sample when immersed in water at 25°C and 40°C are displayed in **Table 3**. Overall, the swelling ratio of multilayer gel films in water is the same or less when compared with single-network gel films, keeping the responsive properties to temperature. Take the sample LbL_541 as an example, it swells with a ratio of 3.0 in water at 25°C, less than 3.4 for SN65 and 4.0 for SN421. These results may be indicative of the formation of thin interpenetrating networks between every two layers, which could restrain partly the swelling of multilayer gel films, resulting in a relatively smaller swelling ratio. On the other hand, the swelling ratio found in collapsed state at 40°C is around 1.5, which is the same value for single-network films. The presence of the hypothetical thin connecting networks between two adjacent layers predictably has no effect on the collapse of PNIPAM networks. The amplitude of the collapse of PNIPAM gel films is independent of the architecture and the thickness of the gel films. On the basis of

these observations, it is clear that multilayer PNIPAM gel films prepared by layer-by-layer assembly retain the same temperature sensitive behavior but exhibit a smaller swelling ratio, comparing to single-network gel films.

1.2.3. Characterization by neutron reflectivity

Neutron reflectivity technique is well suited for the characterization of multilayer gel films, as they allow the determination of the internal structures of multilayer gel films owing to the use of isotopic contrast.

In order to investigate the swelling behavior of PNIPAM network within the multilayer gel films, we apply the contrast matching procedure using a suitable ratio D_2O/H_2O to adjust the neutron contrast of the solvent to PAA_D network. As PAA-d contains precisely 95% of deuterium and 5% of proton (see ^1H NMR spectrum in chapter 2) and is considered to be 100% ionized in the experimental conditions (pH = 9), the values of Nb obtained by calculation are: 5.56 10^{-6} $Å^{-2}$ for dry PAA-d (without any water) and 4.95 10^{-6} $Å^{-2}$ for PAA-d in air (with 10% of water) assuming that the density for poly(sodium acrylate) as 1.6 g cm^{-3}. Taking into account the scattering length densities of H_2O (ρ_{H_2O} = -0.55.10^{-6} $Å^{-2}$), and D_2O (ρ_{D_2O} = 6.34.10^{-6} $Å^{-2}$), the contrast matching of PAA-d network can be achieved with the following volume ratio: D_2O/H_2O = 0.88/0.12. In these conditions only PNIPAM network is visible due to the contrast-matching by the solvent blend. In addition, the pH of the mixed solvent D_2O/H_2O is adjusted to 9.4 (pD = 9.4 corresponds to pH = 9), so that PAA is ionized to avoid from the hydrogen bond interaction between PAA and PNIPAM.

The objective is to determine the proximity of PNIPAM network from the silicon substrate. It is a definitive proof of the formation of either multilayer networks or interpenetrating networks. In addition, the multilayer gel films are investigated in water below and above the LCST of PNIPAM. We determine then the effect of the confinement on the swelling and collapse of the PNIPAM network in multilayer gel films.

The results are shown later in part 4 of this chapter where films of bilayers and interpenetrating networks are compared.

2. Interpenetrating networks (IPN) gel films

Similar to the synthesis of LbL networks gel films, we prepare interpenetrating networks gel films guided by the successful strategy of synthesis for single-network gel films with thiol-ene reaction. We expect that the formation of strong covalent cross-links and eventually physical entanglements inside the networks, stable IPN hydrogel thin films which are covalently grafted to the substrate can be obtained.

The polymer chains with ene groups synthesized in Chapter 2 are applied to realize cross-linking of the IPN gel films and attachment to the thiol-modified substrate in the presence of cross-linkers, while indicating their responsive properties. Different polymers with responsiveness to different stimuli can be used in preparing IPN gel films as different composition of each network, if proper conditions are chosen (in particular the solvent for spin-coating for each network and the cross-linking reaction).

To make clear the structure of IPN gel films and to understand their properties, we investigate the IPN gel films using ellipsometry, AFM and neutron reflectivity, and then compare the results with that from single-network gel films and multilayers gel films. The ellipsometry measures in air cannot distinguish the architecture of multilayers or interpenetrating networks because it is sensitive to the whole amount of polymer. On the other hand, the measures in water which provide the swelling behavior should be helpful to discern each of the two architectures. Neutron reflectivity measures both in air and in water should definitely differentiate multilayers or interpenetrating networks since it allows the determination of the internal structure of each network owing to the isotopic contrast.

2.1. Synthesis

2.1.1. General strategy

As known, an interpenetrating network consists of two or more polymer networks, at least one of which is polymerized and/or cross-linked in the immediate presence of the other [8]. As a basis, interpenetrating networks composed of two interpenetrated polymer networks are emphasized in our study.

For the synthesis of the first network gel films, we follow exactly the same process as that of the first layer for multilayers gel films by LbL assembly. However, afterwards the preparation of IPN is different from multilayers assembly as shown in **Figure 5**. After the coating of the polymer chains on the first network in the presence of cross-linkers, one more step is carried out before cross-linking, in order to facilitate the interpenetration of the polymer chains into the first network. The whole system is kept in a sealed container which is filled with saturated vapor of a good solvent for the first network for 24 h. This step aims to swell the first network by prestretching the polymer chains of the first network, and thus help the interpenetration of the polymer chains of the second network into the first network. When the interpenetration process is finished, cross-linking of the second network is realized, resulting in interpenetrating networks composed of two polymer networks. It is important to note that short polymer chains (polymer with smaller Mw) are preferred to prepare the second network as they enable to more diffuse in the first network than long polymer chains. Actually, the relaxation time is proportional to the cube of the molecular weight of chains

assuming the reptation theory. For the synthesis of LbL-inspired gel films, there is no preference because the second layer is supposed to be simply stacked on the first one.

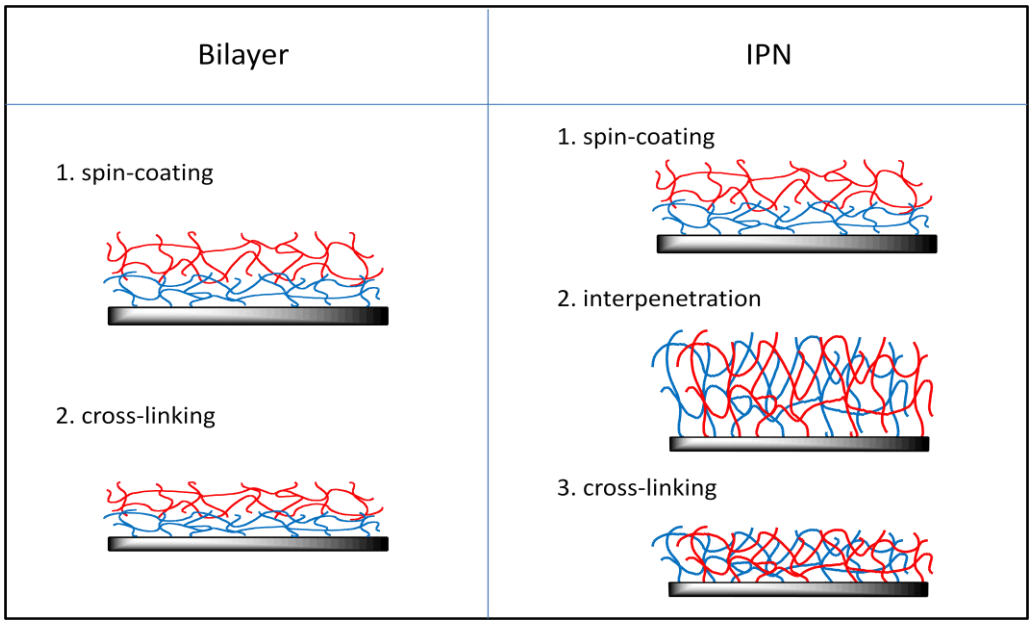


***Figure 5**: Comparison between synthesis of bilayers and interpenetrating networks.*

The essence lies in the selection of a good solvent for the interpenetration, as a poor solvent cannot yield in interpenetration between the two networks, thus, in IPN formation. Here a "good" solvent refers to a solvent in which the polymer chains of the first network can solubilize well to realize the swelling of the first network, and meanwhile who has a low boiling point to ensure that the system is surrounded by saturated vapor during the process of interpenetration.

The film thickness of each network can be easily controlled by adjusting polymers with different molar mass, the concentration of the solution and the final spinning speed in coating. Thus the thickness of the IPN gel film is controllable, ranging from nanometers to micrometers.

Our general strategy to prepare IPN hydrogel films composed of two polymer networks is summarized as follows:

1) the solution of an ene-functionalized polymer is deposited on the thiol-modified silicon wafer in the presence of cross-linkers and then spin-coated; the cross-linking and grafting-to-surface processes are achieved simultaneously by the thiol-ene reaction under certain conditions;
2) the solution of another (or the same) ene-functionalized polymer is deposited on the first network film in the presence of cross-linkers and then spin-coated; the whole system is kept in a sealed container for a given reaction time (24 h

is tried here), the container being filled with saturated vapor of a good solvent for the first network;

3) the sample is afterwards put in oven at 120°C to activate the cross-linking of the second network; the cross-linking of the 2nd network and connecting-to-the 1st network processes are simultaneously achieved by the thiol-ene reaction.

2.1.2. Synthesis of PNIPAM IPN gel films

Here we take the thermo-responsive PNIPAM IPN hydrogel films as an example to show the details of fabrication of IPN gel films.

Synthesis of the 1st network:

The synthesis of the 1st network is exactly the same as that of the 1st layer for single-network and LbL-inspired gel films. This provided a film of PNIPAM network, which is used as a substrate for coating the second layer.

Synthesis of the 2nd network:

The synthesis of the 2nd network is similar to that of the 1st network. The only difference is that after spin-coated before put in oven, the wafer is kept in a sealed container which is filled with saturated vapor of a good solvent for the first network for 24 h to fulfill the interpenetration process. The gel films are then stored at room temperature for later use.

In **Table 4**, we list out some of the PNIPAM IPN gel films prepared and their compositions.

Name of samples	Number of networks	Mw of polymer (Kg/mol)	Concentration of polymer (wt%)	Thickness of 1st network in air (nm)	Total thickness in air (nm)	Solvent for interpenetration
IPN_109	1st	400	1.0%	64	109	butanol+methanol (V/V = 1/1)
	2nd	66	1.0%			
IPN_139	1st	400	1.0%	69	139	butanol+methanol (V/V = 1/1)
	2nd	400	1.0%			
IPN_417	1st	400	3.0%	223	417	butanol+methanol (V/V = 1/1)
	2nd	400	3.0%			

***Table 4**: Formulation of PNIPAM IPN gel films.*

From **Table 4**, we can see that PNIPAM IPN gel films made from copolymers of different molar mass or at different polymer concentrations are available. To prepare PNIPAM IPN gel films, a blend of butanol and methanol (V/V = 1/1) is a proper solvent for the interpenetration process. Samples IPN_109 and IPN_139 have comparable thickness of single-network networks and the difference is the chain length of the second network, IPN_109 being preparing with shorter chains. For samples IPN_139 and IPN_417, the total

thickness and the thickness of the two networks are different since they are prepared with polymer solution of different concentrations. The comparison between these samples should give an indication of the interdiffusion of the two networks depending on the chain length and the thickness of the first network (for a same relaxation time). If the networks choosen here consist of only PNIPAM polymer, it should be interesting to extend the study to different kinds of polymer. It is opportunely investigated with poly(acrylic acid) instead of PNIPAM, as described in the following.

2.1.3. Synthesis of IPN films for neutron reflectivity experiments

IPN gel films composed of two networks which have isotopic contrast are required to determine their internal structure in air and also in water by neutron reflectivity. Thus interpenetrating networks films of deuterated poly(acrylic acid) (PAA-d) and protonated poly(N-isopropylacrylamide) (PNIPAM-h) gels are synthesized, poly(acrylic acid) being used here for its unresponsiveness to temperature. For the study in water, PAA-d network can be contrast-matched with D_2O/H_2O mixture, leaving only PNIPAM-h network visible.

Interpenetrating networks films are prepared with PAA-d network as the first network and PNIPAM-h network as the second network. These IPN gel films are chosen to make a comparison with bilayers gel films studied by neutron reflectivity. The fabrication process of these IPN films is similar to that of IPN films made of only PNIPAM networks, with the only difference that we use deuterated poly(acrylic acid) (PAA-d) to prepare the first network. The solvent for spin-coating PAA-d chains is a blend of methanol and formic acid with the ratio V/V = 7/3. And THF is chosen as the solvent for the interpenetration process of PNIPAM chains into PAA-d network since it is a good solvent for both PAA and PNIPAM polymers and has a very low boiling point.

In **Table 5**, we list out all the IPN hydrogel films for neutron experiments.

Name of samples	Number of networks	Polymer	Mw of polymer (Kg/mol)	Concentration of polymer (wt%)	Thickness in air (nm)	Solvent for spin-coating	Solvent for interpenetration
IPN5	1st	PAA Deuterated	92	0.18%	10.1	Methanol+Formic acid V/V=7/3	THF
	2nd	P(AA-co-NIPAM)	66	0.17%	4.6	Butanol+Methanol V/V=1/1	
IPN11	1st	PAA Deuterated	92	0.20%	7.6	Methanol+Formic acid V/V=7/3	THF
	2nd	P(AA-co-NIPAM)	66	0.20%	11.1	Butanol+Methanol V/V=1/1	
IPN14	1st	PAA Deuterated	92	0.18%	11.4	Methanol+Formic acid V/V=7/3	THF
	2nd	P(AA-co-NIPAM)	66	0.20%	13.6	Butanol+Methanol V/V=1/1	
IPN31	1st	PAA Deuterated	92	0.40%	16.0	Methanol+Formic acid V/V=7/3	THF
	2nd	P(AA-co-NIPAM)	66	0.50%	30.5	Butanol+Methanol V/V=1/1	

***Table 5**: Formulation of IPN hydrogel films for neutron experiments. The number in the name is the value of the thickness of PNIPAM gel (in air) in the IPN films.*

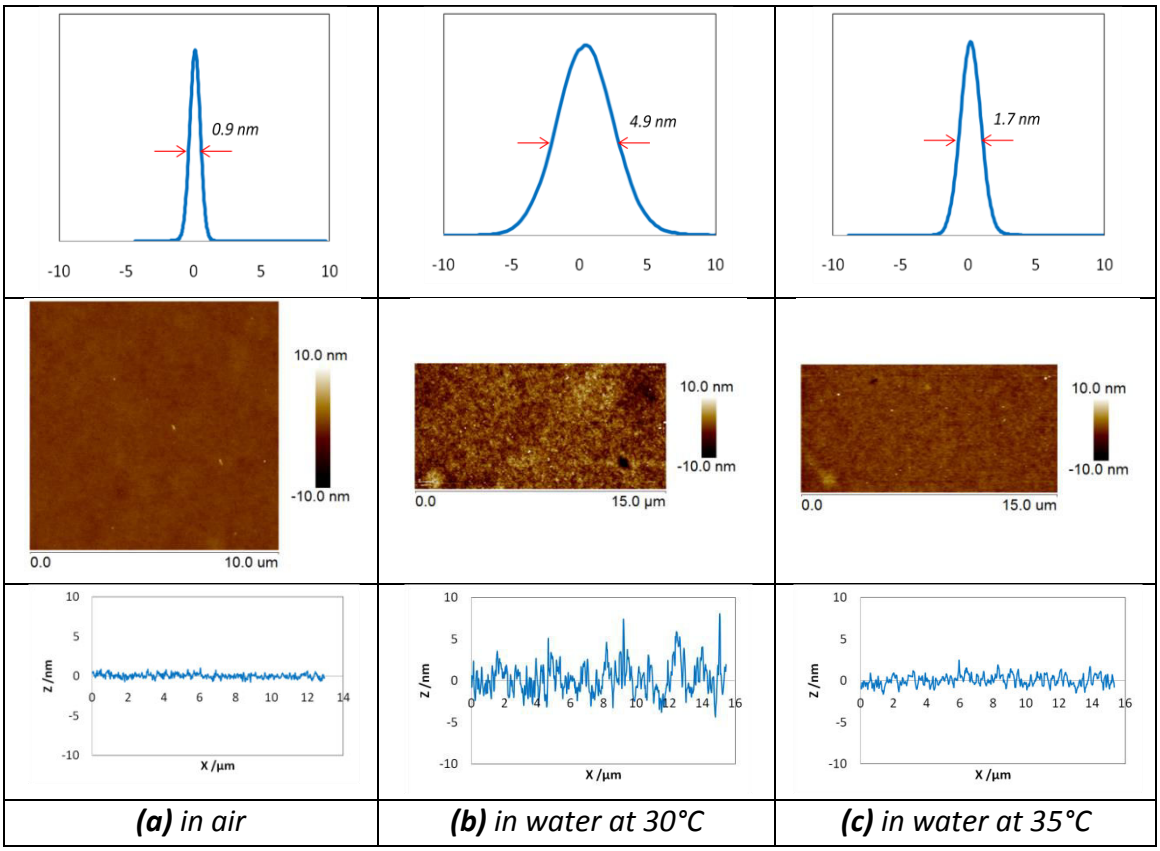
From **Table 5**, we can see that very thin IPN films made from PAA-d chains and PNIPAM-h chains with various thicknesses in air are available. However, the uncertainty of thickness shows up when preparing gel films with low polymer concentration as already informed for the bilayer films.

2.2. Structure of the PNIPAM IPN gel films in water

2.2.1. Topography

We choose sample IPN_417 in **Table 4** to perform AFM investigation. Sample IPN_417 has the total thickness of 417 nm in air. Peak Force QNM mode is used to characterize the free surface topography of IPN gel films.

AFM images of IPN_417 in air and in water are presented in **Figure 6**. The small roughness in air implies formation of a uniform and continuous pattern on the IPN film. When immersed in water, the roughness of the free surface increases. But it decreases with the growth of temperature. The FWHM found is the comparable to the values obtained with single-network films and LbL-inspired films. The LbL-inspired films and the IPN films are as little rough as the single-network films.



***(a)** in air* | ***(b)** in water at 30°C* | ***(c)** in water at 35°C*

***Figure 6**: AFM images of IPN_417 in air (a), in water at 30°C (b) and 35°C (c), with thickness in air h_a = 417 nm.*

2.2.2. Swelling behavior

Swelling behavior of IPN films made of PNIPAM chains in water at 25°C (swollen state) and 40°C (collapsed state) is characterized by ellipsometry. The sample IPN_139 in **Table 4** is used for the study. In addition, to make a comparison with bilayers and single-network films, the bilayers gel film LbL_128 in **Table 1** and the single-network film SN149 (see Chapter 2) are also investigated together. Note that the three samples have comparable thickness in air. Results are shown in **Table 6**.

As for the bilayer gel film, both of the two layers are made from the same polymer, when we treat the experimental data obtained from ellipsometry, we suppose the bilayers network as a single network, which is the same situation for the IPN film. Also, it is taken into account that the refractive index of water is temperature independent.

Samples	Thickness in air h_a (nm)	Swollen thickness h_w (nm)		Swelling ratio $r = h_w/h_a$	
		in water at 40°C	in water at 25°C	in water at 40°C	in water at 25°C
SN149	149	240	615	1.6	4.1
IPN_139	139	195	350	1.4	2.5
LbL_128	128	190	400	1.5	3.1

Table 6*: Swelling behavior of an IPN film is compared with a bilayers gel film and a single network film. The film is characterized by ellipsometry.*

The swollen thickness and swelling ratio of each sample when immersed in water at 25°C and 40°C are displayed in **Table 6** respectively. Comparing with the single-network film, the bilayers gel film swells less, with a swelling ratio of 3.1 (against 4.1) in water at 25°C, which is consistent with the results shown in **Table 3**. The swelling of the IPN film is much less, with a swelling ratio of 2.5 compared to 4.1 for the SN film.

Multilayers gel films are supposed to be the combination of many single network films simply by stacking one onto the other, but thin interpenetrating networks may exist between every two layers, which could restrain partly the swelling of multilayer gel films, resulting in a relatively smaller swelling ratio. Different from that, during the fabrication of IPN gel films, interpenetration process between the two networks is targeted, making the two networks go into each other and then connected by covalent bonds and eventually physical entanglements. The strong connection between the two networks restricts the swelling of the IPN film strongly leading to a smaller swelling ratio. For the two symmetric networks with same cross-linking density and the same amount of polymer (or same thickness in air), the complete interpenetration of the two networks is expected to restrict the swelling of the films to half such as the double of the cross-linking density. The swelling ratio of 2.5 of the IPN film studied (instead of the value of 2 expected for an ideal interpenetrating networks film) suggests that the two networks are not completely

interdiffused and that only partial interpenetration occurs.

However, the difference in swelling ratio between the IPN film and the bilayers gel film (2.5 and 3.1) happens to confirm our relative success in building these two different systems. If the IPN and bilayers are not ideal interpenetrating networks and stacked layers, the swelling behavior shows that in the IPN film, the two networks are more interdiffused than in bilayers films. This observation has to be confirmed by neutron reflectivity which allows the determination of the internal structure of the layers owing to the isotopic contrast.

3. Hybrid gel films

Hydrid hydrogel films containing silica particles and polymer networks are developed. The hybrid gel films are expected to have their mechanical properties improved similarly to macroscopic hybrid hydrogels [9] due to the presence of solid (silica) particles and because physical interactions between silica particles and polymer chains inside hybrid gels exist. The synthesis of surface-attached silica-polymer hybrid networks follows the same strategy as used for single network gel films. The polymer chains with ene groups synthesized in Chapter 2 are applied to realize cross-linking of the hybrid gel films and attachment to the thiol-modified substrate in the presence of cross-linkers, while indicating their responsive properties.

To make clear the structure of hybrid gel films and to understand their properties, we investigate silica-polymer hybrid gel films using ellipsometry and AFM and then compare the results with that from single network gel films. Since as an environmental parameter temperature is easier to control compared with light and electric field, for the study of properties of hybrid gel films, we choose thermo-responsive PNIPAM chains as the polymer composition of hybrid gels. The dispersion of silica particles is observed by AFM and the swelling behavior of PNIPAM network in silica-PNIPAM hybrid gel films is characterized by ellipsometry. We will show that silica nanoparticles are mechanically trapped inside the polymer matrix, even during swelling experiments. Also, the impact of silica nanoparticles on the swelling behavior of hybrid hydrogels will be discussed.

3.1. Synthesis

3.1.1. General strategy

Hybrid hydrogel films are prepared by cross-linking polymer chains in the presence of silica nanoparticles dispersed inside. Before presenting the synthesis procedure of hybrid hydrogel films, a special attention will be given to the inorganic material – silica nanoparticles that have not been introduced before.

One silica suspension named Ludox-TM50 from Dupont is used for the study. The Ludox suspensions are known to be weakly polydisperse and easily available with several sizes. The main characteristics of Ludox-TM50, characterized at 25°C, are the following:

- concentration: 52 wt% in water;
- pH = 9;
- conductivity: 4.9 mS/cm;
- nature of the stabilizing counter ions: Na^+.

Ludox-TM50 is initially dialyzed in pure water during two weeks in order to remove the counter ions and purify the suspension. After dialysis, a stable suspension is obtained, with the silica concentration around 20 wt% and the conductivity nearly 0 mS/cm.

The size of silica nanoparticles in Ludox-TM50 is characterized by different techniques such as dynamic light scattering, small angle neutron scattering and scanning electron microscopy [10]. It is observed that the silica particles present a spherical shape with a mean radius around 15 nm. This indication will be useful for the following characterizations.

The synthesis of silica-polymer hybrid hydrogel films is very similar to that of single network gel films, except that silica nanoparticles are introduced into the polymer solution before spin-coating (see **Figure 7**). The principle consists in coating on the thiol-modified silicon wafers a mixed solution with ene-functionalized polymers, silica suspension and bifunctional thiol molecules as cross-linkers. The polymers are copolymers containing ene-reactive groups and monomer units with stimuli-responsive properties synthesized in Chapter 2. As for the films of single-network, LbL-inspired network and interpenetrating networks, the thiol-ene reaction allows the covalent cross-linking of polymers networks which are also covalently grafted onto the surface of silicon wafers, the hybrid hydrogel networks being obtained with silica particles trapped inside.

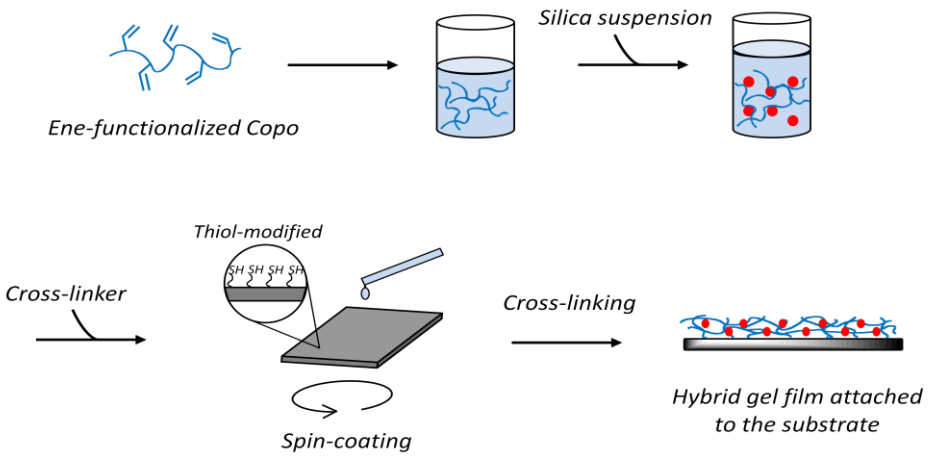


***Figure 7**: Synthesis of silica-polymer hybrid gel thin films.*

Typically, the thickness of the silica-polymer hybrid hydrogel thin film can be easily controlled by adjusting polymers with different molar mass, the polymer concentration, the concentration of silica particles, and the final spinning speed in coating, ranging from nanometers to micrometers.

Our general strategy to prepare hybrid hydrogel films is presented as follows:

1) the ene-functionalized copolymer is dissolved in a proper solvent stirring for one night and then the dialyzed Ludox-TM50 suspension is introduced into the solution stirring for about 3 hours;
2) the mixed solution is deposited on the thiol-modified silicon wafer in the presence of cross-linkers and then spin-coated;
3) cross-linking and grafting-to-surface processes are achieved simultaneously by the thiol-ene reaction.

3.1.2. Synthesis of silica-PNIPAM hybrid gel films

Here we take the thermo-responsive silica-PNIPAM hybrid hydrogel films as an example to show the details of fabrication of silica-polymer hybrid gel films.

Firstly poly(AA-co-NIPAM) is dissolved in the mixture of methanol and pure water at a certain concentration, the solution stirred for one night to help dissolution. Then the dialyzed Ludox-TM50 suspension is introduced into the solution, whose amount is decided by the ratio between polymer chains and silica particles, meanwhile with respect to the ratio between methanol and water as V/V = 4/1 in the solution. After the solution stirred for about 3 hours, the cross-linker dithioerythritol (DTE), of an access with respect to a certain ratio of the ene groups in the polymer chains, is added into the solution. The mixture is then spin-coated on the silicon wafer at 3000 rpm for 30 s. After spin-coating, the wafer is immediately put under vacuum at 120°C for one night. Afterwards the silicon wafer is taken out of the oven and cools down naturally. It is rinsed in methanol using ultrasonic bath for 1 minute to remove the unreacted polymers and then dried with N_2 flow. The thickness of the obtained film is measured by ellipsometry.

In **Table 7**, we list out some of the silica-PNIPAM hybrid gel films synthesized with their characteristics.

As shown in **Table 7**, the nomenclature used in this study is: “Mw of polymer”_Px_Sy, while x stands for the concentration of polymer in the solution by weight, and y stands for the volume fraction of silica particles in the film in air. All the samples listed above have been put in water at room temperature for at least 1 day and then the thicknesses are measured by ellipsometry, to test whether there’s detachment of the silica nanoparticles from the gel films in swollen state. Results indicate that stable silica-PNIPAM hybrid gel films made from polymers with different molar mass at various concentrations are available. Reasonably, the

addition of silica particles increases the thickness of the gel film in air. We also vary the silica nanoparticles content in the gel film to tune its architecture: from pure polymer network to hybrid gel. These samples are stored at room temperature for later use.

Name of samples	Mw of polymer (Kg/mol)	Concentration of polymer (wt%)	Silica/Polymer (w/w)	Volume fraction of silica particles*	Thickness in air (nm)
66K_P1_S0	66	1.0%	0	0	70
66K_P1_S61.7			5/1	61.7%	198
66K_P2_S0		2.0%	0	0	90
66K_P2_S41.9			2/1	41.9%	277
66K_P2_S61.7			5/1	61.7%	420
66K_P5_S0		5.0%	0	0	200
66K_P5_S0.39			1/100	0.39%	230
66K_P5_S0.77			1/50	0.77%	251
66K_P5_S1.8			1/20	1.8%	293
66K_P5_S3.6			1/10	3.6%	340
66K_P5_S7.2			1/5	7.2%	352
66K_P5_S16.2			1/2	16.2%	400
66K_P5_S27			1/1	27,0%	455
681K_P1_S0	681	1.0%	0	0	80
681K_P1_S61.7			5/1	61.7%	237
681K_P2_S0		2.0%	0	0	170
681K_P2_S0.77			1/50	0.77%	178
681K_P2_S1.8			1/20	1.8%	201

**10% of water (by volume) in the film in air is taken into account. ρ_{Silica} = 2.3 g/cm^3; $\rho_{Polymer}$ = 1 g/cm^3.*

***Table 7**: Formulation of silica-PNIPAM hybrid gel films. The nomenclature is: "Mw of polymer"_Px_Sy, while x stands for the concentration of polymer in the solution by weight (%), and y stands for the volume fraction of silica particles in the film in air (%).*

In **Figure 8**, we display the curve of thickness of silica-PNIPAM hybrid gel film in air as a function of the volume fraction of silica particles, using the samples from **Table 7**. The molecular weight (66 kg/mol) and the concentration of polymer in the solution for spin-coating (5%) are kept constant. The curve shows that the thickness in air rises along with the increase of the content of silica particles. We can observe that the curve is composed of two linear parts with the cross-over volume fraction at around 4%. When the volume fraction of silica particles is less than this cross-over concentration, the slope of the line is bigger than that when the volume fraction is more, which means that the effect of silica particles content on the thickness of the hybrid gel film in air is stronger when there are relatively less silica particles.

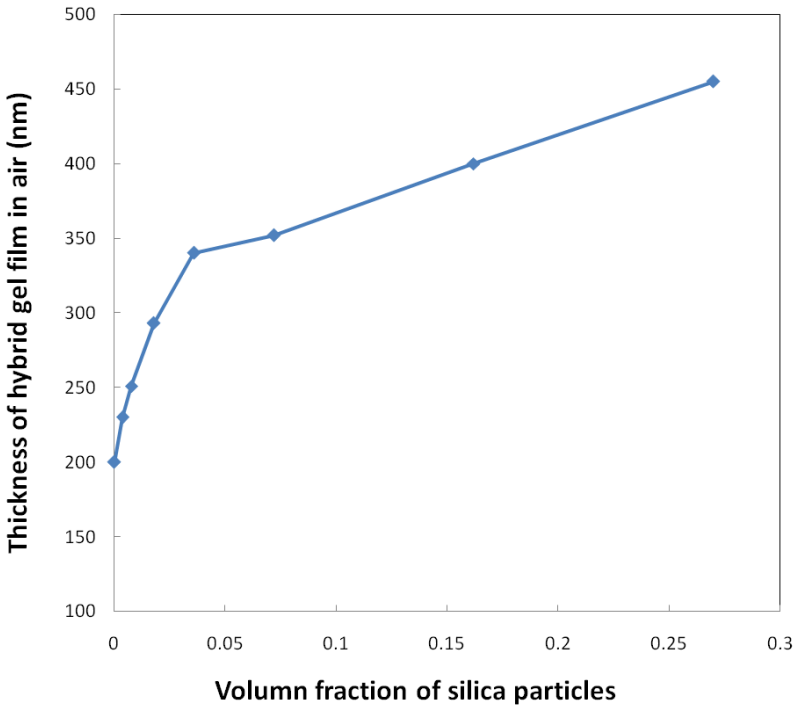


***Figure 8**: Thickness of silica-PNIPAM hybrid gel film in air as a function of the volume fraction of silica particles. Mw of P(AA-co-NIPAM): 66Kg/mol; concentration of polymer by weight: 5.0%.*

3.2. Structure of silica-PNIPAM hybrid gel films in water

3.2.1. Topography of the free surface

AFM can provide information on the topography and roughness of the free surface of the hybrid gel films with qualitative information on the dispersion of silica nanoparticles at the free surface of the hybrid gel films.

Firstly the silica-PNIPAM hybrid gel films are studied in dry state (in air at room temperature) to determine the amount of silica nanoparticles on the surface and their distribution. Then measurements in water at room temperature are carried out, using the temperature-controllable cell as presented in Chapter 3. The measurements are not easy due to the big difference in hardness between silica particles and the swollen polymer network. Finally, the effect of temperature on the morphology of the hybrid gel films in water is also investigated.

All the samples used for AFM study are from **Table 7**.

In dry state

All the AFM measurements in dry state are carried out in tapping mode with a standard tapping cantilever of resonance frequency equal to 300 Hz and stiffness 40 N/m.

The results are displayed using height images together with the corresponding phase images. Along with the height images, we also show the height histogram of the image at the top. So in each figure, the first and the second rows are the height histogram(s) and height image(s) respectively, and the third row is the phase image(s). In addition, the value of full width at half maximum (FWHM) of the histogram curve is also indicated in the height histogram.

The silica-PNIPAM hybrid gel film 66K_P1_S61.7 is firstly studied in dry state, with results shown in **Figure 9**.

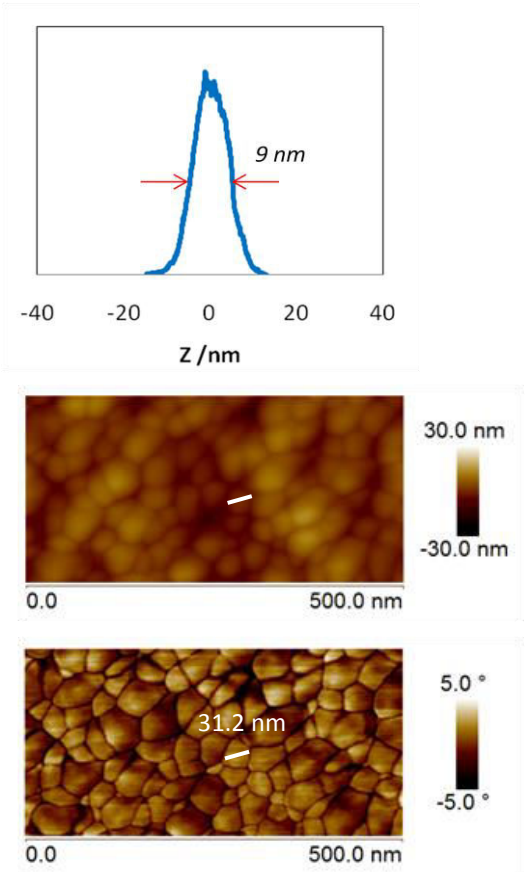
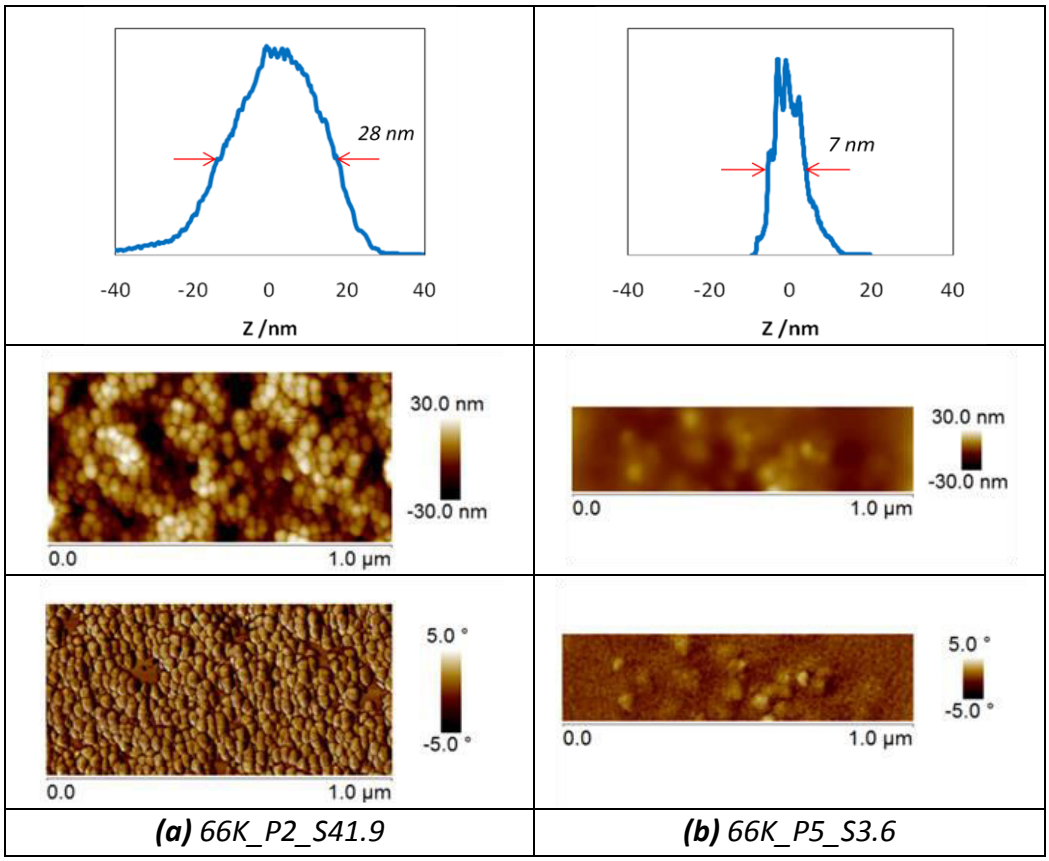


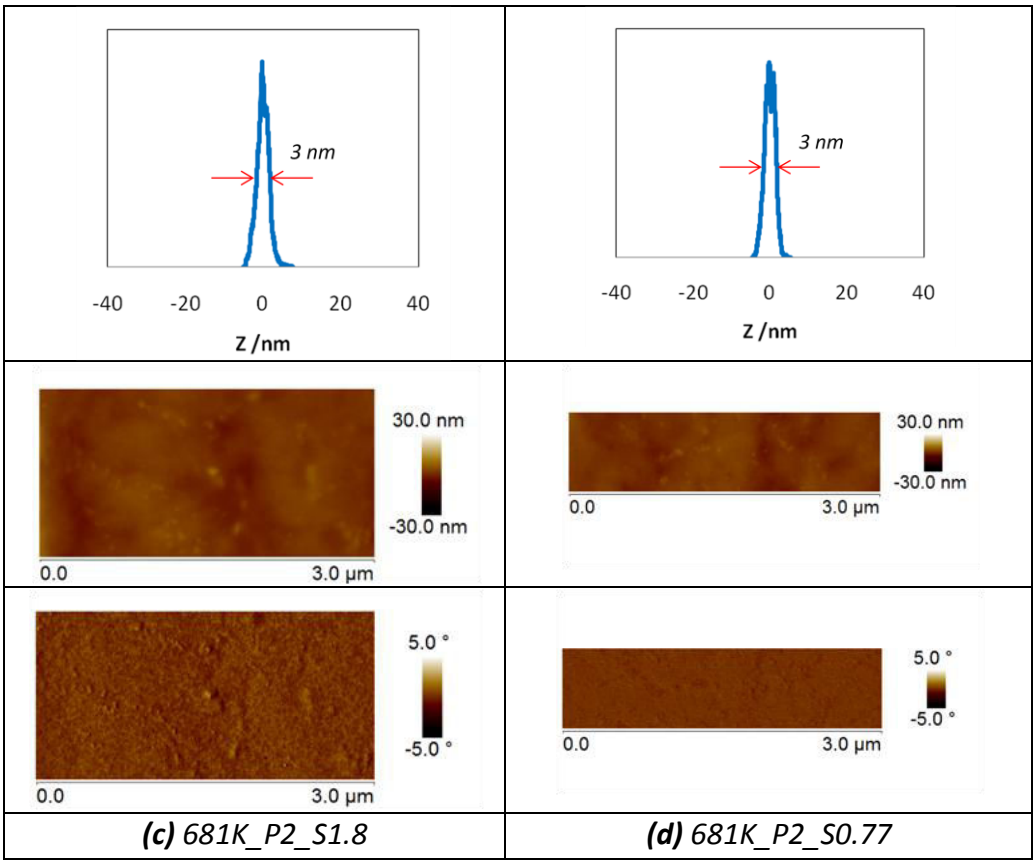
***Figure 9**: AFM tapping images of a silica-PNIPAM hybrid gel film 66K_P1_S61.7 in dry state.*

In the height and phase images presented in **Figure 9**, silica nanoparticles with a radius equal to about 30 nm can be clearly observed on the surface of the hybrid gel film. Actually, due to their high volume fraction (up to 61.7%) in the hybrid gel film, silica nanoparticles distribute on the surface in very high density, with almost no polymer network showing up. Moreover, compared with the single network PNIPAM gel films studied in Chapter 3, the addition of silica particles in the polymer network makes its surface become rougher, with FWHM of the height histogram greatly increased from about 0.6 nm to 9 nm.

The same experiments are carried out on silica-PNIPAM hybrid gel films with different contents of silica nanoparticles, varying between 0.77% and 61.7%. The results are displayed in **Figure 10**.



(a) *66K_P2_S41.9* | ***(b)*** *66K_P5_S3.6*



(c) *681K_P2_S1.8* | ***(d)*** *681K_P2_S0.77*

Figure 10*: AFM tapping images of silica-PNIPAM hybrid gel films with different silica nanoparticles contents in dry state.*

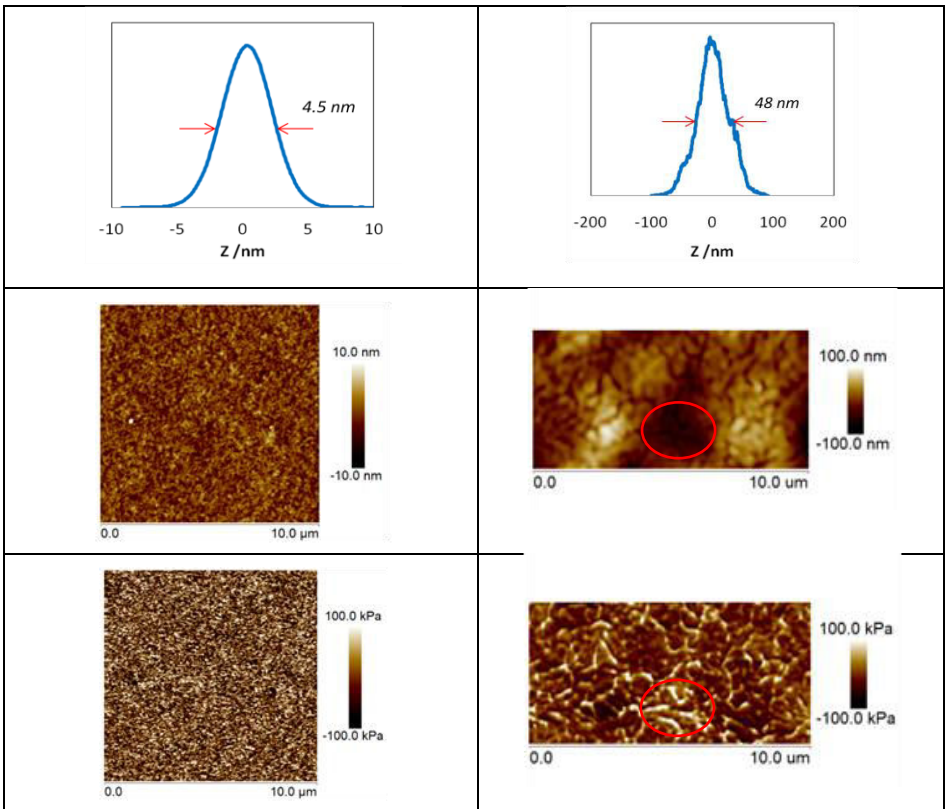
From the height and phase images shown in **Figure 10**, we can easily find out that the density of silica particles on the surface decreases with the decrease of their volume fraction in the hybrid gel film, which is quite reasonable. And generally, the surface becomes smoother when there are less silica particles, with a smaller FWHM of the height histogram.

In water at 25°C

All the AFM measurements in water are carried out in QNM mode.

The results are displayed using height images together with the corresponding DMT Modulus images. It has to be pointed out that the modulus obtained from AFM experiments is not absolute value, while we just use it to make a comparison between silica particles and the polymer network. Along with the height images, we also show the height histogram of the image at the top. So in each figure, the first and the second rows are the height histogram(s) and height image(s) respectively, and the third row is the DMT Modulus image(s). In addition, the value of full width at half maximum (FWHM) of the histogram curve is also indicated in the height histogram.

The silica-PNIPAM hybrid gel film 681K_P2_S1.8 is firstly studied in water at 25°C, with results shown in **Figure 11**, comparing with a single network PNIPAM gel film.



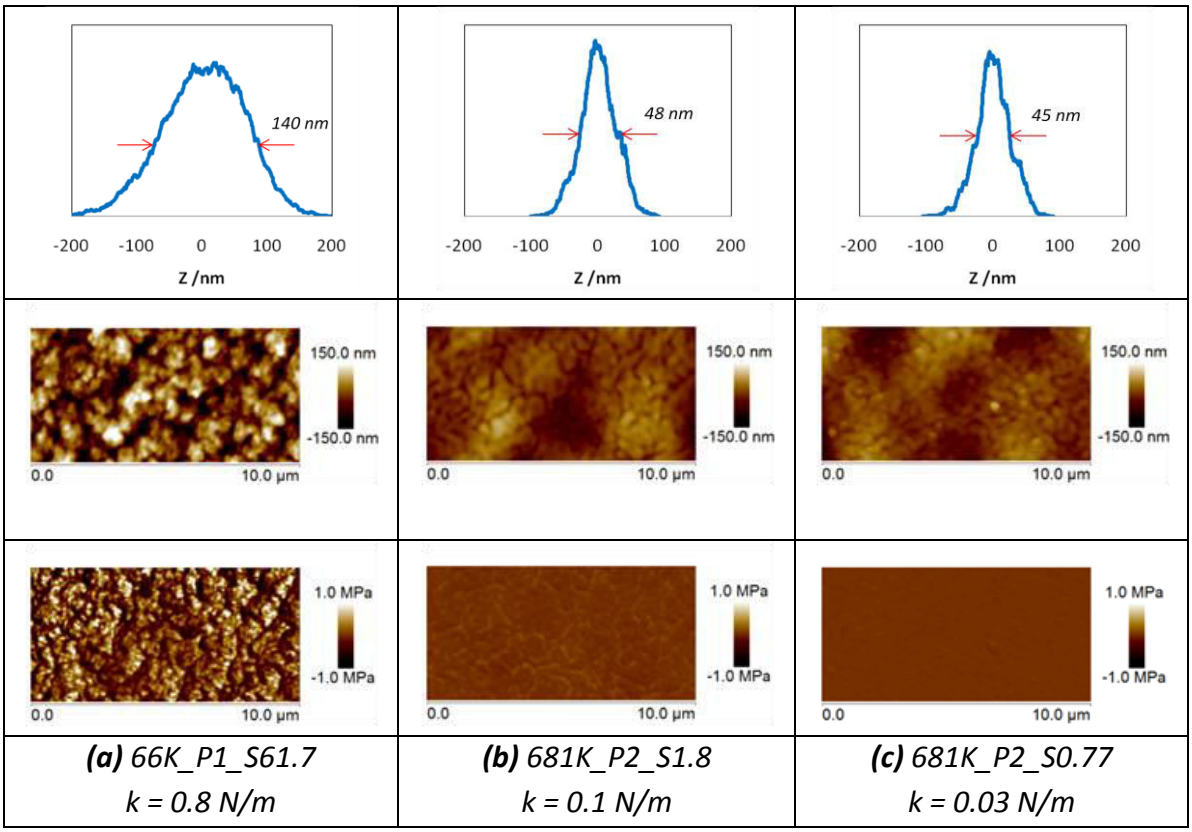
(a) *SN249, k = 0.7 N/m* | ***(b)*** *681K_P2_S1.8, k = 0.1 N/m*

Figure 11*: AFM QNM images of a single network PNIPAM gel film (a) S2_629K_249nm (Chapter 3) and a silica-PNIPAM hybrid gel films (b) 681K_P2_S1.8 in water at 25°C.*

When immersed in water at 25°C, both of the two gel films are in swelling state. Comparing the height images and height histograms of the two samples SN249 (see Chapter 3) and 681K_P2_S1.8 presented in **Figure 11**, we observe that the addition of silica particles in the polymer network, even a small amount (volume fraction equal to 1.8%), can make its surface become much rougher, with FWHM of the height histogram greatly increased from 4.5 nm to 48 nm.

Moreover, large zones of different height can be observed in water, the zones being larger than those found in air, which is consistent with the swelling of the hybrid network film. The relatively lower part in the height image (marked with a red circle) has higher modulus in the DMT Modulus image. It could be explained by the presence of aggregated silica particles at this place. The other place which appears clear in the height image is explained by the presence of the swollen polymer, this zone showing lower modulus in the DMT Modulus image. It is consistently comprehended by the hardness of silica particles and the softness of polymer network.

The same experiments are carried out on silica-PNIPAM hybrid gel films with different contents of silica nanoparticles, varying between 0.77% and 61.7%. The results are displayed in **Figure 12**.



(a) *66K_P1_S61.7* *k = 0.8 N/m*	***(b)*** *681K_P2_S1.8* *k = 0.1 N/m*	***(c)*** *681K_P2_S0.77* *k = 0.03 N/m*

Figure 12*: AFM QNM images of silica-PNIPAM hybrid gel films with different silica nanoparticles contents in water at 25°C.*

From the height images and height histograms shown in **Figure 12**, we can easily find out that the roughness of the surface in water decreases with the decrease of the volume fraction of silica particles in the hybrid gel film, with a decreasing FWHM of the height histogram. For hybrid networks with less silica particles, the zones of different height are large, showing more diffuse morphologies due to the presence of more (swollen) polymers. In addition, the DMT Modulus images demonstrate that hybrid gel films are harder when containing more silica particles with a bigger DMT Modulus, which may be due to the aggregation of silica particles and the thus-caused less swelling of the hybrid gel films.

Effect of temperature

All the AFM measurements here are carried out in QNM mode.

The silica-PNIPAM hybrid gel film 681K_P2_S0.77 is studied in water at 30°C and 40°C, with results shown in **Figure 13**.

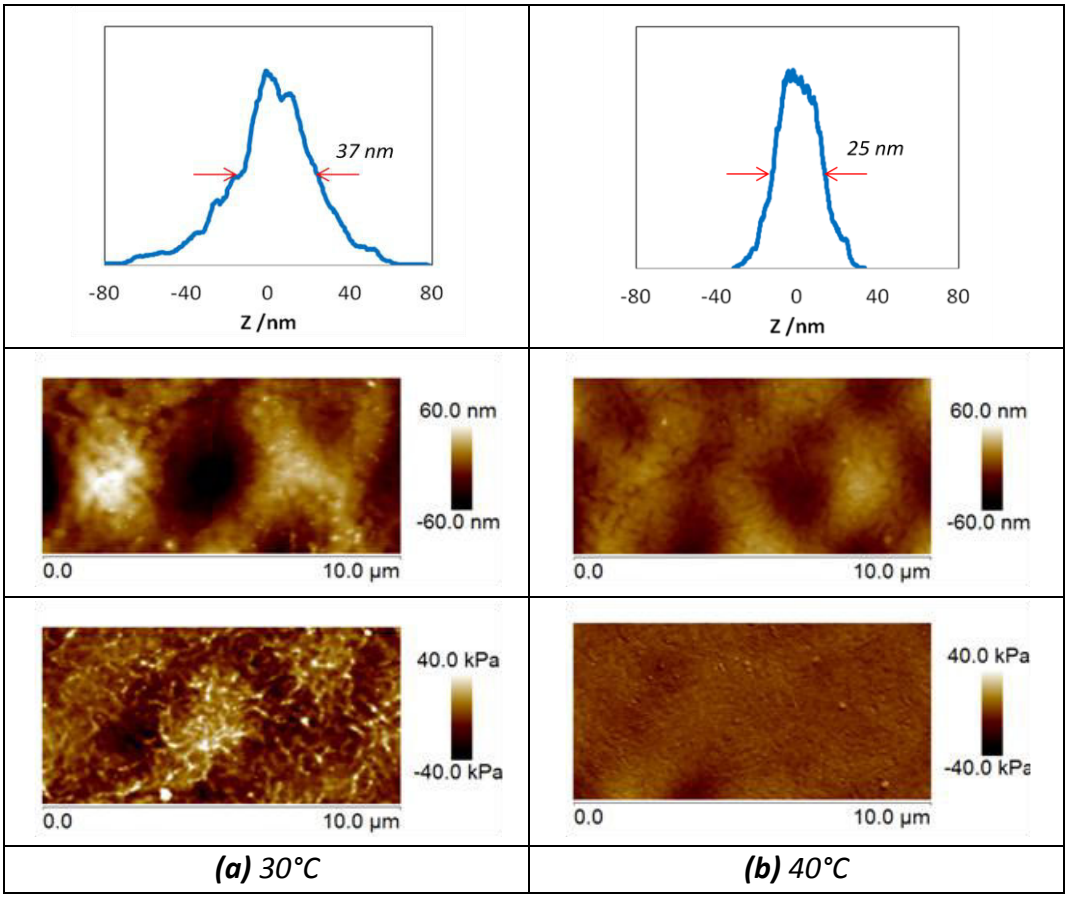


***Figure 13**: AFM QNM images of the silica-PNIPAM hybrid gel film 681K_P2_S0.77 in water at different temperatures probed using a cantilever of stiffness k = 0.2 N/m.*

From the height images and height histograms shown in **Figure 13**, we observe that the roughness of the surface decreases when the temperature rises up from 30°C (swollen state)

to 40°C (collapsed state), with a decreasing FWHM of the height histogram from 37 nm to 25 nm. This decrease in the roughness is consistent with the results already obtained for single network films in Chapter 3. In the height image, we can observe that the size of the clear zone and the dark zone decreases at 40°C, due the collapse of the polymer network. While the DMT Modulus images demonstrate that the stiffness of the free surface of the hybrid gel film is more homogeneous at 40°C than 30°C. As the polymer network collapses and contains less water at 40°C than at 30°C, the hybrid network has a higher modulus so that the difference of modulus between the dark zone (with more aggregated silica particles) and the clear zone (which contains more polymer) is attenuated.

3.2.2. Swelling ratio

In this part, the impact of silica nanoparticles on the swelling behavior of hybrid hydrogel films is investigated by ellipsometry.

In situ measurements are performed using a liquid cell which can be regulated in temperature, as what has been done for single network films. Silica-PNIPAM hybrid hydrogel films which are grafted to the silicon wafers are immersed in pure water, and then measurements are executed at 25°C (swollen state). After treatment of the experimental data, both the refractive index and thickness of the swollen hybrid gel film are able to be extracted from the ellipsometry data fit. It is taken into account that the refractive index of water is temperature independent.

Since the silica-PNIPAM hybrid gel films are attached to the substrate by covalent bonds, with silica particles trapped inside, the amount of the polymer chains and silica particles in the films should keep the same when immersed in water. Based on this, we can have a numerical test to ensure that the fitting of the experimental data from ellipsometry is logical, as for the analysis of single network, LbL-inspired and interpenetrating networks.

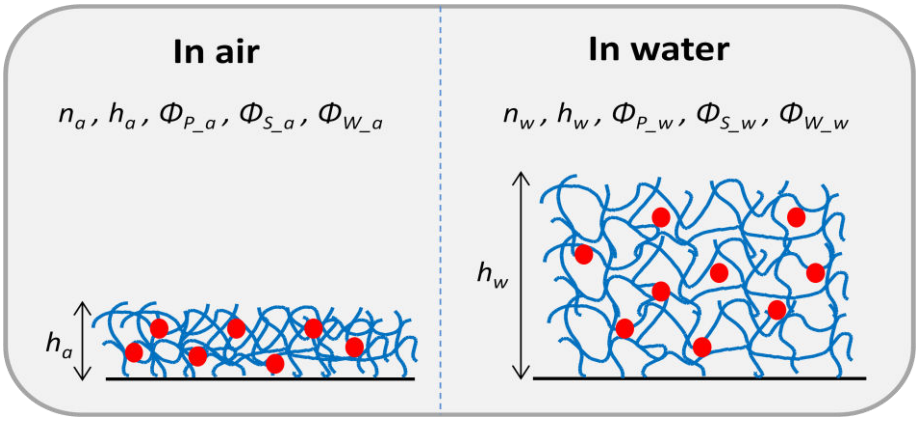


***Figure 14**: Sketch of the hybrid gel film in air and in water. The parameters in air are: n_a which is the refractive index of the film, h_a the thickness of the film, Φ_{P_a} the volume fraction*

of polymer in the film, Φ_{S_a} the volume fraction of silica particles in the film and Φ_{W_a} the volume fraction of water in the film. The parameters in water are: n_w which is the refractive index, h_w the swollen thickness, Φ_{P_w} the volume fraction of polymer, Φ_{S_w} the volume fraction of silica particles, Φ_{W_w} the volume fraction of water.

In **Figure 14**, the sketch of the hybrid gel film in air and in water is shown, with all the related physical parameters listed out. As for films of single network (which contain only polymer and water), we can use two relations with the measured parameters, refractive index *n* and the thickness *h,* and the volume fraction ϕ allowing the connection between the measured parameters:

$$\begin{cases} n = \sum n_i \phi_i & \textbf{[Eq 1]} \\ h_{water} \times \phi_{water} = h_{air} \times \phi_{air} & \textbf{[Eq 2]} \end{cases}$$

In the first equation, the variation of the refractive index is considered as linear with the volume fraction (of polymer, silica and water) and in the second equation, the amount of the polymer chains and silica in the films should always keep the same when immersed in water since the gel films are attached to the substrate by covalent bonds.

The two equations have to be written in air (with the second index as a) and in water (with the second index as w) and all the species (polymer with the first index as P, silica with the first index as S and water with the first index as W) have to be considered.

Considering the refractive index, we have the following system with three equations:

$$\begin{cases} n_a = 1.52\Phi_{P_a} + 1.46\Phi_{S_a} + 1.33\Phi_{W_a} & \textbf{[Eq 3]} \\ n_w = 1.52\Phi_{P_w} + 1.46\Phi_{S_w} + 1.33\Phi_{W_w} & \textbf{[Eq 4]} \\ \frac{\Phi_{S_w}}{\Phi_{P_w}} = \frac{\Phi_{S_a}}{\Phi_{P_a}} & \textbf{[Eq 5]} \end{cases}$$

In the equation 5, we consider that the ratio of polymer to silica is the same in air and in water. The system of linear equations is also equivalent to the following system if we assume that the water content in hybrid gel films is 10% like the value measured in single network films:

$$\begin{cases} n_a = 0.06\Phi_{P_a} + 1.447 & \textbf{[Eq 6]} \\ n_w = 0.19\Phi_{P_w} + 0.13\Phi_{S_w} + 1.33 & \textbf{[Eq 7]} \\ \frac{\Phi_{S_w}}{\Phi_{P_w}} = \frac{0.9}{\Phi_{P_a}} - 1 & \textbf{[Eq 8]} \end{cases}$$

Once n_a and n_w are measured, the system of linear equations is entirely resolved so that the volume fraction ϕ_{p_a}, ϕ_{p_w} and ϕ_{s_w} can be determined.

Considering the thickness, we have:

$$h_w(\Phi_{P_w} + \Phi_{S_w}) = h_a(\Phi_{P_a} + \Phi_{S_a}) \qquad \textbf{[Eq 9]}$$

or

$$h_w(\Phi_{P_w} + \Phi_{S_w}) = 0.9h_a \qquad \textbf{[Eq 10]}$$

assuming that the water content in hybrid gel films is 10%. As the values ϕ_{p_w} and ϕ_{s_w} are determined from the equations with the refractive index, we compare the thickness of the film in water h_w and the thickness of the film h_a in air extracted from the fitting so that the values are consistent with the equation 10.

Once we get the swollen thickness of the hybrid gel film, the swelling ratio of the hybrid gel film and the inside polymer network are able to be inferred separately. The calculation method is shown as follows:

$$r_{gel} = \frac{h_w}{h_a}$$

$$r_{polymer} = \frac{h_w - \Phi_{S_a} * h_a}{h_a - \Phi_{S_a} * h_a}$$

r_{gel} is the swelling ratio of the hybrid gel film in water and $r_{polymer}$ is the swelling ratio of the pure polymer network in the hybrid gel assuming that silica particles are incompressible.

Results of swelling experiments carried out on cross-linked PNIPAM hybrid hydrogel films containing silica nanoparticles at different amounts are represented in **Figure 15**.

The swelling ratio of the hybrid gel film at 25°C (swollen state) is displayed as a function of the volume fraction of silica particles. Also represented is the swelling ratio of the PNIPAM network assuming that the silica particles are incompressible. The obvious trend is a clear decrease of the swelling ratio at 25°C as the silica particles content is increased, from a swelling ratio of 4 (for the pure polymer matrix without silica particles) to 1.21 and 1.56 (for the highest silica particles content), for the hybrid gel film and the PNIPAM network respectively. As a matter of fact, the presence of silica nanoparticles in the hybrid gel film provides two opposite contributions to its swelling properties. The main effect is a decrease of the swelling ability of the hybrid gel network as a consequence of the attractive interactions between the silica nanoparticles and the PNIPAM network. The strong interactions at the silica-polymer interface give rise to geometrical constrains which restrict

the swelling of the polymer network. The second effect is a slight increase of the swelling ability due to the additional osmotic pressure generated by the counter-ions present at the surface of the silica nanoparticles. Obviously, the latter one can be neglected here.

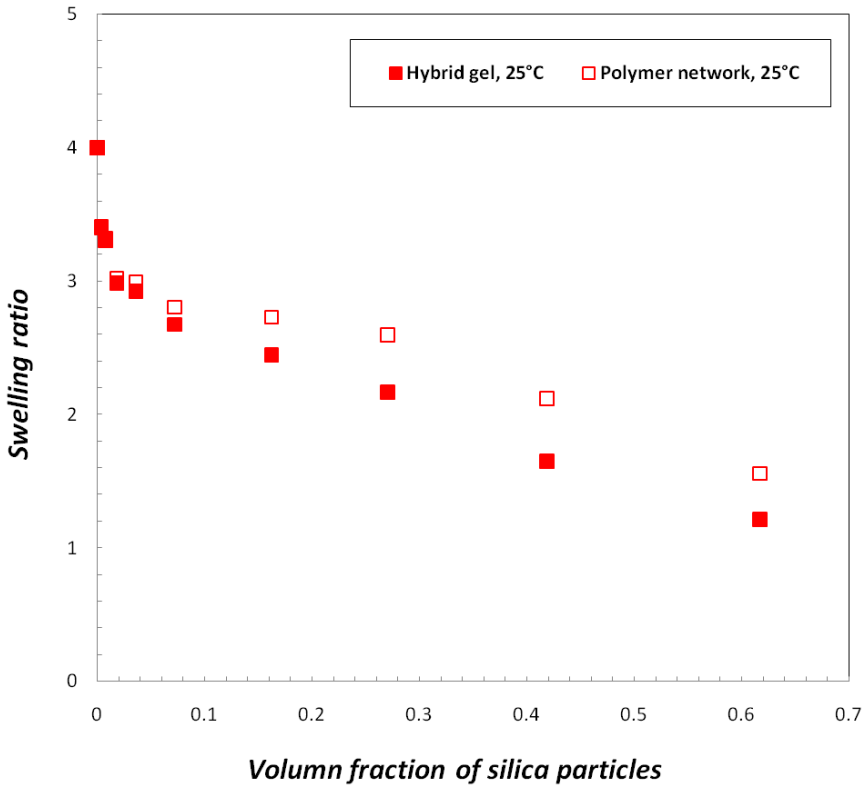


***Figure 15**: Swelling ratio of the silica-PNIPAM hybrid gel film and the PNIPAM network in water at 25°C as a function of the volume fraction of silica particles in the film in air (Φ_{S_a}) respectively.*

3.2.3. Effect of temperature on the swelling ratio

Based on the study of the swelling ratio of the silica-PNIPAM hybrid gel films at 25°C (swollen state), the same measurements are executed on the same samples (which contain silica nanoparticles at different amounts) at 40°C (collapsed state) to have an idea on their collapse behavior. Results are shown in **Figure 16**, with a comparison to those at 25°C.

The swelling ratio of the hybrid gel film at 25°C (swollen state) and 40°C (collapsed state) is displayed as a function of the volume fraction of silica particles, as well as for the PNIPAM network. With the decrease of the silica particles content, the swelling ratio at 40°C has no obvious variation, for both the hybrid gel film and the PNIPAM network. However, the gap of swelling ratio between 25°C and 40°C is smaller when there are more silica particles. In particular, when the amount of silica particles in the hybrid gel film reaches a certain value

(up to 61.7%), the swelling ratio of the hybrid gel film doesn't change from swollen state to collapse state, showing no thermo-responsive property.

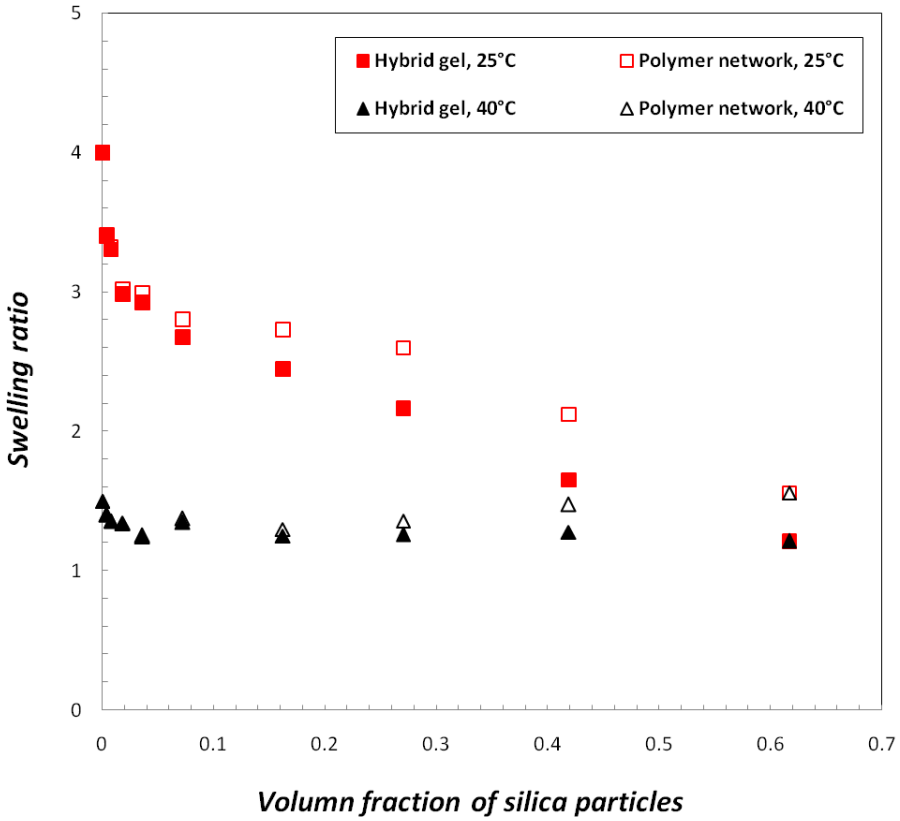


***Figure 16**: Swelling ratio of the silica-PNIPAM hybrid gel film and the PNIPAM network in water at 25°C and 40°C as a function of the volume fraction of silica particles in the film in air (Φ_{S_a}) respectively.*

To detail the effect of temperature on the swelling ratio, a silica-PNIPAM hybrid gel film which contains a small amount of silica particles (with volume fraction equal to 1.8%) is investigated in water at various temperatures, from 25°C to 40°C. Results are shown in **Figure 17**.

In **Figure 17**, the swelling ratio is represented as a function of temperature, for both the hybrid gel film and the PNIPAM network. From a general point of view, the swelling ratio of the hybrid gel film decreases along with the growth of temperature, from about 3 (25°C) to 1.6 (40°C), with a transition at around 33°C, close to that for single network PNIPAM gel film (34°C).

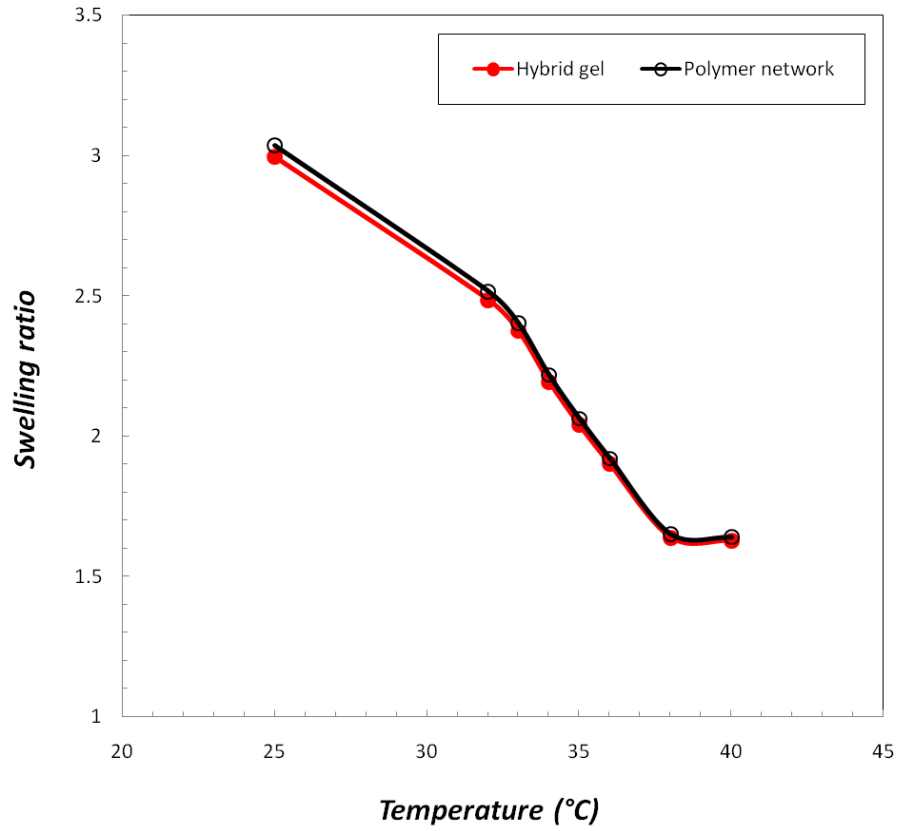


***Figure 17**: Swelling ratio of silica-PNIPAM hybrid gel film and the PNIPAM network in water as a function of temperature. Here the sample is 66K_P5_S1.8.*

4. LbL or IPN networks? A study by neutron reflectivity

We showed that the synthesis strategy used for single-network gel films is also appropriate for the development of new assemblies such as layer-by-layer LbL multilayers and interpenetrating networks IPN. LbL multilayers, bilayers and trilayers (and more), are built by stacking one layer on top of the other as in layer-by-layer assemblies [3]. Interpenetrating networks are obtained by first synthesizing the first network and then adding the chains of the second network for which the interpenetration inside the first network layer is favored before being cross-linked.

The hydrogel films were characterized by ellipsometry and AFM. AFM provided information on the topography of the free surface of the gel films. Ellipsometry allowed global measures: the thickness at silicon-air interface corresponds to the total amount per unit area and the thickness at silicon-water interface gives the swelling ratio of the whole film. Indeed, neutron reflectivity is necessary for determining the internal structure of the film owing to the isotopic contrast:

- the structure of multilayers or interpenetrating networks can be distinguished.

- the swelling behavior of each single network (in multilayers or interpenetrating networks) can be extracted.
- the collapse behavior of the PNIPAM network with temperature in the two different architectures can be studied.

In this chapter, we use neutron reflectivity to investigate bilayers and interpenetrating networks containing protonated PNIPAM-h and deuterated PAA-d networks, poly(acrylic acid) being used for its unresponsiveness to temperature.

How stacked are the bilayers containing PAA-d and PNIPAM-h networks?

How inter-diffused are the interpenetrating networks with PAA-d and PNIPAM-h?

4.1. Measures in air

The characteristics of the gel films studied are summarized in Table 1. The bilayers samples called BL were synthesized by stacking the second network (PNIPAM-h) on the surface-attached and first network (PAA-d): the PNIPAM-h layer was spin-coated on the top of PAA-d network and heated at 120°C for cross-linking. The interpenetrating networks called IPN were synthesized by favoring the diffusion of the second networks (PNIPAM-h) inside the surface-attached and first network (PAA-d) before cross-linking: after the spin-coating of the PNIPAM-h layer on the top of PAA-d network, the sample is let at ambient temperature in a reactor under saturating vapor pressure of methanol (which is a good solvent for both PAA and PNIPAM) to favor the swelling of the PAA-d network and the interpenetration of the PNIPAM-h chains, finally the sample was heated at 120°C for the cross-linking of the PNIPAM-h chains inside the PAA-d networks.

The thickness of the layers in air was measured after each step of spin-coating. The BL and IPN samples were also characterized after all the steps and rinsing. The total thickness measured remain the same indicating that none chains were removed.

In **Table 8**, the samples are classified by pair BL/IPN with the same ratio of deuterated and protonated polymers, the thickness (or amount of polymer per unit area) of PAA-d and PNIPAM-h being comparable. BL9/IPN14 has a ratio H/D close to 1, BL4/IPN5 has a ratio around 3, the ratio for BL10/IPN11 and BL26/IPN31 is less than 1 (around 0.7).

Figures 18 display the neutron reflectivity curves for the four pairs. Also are shown, for comparison, the simulations for ideal bilayers (with stacked layers) and (completely interdiffused) interpenetrating networks with the same thickness of deuterated and protonated polymers as the four pairs. The characteristics of the simulations including the

thickness, the interface width σ and the scattering length density Nb of the layers are indicated in **Table 9**. For bilayers, the first line corresponds to the PAA-d first layer and the second line to the PNIPAM-h second layer, the width σ of the first line using erf error function allows the connection of the two layers, the width σ of the second line corresponds to the free interface width of the gel film. The interpenetrating networks contain a single layer of mixed PAA-d and PNIPAM-h networks with σ as the free interface width. The values of Nb obtained by calculation are: 5.56 10^{-6} $Å^{-2}$ for dry PAA-d (without any water) and 4.95 10^{-6} $Å^{-2}$ for PAA-d in air (with 10% of water). The Nb of PNIPAM-h in air calculated is 0.9 10^{-6} $Å^{-2}$, as explained in Part 3.1 of Chapter 3.

Samples	h_a (nm)	h_a (nm)	Samples
BL9	9.2	11.4	IPN14
	9.5	13.6	
BL4	12.5	10.1	IPN5
	4.2	4.6	
BL10	7.9	7.6	IPN11
	10.0	11.1	
BL26	17.7	16.0	IPN31
	25.9	30.5	

***Table 8**: Characteristics of bilayers films and interpenetrating networks films: the thickness measured in air by ellipsometry ha for each network (PAA-d for the first line and PNIPAM-h for the second line). The samples are classified by pairs for which h_a are comparable.*

Samples	h_a (nm)	σ (nm)	Nb (10^{-6} $Å^{-2}$)
BL9	9.2	2.0	4.9
	9.5	5.0	0.9
IPN14	25.0	5.0	2.9
BL4	12.5	2.0	4.9
	4.2	5.0	0.9
IPN5	14.7	5.0	2.9
BL10	7.9	2.0	4.9
	10.0	5.0	0.9
IPN11	19.6	5.0	2.9
BL26	17.7	5.0	4.9
	25.9	8.0	0.9
IPN31	46.5	8.0	2.9

***Table 9**: Characteristics of the simulations of neutron reflectivity for bilayers films and interpenetrating networks films in air, the samples being classified by pairs. For bilayers, the*

first line corresponds to the PAA-d first layer and the second line to the PNIPAM-h second layer, the width σ of the first line allows the connection of the two layers, the width σ of the second line corresponds to the free interface width of the gel film. The interpenetrating networks contain a single layer of mixed PAA-d and PNIPAM-h networks with σ as the free interface width.

The neutron experiments for BL9/IPN14 and BL4/IPN5 pairs were performed on PRISM reflectometer which works with angle variation (and not time of flight, see Annex). Even if the angle variation 0.002° is the smallest as possible, the resolution on small wave vectors is not as good as that obtained with EROS which works with time of flight.

The experimental curves are all different from the simulated curves. For all pairs, it seems that the experimental curves are a little closer to the simulated curves of the interpenetrating networks than the curves of the bilayers. It means that the BL samples are less stacked or more interpenetrated than they were supposed to be whereas the IPN samples are not completely interpenetrated with a partial diffusion of the second network inside the first one.

The neutron reflectivity curves of BL9/IPN14 pair and their best fittings are displayed in **Figure 19**. As explained above, the resolution on wave vector is not satisfying and so the relevance of the fit should be cautiously evaluated. The characteristics of the layers corresponding to the best fitting are also shown in Table 3. For BL9 and IPN14, two layers were necessary for the fit. Even for the IPN sample, the fit using a single layer is not satisfying, confirming that the interpenetration of the two networks is only partial. By comparison with the characteristics of the simulated curves shown in **Table 9**, we can note that the values of Nb for BL9 are different from the values 4.9 and 0.9 that should be found if the two layers are stacked, confirming that BL9 contain two networks which are not stacked but partially interpenetrated. Nevertheless, IPN14 is more interpenetrated than BL9 with a higher interface width connecting the two layers (4.8 nm instead of 3.8 nm) and a more balanced $\phi_D/(\phi_D+\phi_H)$ ratio for the first and second layers (0.65 and 0.30 instead of 0.9 and 0.1).

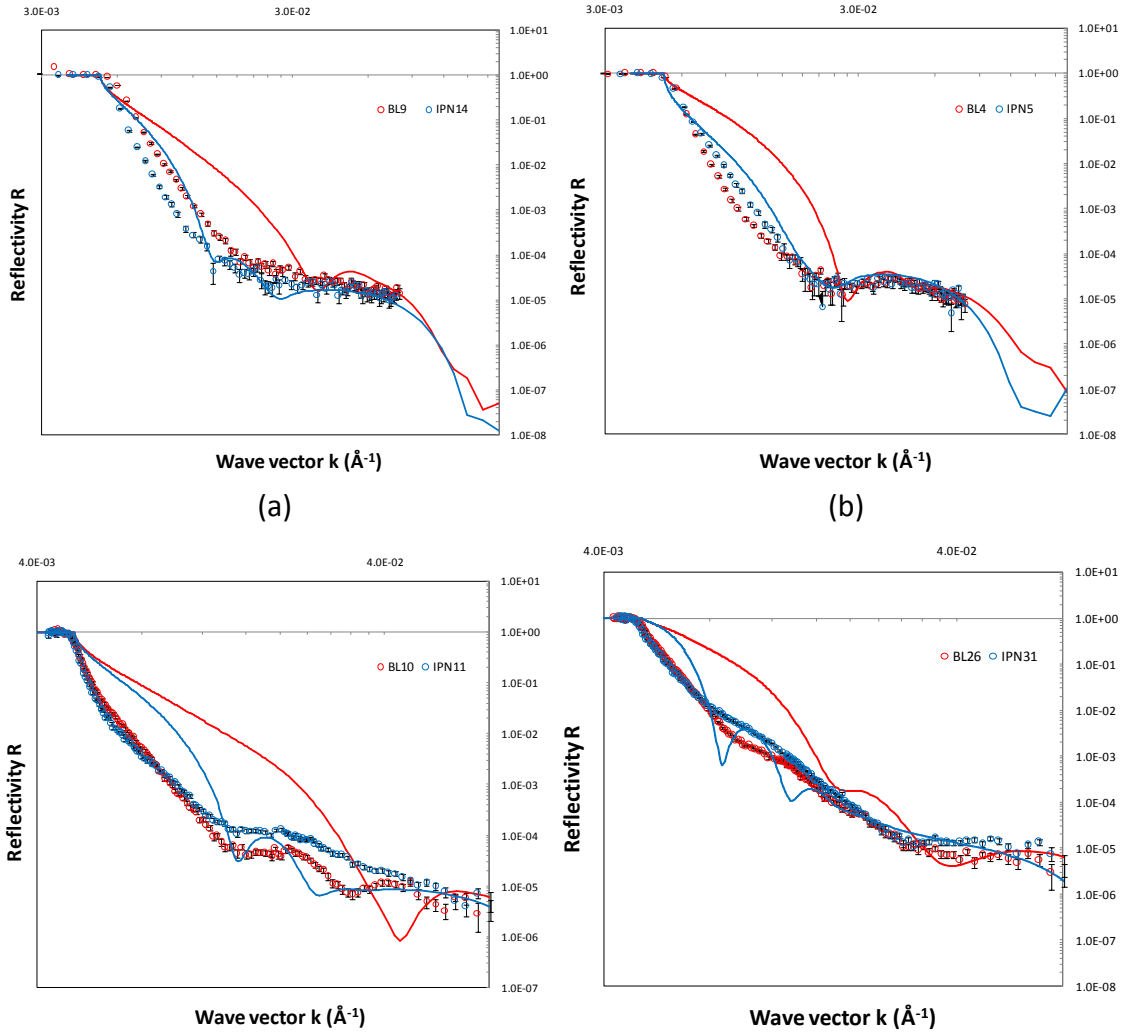


***Figure 18**: Neutron reflectivity curves of bilayers and interpenetrating networks films in air. Also are shown for comparison the simulation curves of ideal bilayers (stacked layers) and ideal interpenetrating networks (completely interdiffused networks) for films with same thickness, the characteristics of the simulations being indicated in **Table 9**. The samples are classified by pairs: BL9/IPN14 (a), BL4/IPN5 (b), BL10/IPN11 (c) and BL26/IPN31 (d). Circle: data; line: simulation.*

Samples	h_a (nm) by ellipsometry	h_a (nm) by neutrons	σ (nm)	Nb (10^{-6} Å^{-2})	$\frac{\phi_D}{\phi_D + \phi_H}$
BL9	9.2	6.1	3.8	4.5	0.90
	9.5	10.9	4.0	1.3	0.10
IPN14	11.4	6.3	4.8	3.3	0.60
	13.6	15.2	6.1	2.3	0.35

***Table 10**: Characteristics of the fittings of neutron reflectivity data of bilayers film BL9 and interpenetrating networks film IPN14 in air. The thickness measured in air by ellipsometry is*

reminded for comparison. The ratio ϕ_D/ϕ_H is deduced from the value of Nb assuming that the ratio of polymer in air is 90%.

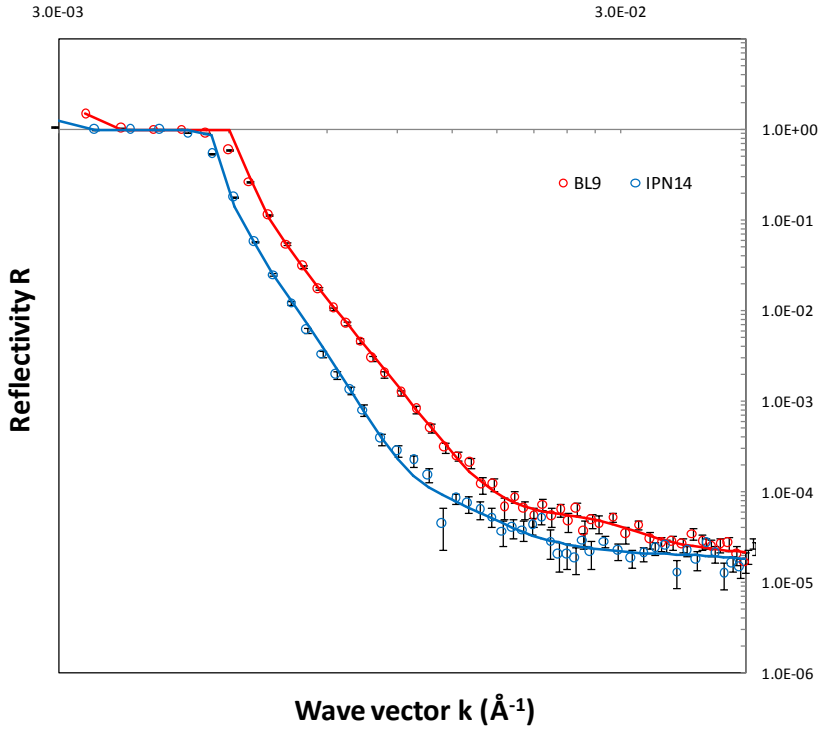


***Figure 19**: Neutron reflectivity curves of bilayers film BL9 and interpenetrating networks film IPN14 in air and their best fittings. The characteristics of the fittings are indicated in **Table 10**. Circle: data; line: fitting.*

The neutron reflectivity curves of BL10/IPN11 and BL26/IPN31 pairs and their best fittings are displayed in **Figure 20**. Contrarily to the former BL9/IPN14 pair, BL10/IPN11 and BL26/IPN31 were performed on EROS reflectometer. As the resolution on wave vector is good here, the fit is clearly relevant. The characteristics of the layers corresponding to the best fitting are summarized in **Table 11**. Three layers were necessary for the fit. As the ratio H/D is less than 1, the gel film should be divided in three parts: the first layer near the substrate mainly contains deuterated polymer, the second layer is a mixture of PAA-d and PNIPAM-h and the third layer contains only protonated polymer that cannot (unfeasibly) diffuse in PAA-d network. The $\phi_D/(\phi_D+\phi_H)$ ratio found decreases logically from the first layer to the third one. Comparing BL and IPN samples, it should be noticed that the thickness of the first (deuterated) layer is lower for IPN (0.5 nm for IPN11 and 6.3 nm for IPN31) than for BL (1.7 nm for BL10 and 7.5 nm for BL26) and the interface width σ is higher for IPN (3.7 nm for IPN11 and 8.8 nm for IPN31) than for BL (2.4 nm for BL10 and 6.0 nm for BL26). It demonstrates that even if the H/D ratio is less than 1, there is a difference between BL and IPN networks, with more interpenetration between deuterated and protonated chains in IPN films.

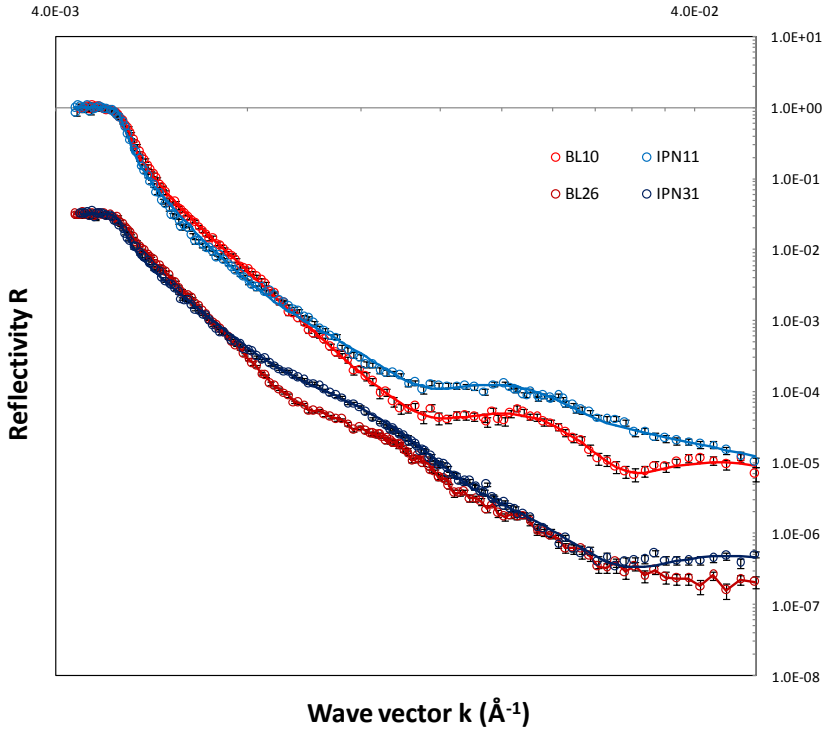


***Figure 20**: Neutron reflectivity curves of the pairs BL10/IPN11 and BL26/IPN31 in air and their best fittings. The characteristics of the fittings are indicated in **Table 11**. Circle: data; line: fitting.*

4.2. Effect of temperature

Figures 21 display the neutron reflectivity curves of BL10 and IPN11 films in water at 25°C. D_2O/H_2O mixture (with 88% of D_2O and 12% of H_2O) was used in order to contrast-match the PAA-d gel (with Nb = 5.56 10^{-6} $Å^{-2}$) and then only the PNIPAM gel is visible. Also are shown the simulations for ideal bilayers and interpenetrating networks. The characteristics of the simulations with the thickness in air ha and in water h_w, the interface width σ and the scattering length density Nb of the layers, are indicated in **Table 12**. h_w is calculated from ha considering that for ideal bilayers, the swelling ratio is 3 for separately deuterated and protonated networks. For ideal interpenetrating networks, the swollen thickness of the mixed deuterated/protonated network is considered to be 1.5 times the thickness in air.

As BL26 and IPN31 films in water are too thick for neutron reflectivity (as observed and discussed for SN60 film in water, see Chapter 3), it is useless to analyze the data. On the other hand, the data of the BL9/IPN14 pair are not analyzed because of the lack of resolution on small wave vectors.

Samples	h_a (nm) by ellipsometry	h_a (nm) by neutrons	σ (nm)	Nb (10^{-6} Å^{-2})	$\frac{\phi_D}{\phi_D+\phi_H}$
BL10	7.9	1.7	0.7	4.9	1
		8.0	2.4	3.9	0.75
	10.0	10.0	4.5	1.0	0.03
IPN11	7.6	0.5	0	4.5	0.90
		8.9	3.7	3.2	0.58
	12.0	12.0	4.8	1.5	0.15
BL26	17.7	7.5	4.7	4.8	0.98
		13.0	6.0	2.3	0.35
	25.9	14.8	6.0	1.1	0.05
IPN31	16.0	6.3	6.3	4.7	0.95
		18.3	8.8	2.6	0.42
	30.5	19.5	9.7	1	0.03

***Table 11**: Characteristics of the fittings of neutron reflectivity data of bilayers and interpenetrating networks films, the samples being classified by pairs BL10/IPN11 and BL26/IPN31. The thickness measured in air by ellipsometry is reminded for comparison. The ratio $\phi_D/(\phi_D+\phi_H)$ is deduced from the value of Nb assuming that the ratio of polymer in air is 90%.*

Samples	h_a (nm)	h_w (nm)	σ (nm)	Nb (10^{-6} Å^{-2})
BL10	7.9	23.7	5.0	3.5
	10.0	30.0	10.0	2.1
IPN11	19.6	29.4	10.0	2.7

***Table 12**: Characteristics of the simulations of neutron reflectivity for bilayers film BL10 and interpenetrating networks film IPN11 in water at 25°C. For the bilayers, the first line corresponds to the PAA-d first layer and the second line to the PNIPAM-h second layer, the width σ of the first line allows the connection of the two layers, the width σ of the second line corresponds to the free interface width of the gel film. The interpenetrating networks contain a single layer of mixed PAA-d and PNIPAM-h networks with σ as the free interface width.*

As observed in air, the experimental curves and the simulated curves in water are different. The experimental curves of BL10 and IPN11 are quite close and between the simulated curves of the interpenetrating networks and that of bilayers. It means that BL10 film contains networks which are more interpenetrated than they were supposed to be whereas the IPN sample is partially inter-diffused.

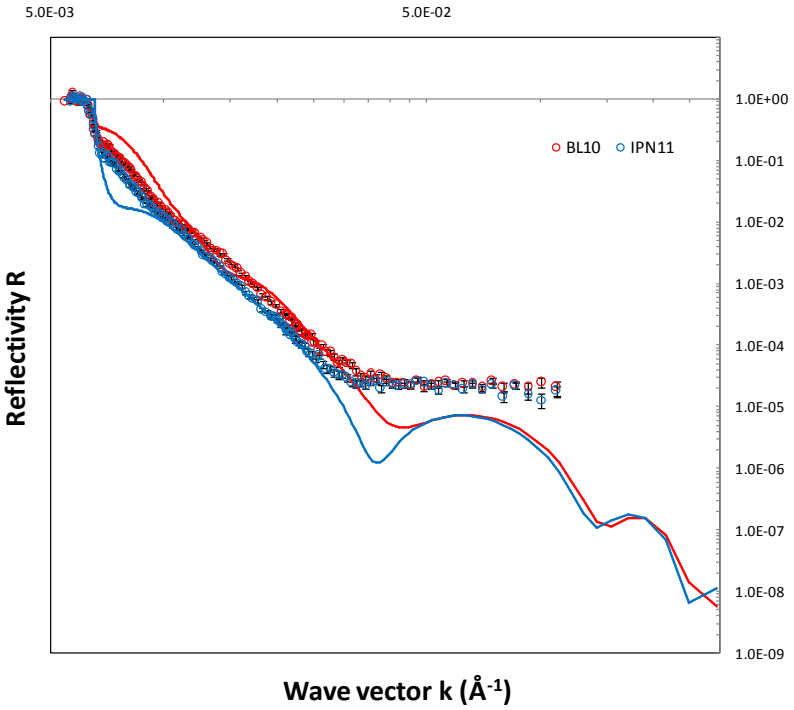


***Figure 21**: Neutron reflectivity curves of the bilayers films BL10 and the interpenetrating networks films IPN11 in water at 25°C. Also are shown for comparison the simulation curves of ideal bilayers (stacked layers) and ideal interpenetrating networks (completely interdiffused networks), the characteristics of the simulations being indicated in **Table 12**. Circle: data; line: simulation.*

The neutron reflectivity curves of BL10 and IPN11 films in water at 25°C and 40°C are displayed in **Figure 22**. The best fittings of the experimental data are also shown for comparison to evaluate the relevance of the fit. The curves at 25°C and 40°C are very close, suggesting that both for BL10 and for IPN11, the PAA-d and PNIPAM-h chains are interpenetrated and there is very low effect of the temperature on the mixed networks.

The characteristics of the layers corresponding to the best fitting are summarized in **Table 13**. Two layers were here necessary for the fit whereas three layers were required in air, suggesting that the networks chains diffuse more in swollen layers. The ratio $\phi_D/(\phi_D+\phi_H)$ is not calculated here as it was for the measures in air. Actually, as the volume fraction of monomers (for the whole layer) in air was assumed to be 0.9, the volume fractions of deuterated and protonated polymers can be then easily calculated. For the samples in air, it is difficult to know the volume fraction of polymers (and so those of deuterated and protonated parts) because the swelling ratio of internal layers, which depends on the interpenetration between the networks, cannot be assumed. Comparing with the characteristics of the simulated curves shown in **Table 12**, the values of Nb for BL10 are not so far from the values 3.5 and 2.1 that should be found if the two layers are stacked. For

IPN11, even if two layers were required (instead of one for ideal interpenetrating networks), the values of Nb (2.7 and 2.0) are close together in comparison with those obtained for BL10. It is coherently confirmed by the values of ϕ_D/ϕ_H ratio. The values of thickness at 40°C (4.1 + 8.7 nm) are lower than those at 25°C (6.2 + 10.1 nm) for BL10 whereas they are almost the same for IPN11 (6.1 + 15.4 nm at 40°C against 7.0 + 15.7 nm at 25°C), indicating that there is a (little) LCST effect on BL10 but no effect on IPN11. As for the measures in air, it proves that even if the H/D ratio is less than 1, there is a difference between BL10 and IPN11 networks, with more interpenetration between deuterated and protonated chains in IPN11 films.

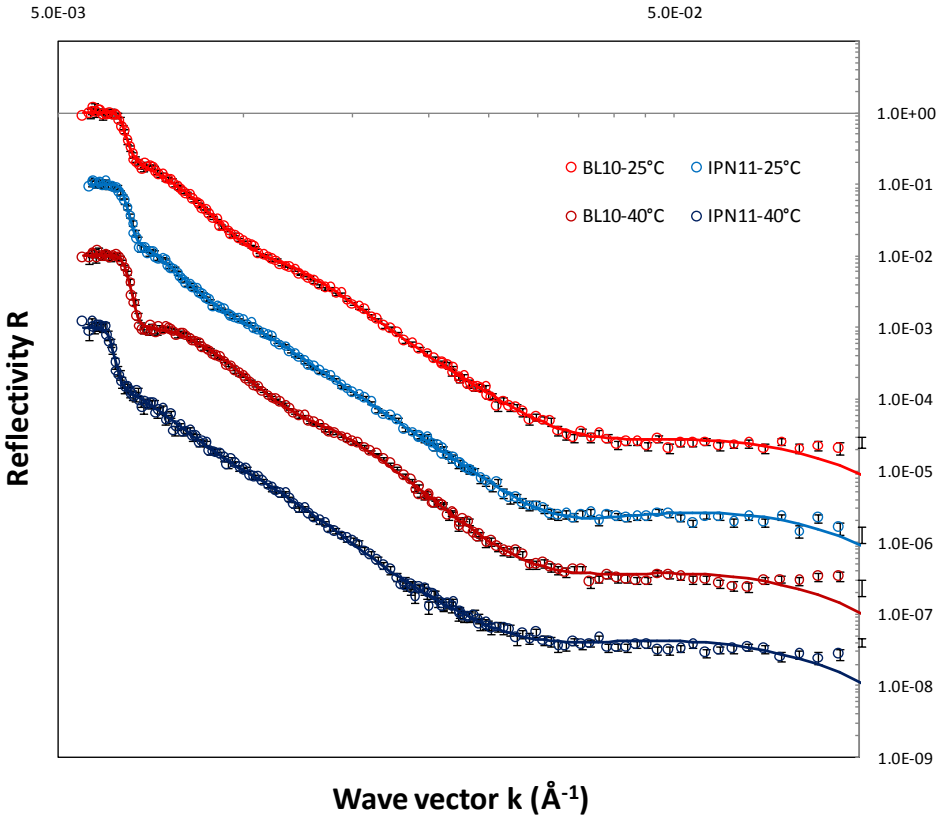


***Figure 22**: Neutron reflectivity curves of the pairs BL10/IPN11 in water at 25°C and 40°C and their best fittings. The curves are shifted on the y axis for more clarity. The characteristics of the fittings are indicated in **Table 13**. Circle: data; line: fitting.*

4.3. Discussion

Neutron reflectivity is a powerful technique which allows the determination of the internal structure of the film owing to isotopic contrast. This technique was used in order to prove the formation of either bilayers or interpenetrating networks.

In fact, we found that bilayers samples were not completely stacked as they were supposed to be. The two networks are a little interpenetrated. These results are coherent with those obtained in ellipsometry. Actually, the swelling ratio at 25°C found by ellipsometry is 3 for

multilayers whereas it is expected to be 4 for ideal multilayers (or monolayer of same thickness in air). Using neutron reflectivity on thinner layers for which the swelling ratio at 25°C (respectively at 40°C) is expected to be around 3 (respectively 1.5), we found 2.76 at 25°C and 2.35 at 40°C. The low collapse of the gel films at 40°C is coherent with the presence of PAA networks and the formation of a more or less mixture of PAA/PNIPAM networks instead of plainly stacked bilayers.

Samples	h_a (nm) by neutrons	h_w (nm) by neutrons	σ (nm)	Nb (10^{-6} Å^{-2})
BL10-25C	6.1	11.4	6.2	3.1
	10.9	35.6	10.1	1.6
BL10-40C	6.1	10.9	4.1	3.1
	10.9	29.0	8.7	1.7
IPN11-25C	9.7	14.0	7.0	2.7
	10.0	38.3	15.7	2.0
IPN11-40C	9.7	15.2	6.1	2.4
	10.0	32.4	15.4	1.4

***Table 13**: Characteristics of the fittings of neutron reflectivity data of the bilayers film BL10 and the interpenetrating networks film IPN11 in water at 25°C and 40°C. The thickness measured in air by neutrons is reminded for comparison. The ratio ϕ_D/ϕ_H is deduced from the value of Nb.*

The interpenetrating networks are partially interdiffused. Again, the results are consistent with those obtained in ellipsometry. The swelling ratio at 25°C found by ellipsometry is 2.5 whereas it is expected to be 2 for ideal interpenetrating networks containing the same amount of polymers for each network (or the same thickness in air). The gel film studied by neutron reflectivity (in air and in water) has a D/H ratio less than 1 or in other words, the thickness in air of the first network is higher than that of the second network. Accordingly, the deuterated and protonated networks cannot be completely interpenetrated and there is predictably a part of the second network that cannot diffuse inside the first network. We found a swelling ratio of 2.65 at 25°C and 2.41 at 40°C. The almost comparable values of the swelling ratio of BL10 and IPN11 are coherent with the formation of partially interpenetrated PAA/PNIPAM networks. Nevertheless, combining the measures in air and in water, it proves that even if the H/D ratio is less than 1, there is a difference between BL10 and IPN11 networks, with more interpenetration between deuterated and protonated chains in IPN11 films.

Another point is that the gel films measured by ellipsometry and by neutron reflectivity are not exactly the same. The first (ellipsometry) contain only PNIPAM species whereas the last (neutron reflectivity) comprise PAA and PNIPAM. For interpenetrating networks, the

compatibility of PNIPAM with PNIPAM chains is surely larger than the compatibility of PAA with PNIPAM. It could explain that the PNIPAM/PNIPAM IPN are more interdiffused than the PAA/PNIPAM IPN.

Progress in the synthesis of bilayers (or multilayers) and interpenetrating networks could be suggested. For bilayers, the use of UV-irradiation to activate the thiol-ene reaction and then the cross-linking could be more appropriate than temperature activation. It is shown that the UV-irradiation at a wavelength 254 nm (without any initiator) for a few hours (instead of more than 20 hours with temperature) allows the formation of the network films (Benjamin's PhD). The short reaction time by UV-irradiation is expected to limit the diffusion of the chains (coated for the formation of the second network) inside the first network.

For interpenetrating networks, the shorter the chains (coated for the formation of the second network), the more they enable to diffuse in the first network as the relaxation time is proportional to the cube of the molecular weight of chains from the reptation theory. As for bilayers, the thickness of the layers is an important parameter. The compatibility of the polymers used (through Flory parameter χ) for the formation of the networks should be also considered. For example, it should be interesting to compare the compatibility of the couples PAA/PNIPAM and PNIPAM/PNIPAM.

Neutron reflectivity experiments on thick bilayers and interpenetrating networks could also be planned. **Figures 23** display the simulations for ideal bilayers (stacked layers) and ideal interpenetrating networks (with complete interdiffusion between chains) with the characteristics of the thickness, the interface width σ and the scattering length density Nb of the layers indicated in **Table 14** (as shown in **Figure 18** and **Table 9**). The simulations are achieved for the thickness of deuterated and protonated polymers in air equal to 100 nm and 1 μm. The reflectivity curves of the bilayers and the interpenetrating networks are highly shifted (2.8 10^{-3} $Å^{-1}$). The critical wave vector k_c can be calculated using the relation $k_c = \sqrt{4\pi \times Nb}$, then k_c is equal 7.8 10^{-3} $Å^{-1}$ (with Nb = 4.9 10^{-6} $Å^{-2}$) for bilayers whereas for interpenetrating networks, k_c is equal 6.0 10^{-3} $Å^{-1}$ (Nb = 2.9 10^{-6} $Å^{-2}$). The decrease of the reflectivity curves for both bilayers and interpenetrating networks is the same for a total thickness in air higher than 100 nm. The curves can be however distinguished (with small oscillations) for the values of the interface width lower than 15 nm.

Samples	h_a (nm)	σ (nm)	Nb (10^{-6} Å^{-2})
BL200nm-stacked	100	10	4.9
	100	10	0.9
BL200nm-rough	100	10	4.9
	100	50	0.9
IPN200nm	200	20	2.9
IPN2µm	2000	200	2.9

***Table 14**: Characteristics of the simulations of neutron reflectivity for bilayers and interpenetrating networks films in air. For the bilayers, the first line corresponds to the PAA-d first layer and the second line to the PNIPAM-h second layer, the width σ of the first line allows the connection of the two layers, the width σ of the second line corresponds to the free interface width of the gel film. The interpenetrating networks contain a single layer of mixed PAA-d and PNIPAM-h networks with σ as the free interface width.*

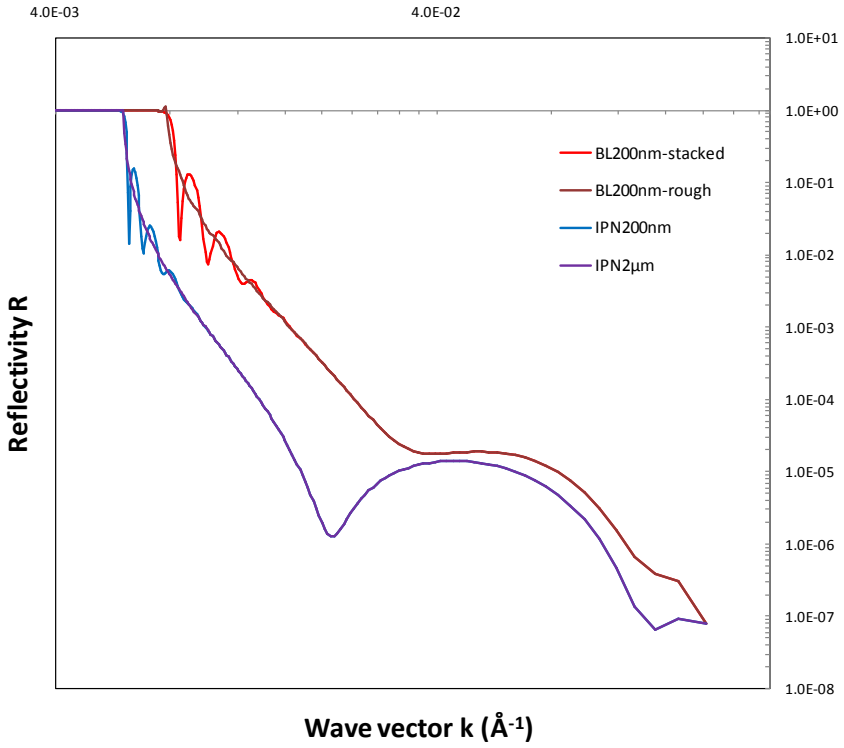


***Figure 23**: Neutron reflectivity simulations of bilayers and interpenetrating networks films in air, the characteristics of the simulations being indicated in **Table 14**. Circle: data; line: simulation.*

References

1. Richtering, W. and B.R. Saunders, *Gel architectures and their complexity.* Soft Matter, 2014. **10**(21): p. 3695-3702.
2. Stuart, M.A.C., et al., *Emerging applications of stimuli-responsive polymer materials.* Nat Mater, 2010. **9**(2): p. 101-113.
3. Decher, G., *Fuzzy Nanoassemblies: Toward Layered Polymeric Multicomposites.* Science, 1997. **277**(5330): p. 1232-1237.
4. Decher, G., J.D. Hong, and J. Schmitt, *Buildup of ultrathin multilayer films by a self-assembly process: III. Consecutively alternating adsorption of anionic and cationic polyelectrolytes on charged surfaces.* Thin Solid Films, 1992. **210–211, Part 2**(0): p. 831-835.
5. Glinel, K., et al., *Responsive polyelectrolyte multilayers.* Colloids and Surfaces A: Physicochemical and Engineering Aspects, 2007. **303**(1–2): p. 3-13.
6. Gong, J.P., et al., *Double-Network Hydrogels with Extremely High Mechanical Strength.* Advanced Materials, 2003. **15**(14): p. 1155-1158.
7. Gong, J.P., *Why are double network hydrogels so tough?* Soft Matter, 2010. **6**(12): p. 2583-2590.
8. Sperling, L.H. and V. Mishra, *The current status of interpenetrating polymer networks.* Polymers for Advanced Technologies, 1996. **7**(4): p. 197-208.
9. Rose, S., et al., *Time Dependence of Dissipative and Recovery Processes in Nanohybrid Hydrogels.* Macromolecules, 2013. **46**(10): p. 4095-4104.
10. Rose, S., *Thèse de Doctorat.* Paris VI, 2013.

General conclusion

We have developed a very simple and versatile strategy to synthesize chemically cross-linked hydrogel thin films that are covalently grafted to the surface. We are able to vary the thickness of the hydrogel films on a large range from nanometers to microns. Our strategy allows easily the adjustment of chemical properties (e.g. responsiveness) and physical properties (e.g. size and structure) of the films. It consists in cross-linking preformed and functionalized polymers rather than polymerizing and cross-linking monomers. For the cross-linking of polymer chains, the click chemistry selected is based on thiol-ene chemistry. The surface-attached hydrogel films are obtained by spin-coating ene-functionalized polymers in the presence of dithiol molecules as cross-linkers on thiol-modified substrates. The thiol-ene reaction allows both the chemical cross-linking of the polymer chains and their covalent attachment to the surface, which is performed under air atmosphere and can be activated without initiator by temperature or UV-irradiation at 250 nm. The hydrogel films can be obtained on glass subtrates, silicon substrates or gold surfaces, enlarging the range of applying this strategy. The technique of spin-coating brings the additional advantage to coat a film in the melt state using only a little polymer.

We have synthesized hydrogel films which can response to three different stimuli: temperature, light and electric field. The response of the hydrogel films to external stimuli results from the polymer chains used for cross-linking. So, different polymers are chosen according to their specific responsiveness properties. The thermo-sensitive hydrogel films are obtained using poly(*N*-isopropylacrylamide) for its Lower Critical Solution Temperature (LCST) properties. The copolymeration of these acrylamide-like monomers and acrylic acid, and the ene-functionalization of the copolymers, can both be carried out in water. The light-responsive properties of the hydrogel films can be achieved with the addition of azobenzene UV-activated groups on the PNIPAM chains. The UV-irradiation induces the change of trans-conformation to cis-conformation, resulting in the shift of the LCST to higher temperature, even with a small ratio of azobenzene in the hydrogel. The response to electric field is expected with the use of polyelectrolyte hydrogels. With the electric field applied on the hydrogel film, the change of the osmotic pressure due to the moving of the counterions from inside to outside of the hydrogel should induce the swelling to collapse phase transition of the hydrogel film. Weak polyelectrolyte such as poly(acrylic acid) hydrogels used at high pH for a complete ionization and strong polyelectrolyte such as poly(2-acrylamido-2-methylpropane sulfonate sodium) are suitable. The light-responsive and electro-responsive properties were not investigated in the present thesis. Some specific conditions are required. These properties are studied in miniaturized systems with microfluidic devices. This work is a part of Benjamin Chollet's thesis and is currently achieved with the collaboration of Gulliver laboratory in ESPCI. Here, the thermo-responsive properties were investigated using PNIPAM hydrogel films as model networks films since

temperature is easy to control and the working temperature is very comfortable (around 32°C which is the LCST of PNIPAM).

Based on the synthesis, we have systematically investigated the structure of the hydrogel films to make clear the effects of confinement and lateral constraints on their stimuli-responsive behaviors. The swelling of hydrogels in the confinement state such as films is supposed to be likely rather anisotropic than isotropic as for macroscopic hydrogels. The constraints on lateral swelling due to the covalent attachment of the hydrogel film on the solid substrate may induce a mechanical stress which causes the deformation of the free surface of the hydrogel film. Ellipsometry has been employed to determine the swelling ratio of the hydrogel films in the direction normal to the substrate. Neutron reflectivity experiments have been performed for defining the interface width on the free surface side of the hydrogel films, together with the swelling ratio for very thin films (< 50 nm) as a complement for ellipsometry. The topography of the free surface (in-plane) has been investigated using AFM.

Experimental results were obtained on hydrogel films (with same cross-linking ratio) with thickness widely ranging from nanometer to a few microns. The cross-linking ratio of the hydrogels, even not directly measured, can be supposed the same for all samples studied. Actually, the ratio of ene-functionalized polymer chains (characterized by ^{1}H NMR) is the same and the cross-linking between chains is achieved by thiol-ene click reaction using an excess of dithiol. The assumption of a homogeneous distribution of the cross-linking in the (whole) micrometric film, even tricky to prove, is also realistic. It was shown that the swelling behavior of the (single-network) gel films is independent of the film thickness in the middle range studied from 150 nm to 420 nm. The swelling ratio decreases from about 4 at 25°C to about 1.5 at 40°C, showing a LCST around 34°C. Below the LCST, the gel films are highly swollen with a large volume fraction of water (around 80%). Above the LCST, the gel films are collapsed, containing less water (40%). The swelling ratio around 1.5 at 40°C indicates that the films are unable to fully collapse as in air (only 10% of water). It was also found that the swelling behavior of the gel films is independent of the length of polymer chains used for the synthesis.

The combination of results obtained with ellipsometry and neutron reflectivity allowed the determination of the swelling ratio of (single-network) hydrogel films on a larger range of thickness. At 25°C for swollen gels, the swelling ratio is about 3 for films with thickness (in air) less than 50 nm. It increases to 3.5 at 90 nm to reach 4.0 for thickness up to 1.2 microns (measured by microfluidics tools). If the distribution of the cross-links is supposedly homogeneous in the whole film, it means that the surface attachment has a strong effect on

the swelling of the films, particular for very thin films below 100 nm. If the surface attachment of the gel films has a clear effect on the swelling of the films, it has less influence on the collapse of the films. At 40°C for collapsed gels, the swelling ratio is 1.5 for the whole range of thickness studied. As a final point, the linear swelling ratio of the surface-attached networks measured exceeds the supposed one-dimension swelling ratio of the bulk (or macroscopic) networks. It is in good agreement with the scaling laws predicted for the swelling of hydrogels with the extension of Flory-Rehner theory to one-dimension swelling. In that case, the power law relating the volumetric swelling ratio for gel films and for bulk networks is more properly equal to 5/9 rather than 1/3 found with simple geometric considerations.

The topography of the free surface of hydrogel films in air (characterized by usual AFM tapping mode) and in water (characterized by AFM QNM mode) showed the formation of uniform and continuous patterns. It seemed that there is no effect of the constraints of the surface-attachment on the lateral swelling which induce the deformation of the free surface of the hydrogel. The hydrogel films are flat, the roughness being small in comparison with the thickness of the film. In air, the values of the width of the height histogram are a few nanometers for 300 nm-thick films for images of 10 microns-size. For swollen hydrogel films in water, the width of the height histogram is at the maximum 10 nm for images of 10 microns-size while the thickness of the films can reach 1 micron. The topography also demonstrated that the swelling of the hydrogel film is rather vertical than lateral. The comparison between the experiments in air and in water indicated that the swelling leads to an increase of the (vertical) roughness while it has no obvious effect on the (horizontal) size of the patterns.

The density profile of the gel films obtained from neutron reflectivity is coupled with a topographic (in-plane) description of the free surface, resulting from AFM experiments. As the size of the in-plane irregularities (100 nm at the great maximum) is much smaller than the coherent length of neutrons (a few microns), specular neutron reflection cannot distinguish a diffuse film from a rough film. It is then helpful to compare the roughness of the surface of the hydrogel film determined by AFM and the free interface width deduced from neutron reflectivity. The discrepancy between the roughness of the surface and the free interface width shows that the smoothness of the free surface of the hydrogel is not due to the roughness (in-plane irregularities) but mainly to the diffusion of the interface. The surface is most diffuse in the swollen state indicating that the hydrogel in the film is far from a model network. The diffuse surface might be explained by the presence of pendant chains at the outside edge of the film. The peripheral chains are more likely to penetrate into the aqueous environment (rather than into the network, which is entropically unfavorable) giving rise to a diffuse interface.

On the basis of studies on single-network thin films, we have exploited new and complex hydrogel films by targeting the architecture of the polymer networks. Thanks to the versatility of hydrogels architecture, we manage to develop various architectures such as multilayer hydrogel films through layer-by-layer assembly, interpenetrating networks (IPN) hydrogel films and hybrid hydrogel films containing silica nanoparticles. The structure and swelling properties of these complex systems have been investigated by the three techniques in the same way as for single-network hydrogel films, and then comparisons are made among them.

Multilayers gel films are supposed to be the combination of many single-network films simply by stacking one onto the other, but thin interpenetrating networks may exist between every two layers, which could restrain partly the swelling of multilayer gel films. The swelling ratio of the (whole) multilayers films is about 3 against 4 for single-network films. Different from that, for IPN gel films, interpenetration process between the two networks is targeted, making the two networks go into each other and then connected by physical entanglements. The strong connection between the two networks restricts strongly the swelling of the IPN film leading to a smaller swelling ratio, about 2.5 compared to 4 for single-network films.

If ellipsometry only provided global measures, in particular the swelling ratio of the whole film, neutron reflectivity allowed the determination of the internal structure of the hydrogel films (owing to the isotopic contrast) and thus the proof of the formation of either bilayers or interpenetrating networks. Hydrogel films with architectures of supposed bilayers and interpenetrating networks, which contain protonated PNIPAM-h and deuterated PAA-d networks, poly(acrylic acid) being used for its unresponsiveness to temperature, were compared. It is found that bilayers samples are not completely stacked as they are supposed to be. The two networks are a little interpenetrated. These results corroborated those obtained in ellipsometry. For example, the swelling ratio is 2.8 at 25°C and 2.3 at 40°C for thinner layers, which is expected to be around 3 and 1.5 respectively. While the interpenetrating networks films are partially interdiffused and not completely, also confirming the results obtained by ellipsometry.

The swelling behavior of silica-PNIPAM hybrid gel films and the dispersion of silica nanoparticles inside the polymer matrix (at the free surface of the gel film) were investigated as function of the ratio of silica particles (large range from 0.3% to 62%) and the temperature. For small ratio of silica particles (below 1%), the solid particles are quite homogeneously dispersed while for high ratio, the formation of particles aggregates is unsurprisingly observed. The swelling ratio at 25°C decreases strongly from 4 to 1.5 with the

increase of the silica particles content. While at 40°C, the swelling ratio has no obvious variation being constant at around 1.5. The change of the swelling ratio from 25°C to 40°C is reduced with the increase of the silica particles content. In particular, when the amount of silica particles in the hybrid gel film reaches a certain value (up to 60%), the swelling ratio is the same at 25°C and 40°C, showing no thermo-responsive property.

This work could be continued following various attractive directions.

The development of other stimuli-responsive properties of hydrogel films for specific applications should be envisaged. For instance, thermo-responsive hydrogel films with an Upper Critical Solution Temperature (UCST) show a converse responsive property to temperature compared with PNIPAM hydrogel films. These systems are of great interest in controlled drug delivery and bioseparation. UCST polymers such as poly(sulfobetaine) are good candidates. These polyzwitterion have the advantages to combine the UCST properties with anti-fouling properties which are very interesting for biological applications. Last but not least, UCST properties are preferred to LCST properties for some specific applications in microfluidics.

Improvement could be brought to the synthesis of hydrogel films with targeted architecture, in particular layer-by-layer hydrogel films and interpenetrating networks films. For LbL hydrogel films, the use of UV-irradiation to activate the cross-linking could be more appropriate than temperature activation. The short reaction time by UV-irradiation should limit the diffusion of the networks between two adjacent layers. For IPN films, the shorter the chains coated for the second network, the more they enable to diffuse in the first network as the relaxation time is proportional to the cube of the molecular weight of chains from reptation theory.

LbL hydrogel films with multifunctions could be effectively exploited if the multilayers in the hydrogel film are completely stacked. For example, a double response to temperature (with PNIPAM network layers) and pH (with PAA network layers) of hydrogel films could be achieved for completely stacked multilayers. Otherwise, architecture with mixed networks should reduce the amplitude of the response to pH and temperature. On the other hand, ideal IPN hydrogel films should be completely interdiffused (and not only partially). The properties of mixtures are aimed in that case. For example, using IPN architecture, it would be interesting to generate both chemical and physical cross-links. In this IPN architecture in which each network is (separately) chemically cross-linked and the two networks are mechanically entangled together, physical interactions between the two networks can be

reversibly tuned by a stimulus such as pH which does not change the structure (or swelling) properties of the hydrogel film.

The combination of chemical and physical cross-links could be exploited to improve mechanical properties of hydrogel films by analogy with macroscopic hydrogels. From a basic point of view, the chemical cross-links contribute to the elastic properties of the network while the physical cross-links add the viscous dissipation to the network, reducing structural inhomogeneities inside the networks. The incorporation of objects which provide multiple cross-linking points shows much potential for reinforced hydrogel films. If solid objects such as silica nanoparticles were investigated in this thesis, organic objects such as microgels could be an interesting alternative. For example, soft nanocomposite hydrogel films which consist of PAA nanogels entrapped inside a PNIPAM (network) matrix can be envisaged. In such hydrogel films, temperature would greatly change the modulus elastic of the whole film by tuning the water content (and the swelling behavior) while keeping the same size for the hydrogel particles. The physical interactions between the PAA nanogels and the PNIPAM matrix (which modulate the viscous properties of the hydrogel films) could be reversibly triggered by pH with minor change of the structure (size) of the nanogels.

Beyond the reinforced materials properties, the hydrogel films are a great tool box to control and improve many other properties such as healing or adhesion or also wetting.

Annexes

Annex 1: NMR & SEC experiments

1. The light-responsive copolymer

The copolymer P(AA-co-NIPAM) modified by azobenzene is characterized by ^{1}H NMR in CD_3OD to determine the ratio of azobenzene groups in the copolymer (see **Figure 1**).

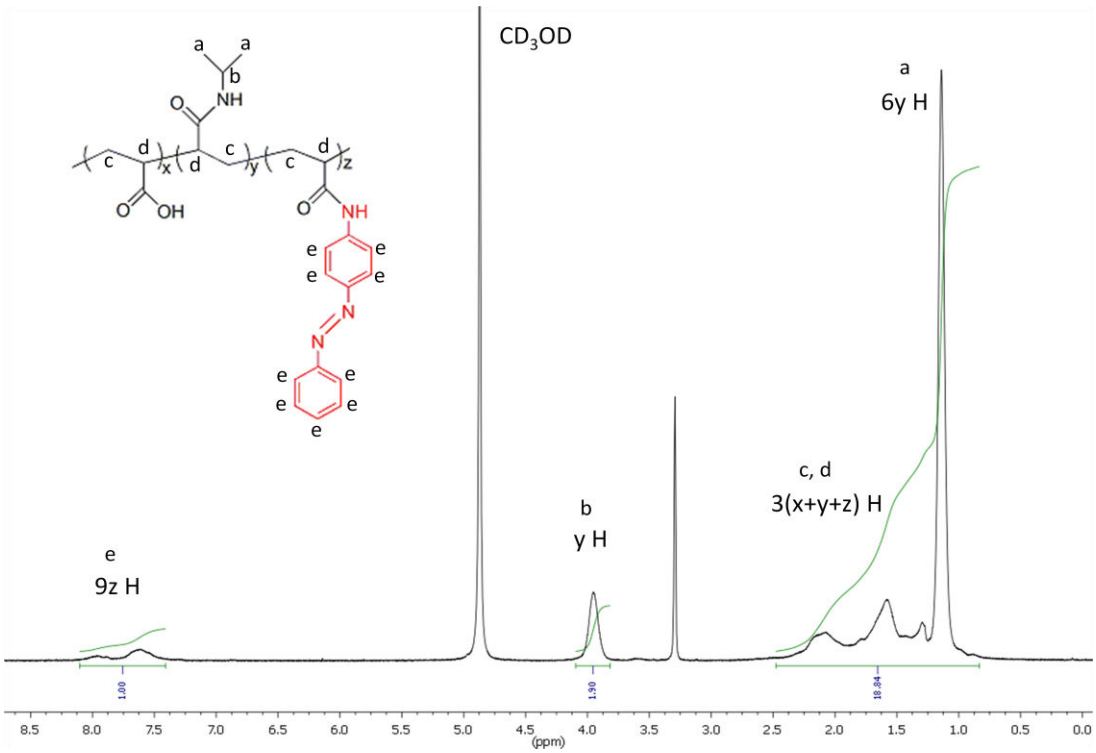


***Figure 1**: ^{1}H NMR spectra of copolymer P(AA-co-NIPAM) modified by azobenzene in CD_3OD.*

The ratio of azobenzene-functionalization can be determined with the following calculation process:

$$\begin{cases} y = 1.9 \\ 9z = 1.0 \\ \dfrac{y}{x+y+z} = 0.8 \end{cases}$$

$$\Longrightarrow \quad \frac{z}{x+y+z} = 4.6\%$$

The result shows that the ratio of azobenzene groups in the copolymer is 4.6%.

The ene-functionalized copolymer P(AA-co-NIPAM) modified by azobenzene is characterized

by ^{1}H NMR in CD_3OD to determine the ratio of ene groups in the copolymer (see **Figure 2**).

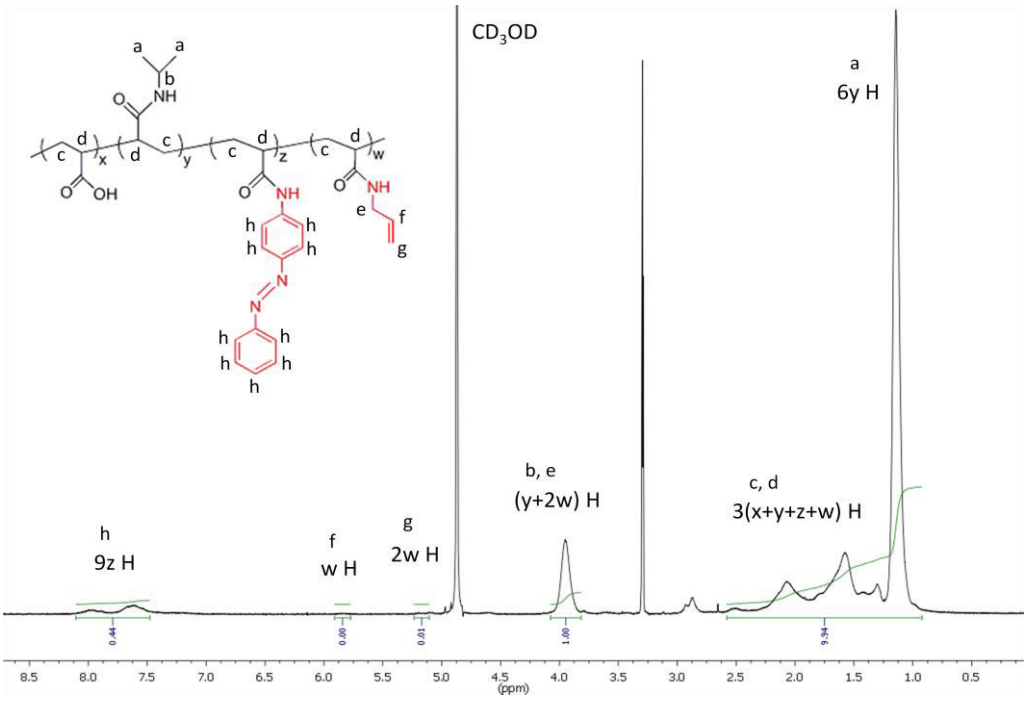


***Figure 2**: ^{1}H NMR spectra of ene-functionalized copolymer P(AA-co-NIPAM) modified by azobenzene in CD_3OD.*

The ratio of ene-functionalization can be determined with the following calculation process:

$$\begin{cases} y + 2w = 1 \\ 2w = 0.01 \\ \dfrac{y}{x+y+z+w} = 0.8 \end{cases}$$

$$\Longrightarrow \quad \frac{w}{x+y+z+w} = 0.4\%$$

The result shows that the ratio of ene groups in the copolymer is 0.4%, which is lower than that obtained with PNIPAM groups.

2. The electro-responsive poly(AA-co-AMPS) copolymer

The reaction process for the synthesis of poly(AA-co-AMPS) can be followed in time by size exclusion chromatography (SEC). In **Figure 3**, the red curve is the SEC result from passing the solution taken at the time t=0, i.e. before the addition of the initiators. While the blue curve is the SEC result from passing the solution taken at the time t=24h, i.e. 24 hours after the addition of the initiators. Since the molecular weight of the copolymer is much bigger than that of the monomers, the peak of the copolymer should come out first. By comparing the two curves, we can figure out all the peaks, as shown in the figure (the minus peak refers to

the solvent). It tells that after 24 hours, there are no more monomers, which means that the polymerization is totally finished, as it was observed for the synthesis of poly(AA-co-NIPAM) copolymers.

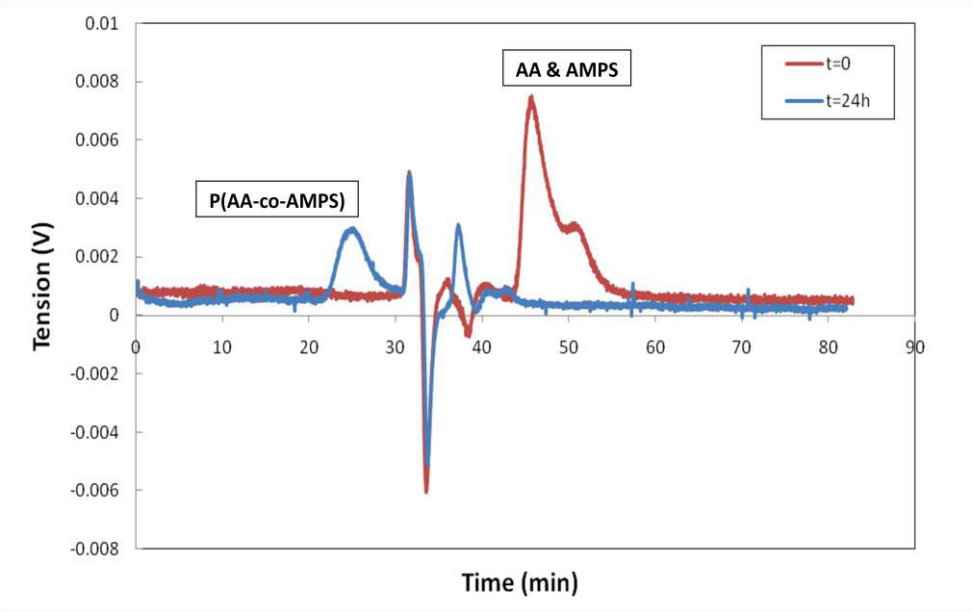


***Figure 3**: Monitoring of the synthesis process of P(AA-co-AMPS) by SEC.*

After synthesis, the copolymer P(AA-co-AMPS) is characterized by ^{1}H NMR spectroscopy in D_2O to determine the ratio of acrylic acid in the copolymer (see **Figure 4**).

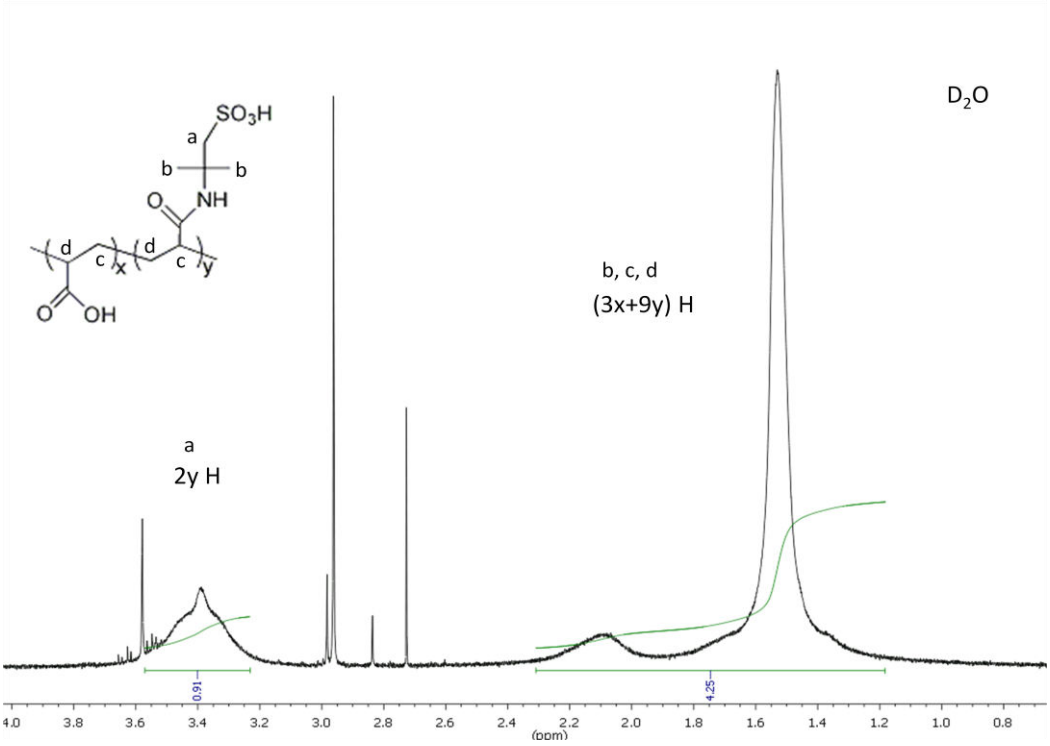


***Figure 4**: ^{1}H NMR spectra of copolymer P(AA-co-AMPS) in D_2O.*

The ratio of AA in the polymer can be determined with the following calculation process:

$$\begin{cases} 3x + 9y = 4.25 \\ 2y = 0.91 \end{cases}$$

$$\Longrightarrow \frac{x}{x+y} = 10.3\%$$

The result shows that the ratio of AA in the copolymer is 10.3%.

As shown previously, the ene-functionalization process can be followed in time by size exclusion chromatography (SEC). In **Figure 5**, the green curve is the SEC result from passing the solution taken at the time t=0, i.e. before the addition of EDC and NHS. While the purple curve is the SEC result from passing the solution taken at the time t=20 min, i.e. 20 minutes after the addition of EDC and NHS. Other curves have similar meanings with the time to take the solution different. By comparing all the curves, we can figure out that after the reaction starting for 1 hour, there's almost no more decrease in the amount of allylamine, as already observed with the previous polymers.

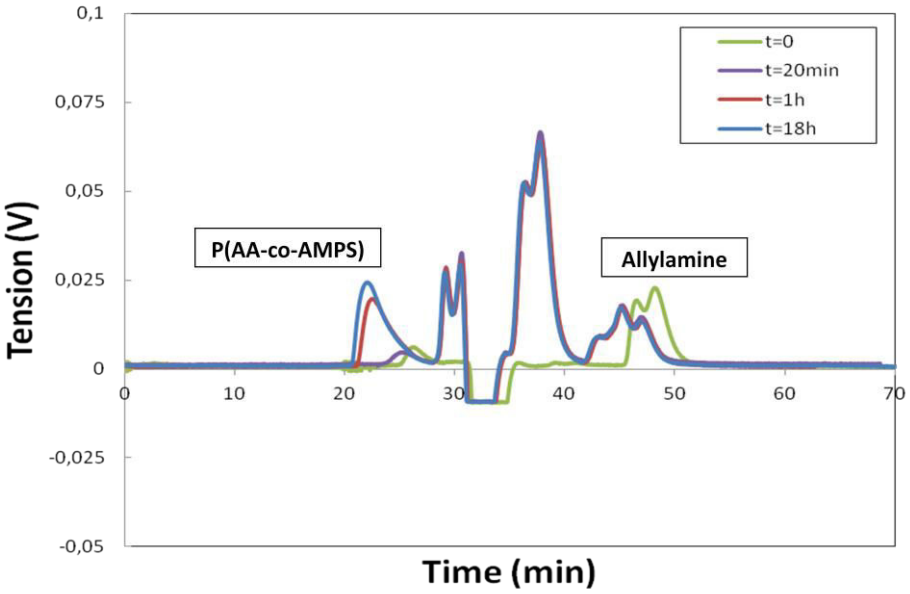


***Figure 5**: Monitoring the process of modification of P(AA-co-AMPS) by SEC.*

The ene-functionalized copolymer P(AA-co-AMPS) is also characterized by ^{1}H NMR in D_2O to determine the ratio of ene groups in the copolymer (see **Figure 6**).

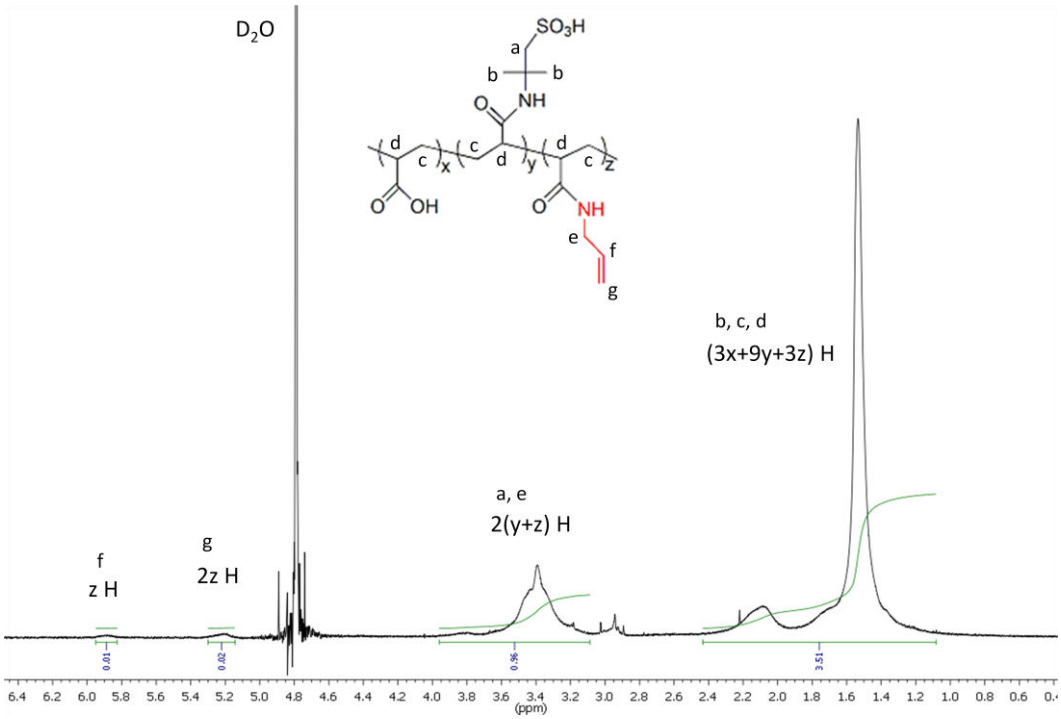


***Figure 6**: [1]H NMR spectra of ene-functionalized copolymer P(AA-co-AMPS) in D_2O.*

The ratio of ene-functionalization can be determined with the following calculation process:

$$\begin{cases} 3x + 9y + 3z = 3.51 \\ \frac{x+z}{x+y+z} = 0.1 \\ 2z = 0.02 \end{cases}$$

$$\Longrightarrow \frac{z}{x+y+z} = 2.4\%$$

The result shows that the ratio of ene groups in the copolymer is 2.4%.

3. Deuterated PAA (PAA_D)

The ene-functionalized homopolymer PAA_D is characterized by [1]H NMR spectroscopy in D_2O to determine the ratio of ene groups in the polymer (see **Figure 7**). In the NMR sample, methanol is added as a reference for quantitative analysis.

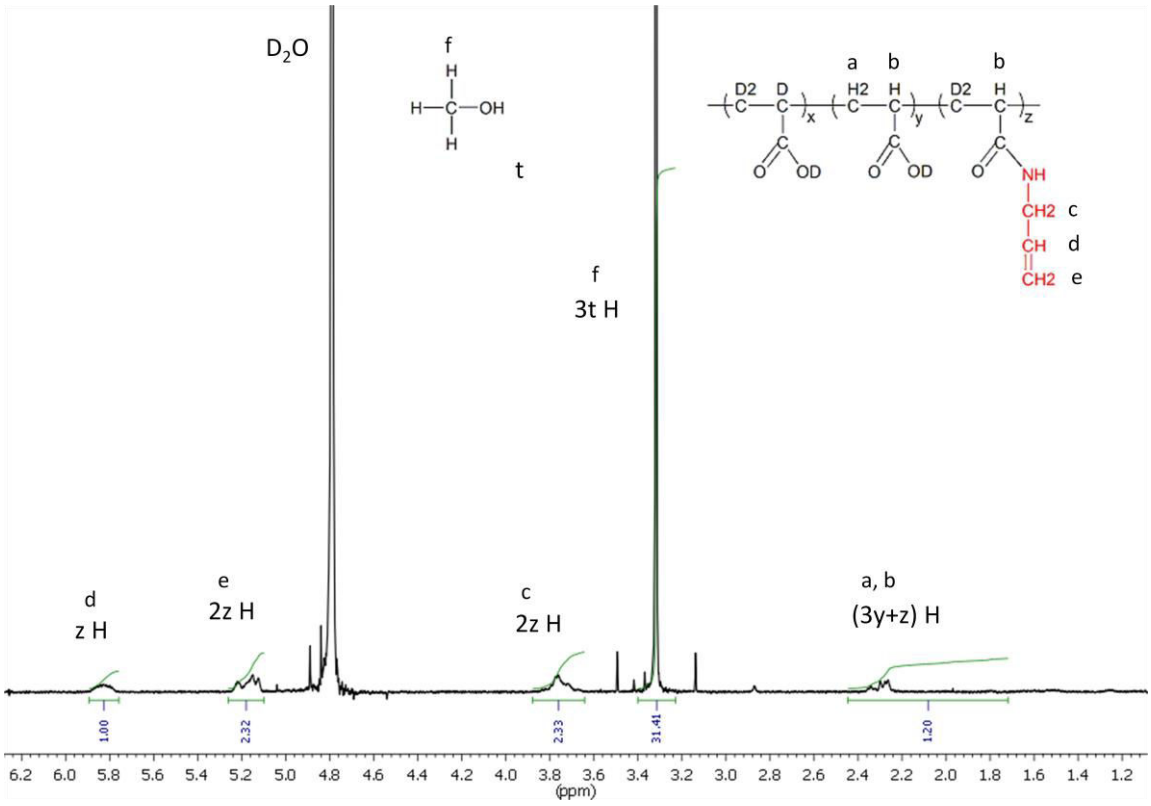


***Figure 7**: [1]H NMR spectra of ene-functionalized homopolymer PAA_D in D_2O. The mass of PAA_D and methanol is 15.4 mg and 2.054 mg respectively.*

The ratio of ene-functionalization can be determined with the following calculation process:

$$\begin{cases} 3y + z = 1.20 \\ 5z = 5.65 \\ 3t = 31.41 \end{cases}$$

$$\Longrightarrow \begin{cases} y = 0.0233 \\ z = 1.13 \\ t = 10.47 \end{cases}$$

Taking into account the mass of PAA_D and methanol, we can deduce:

$$x : y : z = 829.6 : 1 : 48.5$$

or

$$\frac{z}{x+y+z} = 5.5\%$$

The result shows that the ratio of ene groups in the homopolymer is 5.5%. Moreover, we also can see that the homopolymer PAA_D is not totally deuterated but the ratio of proton is very weak.

The proportion of proton and deuterium determined by NMR is very useful for the calculation of the scattering length density, as discussed in Chapter 4.

Annex 2: Ellipsometry

Ellipsometry is an optical method for determining the thickness and refractive index of a homogeneous film on the surface of a reflective substrate. The principle of measurement is to measure and analyze the variation of amplitude and phase of a laser beam after its reflection on the substrate.

1. Principle

When a plane wave is emitted directly onto a reflecting surface, the state of polarization of the reflected wave is changed compared to the incident beam. To describe this change, the reflection coefficients in the directions parallel and perpendicular to the incidence plan are defined as r_p and r_s respectively by:

$$r_p = \frac{E_{pr}}{E_{pi}} = |r_p| \exp(i\delta_p)$$

$$r_s = \frac{E_{sr}}{E_{si}} = |r_s| \exp(i\delta_s)$$

where E_{pi} and E_{si}, are the electric fields of the incident wave in the directions parallel and perpendicular to the incidence plane respectively, and E_{pr} and E_{sr} are the electric fields of the reflected wave in the directions parallel and perpendicular to the incidence plane respectively. The reflection coefficients r_p and r_s are complex numbers. There absolute values $|r_p|$ and $|r_s|$ represent the change in the amplitude of the electric field, and their phases δ_p and δ_s, the delay produced by the reflection on the substrate.

Ellipsometry is based on the measurement of the polarization states of the incident and reflected waves, which leads to the determination of the ellipticity G, defined as the ratio of the reflection coefficients r_p and r_s:

$$G = \frac{r_p}{r_s} = \left|\frac{r_p}{r_s}\right| e^{i(\delta_p - \delta_s)} = \tan\Psi e^{i\Delta}$$

where $\tan\Psi = \left|\frac{r_p}{r_s}\right|$ is the ratio of the absolute values which represents the change in the amplitude of the wave after reflection on the surface, and $\Delta = \delta_p - \delta_s$ represents the change in the phase.

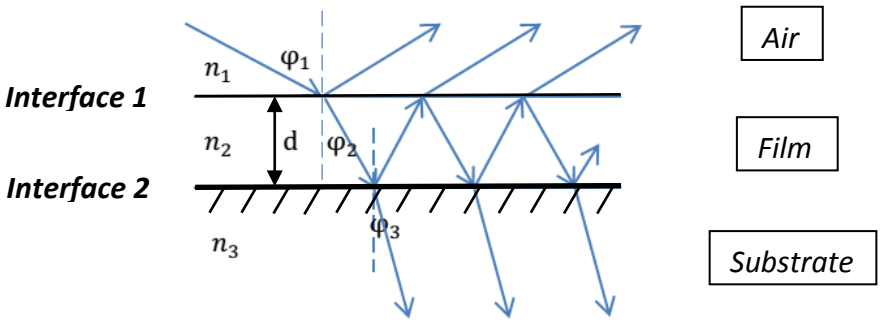


***Figure 1**: Schematic representation of the principle of ellipsometer.*

In our case, the incident light is emitted onto a thin film which is grafted on a reflective substrate, as shown in **Figure 1**. After the incident light is reflected and refracted for several times at the two interfaces, we get the final reflected beam. Similar to what is presented above, we can deduce the reflection coefficients as:

$$r_p = \frac{E_{pr}}{E_{pi}} = \frac{r_{1p} + r_{2p}e^{-2i\delta}}{1 + r_{1p}r_{2p}e^{-2i\delta}}$$

$$r_s = \frac{E_{sr}}{E_{si}} = \frac{r_{1s} + r_{2s}e^{-2i\delta}}{1 + r_{1s}r_{2s}e^{-2i\delta}}$$

in which

$$\begin{cases} r_{1p} = \left(n_2 \cos \varphi_1 - n_1 \cos \varphi_2\right)/\left(n_2 \cos \varphi_1 + n_1 \cos \varphi_2\right) \\ r_{2p} = \left(n_3 \cos \varphi_2 - n_2 \cos \varphi_3\right)/\left(n_3 \cos \varphi_2 + n_2 \cos \varphi_3\right) \\ r_{1s} = \left(n_1 \cos \varphi_1 - n_2 \cos \varphi_2\right)/\left(n_1 \cos \varphi_1 + n_2 \cos \varphi_2\right) \\ r_{2s} = \left(n_2 \cos \varphi_2 - n_3 \cos \varphi_3\right)/\left(n_2 \cos \varphi_2 + n_3 \cos \varphi_3\right) \\ 2\delta = 4\pi d n_2 \cos \varphi_2 / \lambda \\ n_1 \sin \varphi_1 = n_2 \sin \varphi_2 = n_3 \sin \varphi_3 \end{cases}$$

where r_{1p} and r_{1s} are the reflection coefficients in the directions parallel and perpendicular to the incidence plane respectively at interface 1, while r_{2p} and r_{2s} at interface 2; d represents the thickness of the film; λ represents the wavelength of the incident light; n_1, n_2 and n_3 represent the refractive index of air, the film and the substrate respectively.

So then we can infer the ellipticity G:

$$G = tan\Psi e^{i\Delta} = \frac{r_p}{r_s} = \frac{r_{1p} + r_{2p}e^{-2i\delta}}{1 + r_{1p}r_{2p}e^{-2i\delta}} * \frac{1 + r_{1s}r_{2s}e^{-2i\delta}}{r_{1s} + r_{2s}e^{-2i\delta}}$$

From all the equations above, we can see that G is the function of $n_1, n_2, n_3, d, \lambda, \varphi_1$, which gives:

$$G = f\left(n_1, n_2, n_3, d, \lambda, \varphi_1\right)$$

and then

$$\begin{cases} \Psi = tan^{-1}|G| & \text{[eq. 1]} \\ \Delta = arg(G) & \text{[eq. 2]} \end{cases}$$

Since the refractive index of air n_1 and the substrate n_3 are already known, theoretically if we fix the wavelength λ and the incident angle φ_1, we can deduce the thickness d and the refractive index n_2 of the film based on the measured Ψ and Δ by ellipsometry. Actually, it is impossible to infer the analytical solutions of d and n_2 from equations 1 and 2.

So we fix the incident angle φ_1 and then vary the wavelength of the incident light λ, it is easy to obtain two curves: the measured Ψ and Δ as function of λ respectively. Then d and n_2 can be found out which give the best fit of the two curves based on the equations above.

2. Experimental setup

2.1 Ellipsometer

The *in situ* measurements are performed using the auto-nulling imaging ellipsometer "Nanofilm_EP3" (Accurion) equipped with a spectroscopic-ellipsometry box containing a monochromator which enables the optical parameters to be determined over a wide range of wavelengths. The ellipsometer system EP3 is a computer-controlled precision measuring instrument for the measurement and graphical evaluation of layer thickness and optical properties. It is schematically represented in **Figure 2**.

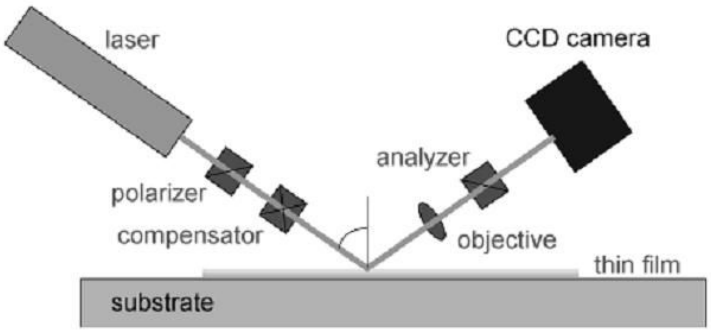


***Figure 2**: Schematic representation of the components of ellipsometer system EP3.*

As shown in **Figure 2**, after passing through the linear polarizer (P) and compensator (C), the light (a plane wave) becomes an ellipse-polarized light by adjusting the relative position between P and C. Then the ellipse-polarized light is reflected on the surface of the sample, and turns into a linearly polarized light, which can be easily detected by using a second polarizer named analyzer (A). In fact, the reflected beam can be extinguished by setting A to a 90° position with respect to the axis of the polarization. Doing this is called "nulling". Especially, the compensator (C) can be fixed at a certain angle (normally 45° for ellipsometric measurements), so a rotation of P is followed by a rotation of A to detect the reflected light which is linearly polarized. The EP3 system is also equipped with a sensitive CCD camera which enables the imaging of the sample.

The light source is a xenon arc lamp. The monochromator with 46 interference filters can result in various monochromatic lights with the wavelength ranging from 360 to 1000 nm, and the bandwidth ± 8 nm. The ellipsometric resolution of Ψ and Δ is 0.001°.

The experimental data is recorded by a connected PC and then analyzed with the software EP4 Model supplied by the manufacturer.

2.2 Measurements in air

For the measurements in air, an optical model is used as shown in **Figure 3**, which contains two layers between two semi-infinite media. One of the semi-infinite media is the substrate consisted of silicon with the refractive index (3.874 + 0.016i), and the other is ambient air with the refractive index 1.00. Here, we suppose that the refractive indices are independent of temperature and the wavelength of the light.

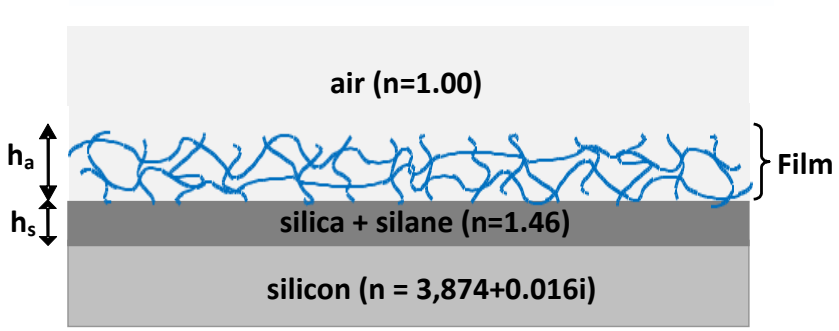


***Figure 3**: Schematic representation of the model for measurements in air.*

In the optical model, silica and silane form the first layer together, with the refractive index 1.46 and the thickness h_s, which is already determined before grafting the film onto the substrate. The second layer is the hydrogel film with an unknown thickness h_a, while its refractive index depends on the polymer used to make the gel film. For example, the

refractive index of a PNIPAM gel film is 1.52.

The thickness of the hydrogel film in air is determined by ellipsometry. The refractive index of the hydrogel film in air depends on the water content in the hydrogel film and so on the humidity ratio in air. We show that the water content is around 10% for a large range of humidity ratio between 20% and 60% which includes standard humidity ratio of air.

2.3 Measurements in water

In situ measurements in water are performed using a liquid cell with thin glass walls fixed perpendicularly to the light path. The angle of incidence is fixed at 60° depending on the liquid cell. The whole system of the setup for the measurements in water is sealed. The liquid cell is temperature-controllable with the temperature regulated within ± 0.1°C.

Similar to the optical model used for measurements in air, an optical model containing two layers between two semi-infinite media is applied, as shown in **Figure 4**. One of the semi-infinite media is the substrate, and the other is pure water with the refractive index 1.33.

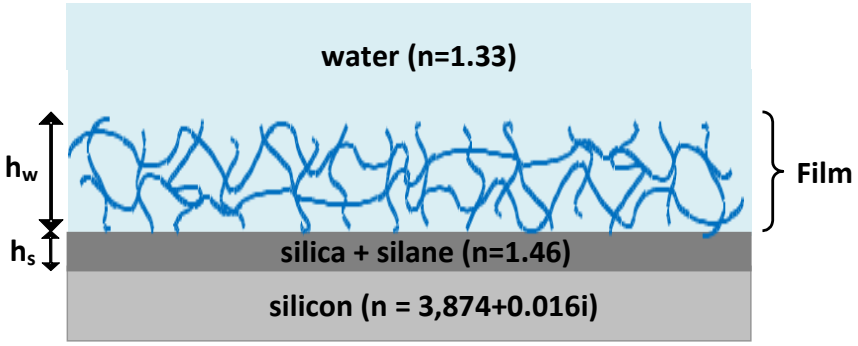


***Figure 4**: Schematic representation of the model for measurements in water.*

Silica and silane form the first layer together, the same as in air. The second layer is the swollen hydrogel film with an unknown thickness h_w. Since water is kept in the polymer network, the refractive index of the gel film is in-between that of water and that of the polymer. For example, the value of the refractive index of a swollen PNIPAM gel film in water is between 1.33 (refractive index of water) and 1.52 (refractive index of PNIPAM).

Both the refractive index and the swollen thickness of the hydrogel film in water are able to be extracted from the ellipsometry data fit.

Annex 3: QNM-AFM

1. Principle

PeakForce QNM (Quantitative NanoMechanics) is an extension of tapping mode. As in PeakForce QNM mode the force applied to the sample by the tip is controlled at a relatively low frequency (typically 1 kHz or 2 kHz), the deformation depth of the sample and the lateral force are small, which ensures the minimal damage to the probe and the sample, and also the effect of the substrate is decreased. With a calibrated cantilever, the measurement with PeakForce QNM mode has higher spatial resolution compared with tapping mode, and enables the quantitative definition of mechanical properties such as modulus, adhesion, deformation and dissipation. In fact, with Peak Force QNM mode we can detect a large range of elasticity.

In Peak Force QNM mode, the cantilever oscillates, but far below its resonant frequency. The vertical motion of the cantilever using the Z piezo element relies on the peak force between the tip and the probed sample as a feedback. The peak interaction force between the tip and the probed sample along with the property information of the sample are collected for each individual tap. Since the cantilever is not resonated, the tuning of the cantilever is not required, which is particularly advantageous in measurements in fluids.

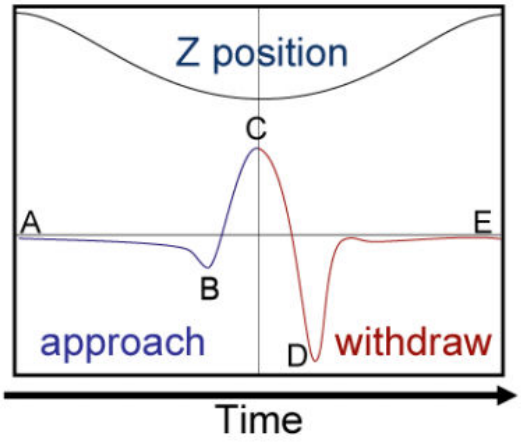


***Figure 1**: The approach-retract curve in the form of "Force-Time". Blue indicates approach of the tip while red indicates retract of the tip.*

Peak Force QNM performs a very fast approach-retract curve at every pixel in the image obtained. As shown in **Figure 1**, the approach-retract curve is presented in the form of "Force-Time". The initial contact of the probe with the sample (B), peak force (C) and adhesion (D) points are labeled. The peak interaction force of each approach curve is then used as the imaging feedback signal.

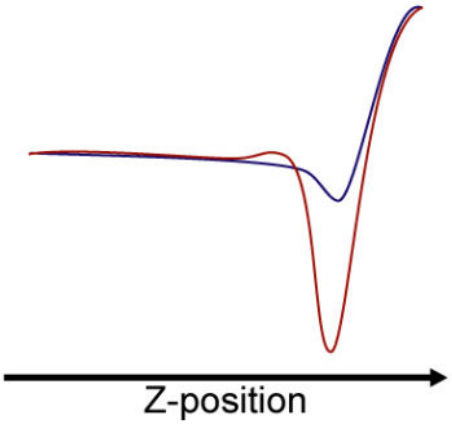


***Figure 2**: The approach-retract curve in the form of "Force-Distance". Blue indicates approach of the tip while red indicates retract of the tip.*

Using the Z-position information, the approach-retract curve can also be presented in the form of "Force-Distance", shown in **Figure 2**. The curve is analyzed during the probing to produce the peak interaction force as the controlling feedback signal, while providing a map of multiple mechanical properties of the sample (adhesion, modulus, deformation, dissipation) that has the same resolution as the height image.

2. Measurements in water

In situ imaging of the PNIPAM hydrogel thin films grafted on silicon wafers is performed using a Dimension Icon Scanning Probe Microscope (SPM) equipped with a NanoScope V Controller (Bruker), shown in **Figure 3**.



***Figure 3**: Dimension Icon SPM System.*

This Dimension Icon SPM System produces high resolution, three-dimensional images by scanning a sharp tip over the sample surface. The tip is part of a flexible cantilever mounted

on one end of a cylindrical piezoelectric tube mounted near the top of the microscope. Voltages applied to the X and Y electrodes on the piezoelectric tube deflect the tube horizontally to produce a precise raster scan over the sample surface. A voltage applied to the Z electrodes on the piezo tube controls the vertical height of the tip. The Dimension Icon head includes X, Y and Z position sensors. The sensed XYZ position information provides the feedback for closed loop control of probe tip location, ensuring that the probe completes each move command at the intended position. Stepper motors coupled to lead screws translate slides with the sample attached. A separate motor drive controls the height of the microscope and tip relative to the sample surface.

For the measurements in water, the samples with grafted gel films on silicon wafers are placed on a specially designed temperature-controllable cell with a few of water droplets on them, as presented in **Figure 4**, and the temperature is regulated within ± 0.1°C.

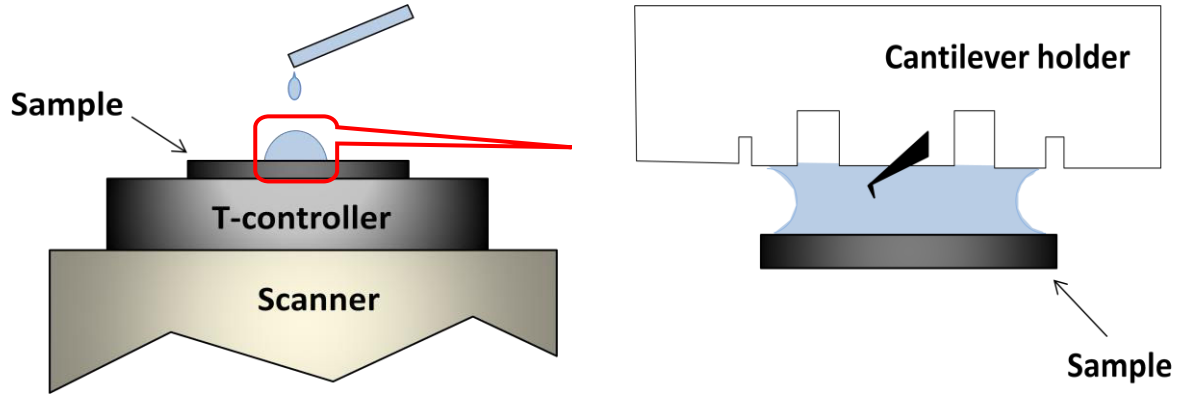


***Figure 4**: Imaging a Sample Covered by a Drop of Fluid.*

Specially, for each temperature, probing is started after at least 15 minutes of equilibration of the whole system to ensure the stability of the water flow and the surface topography of the gel films, which is important for getting high quality images with the true surface morphology.

The PeakForce QNM mode is selected for the measurements in water with the lowest possible peak force set point in order to minimize the damage to the gel film. Triangular cantilevers of different stiffness (k) with an integral silicon nitride tip (NanoProbe, Olympus) are used.

It needs to be pointed out that the cantilever holder used for measurements in fluid is different from the standard one used for operation in air. As shown in **Figure 5**, it has a clear glass window.

The cantilever holder is a small printed circuit card or acrylic block that holds the cantilever firmly at the proper angle. The cantilever holder used for measurements in fluid in **Figure 5**

provides an optically transparent cover over the back of the cantilever to maintain the optical path of the laser beam constant when the tip is submerged in a fluid medium.



***Figure 5**: The cantilever holder used for measurements in fluid.*

3. Data analysis

The images obtained are analysed in the NanoScope Analysis package. Generally, the images are firstly flattened using a standard algorithm within the NanoScope software before further quantitative analysis, to remove background slope and artificial height offsets between consecutive scan lines of the raw images.

Specially, the reduced Young's Modulus E^* is referred as the so-called DMT modulus, which is obtained by fitting the retract curve (in the form of "Force-Distance") using the Derjaguin, Muller, Toropov (DMT) model[1] given by

$$F_{tip} = \frac{4}{3} E^* \sqrt{R d^3} + F_{adh}$$

where F_{tip} is the force on the tip, F_{adh} is the adhesion force, R is the tip end radius and d is the tip-sample distance.

[1]. Derjaguin B.V., Muller V.M., Toropov Yu.P., J. Colloid. Interface Sci. 53, 314 (1975).

Annex 4: Neutron reflectivity

As mentioned previously, neutron is the only available methods with a sufficient resolution to investigate the conformation of solvated polymer networks grafted on planar solid surfaces. The strength of the neutron reflectivity or neutron scattering techniques comes from the strong difference between the neutron scattering lengths of hydrogen and deuterium. It is then possible to create an enhanced contrast by the selective deuteration of one of the components of the system while keeping a nearly equivalent chemical structure. In our case, hydrogenated polymer networks (i.e. hydrogel films) are swollen in a deuterated solvent (water).

1. Principle

The specular neutron reflectivity is sensitive to the coherent scattering length density profile in the direction normal to the interface, noted $\rho(z)$. The scattering length density can be related to the local atomic composition of the material and its density by:

$$\rho = \sum_i N_i b_i$$

where N_i is the volume density of atoms i and b_i is the coherent scattering length of the atom i. The neutron scattering length density is about 10^{-6} Å^{-2}. As the volume concentration in polymer varies with respect to the distance from the surface z, so does ρ. In the kinematical approximation, the reflectivity $R(k)$ – which is the ratio of the reflected beam intensity to the incident beam intensity – can be expressed as a function of Fresnel reflectivity $R_F(k)$ and the wave vector k:

$$R(k) = R_F(k)\left|\int_0^{+\infty} \frac{dNb(z)}{dz} exp(2ik \cdot z) \cdot dz\right|^2$$

with the wave vector k equal to:

$$k = \frac{2\pi}{\lambda}\sin\theta$$

where λ is the neutron wavelength and $(\pi/2 - \theta)$ the angle of incidence.

Fresnel reflectivity corresponds to the reflectivity of the abrupt interface between two homogeneous media with two different coherent scattering length densities Nb_1 and Nb_2. Fresnel reflectivity $R_F(k)$ is related to the critical wave vector k_c, which can be expressed as:

$$k_c = \sqrt{4\pi(Nb_2 - Nb_1)}$$

by the following relationship:

$$R_F(k) = \left| \frac{1 - \sqrt{1 - \frac{k_c^2}{k^2}}}{1 + \sqrt{1 - \frac{k_c^2}{k^2}}} \right|^2$$

For wave vectors inferior to the critical wave vector, total reflection is observed ($R(k \leq k_c) = 1$).

2. Experimental setup

2.1 Neutron reflectometer

Neutron reflectivity measurements were performed on the reflectometers EROS (Etude par Réflectivité de l'Organisation des Surfaces) and PRISM (Polarised Reflectometer for the Investigation of Surface Magnetism) at the Laboratoire Léon Brillouin, CEA-Saclay (France), under Fabrice Cousin's watchful and kind eye. We used protonated hydrogel films and deuterated solvent in order to enhance the contrast between the hydrogel and the solvent and to optimize the reflectivity signal.

2.1.1 EROS

This reflectometer is dedicated to the study of interfaces by neutron reflection. The reflected intensity at grazing angle of a non polarized white neutron beam is measured as a function of wavelength. The variation of this reflection coefficient (reflectivity) with the wave vector is linked to the concentration profile perpendicular to the interface. If this profile is represented by a succession of different layers, the thickness, composition and roughness of each layer may be determined within the range from 2 to 500 nm for thickness and 1 to 20 nm for roughness. All type of interfaces might be studied, including air-solid and solid-liquid interfaces.

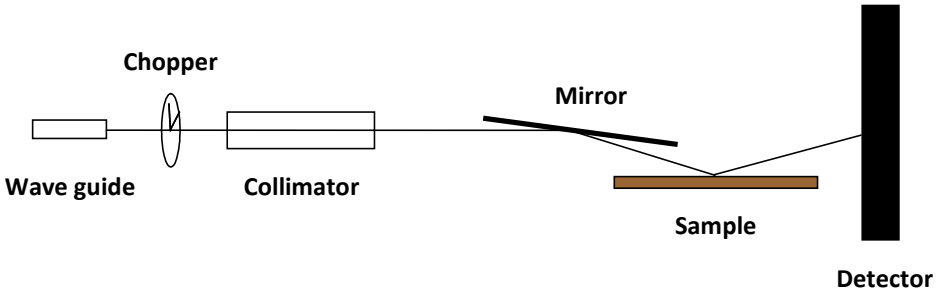


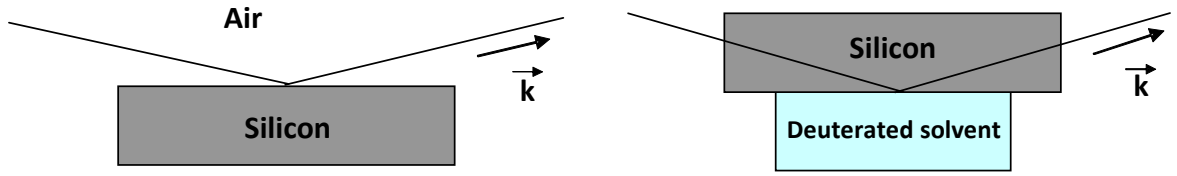
***Figure 1**: Schematic representation of the reflectometer EROS.*

As shown in **Figure 1**, out of the wave guide, the multi-wavelength neutron beam first goes

through a chopper which selects the wave packets with the fastest propagating wavelength equal to 3 Å and the slowest 25 Å, as the velocity of the neutron (of mass m_n) v depends on its wavelength λ through De Broglie's relation:

$$v = \frac{h_p}{m_n \lambda}$$

with h_p the Planck constant. The selected beam is collimated, and then sent onto the solid-air interface directly (**Figure 2a**), or the solid-liquid interface through the silicon wafer (**Figure 2b**). After reflected at the interface, the neutron beam is finally detected by the detector. The "time of flight" method is used to determine the wavelength of the detected neutron beam according to the equation above.



(a) In air (b) In liquid

***Figure 2**: Two types of geometry are used in measurements with EROS: solid-air interface (a) and solid-liquid interface (b).*

For the measurements in air, the neutron beam firstly passes through the grafted hydrogel film and then arrives at the silica-silicon interface, where it is reflected to reach the detector. For the measurements in liquid, the geometry in **Figure 2b** is applied because silicon is a material that absorbs very few neutrons compared to heavy water. The neutron beam crosses the silicon wafer, is reflected at the hydrogel-solvent interface, re-crosses the silicon wafer and then reaches the detector.

A system is specially developed to adapt to the measurements in liquid, as shown in **Figure 3**. A liquid cell made of stainless steel is designed, which contains a teflon trough filled with the deuterated solvent and a copper heater whose temperature can be regulated within ± 0.1°C. During measurements, the sample is tightly clamped against the teflon trough with the film-grafted surface touching the solvent.

The sample was tilted to optimize the signal measured and the detector was placed accordingly to the second semi-infinite media (air or solvent). Two angles θ were set for the measurements to get the largest range of wave vector as possible. In air, the experiments were achieved at 0.93° and 1.6° so that the wave vector ranges from 4 10^{-3} $Å^{-1}$ to 9 10^{-2} $Å^{-1}$. In heavy water, the two angles were set to 1.19° and 2° so that the wave vector ranges from

5 10^{-3} Å^{-1} to 8 10^{-2} Å^{-1}.

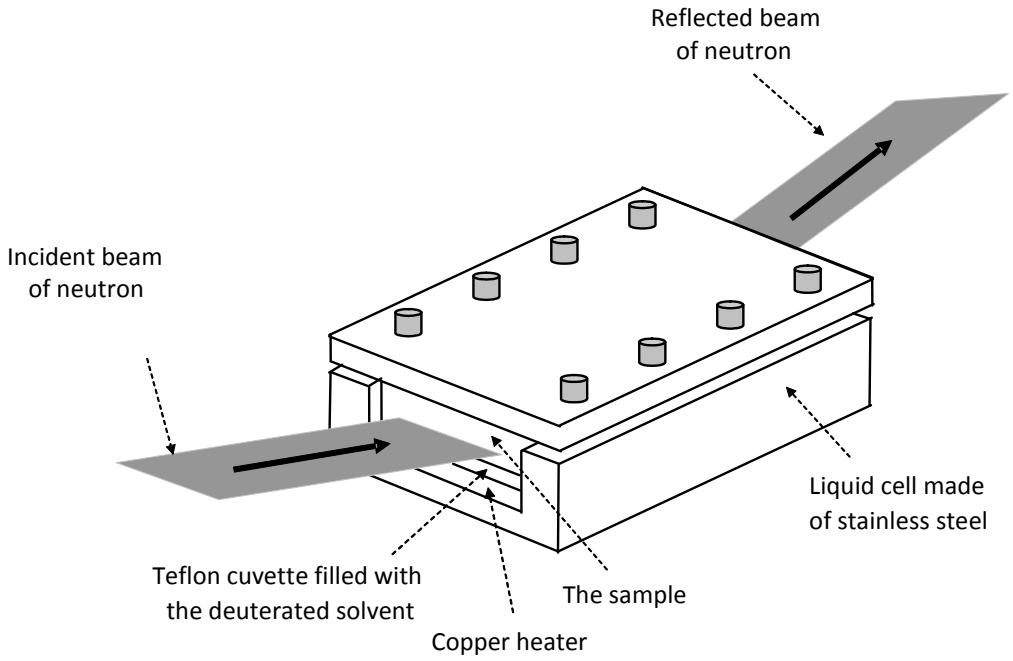


***Figure 3**: Schematic representation of the system for measurements in liquid: a liquid cell containing a teflon trough filled with the deuterated solvent and a copper heater.*

2.1.2 Prism

This spectrometer is suited for the study of thin films and multilayers with polarization analysis. The general view of the spectrometer is shown in **Figure 4**.

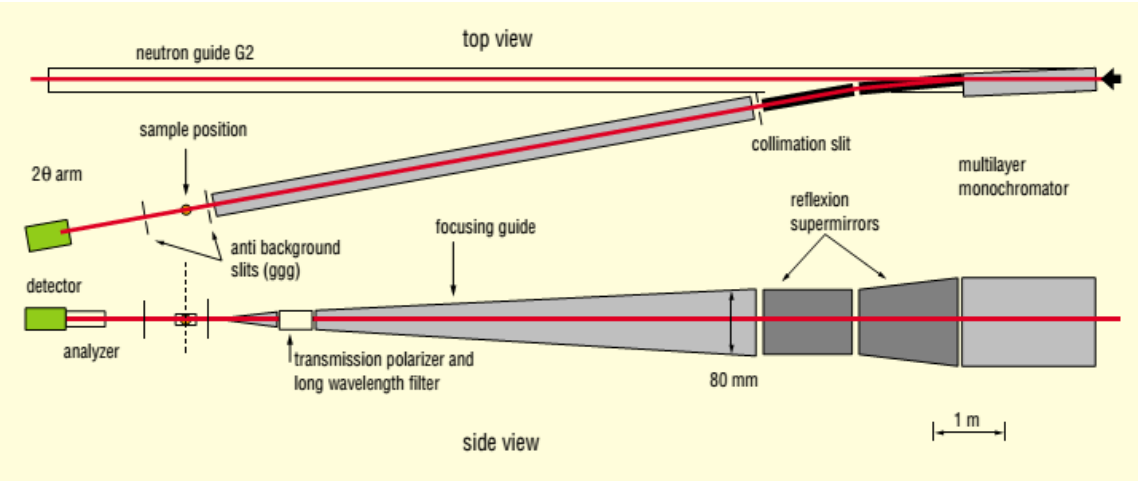


***Figure 4**: Schematic representation of the reflectometer PRISM. Slits are made of single crystal Gallium Gadolinium Garnet to reduce small angle neutron scattering. The incident beam is produced by a multilayer monochromator mounted in the guide G2.*

PRISM reflectometer works with angle variation (and not time of flight). The wavelength is

fixed at 4.3 Å and the scattering angle 2θ can be varied up to 120°. Even if the angle variation 0.002° is the smallest as possible, the resolution on small wave vector is not as good as that obtained with EROS which works with time of flight. This spectrometer allows to measure reflectivity curves with a dynamic range of 10^5 - 10^6. Variation of angles, range of k.

The setup for measurements in air and in liquid with PRISM is very similar to that used in EROS, except that the position of the measured surface is vertical (which is horizontal with EROS).

3. Fitting of experimental data and deduction of the density profile

To determine the profile of scattering length density, we assume a model of $Nb(z)$ which has a number of adjustable parameters, and we are able to deduce the reflectivity corresponding to this profile using the formula of $R(k)$ given above. Then the calculated reflectivity is compared with the experimental one, and with an optimization algorithm, we can find out the values of the parameters which give the best fitting of the experimental data.

For the model of $Nb(z)$, we suppose that the thin film is divided into many layers with a constant scattering length density for each layer. The layers are connected between each two layers by the "error" function which reflects the interpenetration of the layers (i.e. roughness). With this model we don't need to define the shape of the density profile *a priori*. The thickness, the roughness and the scattering length density of each layer are the adjustable parameters. We define Nb_i and h_i are the scattering length density and the thickness of layer i respectively. While σ_i is the roughness which connects the layer i and $i+1$, and it is also the standard deviation of Gaussian function that describes the error function.

$$Nb_{i,j+1}(z) = Nb_i + \frac{Nb_{i+1} - Nb_i}{\sigma_i \sqrt{\pi}} \int_{-\infty}^{z} \exp\left(- \frac{(u - h_i)^2}{{\sigma_i}^2} \right) du$$

$$Nb_{i,j+1}(z) = Nb_i + \frac{Nb_{i+1} - Nb_i}{2} \left[1 + erf\left(\frac{z - h_i}{\sigma_i} \right) \right]$$

where $erf(z) = \frac{2}{\sqrt{\pi}} \int_0^z \exp\left(-t^2\right) dt$ is the error function described above.

The optimization program we use was developed by Alain Menelle of the Laboratoire Léon Brillouin at Saclay. It is employed to minimize the following function:

$$\chi^2 = \frac{1}{M-p}\sum_j^M \left[\log R_j - \log R(k_j)\right]^2 \frac{R_j^{\,2}}{\varepsilon_j^{\,2}}$$

where M is the number of data points, p is the number of adjustable parameters, R_j is the calculated reflectivity for $k = k_j$, $R(k_j)$ is the experimental reflectivity, and ε_j is the measurement error. The number of adjustable parameters must be very small compared to the number of data points, because if not, the probability that the algorithm "blocks" on a local minimum value of χ^2 can grow rapidly.

Films of single network

The single network gel films were measured in air and in (heavy) water. For all sample, the fitting of the experimental data using a unique layer for the hydrogel film is adequate. There is no need to suppose many layers as for polymer brushes for which the density profile is very soft. As a result, the films of single network can be described by one single layer with an interface width defined by an error function.

For the measurements in air, the thickness found h_a is compared with the value measured by another technique such as ellipsometry. The roughness σ provides the interface width of the hydrogel film. The scattering length density *Nb* obtained is compared to the theoretical value (provided by the calculation or the literature). This comparison allows the determination of the water content in the hydrogel film.

For the measurements in water, once we get the profile of scattering length density $Nb(z)$ by fitting of experimental data, the polymer density profile $\Phi(z)$ is deduced from $Nb(z)$, knowing the coherent scattering densities of the polymer Nb_{pol} and of deuterium oxide Nb_{D_2O}:

$$\Phi(z) = \frac{Nb(z) - Nb_{D_2O}}{Nb_{pol} - Nb_{D_2O}}$$

Calculated from the polymer density profile using:

$$h_a = \int_0^{+\infty} \Phi(z) \cdot dz$$

for which the thickness h_a is an important parameter because it corresponds to the thickness of the film in air. Profiles fitting well the experimental date but corresponding to an unsuitable thickness h_a are naturally not selected.

Films of IPN and LbL networks

The IPN and LbL multilayer gel films were investigated in air and in water. For the measurements in water, the contrast-matching of the solvent with the PAA deuterated polymer was performed to make visible only the PNIPAM hydrogenated polymer network. The contrast-matching was achieved by using D_2O/H_2O mixture (with 88% of D_2O and 12% of H_2O). The same incident angles as for films of single network were set: 1.19° and 2° as the D_2O/H_2O mixture contains a majority of D_2O so that the range of wave vector is comparable with that obtained for films of single network: from 4 10^{-3} $Å^{-1}$ to 8 10^{-2} $Å^{-1}$.

For the measurements in air, the thickness h_a found is not unique as the samples contain many networks. However, the number of layers is not necessary the same used for the ellipsometry measurements. Actually, the ellipsometry allowed the control of each step of the synthesis or each step of the *addition* of the networks in the whole film. The neutron measurements are performed on the whole film and the structure of the hydrogel film depends strongly on the interpenetration between the networks. Also, the total thickness in air h_a found after fitting should be the same as the value measured by ellipsometry. The roughness σ given by the error function which connects two adjacent layers provides exactly the interpenetration of the networks. The scattering length density *Nb* obtained for each network is compared to the theoretical value (provided by the calculation or the literature). However, as it depends both on the interpenetration between networks and on the water content in the hydrogel film, we assume that the water content for films of LbL and IPN networks is reasonably the same as for films of single network. The interpenetration between networks with the ratio of deuterated and hydrogenated networks for a given layer is then deduced.

The **Table 1** lists the scattering length densities used along the fitting process.

Material	$Nb.10^6$ (Å^{-2}) for the interface Si-Air	$(Nb-Nb_{Si}).10^6$ (Å^{-2}) for the interface Si-D_2O
Silicon	2.07	0.00
Silica	3.47	1.40
Silane	0.28	-1.79
Deuterium oxide D_2O	6.40	4.33
Water H_2O	-0.56	-2.63
Hydrogenated PNIPAM-h [1]	1.00	-1.07
Deuterated PAA-d [2]	5.56	3.49

***Table 1**: Neutron coherent scattering length densities of various materials.*

[1] see discussion detailed on the part 3.1 of chapter 3

[2] the PAA-d contains 95% of deuterated species and 5% of hydrogenated species as shown by ^{1}H NMR spectrum and is assumed to be 50% ionized in pure water, the calculation of Nb for totally deuterated PAA is 6.00 10^{-6} Å^{-2} for non-ionized state (using density equal to 1.3 g/cm^3) and 5.48 10^{-6} Å^{-2} for fully ionized state (using density equal to 1.6 g/cm^3) respectively, the calculation of Nb for totally protonated PAA is 1.80 10^{-6} Å^{-2} for non-ionized state (using density equal to 1.3 g/cm^3) and 2.46 10^{-6} Å^{-2} for fully ionized state (using density equal to 1.6 g/cm^3) respectively.

Abstract

Thin films of hydrogels we study are chemical polymer networks covalently grafted on solid substrates. These versatile coatings allow the control of various interfacial properties such as responsive properties, wetting or mechanical properties. Here, thin films of stimuli-responsive hydrogels (with temperature, light or electric field) are the point of interest.

The surface-attached gel films are synthesized by following a straightforward strategy based on thiol-ene click chemistry. The formation of the films is achieved by adding bifunctional thiol molecules as cross-linkers to the ene-reactive polymers on thiol-modified surfaces. This strategy allows us to obtain hydrogel films with a wide range of thickness and with the desired properties.

We study the structure of surface-attached poly(*N*-isopropylacrylamide) gel films which show thermo-responsive properties. We determine the effect of confinement and constraints due to the surface-attachment on the swelling/collapse phase transition of hydrogels with two approaches: the one-dimension swelling normal to the surface using ellipsometry and neutron reflectivity and the in-plane observation of the free surface of the gel using AFM. The transition temperature (LCST) and the swelling ratio of the hydrogel films are investigated on a range of thickness varying from nanometer to microns. The swelling ratio of hydrogel films is in good agreement with the scaling laws predicted with the extension of Flory-Rehner theory to one-dimension swelling. It is also shown that the smoothness of the free surface of the hydrogel films is not due to the roughness (in-plane irregularities) but mainly to a diffuse interface, indicating that the hydrogel in the film is far from a model network.

New and complex hydrogel films are also developed by targeting the architecture of the polymer networks. Inspired from macroscopic hydrogels architecture, we design various architectures: multilayer gel films, interpenetrating networks (IPN) gel films and hybrid gel films. Multilayers gel films are the combination of many functional single-network films simply by stacking one onto the other as in layer-by-layer assemblies. In IPN gel films, the two chemical networks are interpenetrated one into the other. Hybrid hydrogels films studied are hydrogels containing solid particles such as silica nanoparticles.

Résumé

Les films minces d'hydrogels que nous étudions sont des réseaux chimiques de polymères greffés par liaison covalente sur des substrats solides. Ces revêtements versatiles permettent le contrôle des propriétés interfaciales tel que les propriétés stimulables, le mouillage ou les propriétés mécaniques. Ici, nous nous intéressons aux films minces d'hydrogels stimulables (par la température, la lumière ou le champ électrique).

La synthèse des films de gels greffés suit une stratégie simple basée sur la chimie click thiol-ène. Les films sont fabriqués en déposant les polymères stimulables fonctionnalisés par des groupes diène en présence de réticulants dithiols sur des surfaces modifiées thiol. Cette stratégie permet d'obtenir des films d'hydrogels sur une large gamme d'épaisseur avec les propriétés stimulables visées.

Nous nous intéressons à la structure des films d'hydrogels greffés de poly(N-isopropylacrylamide) aux propriétés thermo-stimulables. Nous étudions l'effet du confinement et des contraintes dues au greffage sur la surface sur la transition de phase gonflement/dégonflement des gels avec deux approches : le gonflement unilatéral (perpendiculaire à la surface) par ellipsométrie et réflectivité de neutrons, et la topographie (dans le plan) de la surface libre du gel par AFM. La température de transition (LCST) et le degré de gonflement des films de gel sont étudiées sur une large gamme d'épaisseur du nanomètre aux microns. Le degré de gonflement des films de gel est en bon accord avec les lois d'échelle établies à partir de la théorie de Flory-Rehner adaptée à un gonflement unidirectionnel. Nous montrons que la surface libre des films de gel est plus diffuse que rugueuse, l'hydrogel dans le film étant loin d'un réseau modèle.

Nous développons également de nouveaux films d'hydrogels avec des réseaux d'architectures ciblées. En s'inspirant de l'architecture des gels macroscopiques, nous élaborons diverses architectures : films de gels multicouches, films de réseaux interpénétrés et films de gels hybrides. Les films de gels multicouches permettent de combiner plusieurs réseaux simples fonctionnels empilés les uns sur les autres à la manière des assemblages layer-by-layer. Dans les films de réseaux interpénétrés, les deux réseaux chimiques sont interpénétrés l'un dans l'eau. Les films de gels hybrides contiennent des particules solides telles les nanoparticules de silice.